

## **Distribution Agreement**

In presenting this thesis or dissertation as a partial fulfillment of the requirements for an advanced degree from Emory University, I hereby grant to Emory University and its agents the non-exclusive license to archive, make accessible, and display my thesis or dissertation in whole or in part in all forms of media, now or hereafter known, including display on the world wide web. I understand that I may select some access restrictions as part of the online submission of this thesis or dissertation. I retain all ownership rights to the copyright of the thesis or dissertation. I also retain the right to use in future works (such as articles or books) all or part of the thesis or dissertation.

Signature:

---

Muhsinah Holmes Morris

---

Date

Photolabeling of the Human Dopamine Transporter  
and the Reactivity of Aryl Azides with Amino Acid Analogs

By

Muhsinah Holmes Morris  
Doctor of Philosophy

Chemistry

---

Joseph B. Justice, Jr., Ph. D.  
Advisor

---

Dale E. Edmondson, Ph. D.  
Committee Member

---

David Lynn, Ph. D.  
Committee Member

Accepted:

---

Lisa A. Tedesco, Ph.D.  
Dean of the Graduate School

---

Date

Photolabeling of the Human Dopamine Transporter  
and the Reactivity of Aryl Azides with Amino Acid Analogs

By

Muhsinah Holmes Morris

B.S., Clark Atlanta University, 2000

M.S., Emory University, 2005

Advisor: Joseph B. Justice, Jr., Ph.D.

An Abstract of

A dissertation submitted to the Faculty of the Graduate

School of Emory University in partial fulfillment

of the requirements for the degree of

Doctor of Philosophy in Chemistry

2008

## Abstract

### Photolabeling of the Human Dopamine Transporter and the Reactivity of Aryl Azides with Amino Acid Analogs By Muhsinah Holmes Morris

This work explored the site of photolabeling of the human dopamine transporter (hDAT) by the photoaffinity agent [<sup>125</sup>I]-DEEP, an aryl azide photoaffinity label, and also the selectivity of aryl azides using phenyl azide and amino acid analogs. The site of incorporation of [<sup>125</sup>I]-DEEP had been shown to incorporate within transmembrane domains 1 and 2 of hDAT by Vaughan and Kuhar (1996). To further isolate the site of incorporation, [<sup>125</sup>I]-DEEP was photolyzed with hDAT membranes, isolated by SDS-PAGE, and digested with trypsin and cyanogen bromide (CNBr). The peptide, N<sub>93</sub>GGAFLLVPYLLFM<sub>106</sub>, which is located at the top portion of TMD2, was identified as the possible site of [<sup>125</sup>I]-DEEP incorporation.

[<sup>125</sup>I]-DEEP contains a phenyl azide as the photoactive agent. In a follow-up study, the photolabeling selectivity of phenyl azide with amino acids was examined using analogs of amino acid side chains. Phenyl azide (100 μM) and amino acid analogs (1 M) were irradiated at 254 nm for 4 minutes in polar and nonpolar conditions and the kinetics of the reactions determined. 1-Octanethiol, butylamine, guanidine acetic acid, dimethyl sulfide, ethylbenzene, butyric acid, imidazole, and phenol were used to model the side-chains of cysteine, lysine, arginine, methionine, phenylalanine, glutamic acid, histidine, and tyrosine, respectively. *N*-ethylacetamide was used as a model for the peptide backbone.

The order of phenyl azide reactivity with analogs studied in polar conditions was guanidine acetic acid ≈ imidazole > phenol. The order of phenyl azide reactivity with analogs studied in nonpolar conditions was dimethyl sulfide > butyric acid ≈ butylamine ≥ *N*-ethylacetamide ≈ 1-octanethiol ≈ ethylbenzene. Product stability in proteolytic conditions was tested. Trypsin digestions were performed in 100mM ammonium bicarbonate at pH 8.9, while CNBr cleavages were performed in 70% trifluoroacetic acid at pH 1. Histidine, tyrosine and cysteine analogs were the most stable, while all of the other analogs decomposed by greater than 50% within 24 hours. Product stability in proteolytic conditions has implications for photoaffinity labeling of proteins with aryl azides in which proteolysis is used for peptide mapping.

Photolabeling of the Human Dopamine Transporter  
and the Reactivity of Aryl Azides with Amino Acid Analogs

By

Muhsinah Holmes Morris

B.S., Clark Atlanta University, 2000

M.S., Emory University, 2005

Advisor: Joseph B. Justice, Jr., Ph.D.

A dissertation submitted to the Faculty of the Graduate  
School of Emory University in partial fulfillment  
of the requirements for the degree of  
Doctor of Philosophy in Chemistry

2008

## **Dedication**

I would like to dedicate this dissertation work to my father, Mr. Gordon Leonard Holmes, Sr. and my mother, Mrs. Alice Mae Kirkland Holmes. During this time, I leaned on the two of them more than I ever have. Thank you both for letting me lean, for helping me raise my children and fulfill my dreams, and for helping me remain focused on the vision that had been nurtured within me for an entire lifetime.

This is for the both of you. Thank you for teaching me that education was my key to a better future.

In honor of you, Mom and Dad, I pay homage to my grandparents, Grandma Mary, Susie Mae, and Ella; I miss you ladies and Grand Daddy J.C. Holmes, Wyman Moore, and Rufus Mobley.

## Acknowledgements

I would like to thank God for His strength and ability to persevere through the hard times as I was pursuing my goal. "Though He slay me, yet will I trust Him" (Job 13:15). "For I know the plans I have for you," declares the LORD, "plans to prosper you and not to harm you, plans to give you hope and a future" (Jeremiah 29:11). I love you God! Thank you for directing my path and for putting angels at my every turn.

Secondly, thank you to my advisor, Dr. Joseph B. Justice, Jr., who would never let me quit. Whenever I was losing sight of my vision you helped to redirect me back to accomplishing what I wanted to finish. You have taught me about more than science but about life. Life is what happens while you're living it. I learned that from you and just having had your full support has helped me through this program. You are a good, highly esteemed friend. Your kindness has never gone unnoticed. Have a great retirement. I will miss you, your wit, and your wisdom!

To my committee members, Dr. David Lynn and Dr. Dale Edmondson, I appreciate all of your support and ideas that helped to shape this project into something that I could be proud of. To John Lever and Amy Hauck Newman, thank you for providing the photoaffinity ligands that were used to analyze the dopamine transporter. This project could not be possible without you.

Thanks to my current and former lab members, Dr. Uliana Danilenko, Dr. Tamara Jackson Henderson, Chineye Idigo, Matthew Printz, Dr. Sara Wirtz-Simmons, Dr. Brian Reed, Dr. Rachel Whitehead-Spector, Astrid Suantio, and Dr. Anh Pham. You all have helped propel me forward towards my destiny. Thank you all for your encouragement and love through every task that needed completing.

I appreciate the Emory community of mothers that gave me advice and love throughout my matriculation at this institution. Kharen Fulton, Theresa Kenney, Queen Watson, Dr. Virginia Shadron, Dr. Lisa Tedesco, Dr. Pat Marsteller, Rosemary Hynes, Geri Thomas, Sherice Allen-Henry, Ethel Ellington, Deirdre Russell, Jan McSherry, and Cindy Gailliard. I am in awe of you. Thank you for loving me!

To my family-my husband, Christopher Anthony Morris, Sr.-thank you for holding it down while I pursued my goals. My deepest gratitude goes to you for consistently providing for our family. I respect you for that act of love. You are my very best friend, one who I have grown to love more and more each day. To my children, Anthony Christopher, Matthew Joseph, Christopher Anthony II, and Seth Muhsin, you all have pushed me into being who I am today. I am proud to be your mother. Thank you for sharing me with my work and for loving me every day no matter what time of night I drag in from the lab. I love each of you with all that I am. To my in-laws, Hector and Lorna Morris, thank you for the undying love, encouragement and support. To my second mom, Nina Morris, my gratitude for your love and support of me and my family during this time can hardly be expressed. Thank you for your around-the-clock

unconditional love. God bless you! To my little sister-in-law, Ms. Christine Meloney Morris, thank you for letting me be myself, for always accepting me, and helping me regardless of the situation. I adore you and love you little sis. God bless you (and Zyien)! To my Mamauntie Lil and Uncle Charles, you all have made success look effortless. Thank you for the prayers and love from before I was born. I love you both very much! To my big sister, "My Imah", thanks for your early morning wake-up calls and for always letting me cry on your shoulder. Thank you for always stepping up to the plate to help me in my times of need and for providing my "secret batcave". To my little brother, Sabir Ali, thank you for believing that I could do anything. Your admiration for me keeps me going no matter how bad I want to give up. Thank you for the joy you have given me in Sabir Jr. Jaye-thank you for your admiration and your kindness. Take care of my nephew, Sabir Jr., and go for it girl-you can have it ALL! Gordy, you are my inspiration. Because of your illness, I have been propelled to do **more** in this lifetime than I could have ever imagined. I love you Big Brother day and night. I love all of my siblings very much. To my loving parents, Gordon and Alice Holmes, Sr., no greater love have I experienced as that which you both have given me. The character that is the foundation of a willingness to push through until the end is something that is only obtained through God's divine will. **Thank you for your DNA.** I love and adore you!

To my extended family and my ancestors who have gone before me-I stand on your shoulders. Thank you for the strength to stand!

Finally, thank you to Thomas Edison who taught me that "I have not failed but that I have found 1,000 ways that don't work."

**It is finished!**



# Table of Contents

	Page
<b>Chapter One</b>	
<b>Cocaine Addiction and the Human Dopamine Transporter</b>	1
Cocaine Addiction	2
Available Treatments for Addiction	5
Cocaine as an Inhibitor of the Dopamine Transporter	6
Other Inhibitors to the Dopamine Transporter	10
Structure and Function of the Dopamine Transporter	13
Characterization of Membrane Bound Proteins	18
Photoaffinity Labeling as a Method to Identify the Cocaine	
Binding Site of the Human Dopamine Transporter	25
Photoaffinity Labeling of DAT	31
Photochemistry of Aromatic Nitrenes	36
Project Overview and Objectives	39
<b>Chapter Two</b>	
<b>Photoaffinity Labeling of the Human Dopamine Transporter</b>	
<b>with [<sup>125</sup>I]-DEEP</b>	51
<b>Introduction</b>	52
<b>Methods</b>	56
Cell Culture and Photoaffinity Labeling	57
Cell Culture	57
Membrane Preparation	57
Photoaffinity Labeling	58
Purification and Isolation of Radiolabeled hDAT	61
Immobilized Metal Affinity Chromatography	61
Gel Electrophoresis	61
Autoradiography	62
Western Blotting	62
Digestion of Radiolabeled hDAT	64
Enzymatic Digestions of Labeled hDAT	64
Chemical Cleavage	64
Thin Layer Chromatography	65
HPLC	66
SDS-PAGE of Extracted hDAT Peptides	67
Solid-State Photolabeling of hDAT with Radioligands	67
General Protein/Mass Analysis for Windows (GPMW)	67
<b>Results</b>	70
Introduction to the Results	71
Suitability of Photoaffinity Labeling Experimental Conditions	74
Investigations into Localizing the Cocaine Binding Site with the	

GBR Analog, [ <sup>125</sup> I]-DEEP	78
Solid-State Photoreactions of [ <sup>125</sup> I]-DEEP and Amino Acids	89
Effect of Photoaffinity Labeling Conditions on [ <sup>125</sup> I]-DEEP	92
Preliminary Investigations of [ <sup>125</sup> I]-JJC 3-24, a Rimcazole	
Photolabel of DAT	96
<b>Discussion</b>	103
Introduction to the Discussion	104
Investigation of Photoincorporation Site of [ <sup>125</sup> I]-DEEP on hDAT	105
Suitability of Photoaffinity Labeling Experiment Conditions	105
WIN 35, 428 Protection Experiment	106
Analysis of [ <sup>125</sup> I]-DEEP Labeled Peptides Resulting from	
Proteolytic Digestions	107
Primary CNBr Digestion followed by Secondary	
Trypsin Digestion	107
Primary Trypsin Digestion followed by Secondary	
CNBr Cleavage: Gel and TLC Analysis	112
HPLC of [ <sup>125</sup> I]-DEEP Labeled hDAT	112
Solid-state Photolabeling of TM2 Amino Acids	113
Effect of Photoaffinity Labeling Conditions on [ <sup>125</sup> I]-DEEP	114
Analysis of Photolabeling of hDAT with [ <sup>125</sup> I]-JJC 3-24	117
Future Studies	118
<b>Chapter Three</b>	
<b>Photoreactions of Phenyl Azide with Amino Acid Analogs</b>	120
<b>Introduction</b>	121
<b>Methods</b>	124
<b>Photoreactions of Phenyl Azide/<i>Para</i>-azidoacetophenone</b>	
<b>with Amino Acid Analogs</b>	125
General Notes	125
Synthesis of Phenyl Azide	125
Purification of Phenyl Azide	126
<b>Analysis of the Irradiation of Phenyl Azide</b>	
<b>with Amino Acid Analogs</b>	127
Sample Preparation	127
High Pressure Liquid Chromatography Analysis	127
Irradiation of Phenyl Azide and Amino Acid Analogs	
for HPLC and Mass Spectral Analysis	129
Irradiation of <i>para</i> -azidoacetophenone (PAAP) and	
Amino Acid Analogs for HPLC and Mass Spectral Analysis	129
Irradiation of Phenyl Azide and Amino Acid Analogs	
for <sup>1</sup> H Nuclear Magnetic Resonance (NMR)	130
Collection of the Product of the Reaction between	
Phenyl Azide and the Amino Acid Analogs	130
High Resolution Mass Spectrometry Analysis	130
<b>Stability of Products</b>	130
Stability of the Products of Phenyl Azide and	

the Amino Acid Analogs at pH 8.9 in Ammonium Bicarbonate	130
Stability of the Products of Phenyl Azide and the Amino Acid Analogs at 25°C in Trifluoroacetic Acid (TFA), pH 1	131
<b>Data Analysis</b>	131
<b>Results</b>	136
<b>Introduction to the Results</b>	137
<b>Photoreactions with Phenyl Azide and Butylamine as a Model for Lysine</b>	139
Phenyl Azide Photoreactivity with Butylamine as a Model for Lysine	139
Phenyl Azide Photoreactivity with Butylamine as a Model for Lysine under NEAT conditions	148
The Identification of <i>N</i> -butyl-2H-azepin-7-amine by Electrospray Ionization (ESI) Mass Spectrometry (MS) and Proton Nuclear Magnetic Resonance ( <sup>1</sup> H NMR)	154
Product Stability of Butylazepine under Proteolytic Conditions	159
<b>Photoreactions with Phenyl Azide and 1-Octanethiol as a Model for Cysteine</b>	162
Phenyl Azide Photoreactivity with 1-Octanethiol as a Model for Cysteine	162
Phenyl Azide Photoreactivity with 1-Octanethiol as a Model for Cysteine in NEAT Conditions	171
The Identification of 7-(octylthio)-2H-azepine by Atmospheric Pressure Chemical Ionization (APCI) Mass Spectrometry (MS)	177
Product Stability of Octylthioazepine under Proteolytic Conditions	181
<b>Single Exponential First-Order Rate Constants for Phenyl Azide Irradiated with Other Amino Acid Analogs</b>	184
<b>Dimerization of Phenyl Azide</b>	195
<b>Double Exponential Rate Constants Applied to the Photoreactions of Phenyl Azide with Amino Acid Analogs</b>	203
<b>Identification of Products by Mass Spectrometry for Aryl Azides Irradiated with Amino Acid Analogs</b>	213
<b>Products from the Irradiation of Phenyl Azide with Amino Acid Analogs</b>	218
<b>Stability of Products in Proteolytic Conditions</b>	223
<b>Discussion</b>	226
<b>Introduction to the Discussion</b>	227
<b>Reactivity of Phenyl Azide with Amino Acid Analogs</b>	
Interpretation of Results for Photoreactions of Phenyl Azide with Amino Acid Analogs, Butylamine and 1-Octanethiol	229
Butylamine as a Model for Lysine	229
1-Octanethiol as a Model for Cysteine	230
Interpretation of Results for Photoreactions of Phenyl Azide with Amino Acid Analogs in Nonpolar, Aqueous, and NEAT Conditions	233
Nonpolar Conditions	233
Aqueous Conditions	234
NEAT Conditions	234

Phenyl Azide Irradiated in Nonpolar and Aqueous Conditions	238
Interpretation of Phenyl Azide Reactivity with Amino Acid Analog	240
<b>Discussion of the Product Formation of Azepines from the Irradiation of Aryl Azides and Amino Acid Analogs</b>	245
Identification of Butylazepine	247
Analysis of Azepine Products from Phenyl Azide and Amino Acid Analog using Mass Spectrometry	247
<b>Absorbance of Products from Photoreactions of Phenyl Azide and Amino Acid Analogs</b>	248
<b>Azepine Product Stability in Proteolytic Conditions</b>	252
Stability of Product in Basic Conditions	252
Stability of Product in Acidic Conditions	253
Correlation of Rate Constants vs. Product Stability in Proteolytic Conditions	258
So What Gets Labeled?	260
<b>References</b>	262
<b>Appendices</b>	299

## List of Figures

### Chapter One

<b>Cocaine Addiction and the Human Dopamine Transporter</b>	1
Figure 1-1. Forms of Cocaine	3
Figure 1-2. Dopaminergic Neurotransmission	8
Figure 1-3. DAT and VMAT Topology	9
Figure 1-4. DAT Inhibitors	12
Figure 1-5. 2-D Topology of the Human Dopamine Transporter (hDAT)	16
Figure 1-6. Proposed Mechanism for the Glutamate Transporter	20
Figure 1-7. The LeuT <sub>Aa</sub> Topology	23
Figure 1-8. Structure of the LeuT-desipramine Complex	24
Figure 1-9. Steps for Photoaffinity Labeling	27
Figure 1-10. Typical Compounds used as Photoaffinity Labels	28
Figure 1-11. Photolysis of Photophores	29
Figure 1-12. GBR Analogs	34
Figure 1-13. Regions of Incorporation of PALs on hDAT	35
Figure 1-14. Pathways for Photolysis of Phenyl Azide	38
Figure 1-15. Structures of Cocaine and DAT Photolabels	41
Figure 1-16. Analogs of DAT Photolabels	42
Figure 1-17. Intermediates of Singlet and Triplet Nitrenes	49

### Chapter Two

<b>Photoaffinity Labeling of the Human Dopamine Transporter with [<sup>125</sup>I]-DEEP</b>	51
Figure 2-1. Structures of Cocaine and hDAT Inhibitors	53
Figure 2-2. [ <sup>125</sup> I]-DEEP as an Example of a DAT Photolabel	54
Figure 2-3. Western Blot of Purified DAT	75
Figure 2-4. [ <sup>125</sup> I]-RTI-82 Labels Near the Cocaine Binding Site	76
Figure 2-5. Time-Dependent Irradiations with [ <sup>125</sup> I]-RTI-82	77
Figure 2-6. [ <sup>125</sup> I]-DEEP Labels Near the Cocaine Binding Site	80
Figure 2-7. Primary Proteolytic Digestions of [ <sup>125</sup> I]-DEEP Labeled hDAT	81
Figure 2-8. HPLC of Primary Tryptic Digestion of [ <sup>125</sup> I]-DEEP hDAT	82
Figure 2-9. TLC of Secondary Digestions of [ <sup>125</sup> I]-DEEP hDAT	83
Figure 2-10. HPLC Analysis of Secondary CNBr Digestion of Tryptic Peptide, T1	84
Figure 2-11. HPLC Analysis of Secondary CNBr Digestion of Tryptic Peptide, T2	85
Figure 2-12. Primary Digestion of [ <sup>125</sup> I]-DEEP Labeled hDAT with Trypsin TPCK	87
Figure 2-13. HPLC Radioactive Trace of [ <sup>125</sup> I]-DEEP with Methionine	89
Figure 2-14. HPLC Radioactive Trace of [ <sup>125</sup> I]-DEEP with Leucine	90
Figure 2-15. HPLC Radioactive Trace of [ <sup>125</sup> I]-DEEP with Tyrosine	91
Figure 2-16. Effect of Irradiation on [ <sup>125</sup> I]-DEEP	92

Figure 2-17. Effect of Tryptic Conditions on [ <sup>125</sup> I]-DEEP Labeled hDAT	93
Figure 2-18. Effect of CNBr/TFA Solution on the Photoaffinity Label, [ <sup>125</sup> I]-DEEP	94
Figure 2-19. TFA causes Decomposition of [ <sup>125</sup> I]-DEEP Photolabel	95
Figure 2-20. High Concentration of [ <sup>125</sup> I]-JJC 3-24 Labels hDAT	97
Figure 2-21. SDS-PAGE of Primary Tryptic Digestion of hDAT Labeled with [ <sup>125</sup> I]-DEEP and [ <sup>125</sup> I]-JJC 3-24	98
Figure 2-22. Primary CNBr Cleavage of [ <sup>125</sup> I]-JJC 3-24 Labeled hDAT	99
Figure 2-23. [ <sup>125</sup> I]-JJC 3-24 Labels hDAT Peptide, PLFYM	100
Figure 2-24. Effect of Irradiation on [ <sup>125</sup> I]-JJC 3-24	101
Figure 2-25. Effect of CNBr Conditions on [ <sup>125</sup> I]-JJC 3-24	102
Figure 2-26. CNBr Cleavage Sites of hDAT	109
Figure 2-27. Primary CNBr and Secondary Tryptic Digestion Cleavage Sites	110
Figure 2-28. Primary Tryptic and Secondary CNBr Digestion Cleavage Sites	111
Figure 2-29. Effect of [ <sup>125</sup> I]-DEEP on the Retention Time of Amino Acids	116

### Chapter Three

<b>Photoreactions of Phenyl Azide with Amino Acid Analogs</b>	120
Figure 3-1. Phenyl Azide and Butylamine in Cyclohexane Before Irradiation	140
Figure 3-2. Phenyl Azide and Butylamine in Cyclohexane After Irradiation	141
Figure 3-3. Phenyl Azide and Butylamine in Cyclohexane Before and After Irradiation	142
Figure 3-4. Phenyl Azide and Butylamine in Cyclohexane Irradiated over Time	143
Figure 3-5. Single Exponential First-Order Decay Curve Fit for Phenyl Azide and Butylamine in Cyclohexane	144
Figure 3-6. Double Exponential First-Order Decay Curve Fit for Phenyl Azide and Butylamine in Cyclohexane	145
Figure 3-7. Phenyl Azide and Butylamine in Cyclohexane Product Formation	146
Figure 3-8. Phenyl Azide and Butylamine (NEAT) Before and After Irradiation	149
Figure 3-9. Phenyl Azide and Butylamine (NEAT) Irradiated over Time	150
Figure 3-10. Single First Order Exponential Decay Curve Fit for Phenyl Azide and Butylamine (NEAT)	151
Figure 3-11. Phenyl Azide and Butylamine (NEAT) Product Formation	152
Figure 3-12. Mass Spectrometry of the Butylazepine Product	156
Figure 3-13. Experimental Proton NMR of <i>N</i> -butyl-3H-azepin-2-amine.	157
Figure 3-14. Theoretical Proton NMR of <i>N</i> -butyl-3H-azepin-2-amine	158
Figure 3-15. Stability of Butylazepine Product in Basic Conditions	160
Figure 3-16. Stability of Butylazepine in Acidic Conditions	161
Figure 3-17. Phenyl Azide and 1-Octanethiol in Cyclohexane Before Irradiation	163
Figure 3-18. Phenyl Azide and 1-Octanethiol in Cyclohexane After Irradiation	164
Figure 3-19. Phenyl Azide and 1-Octanethiol in Cyclohexane Before and After Irradiation	165
Figure 3-20. Phenyl Azide and 1-Octanethiol in Cyclohexane Irradiated over Twenty Minutes	166
Figure 3-21. Single Exponential First-Order Decay Curve Fit for Phenyl Azide and 1-Octanethiol in Cyclohexane	167

Figure 3-22. Double Exponential Decay Curve Fit for Phenyl Azide and 1-Octanethiol in Cyclohexane	169
Figure 3-23. Product Formation for Phenyl Azide and 1-Octanethiol in Cyclohexane	170
Figure 3-24. Phenyl Azide and 1-Octanethiol (NEAT) Before and After Irradiation	172
Figure 3-25. Phenyl Azide and 1-Octanethiol (NEAT) Irradiated over Sixty Minutes	173
Figure 3-26. Phenyl Azide and 1-Octanethiol (NEAT) First-Order Exponential Decay Curve Fit	174
Figure 3-27. Rate of Product Formation for Phenyl Azide and 1-Octanethiol (NEAT)	176
Figure 3-28. Mass Spectrometry of the Octylthioazepine Product	178
Figure 3-29. Stability of Octylthioazepine in Basic Conditions	182
Figure 3-30. Stability of Octylthioazepine in Acidic Conditions	183
Figure 3-31. Single Exponential First-Order Curve Fit for Phenyl Azide and Imidazole	185
Figure 3-32. Single Exponential First-Order Curve Fit for Phenyl Azide and Guanidine Acetic Acid	186
Figure 3-33. Single Exponential First-Order Curve Fit for Phenyl Azide and Phenol	187
Figure 3-34. Single Exponential First-Order Curve Fit for Phenyl Azide and <i>N</i> -ethylacetamide	188
Figure 3-35. Single Exponential First-Order Curve Fit for Phenyl Azide and <i>N</i> -ethylacetamide (NEAT)	189
Figure 3-36. Single Exponential First-Order Curve Fit for Phenyl Azide and Ethylbenzene	190
Figure 3-37. Single Exponential First-Order Curve Fit for Phenyl Azide and Butyric Acid	191
Figure 3-38. Single Exponential First-Order Curve Fit for Phenyl Azide and Dimethyl Sulfide First-Order Curve Fit	192
Figure 3-39. Loss of Phenyl Azide in Aqueous Conditions for 4 Minutes of Irradiation	197
Figure 3-40. Dimerization of Phenyl Azide in Aqueous Conditions	198
Figure 3-41. Loss of Phenyl Azide in Cyclohexane for 4 Minutes of Irradiation	199
Figure 3-42. Dimerization of Phenyl Azide in Cyclohexane	200
Figure 3-43. Double Exponential First-Order Curve Fit for Phenyl Azide and Guanidine Acetic Acid	204
Figure 3-44. Double Exponential First-Order Curve Fit for Phenyl Azide and Imidazole	205
Figure 3-45. Double Exponential First-Order Curve Fit for Phenyl Azide and Phenol	206
Figure 3-46. Double Exponential First-Order Curve Fit for Phenyl Azide and Dimethyl Sulfide	208
Figure 3-47. Double Exponential First-Order Curve Fit for Phenyl Azide and Butyric Acid	209

Figure 3-48. Double Exponential First-Order Curve Fit for Phenyl Azide and <i>N</i> -ethylacetamide	210
Figure 3-49. Double Exponential First-Order Curve Fit for Phenyl Azide and Ethylbenzene	211
Figure 3-50. Product Peak Heights for Cysteine, Lysine, and Peptide Backbone Analogs	219
Figure 3-51. Product Peak Heights in Nonpolar Environment	220
Figure 3-52. Product Peak Heights in Aqueous Conditions	221
Figure 3-53. Product Peak Heights in NEAT Conditions	222
Figure 3-54. Stability of Products in Basic Proteolytic Conditions	224
Figure 3-55. Stability of Products in Acidic Proteolytic Conditions	225
Figure 3-56. UV Absorbance of Products in Different Solvent Conditions	250
Figure 3-57. Acid Hydrolysis of Azepine	259
Figure 3-58. Azepine becomes the Protonated Salt upon Addition of Acid	259



## List of Tables

### Chapter One

<b>Cocaine Addiction and the Human Dopamine Transporter</b>	1
Table 1-1. Amino Acid Analogs	44

### Chapter Two

<b>Photoaffinity Labeling of the Human Dopamine Transporter with [<sup>125</sup>I]-DEEP</b>	51
Table 2-1. HPLC Gradient Description of Sara3 Method	66
Table 2-2. GPMW Codes for Theoretical Proteolytic Digestions	68
Table 2-3. Summary of Peptides from Primary and Secondary Digestions of [ <sup>125</sup> I]-DEEP Labeled hDAT	86

### Chapter Three

<b>Photoreactions of Phenyl Azide with Amino Acid Analogs</b>	120
Table 3-1. HPLC Gradient Description for Method SHORT1	128
Table 3-2. HPLC Gradient Description for Method 16	128
Table 3-3. Single Exponential First-Order Rate Constants	193
Table 3-4. Single Exponential First-Order Rate Constants Divided by Solvent Conditions	194
Table 3-5. Initial Reaction Rates of Phenyl Azide Reacting with Amino Acid Analogs	201
Table 3-6. Single and Double Exponential Rate Constants for Amino Acid Analogs in Aqueous Conditions	207
Table 3-7. Single and Double Exponential Rate Constants for Amino Acid Analogs in Cyclohexane	212
Table 3-8. Mass Spectrometry Analysis of Amino Acid Analogs with Phenyl Azide	214
Table 3-9. Mass Spectrometry Analysis of Amino Acid Analogs with <i>Para</i> -azidoacetophenone (PAAP)	216
Table 3-10. Rate Constants of Amino Acids in Nonpolar Conditions	235
Table 3-11. Rate Constants of Amino Acids in Aqueous Conditions	237
Table 3-12. Partial List of Amino Acids Labeled by Azido Photolabels	242
Table 3-13. Arylnitrene Reactivity with Amino Acid Functional Groups	244
Table 3-14. Product Stability in Basic and Acidic Conditions	255

## List of Schemes

### Chapter One

<b>Cocaine Addiction and the Human Dopamine Transporter</b>	1
Scheme 1-1. Photolysis of Phenyl Azide	48

### Chapter Two

<b>Photoaffinity Labeling of the Human Dopamine Transporter with [<sup>125</sup>I]-DEEP</b>	51
Scheme 2-1. Localization of Photoaffinity Labels	60

### Chapter Three

<b>Photoreactions of Phenyl Azide with Amino Acid Analogs</b>	120
Scheme 3-1. Irradiation of Phenyl Azide forms 3 <i>H</i> -Azepine and Azobenzene	123
Scheme 3-2. Reaction Schemes for Butylamine and Phenyl Azide	154
Scheme 3-3. Reaction Scheme for 1-Octanethiol and Phenyl Azide	177
Scheme 3-4. Photolysis of Phenyl Azide in Aqueous and Organic Solvents	246
Scheme 3-5. Photoisomerization of 3 <i>H</i> -Azepines	257
Scheme 3-6. Irradiation of <i>N</i> -butyl-3 <i>H</i> -azepin-2-amine	257

## List of Appendices

<b>A. The Amino Acid Sequence of the Flag 6XHis Tagged Human Dopamine Transporter</b>	299
<b>B. Correlations of Physical Properties vs. Rate Constants</b>	302
Table of Physical Constants for the Amino Acid Analog	
Functional Groups	302
Correlation Between Phenyl Azide Reactivity and Electronegativity	303
Correlation Between the Phenyl Azide Reactivity and Dielectric Constant	304
Correlation Between the Phenyl Azide Reactivity and Polarizability	305
<b>C. ANOVA Data Tables for the Rate Constants</b>	306
One-Way ANOVA of Rate Constants in Cyclohexane	306
One-Way ANOVA of Rate Constants in Aqueous Conditions	308
One-Way ANOVA of Rate Constants in NEAT Conditions	309
<b>D. Correlations of Rate Constants vs. Product Stability in Proteolytic Conditions</b>	310
Correlation Between the Phenyl Azide Reactivity and Product Stability in Acidic Conditions	310
Correlation Between the Phenyl Azide Reactivity and Product Stability in Basic Conditions	311

# **Chapter One**

## **Cocaine Addiction and the Human Dopamine Transporter**

“All men dream: but not equally. Those who dream by night in the dusty recesses of their minds wake in the day to find that it was vanity: but the dreamers of the day are dangerous men, for they may act their dreams with open eyes, to make it possible.”

**-T.E. Lawrence**

## Cocaine Addiction

Cocaine is the most powerful stimulant of natural origin (Fisher, 1987.). It is extracted from the leaves of the coca plant, *Erythoxylon* (Kreek *et al.*, 2005). In the mid-19<sup>th</sup> century it was used by South Americans to relieve fatigue (Schultes, 1987). Pure cocaine (cocaine hydrochloride) was used as a local anesthetic for surgeries in the 1880s and the main stimulant drug used in tonics and elixirs for various illnesses in the early 1900s (Koller-Becker, 1962). Crack, however, which became a popular and less expensive form of cocaine in the mid-1980s, derives its name from the crackling sound made when heating cocaine with ammonium bicarbonate or ammonia during production (NIDA, 2004). Crack or “rock” gives its users an immediate high and is smoked (Figure 1-1) (NIDA, 2004). Cocaine most often appears as a white, crystalline powder or an off-white chunky material. It is also commonly diluted with other substances like lactose, mannitol, inositol, and lidocaine to increase the volume of the drug and to increase drug dealer street profits (ONDCP, 1998). Powder cocaine is normally snorted or dissolved in water and injected intravenously (ONDCP, 2003) (Figure 1-1).

In 2001, there were an estimated 27.8 million who had used cocaine at least once in their lifetime (Gorelick *et al.*, 2004; ONDCP, 2003). According to the Office of National Drug Control Policy (ONDCP), there are three million chronic cocaine users in the United States of America (ONDCP, 2003; SAMHSA, 2002). With an increase in cocaine users, has also come a need for better rehabilitation resources. There is a high level for recidivism for cocaine abusers (Butzin, 1999). This is because there are not any medications available that successfully treat cocaine addiction (Herman *et al.*, 2005).

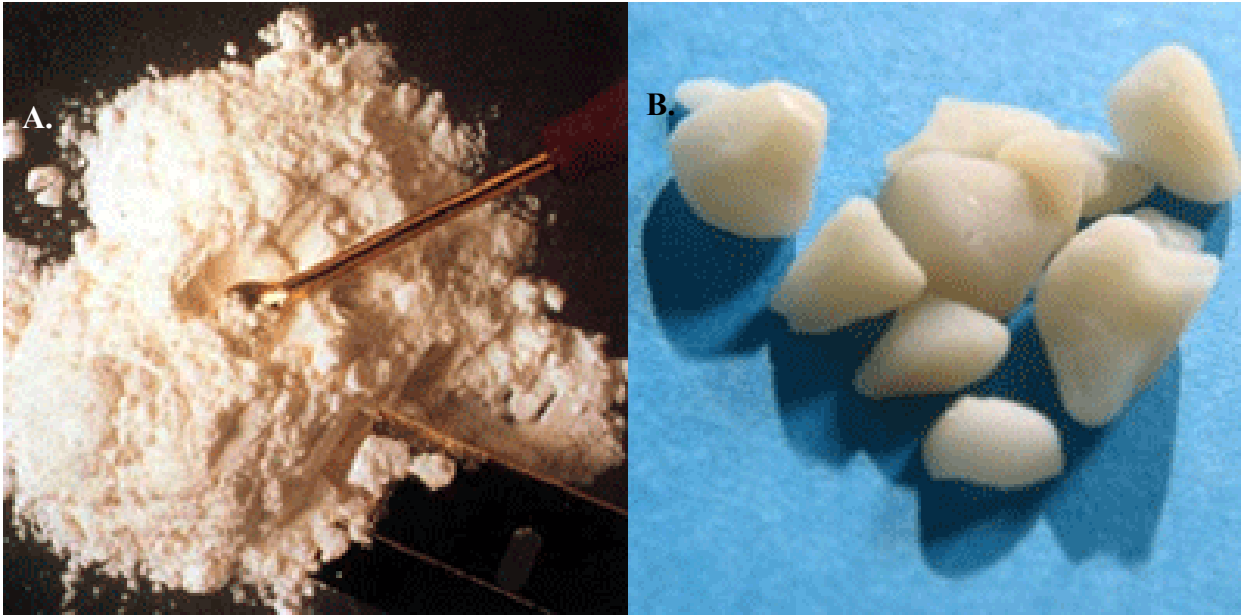


**Figure 1-1. Forms of Cocaine.** A. Cocaine in powder form. B. Crack cocaine.

Cocaine addiction is an expensive habit that has led users to abuse a cheaper form of the drug, “crack”, which is made by mixing the powder form of cocaine with ammonium bicarbonate. Crack is typically smoked from a pipe (adapted from NIDA, 1998).

At least 65 medications have been evaluated as potential treatments for cocaine dependence (Herman, 2005). One experimental medication is selegiline, (L-Deprenyl), which is a specific monoamine oxidase (MAO)-B inhibitor used for the treatment of Parkinson's Disease (Sofuoglu & Kosten, 2005). Selegiline enhances dopamine release and blocks dopamine reuptake, similar to amphetamine (Ebadi *et al.*, 2002). Though it has been used in two prior studies with humans (Bartzokis *et al.*, 1999; Haberny *et al.*, 1995), further controlled studies are needed to determine the utility of selegiline as a treatment for cocaine addiction (Sofuoglu & Kosten, 2005).

Another medication is Disulfiram, an aldehyde dehydrogenase inhibitor that is used to treat alcoholism (Hughes & Cook, 1997). Disulfiram also inhibits dopamine  $\beta$ -hydroxylase or DBH, which converts dopamine to norepinephrine (Nagendra *et al.*, 1997). Disulfiram acts similar to a dopamine agonist (Nagendra *et al.*, 1997). Disulfiram decreased cravings for cocaine in clinical trials involving cocaine abusers (McCance-Katz *et al.*, 1998). A greater reduction of cocaine use has been seen when compared to psychotherapy alone (Carroll *et al.*, 1998). Results suggest that Disulfiram may be an effective medication for reducing cocaine use (Sofuoglu & Kosten, 2005).

Antidepressants, fluoxetine, desipramine, and venlafaxine, are also used to help the patients deal with the mood swings and depression that is most commonly a direct effect of cocaine withdrawal (Herman, 2005). Cognitive-behavioral coping skills are a short-term solution for helping address cocaine addicts. Finally, a cocaine vaccine is a promising treatment but the efficacy of it for relapse prevention is under investigation (Sofuoglu & Kosten, 2005).

With there being such a lack of specific pharmacotherapies available to cocaine abusers, the problem continues to spiral out of control. According to the National Institute on Drug Abuse (NIDA), 2004, the long term medical effects of cocaine are cardiovascular, respiratory, strokes, seizures and gastrointestinal effects including abdominal pain and nausea. As reported to NIDA, 2004, by the Centers for Disease Control and Prevention or the CDC, cocaine abusers that inject the drug intravenously are subjected to infectious diseases such as human immunodeficiency virus (HIV) and hepatitis. Cocaine addicted mothers give birth to premature babies that have very low birth weights and smaller head circumferences (Harvey, 1998). It was previously thought that these babies suffered irreversible neurological damage but now it appears that they recover from the drug exposure (Harvey, 1998). Many still have long term effects that lead to attention deficient problems in childhood (ONDCP 2003). These are just a few of the reasons that it is imperative to find better treatments for abusers of cocaine.

### **Available Treatments for Addiction**

Drug addiction has been defined as the overpowering motivational strength and decreased ability to control the desire to obtain drugs (Kalivas & Volkow, 2007). Methadone is by far the most widely employed and best understood opiate addiction pharmacotherapy. It has been more than 30 years from its inception and there are over 220, 000 patients currently in care, and hundreds of studies documenting its efficacy in treating heroin addiction (Lowinson *et al.*, 1992; Ball & Ross, 1991; Dole & Nyswander, 1983).



Substitution therapies like methadone (Farrell *et al.*, 1994; Garrido & Troconiz, 1999) for heroin addicts and nicotine patches, gums, and tablets for nicotine addicts (Stead *et al.*, 2008), have shown to be effective in assisting the users in breaking the cycle of abuse. It would be ideal for cocaine abusers to have the same alternative. This would take an enormous effort in the research involving cocaine.

### **Cocaine as an Inhibitor of the Dopamine Transporter**

Research consistently suggests that increased synaptic dopamine plays a major role in the abuse of cocaine (Woolverton & Johnson, 1992). Cocaine is a powerfully known inhibitor of synaptosomal uptake of catecholamines and 5-HT (Woolverton & Johnson, 1992). This inhibition includes the dopamine transporter or DAT (Church *et al.*, 1987; Di Chiara & Imperato, 1988; Hurd & Ungerstedt, 1989; Maisonneuve *et al.*, 1990; Nielsen *et al.*, 1983; Pani *et al.*, 1990).

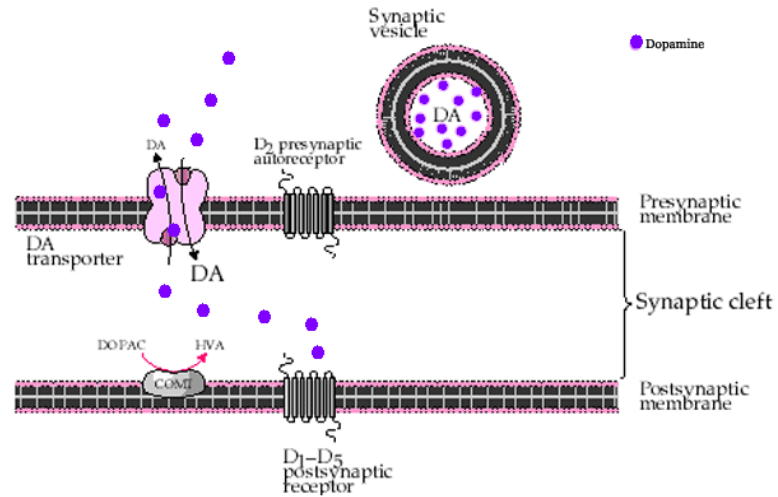
DAT is of particular importance because research has established that cocaine blocks dopamine uptake. Inhibition of dopamine uptake has been linked to the behavioral effects of cocaine. The binding sites for dopamine and cocaine may not be identical. The possibility has been shown by Anderson, 1997 that cocaine binds to DAT, induces a conformation change in the dopamine recognition site resulting in decreased affinity. Others argue that the cocaine and dopamine sites arise from potency differences that relate to how substrate molecules are transported across the membrane (Reith *et al.*, 1989). Regardless, understanding the interaction between cocaine and DAT on a molecular level is the key to developing any type of suitable pharmacotherapy for cocaine addiction.

The role of DAT is to clear dopamine from the synaptic cleft and recycle this dopamine back into the pre-synaptic nerve (Figure 1-2a) (Giros & Caron, 1993; Giros *et al.*, 1996; Uhl *et al.*, 2002; Uhl & Lin, 2003). Once inhibited by cocaine, DAT is unable to clear the dopamine from the synaptic cleft, which leads to an overstimulation of the dopamine receptors on the post-synaptic cell (Figure 1-2b) (Uchimura & North, 1990). This process causes the euphoric effects that cocaine users feel (Griffiths, 1980; Johanson, 1989). An appropriate substitute therapy for cocaine abuse would block the action of cocaine on the dopamine transporter while allowing for the re-uptake of dopamine into the pre-synaptic cell.

According to Nirenberg and Pickel, 1997, dopaminergic neurotransmission is regulated by two distinct membrane-bound transporters: the vesicular monoamine transporter-2 (VMAT2) and the plasmalemmal dopamine transporter (DAT). These transporters play important roles in the initiation and termination of dopaminergic neurotransmission, respectively. They also report that dopaminergic neurotransmission involves the regulated storage, release, and reuptake of dopamine. The vesicular monoamine transporter permits dopamine uptake into synaptic vesicles or other intracellular organelles and the plasmalemmal dopamine transporter reduces extracellular dopamine concentrations through active reuptake of dopamine from the extracellular space (Figure 1-3) (Nirenberg & Pickel, 1997).

The focus of this dissertation research is primarily on the cocaine sensitive dopamine transporter that mediates the uptake of dopamine across the plasma membrane. The overall goal of the research is to localize the cocaine binding site on hDAT using photoaffinity labels. The limiting factor in trying to understand these interactions is that

A.



B.

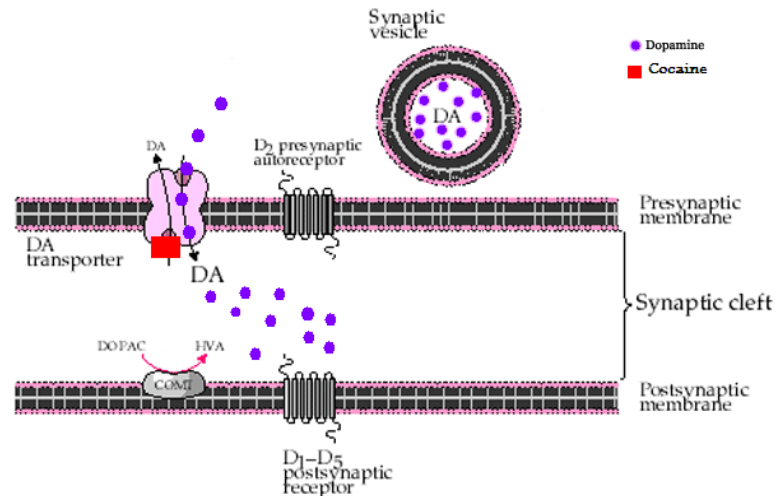


**Figure 1-2. Dopaminergic Neurotransmission.** A. Normal dopaminergic transmission in the synapse. B. Dopamine's inability to be taken up through the dopamine transporter is because cocaine is blocking the pathway. Figures 1-2a and 1-2b are adapted from Figure 8-1 in *Fundamentals of Neuropsychopharmacology* (Feldman, 1984).

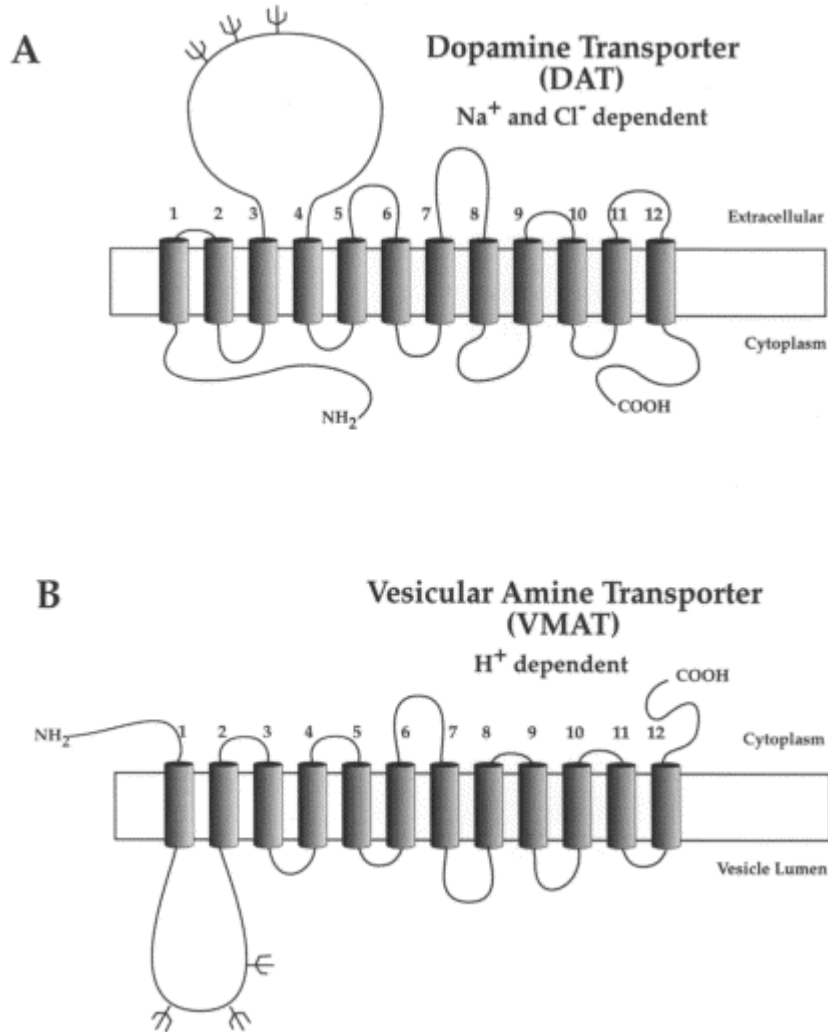


**Figure 1-3. DAT and VMAT Topology.** Proposed topology and structural features of **(A)** the dopamine transporter (DAT) and **(B)** a vesicular monoamine transporter (VMAT). As predicted by hydrophobicity analyses of the predicted protein sequences, the both carrier families have 12 TMs with N- and C-termini within the cytoplasm. Large glycosylated extracellular loops are present between TM 3 and 4 and TM 1 and 2 in DAT and VMATs, respectively (adapted from Amara & Sonders, 1998).

the human dopamine transporter's three-dimensional structure is unknown. Therefore, we do not have a distinct picture of the binding site of cocaine. This information is essential to the further development of cocaine addiction with substitution therapies.

Without a distinct map of its binding site, the mechanism of DAT's transport of substrates (dopamine, amphetamine, PAPEA-2-(para-azidophenyl)ethylamine-photoaffinity label) or inhibition of dopamine uptake by ligands such as cocaine and cocaine analogs (GBR series, phenyltropanes) is limited. The interest in DAT is primarily because DAT is a target for psychostimulant drugs like cocaine and amphetamine (Shimada *et al.*, 1991). It has been hypothesized that the transporter's role is key for the mechanism in the locomotor and rewarding effects as well as the reinforcing properties of psychostimulant drugs (Ritz *et al.*, 1987).

### **Other Inhibitors to the Dopamine Transporter**

Besides cocaine, there are other inhibitors to the dopamine transporter. GBR compounds, benztropine analogs, 3-aryltropane compounds, Mazindol and Methylphenidate are DAT inhibitors and the structures are shown in Figure 1-4 (Carroll *et al.*, 1999). These compounds inhibit dopamine uptake while enhancing dopaminergic activity (Andersen, 1989; Clarke *et al.*, 1973; Coyle & Snyder, 1969; Hyttel, 1982; Janowsky *et al.*, 1985).

GBR compounds are not structural analogs of cocaine but selectively inhibit DA uptake. GBR 12909, a GBR compound, reduces cocaine's effect on the brain (Andersen, 1989). GBR 12909 does not perform as well as cocaine in elevating DA-mediated behavior (Reid *et al.*, 1989) but it does have a high binding affinity for DAT as well as a

slower dissociation from DAT when compared to cocaine (Newman & Kulkarni, 2002). These characteristics make it a good analog to use for research purposes.

3-Aryltropanes are structurally similar to cocaine. They have higher binding affinities to DAT than cocaine (Carroll *et al.*, 1991). WIN 35, 428 is also known as 3 $\beta$ -(4-fluorophenyl) tropan-2 $\beta$ -carboxylic acid methyl ester or  $\beta$ -CFT. WIN 35, 428 is a widely used aryl-tropane because of its high affinity to DAT (Madras *et al.*, 1989).

Benztropine is a drug used in the treatment of Parkinson's disease. It can inhibit DA uptake beyond that of norepinephrine and serotonin (Agoston *et al.*, 1997; Coyle & Snyder, 1969; Newman & Kulkarni, 2002). Benztropines do not cause cocaine-like effects on animal models (Kline *et al.*, 1997). Benztropines are structural hybrids of cocaine and GBR compounds. They bear the tropane ring like cocaine and a diphenyl ether moiety like GBR. This structure makes benztropines ideal to use as a template for synthesizing new DA uptake inhibitors (Newman *et al.*, 1994).

Mazindol is a tricyclic compound used to treat obesity. It inhibits both norepinephrine and dopamine uptake (Hyttel, 1982). Mazindol is not addictive in humans (Chait *et al.*, 1987) yet inhibits DA uptake. Methylphenidate, a psychostimulant, has a higher affinity for DAT than for any other monoamine transporter (Pan *et al.*, 1994). Ritalin or DL-Threo-Methylphenidate is used in the treatment of Attention Deficit Hyperactivity Disorder (ADHD) (Hubbard *et al.*, 1989). Its binding to DAT is twice that of cocaine yet in humans its reinforcing ability is lower (Volkow *et al.*, 1999).

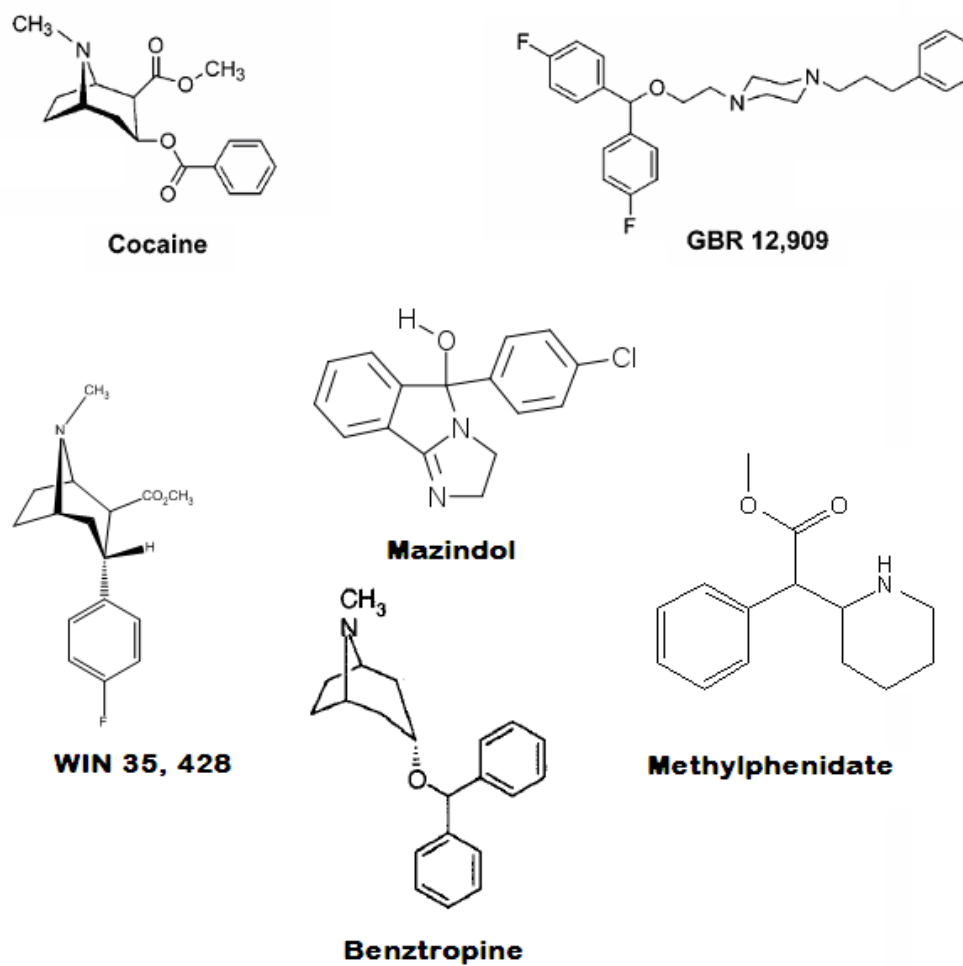


**Figure 1-4. DAT Inhibitors.** Inhibitors of the Dopamine Transporter (DAT) include cocaine, WIN 35, 428, GBR 12909, Mazindol, and Methylphenidate.

## Structure and Function of the Dopamine Transporter

The dopamine transporter (DAT) is a member of the Na<sup>+</sup>- and Cl<sup>-</sup>-dependent neurotransmitter transporter family predicted by hydrophobicity analysis to have 12 transmembrane-spanning helices with intracellular N-terminal and C-terminal ends (Kilty *et al.*, 1991; Shimada *et al.*, 1991). DAT is an 80 kDa integral membrane protein consisting of 620 amino acid residues (Vaughan & Kuhar, 1996). There is a large extracellular loop possessing three putative glycosylation sites between transmembrane domains 3 and 4 (Figure 1-5) (Berger *et al.*, 1991; Grigoriadis *et al.*, 1989; Lew, Grigoriadis *et al.*, 1991; Lew, Vaughan *et al.*, 1991; Sallee *et al.*, 1989). Regulation by PKC and MAP kinases has been identified as direct evidence for phosphorylation (Carvelli *et al.*, 2002; Huff *et al.*, 1997; Kitayama *et al.*, 1994; Uhl & Lin, 2003; Vaughan *et al.*, 1997). In mature functional DAT, there is evidence for the importance of disulfide bonds which link cysteines 180 and 189 in extracellular loop 2 (Chen *et al.*, 2007). When these cysteines are mutated out, DAT is not functional (Chen *et al.*, 2007). DAT may also function as an oligomer (Hastrup *et al.*, 2001) and dimerization may be necessary for the proper trafficking of DAT to the membrane (Torres, 2003). DAT oligomerization may be regulated by substrates dopamine and amphetamine (Chen & Reith, 2008).

It has been shown that Zn<sup>2+</sup> can inhibit DA uptake in hDAT and enhances the binding of cocaine analogs (Loland *et al.*, 2003). Tests have been performed that suggested that DA transport was reversed in the presence of Zn<sup>2+</sup> (Scholze *et al.*, 2002). Prior to that, it had been shown that there is a Zn<sup>2+</sup> binding motif between extracellular loop 2, TM 7 and TM 8 (Norregaard *et al.*, 1998). It can be inferred from the above that



$Zn^{2+}$  mediates changes in hDAT that are significant for the process of transport. In addition, the leucine zipper motif in TM2 contributes to the oligomerization and trafficking of DAT to the plasma membrane (Torres, 2003).

Human DAT (hDAT) has some segments that are similar to the norepinephrine transporter (NET) and the serotonin transporter (SERT). NET has 617 amino acid residues and SERT has 630 amino acids, compared to hDAT's 620 amino acid residues (G. M. Miller *et al.*, 2001). DAT, NET, and SERT are monoamine transporters that co-transport sodium and chloride (Qian *et al.*, 1995). The bacterial leucine transporter, LeuT, is also a sodium chloride dependent transporter which has been crystallized (Yamashita *et al.*, 2005). It has a low level of similarity to DAT (20%), SERT (21%), and NET (24%) (Beuming *et al.*, 2006). However, there are regions of the LeuT that are highly conserved throughout the entire family (Beuming *et al.*, 2006). Thus, the LeuT is the current model that best explains the topology of DAT and other monoamine transporters.

DAT's involvement in the transport of dopamine and the binding of inhibitors has been developed by utilizing site-directed mutagenesis and chimera studies. Aspartate 79 has been identified as being important in the interaction with the amine functionality of substrates. When Aspartate 79 is replaced with alanine, glycine or glutamate, the uptake of [ $^3H$ ]-dopamine and [ $^3H$ ]-MPP+ was dramatically reduced. In addition, the mutant DAT displayed a reduced affinity for [ $^3H$ ]- $\beta$ -CFT, a cocaine analog (Kitayama *et al.*, 1992). Based on the promise of this mutants reduced affinity to  $\beta$ -CFT, several DAT mutants' expression, dopamine uptake and cocaine analog affinities have been assessed. From this study, a phenylalanine-to-alanine mutant in putative DAT transmembrane

domain 3, F154A, retains normal dopamine uptake, lowers cocaine affinity 10-fold and reduces cocaine specificity (Uhl *et al.*, 2002). This work leads one to believe that the possibility of substitution therapy is achievable.

Chimeras of DAT and norephinerphrine transporter (NET) have been constructed (Buck & Amara, 1994, 1995). The technique of creating these chimeras involves constructing a novel transporter by connecting segments from different transporters of the same family. For example, by replacing regions of DAT with NET, regions critical for function can be determined by loss of functionality assessed via binding assays and dopamine uptake experiments. Since DAT and NET have a high homology to one another, functional chimeric transporters have been obtainable. Chimeras can also be constructed from different species of transporters.

Both of these methods have limitations. For instance, with site-directed mutagenesis just because an amino acid that is replaced does not cause total loss of function does not mean that it does not play a role in transporting substrates or binding inhibitors. Furthermore, chimeric studies narrow down the region of interest involved in function so that site-directed mutagenesis can be made more of a direct approach versus a guessing game of choosing amino acids to mutate. Seemingly, the same limitations exist with chimeric studies as with site-directed mutagenesis.

Electron microscopic immunocytochemistry has been used to examine the subcellular distribution of DAT (Hersch *et al.*, 1997). The predicted molecular topology of DAT was confirmed in nigrostriatal dopaminergic neurons (Hersch *et al.*, 1997). This technique combines immunogold labeling with site specific monoclonal antibodies raised

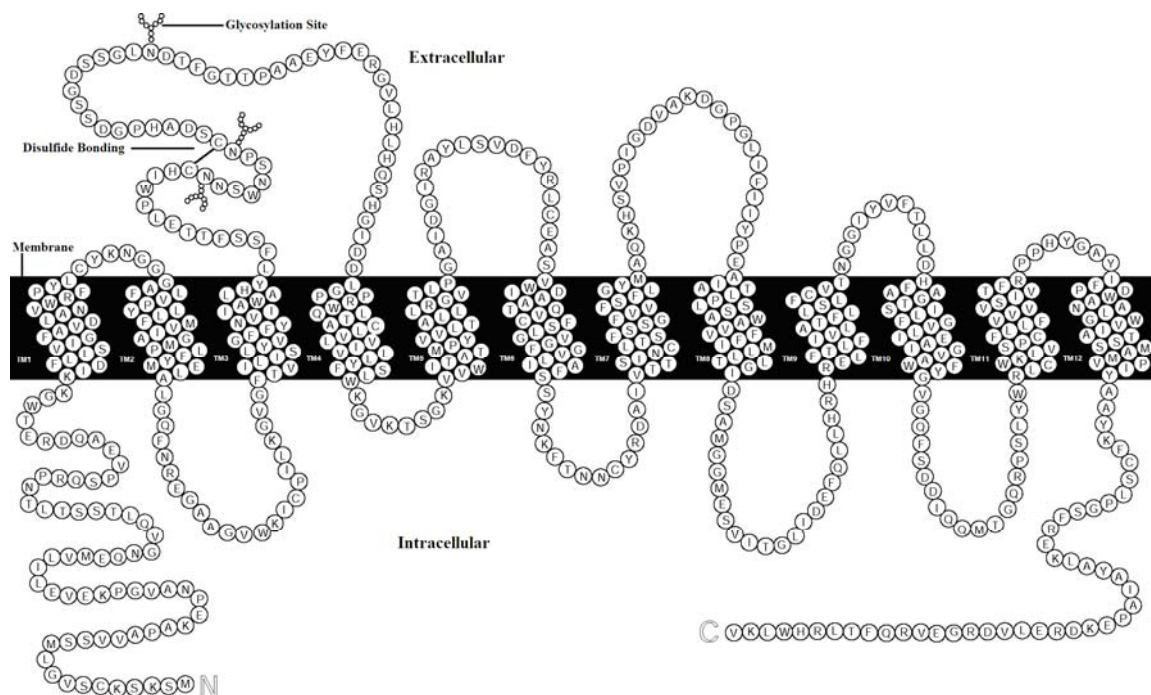


**Figure 1-5. 2-D Topology of the Human Dopamine Transporter (hDAT).**

Illustration of the two-dimensional topology of the human dopamine transporter showing intracellular N and C termini and the amino acid sequence. There are 12 transmembrane domains with alternating intra- and extra-cellular loops. N-linked glycosyl groups are shown at the consensus asparagine glycosylation sites, Asn 181, Asn 188, and Asn 205, in the second extracellular loop. In addition, cysteines 180 and 189 in the second extracellular loop are disulfide bonded (adapted from Giros & Caron, 1993).

against two independent epitopes, the putative cytoplasmic N-terminus and the second extracellular loop (Ciliax *et al.*, 1995). Using a potent and highly selective anti-peptide antiserum allowed electron microscopic visualization of DAT and its relationship to various organelles and membrane compartments within nigral neurons. In each site, immunogold labeling provided suitable detection of the N-terminus being intracellular and the 3<sup>rd</sup> loop being extracellular (Hersch *et al.*, 1997). While this spatial resolution confirmed the positions of DAT in the membrane, it is limited by its sensitivity due to poor penetration and a significant background-to-signal ratio.

## Characterization of Membrane Bound Proteins

The human dopamine transporter is a membrane bound protein. It has been a challenge to determine the three-dimensional structure of most membrane bound proteins because of their amphiphilic nature. Techniques like electron microscopy and molecular modeling are used instead of X-ray crystallography, which is used to determine 3-D structures, to offset the limitations posed because of the proteins' character. However, these other techniques are indirect methods and do not shed but a small amount of light towards better understanding the properties of membrane proteins.

Membrane proteins have been analyzed by a number of instruments including electron microscopy. Electron microscopy has been used in the elucidation of the three-dimensional arrangements of the bacterial homologue of the CLC chloride channel. The images show a homodimeric structure with water filled cavities (aqueous pores) within each monomeric structure (Mindell *et al.*, 2001). The ABC Transporter-YvcC structure has also been resolved with the use of electron microscopy (Chami *et al.*, 2002). The structure was determined to show the existence of three structural domains in the polypeptide TMD (transmembrane domain), stalk and NBD (nucleotide binding domain), the organization of YvcC as a homodimer, the presence of asymmetry for the 2 NBDs forming the homodimer and the putative association of homodimers to form a dimer of homodimers (Chami *et al.*, 2002).

X-ray crystallography serves as a basis for construction of three-dimensional protein models that provide insight into functional mechanisms and molecular structures and enables formulation of new hypotheses regarding transporter structure and function, which may be experimentally validated. As of 2004, there were 90 membrane structures

reported to have crystal structures (Dahl *et al.*, 2004). As of 2005, there were 91 which included a member of the sodium chloride dependent transporter family, of which there is a special interest (Yamashita *et al.*, 2005).

The ABC Transporter, a multi-drug resistant (MDR) transporter, lipid flippase (MsbA) has been crystallized. From the crystal structure, it has been hypothesized that MsbA scans that lower bilayer leaflet substrates, accepts them laterally, and flips them to the outer leaflet (Chang & Roth, 2001). The glutamate transporter has been determined to be a bowl shaped trimer with a solvent-filled extracellular basin extending halfway across the membrane bilayer (Figure 1-6) (Yernool *et al.*, 2004). At the bottom of the basin are three independent binding sites, each cradled by two helical hairpins, reaching from opposite sides of the membrane. Transport of glutamate is achieved by movements of the hairpins that allow alternating access to either side of the membrane (Yernool *et al.*, 2004).

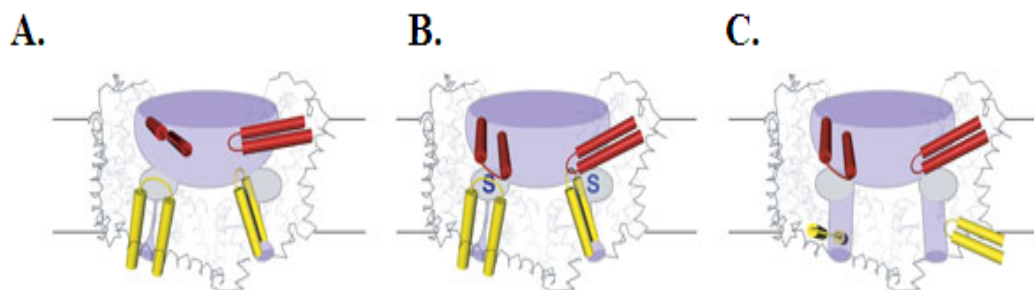


**Figure 1-6. Proposed Mechanism for the Glutamate Transporter.** Glutamate transporters have a large aqueous basin at the bottom. Three substrate-binding sites are located there. In this figure, only two of the three substrate-binding sites and transport pathways are shown. Access to the substrate-binding site, from extracellular or intracellular solution, is mediated by hairpin (HP) 2 (red) or HP1 (yellow), respectively. **A.** HP2 is in an 'open' conformation, providing access to the binding site from the extracellular basin. **B.** Bound state of the transporter where access to the binding site is blocked by HP1 and HP2. The substrate and co-transported ions are represented by the letter S. **C.** Movement of HP1 out of the protomer core, towards the cytoplasm and away from the three-fold axis, opens a transport pathway from the substrate-binding site to the cytoplasm (adapted from Yernool *et al.*, 2004).

X-ray crystallography serves as more than a structural characterization tool but as a tool to help hypothesize regarding the function of proteins. Other membrane proteins that have been successfully characterized by X-ray and their mechanisms postulated are the Lactose Permease Symporter (LacY) (Kaback, 2005) and the potassium channel (Shrivastava & Bahar, 2006). Postulated mechanisms are termed the "alternating access" mechanism for LacY (Kaback *et al.*, 2007) and the S4 shaker mechanism for the K channel (Long *et al.*, 2005; Pathak *et al.*, 2007; Treptow *et al.*, 2004). The ligand-binding site is alternatively accessible to one side of the membrane or the other but not to both sides simultaneously in Lac Y (Abramson *et al.*, 2003). The movement of the shaker mechanism is contradictory and controversial (Long *et al.*, 2005; Pathak *et al.*, 2007; Treptow *et al.*, 2004).

Molecular modeling has opened a door to understanding structural characteristics of large membrane proteins. The ABC Transporter was modeled in 2003 (Seigneuret & Garnier-Suillerot, 2003). They concluded that the interactions between the intracellular domain and the nucleotide-binding domain suggest that an involvement in mediating the coupling between conformational changes of the NBD and reorientation of the TM helices during the transport process. A model of DAT based on the Na<sup>+</sup>/H<sup>+</sup> antiporter (NhaA) projection map has been proposed (Ravna *et al.*, 2003). It was determined that cocaine interacts with Phe 76 in TM 1 of DAT forming a hydrophobic interactions between the benzene ring of this amino acid and the tropane ring of cocaine.

In 2005, the bacterial homologue of the sodium-chloride dependent transporters from *Aquifex aeolicus* (LeuT<sub>Aa</sub>), in complex with its substrate, leucine, and two sodium



ions was crystallized (Yamashita *et al.*, 2005). The protein core consists of the first ten of twelve transmembrane segments, with segments 1-5 related to 6-10 by a pseudo-two-fold axis in the membrane plane. Leucine and the sodium ions are bound within the protein core, halfway across the membrane bilayer, in an occluded site devoid of water. It has been speculated from this structure the mechanism by which the cytoplasmic and extracellular gates open. TMs 1 and 6 cytoplasmic helical segments move relative to TMs 3 and 8 to open and close the gates. Figure 1-7 shows an illustration of the LeuT<sub>AA</sub> topology. The leucine transporter has also been crystallized bound with the inhibitor desipramine (Zhou *et al.*, 2007). This model gives more insight into how inhibitors bind to sodium chloride dependent transporters (Figure 1-8).

# LEUT<sub>AA</sub> STRUCTURE

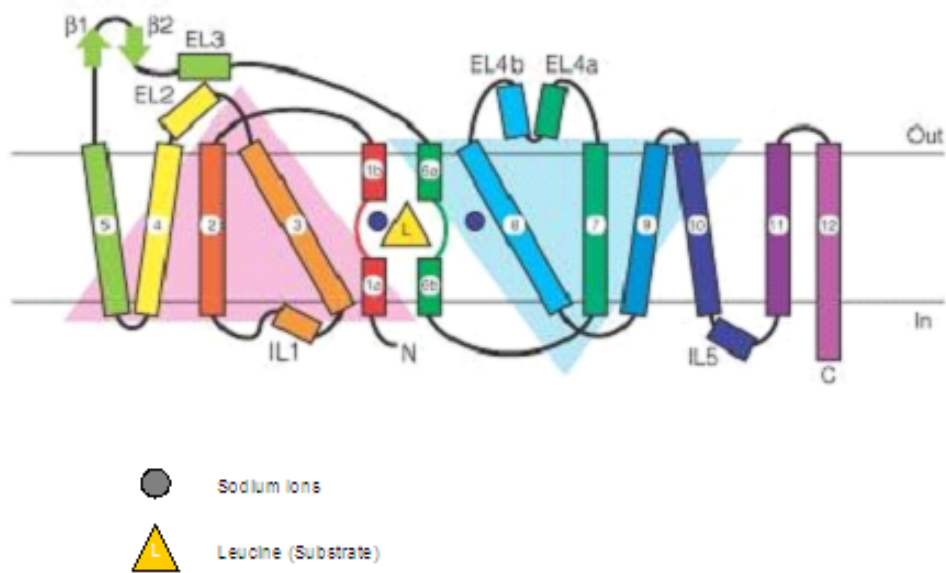


**Figure 1-7. The LeuT<sub>AA</sub> Topology.** The positions of leucine and the two sodium ions are depicted as a yellow triangle and blue circles, respectively (adapted from Yamashita *et al.*, 2005).

## LEUT<sub>AA</sub> THREE-DIMENSIONAL STRUCTURE WITH DESIPRAMINE

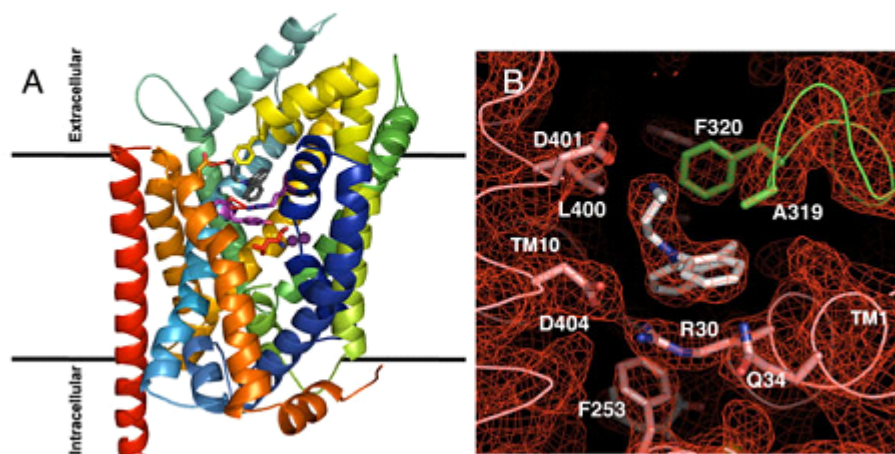


**Figure 1-8. Structure of the LeuT-desipramine complex.** **A.** Over structure of the LeuT-desipramine complex showing the position of the bound desipramine, viewed from within the membrane plane. **B.** 2Fo-Fc map contoured at  $2\sigma$  showing the desipramine binding site in LeuT, viewed from within the membrane plane. Residues R30, Y108, F253 and D404 form the extracellular gate, which separates the leucine substrate from the bound desipramine (adapted from Zhou *et al.*, 2007).

## **Photoaffinity Labeling as a Method to Identify the Cocaine Binding Site of the Human Dopamine Transporter**

Photoaffinity labeling (PAL) is a widely used technique in biochemical applications for studying receptor-ligand interactions (Vodovozova, 2007). Steps for identifying amino acid residues are shown in Figure 1-9. PAL was first proposed more than 40 years ago (Singh *et al.*, 1962). However, more attention has been focused on this method because more sophisticated photophores can be used (Brunner, 1993; Dorman & Prestwich, 1994; Fleming, 1995; Kotzyba-Hibert, *et al.*, 1995).

The most commonly used photoaffinity labels are aryl azides (Fleming, 1995). By definition a photoaffinity label requires the use of a photoactivatable but chemically inert analogue in which the action of light produces a highly reactive species that binds irreversibly to the biological receptor at the site of interaction (Vodovozova, 2007). There are many types of PALs including aryl azides, aryldiazirines, aryldiazonium salts, arylketones and benzophenones (Fleming, 1995). Figure 1-10 shows typical precursors of reactive species in photoaffinity labeling. Figures 1-11 shows three of the major photophores used for photoaffinity labeling (Dorman & Prestwich, 2000).

Reaction of aryl azides occur with the azacycloheptatriene intermediate, which are electrophilic. This happens via intramolecular ring expansion of the nitrene. While they are not as reactive as the singlet nitrene, they are reactive intermediates. They do not insert into non-activated C-H bonds (Brunner, 1993). Fluorines were added to arylazides to increase the lifetime of singlet nitrenes thereby allowing the reaction of the

residue with the nitrene rather than the azepine intermediate (Keana & Cai, 1989; E. Leyva *et al.*, 1989; Poe *et al.*, 1992; Soundararajan & Platz, 1990; Young & Platz, 1989).

<sup>3</sup>H, 3-Aryldiazirines were made first in 1973 (Smith & Knowles, 1973). Smith and Knowles suggested their usefulness as photolabeling reagents (Smith & Knowles, 1975). Aryldiazirines are photolyzed at 360nm and generate a highly reactive carbene. The disadvantage of aryldiazirine was its photolysis generating diazo-isomers as seen

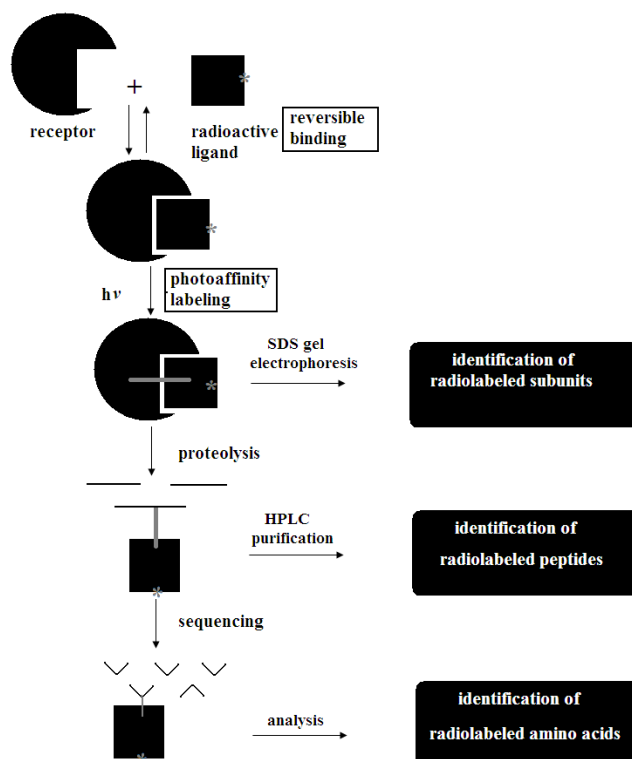


**Figure 1-9. Steps for Photoaffinity Labeling.** Photoaffinity labeling: principle and successive steps for the identification of amino acids (adapted from Kotzyba-Hibert, *et al.*, 1995).

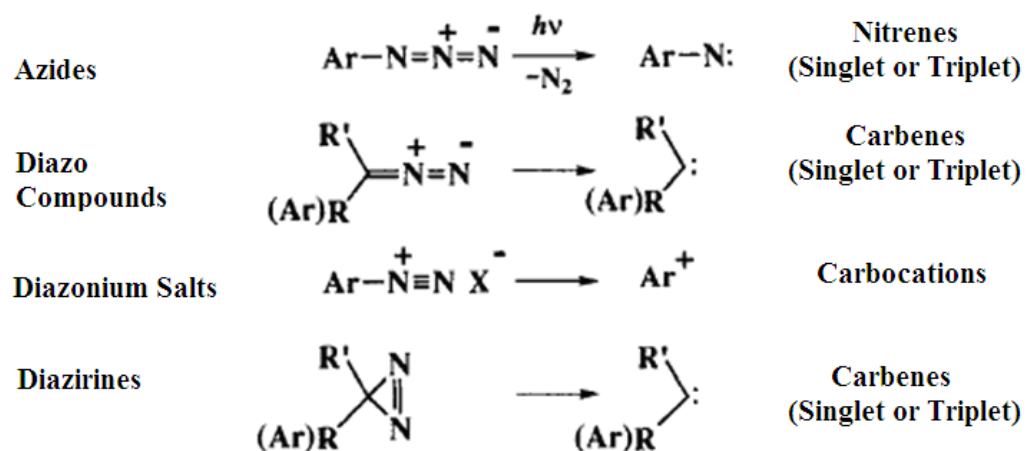


**Figure 1-10. Typical Compounds used as Photoaffinity Labels.** Typical compounds used as precursors of reactive species in photoaffinity labeling (adapted from Kotzyba-Hibert, *et al.*, 1995).

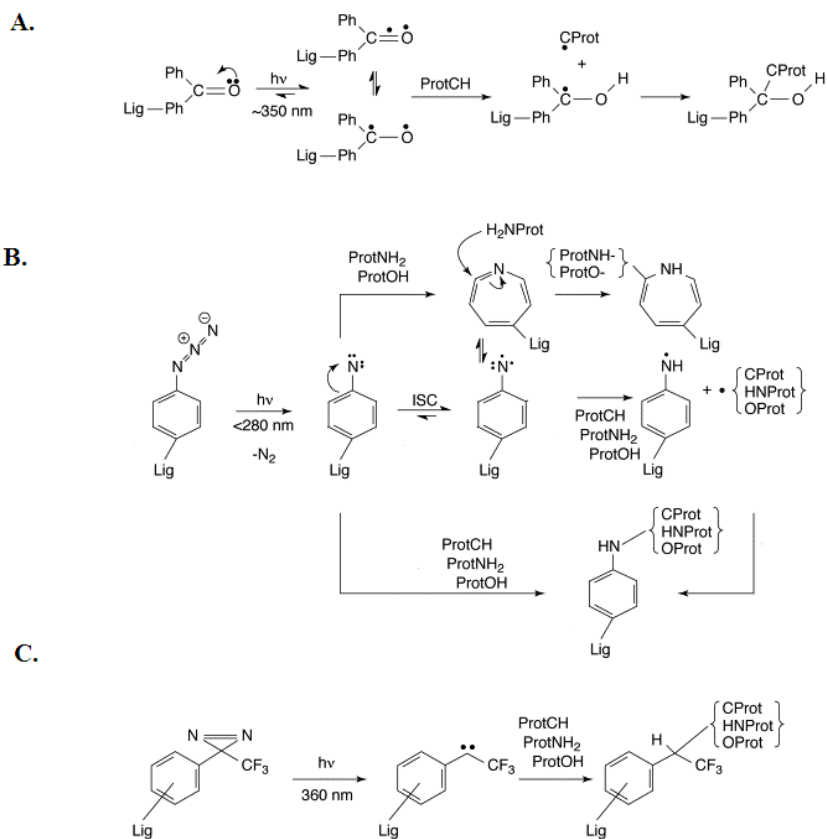


**Figure 1-11. Photolysis of Photophores.** Photochemical events of three major photophores used in photoaffinity labeling: benzophenone, acrylazide and diazirine. **A.** Benzophenone photochemistry, **B.** aryl azide photochemistry and **C.** diazirine photochemistry are illustrated above. ISC; Intersystem crossing (adapted from Dorman & Prestwich, 2000).



with adamantane diazirine, a general hydrophobic labeling reagent (Bayley & Knowles, 1978; Goldman *et al.*, 1979). 3-Trifluoromethyl-3-aryldiazirines were developed in 1980 to offset some of the dark reactions that occur as well as the diazoisomerization (Brunner & Richards, 1980). The effect of the electron withdrawing trifluoromethyl group stabilize the diazo isomer so that it is unreactive under the conditions of labeling and there is no evidence that unintended dark reactions occur (Brunner, 1993).

Aryldiazonium salts fall into the category of a photosuicide labeling reagent (Brunner, 1993). Photosuicide labeling was pioneered by Goeldner, Hirth and colleagues (Ehret-Sabatier, 1989; Goeldner & Hirth, 1980; Goeldner *et al.*, 1982; Goeldner *et al.*, 1983; Kieffer *et al.*, 1981; Langenbuchcachat *et al.*, 1988). Photosuicide labeling is the specific labeling of a receptor binding site through selective activation of the bound ligand molecules (Brunner, 1993). To allow for the selective activation, photosensitive ligands must be designed to account for the specific and different physiochemical properties of the corresponding binding site.

Diazonium salts can be activated through energy transfer from a nearby excited tryptophan residue. This technique has been used to photolabel the digitalis binding site of Na, K-ATPase (Goeldner *et al.*, 1983), the PCP binding site (Kotzyba-Hibert *et al.*, 1985) and the acetylcholine binding site (Langenbuchcachat *et al.*, 1988) of the nicotinic acetylcholine receptor, and the muscarinic receptor binding pocket of muscarinic acetylcholine receptors as potential probes of the gamma-aminobutyric receptor (Autelitano *et al.*, 1997).

Arylketone photochemistry is well understood (Turro, 1978). A triplet biradical that abstracts hydrogens efficiently is formed following excitation. It targets C-H bonds

which may be weaker than O-H bonds making it a very useful reagent in environments accessible to water. Arylketones are stable in harsh chemical conditions. For example, 4'-benzoyl-phenylalanine, an arylketone is compatible with the chemistry of solid phase peptide synthesis using the Fmoc- or Boc-protecting group strategy (Boyd *et al.*, 1991; Kauer *et al.*, 1986; W. T. Miller & Kaiser, 1988; O'Neil *et al.*, 1989) and amino acid microsequencing (Mcnicoll *et al.*, 1992).

Of the PALs, benzophenone is the most stable, can be manipulated in ambient light, and are activated at 350-360 nm avoiding protein damaging wavelengths (Dorman & Prestwich, 1994). Other advantages of benzophenones are that they react preferentially with unreactive C-H bonds, even in the presence of water and bulk nucleophiles (Prestwich *et al.*, 1997). They exhibit remarkable site specificity and the triplet state readily relaxes to the ground state if it does not find an H-donor with the required geometry (Fleming, 1995). Benzophenones relax electronically and maintain their binding and photoactivatable properties and then undergo many excitation-relaxation cycles until a favorable geometry for covalent modification is achieved (Dorman & Prestwich, 1994).

### **Photoaffinity Labeling of DAT**

Radioactive probes have been used to label the dopamine transporter since the 1980s (Andersen, 1987; Janowsky *et al.*, 1987; Maloteaux *et al.*, 1988; Marcusson & Eriksson, 1988). In 1989, Sallee *et al.*, documented one of the first uses of a radioiodinated photoaffinity label. This radioiodinated PAL was an aryl azide derivative of the dopamine uptake inhibitor, GBR 12909 (Sallee *et al.*, 1989) and named [<sup>125</sup>I]-

FAPP. [<sup>125</sup>I]-FAPP was shown to label DAT in canine striatum and thought to be a useful probe for the molecular characterization of the dopamine uptake site in various tissues.

[<sup>125</sup>I]-DEEP, a photosensitive compound related to GBR 12909, was used to covalently label DAT in rat striatal homogenates (Grigoriadis *et al.*, 1989). Covalent attachment was inhibited in a stereospecific manner by (-) and (+) cocaine as well as other cocaine analogs. In addition, DAT was determined to be glycosylated.

Following this study, PAL of DAT with 3 Azido [<sup>3</sup>H] GBR-12935 was performed (Berger *et al.*, 1991). This tritiated azido-diphenylpiperazine derivative was synthesized as a photoaffinity probe of DAT. [<sup>3</sup>H] GBR-12935 was photoincorporated into an 80kDa fragment and was blocked by other DAT inhibitors. Therefore, its use in PAL studies with DAT was found to be acceptable. Figure 1-12 shows the structures of these first DAT PALs.

Epitope-specific immunoprecipitation of proteolytic fragments was performed with several iodinated aryl azide photoaffinity labels of DAT. [<sup>125</sup>I]-MFZ 2-24, a tropane based DAT uptake inhibitor, was shown to be incorporated near transmembrane domains 1-2 (TMD 1-2) of DAT (Lever *et al.*, 2005). Follow-up experiments with [<sup>125</sup>I]-MFZ 2-24 have narrowed the region to TM1 (Parnas *et al.*, 2008). [<sup>125</sup>I]-DEEP, a GBR analog and [<sup>125</sup>I]-GA 2-34 have also been tested with the immunoprecipitation technique and found to label near transmembranes 1-2 (TM 1-2) similar to that of [<sup>125</sup>I]-MFZ 2-24 (Vaughan, 1995; Vaughan *et al.*, 1999). [<sup>125</sup>I]-RTI-82, a photoactivatable cocaine analog, was shown to be incorporated in TMD 4-6 (Vaughan, 1995; Vaughan & Kuhar, 1996). Mutagenesis followed by enzymatic and chemical digestions have allowed the

region to be further narrowed to residues 291-344 of TM6 (Vaughan *et al.*, 2007). [<sup>125</sup>I]-AD 96-129 (Dutta *et al.*, 2001), another photoaffinity inhibitor of DAT, is thought to be covalently labeling TMDs 1-2 and 4-6 (Vaughan *et al.*, 2001). The above results of success with photoaffinity labels of DAT suggest that this technique is worth exhausting until the binding site of DAT is completely mapped out. Thus far, we can infer that the possibility of TMs 1-2 and 4-6 are near the binding site for cocaine. Figure 1-13 shows the sites of incorporation for the above photolabels of DAT. Based on the three-dimensional crystal structure of the LeuT<sub>AA</sub> (Figure 1-7) (Yamashita *et al.*, 2005), where residues from TM 1 and 6 form the binding pocket for desipramine, an inhibitor (Figure 1-8) (Zhou *et al.*, 2007) and leucine, a substrate (Yamashita *et al.*, 2005), the possibility exists that the previous results align with the only known structure of a transporter in the same family. Thus, PAL continues to be a useful way to deduce the information regarding the binding site of cocaine on DAT.

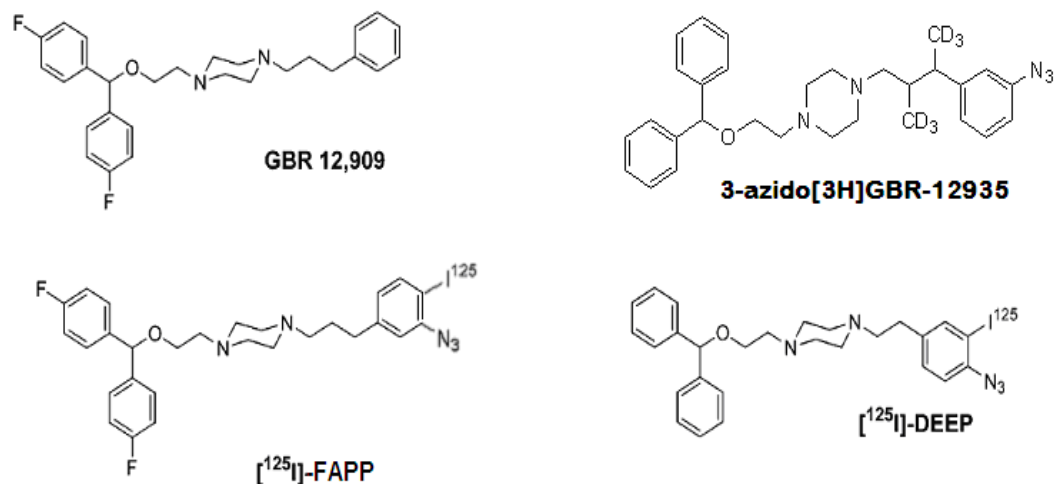


**Figure 1-12. GBR Analogs.** GBR 12, 909 is the dopamine uptake inhibitor that some of the first photoaffinity labels of DAT were modeled after. GBR 12, 909 has a high affinity ( $K_i=36.3\text{nM}$ ) for DAT but is not a structural cocaine analog. 3-azido [<sup>3</sup>H] GBR-12935 is a tritiated photoaffinity label (PAL) while FAPP and DEEP are iodinated.

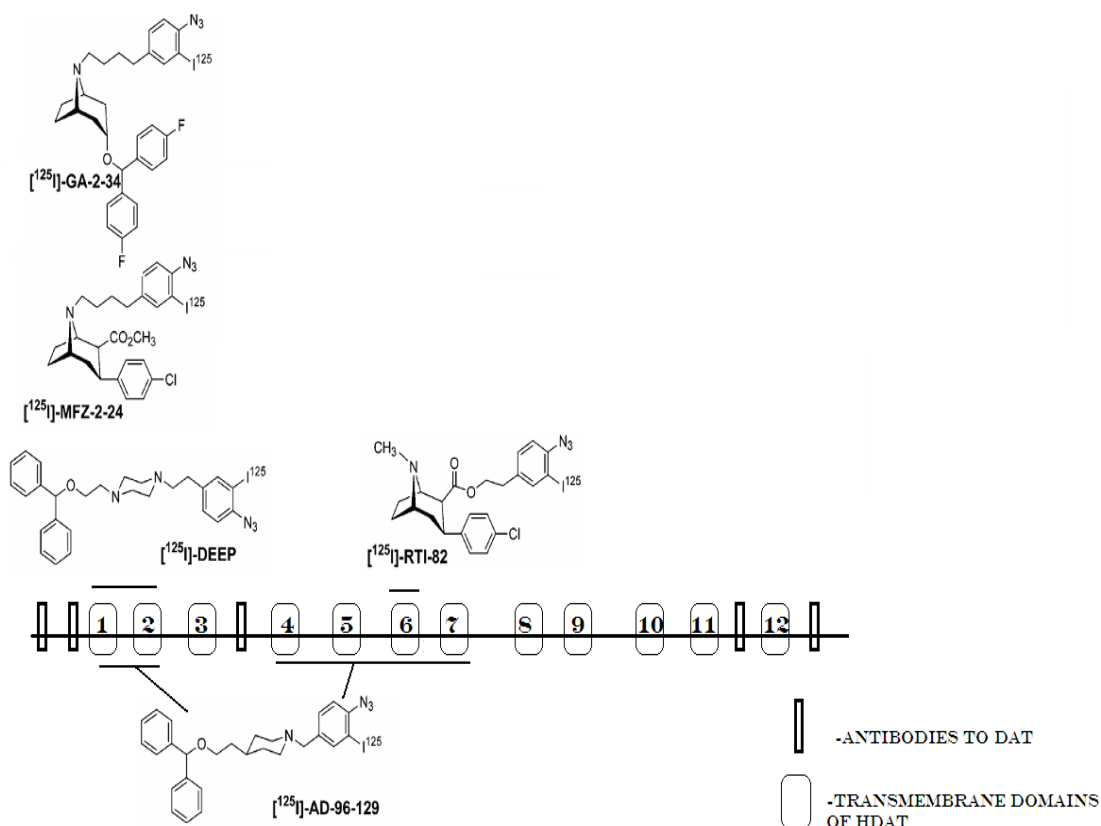


**Figure 1-13. Regions of Incorporation of PALs on hDAT.** An illustration of DAT TMDs from 1-12 as well as the regions in which DAT photoaffinity labels are known to be incorporated based on epitope immunoprecipitation studies (Lever *et al.*, 2005; Parnas *et al.*, 2008; Vaughan, 1995; Vaughan *et al.*, 1999; illustration adapted from Vaughan *et al.*, 2001; Vaughan & Kuhar, 1996; Vaughan *et al.*, 2005; Vaughan *et al.*, 2007).

## Photochemistry of Aromatic Nitrenes

DAT photoaffinity labels are aryl azides thus they form aromatic nitrenes upon excitation by UV light making the discussion of this topic applicable. "Photochemistry" is defined by as a sub-discipline of chemistry. It is the study of the interactions between atoms, small molecules, and light (or electromagnetic radiation). Aromatic nitrenes are used in photoimaging systems and as photoaffinity labels (Bayley & Knowles, 1977). Aryl azides form aromatic nitrenes upon irradiation with ultraviolet (UV) light (Kotzyba-Hibert, *et al.*, 1995). Aromatic nitrenes are very reactive and can insert into C-H bonds. The most commonly researched aryl azide is phenyl azide (Leyva *et al.*, 1991; Leyva *et al.*, 1989; Pandurangi *et al.*, 1994). Most of the studies performed with phenyl azide and derivatives of phenyl azide are to look at the transition states at low temperatures (Dunkin *et al.*, 1997; Gritsan & Platz, 2006).

Phenyl azide forms at least three excited state structures and 6-short lives ground state intermediates upon irradiation (Schrock & Schuster, 1984). The potential reactive intermediates formed from the photolysis of phenyl azide are from 1. the singlet state which forms a singlet nitrene then a dehydroazepine and 2. the triplet state which forms a triplet nitrene, then a benzazirine, and finally an aniline (Schuster, 1992). The nitrogen atom of the nitrene has two non-bonding electrons for distribution into two *p*-orbitals (Platz, 1995). Therefore, it can exist in either the singlet or the triplet state (Platz, 1995). Figure 1-13 shows a scheme of irradiated phenyl azide through both singlet and triplet states along with their resulting products.

It has been shown that the nature of the substituents on the aromatic ring influences the photochemical reaction and this the chemical reactivity of the

photogenerated intermediate (Li *et al.*, 1988b). The photoaffinity ligands that are being used in this study are thought to prefer the triplet state because of the iodine ortho to the azido group on the phenyl ring (Watt *et al.*, 1989). Thus, intersystem crossing (ISC) occurs and the benzazirine/aniline product is favored. Substituents like iodo and nitro enhance the rate of intersystem crossing (ISC) (Turro, 1978). Iodo by heavy atom effect and nitro by mixing in  $n\Pi^*$  states tend to lower the yield of 3H-azepines and raise the yield of azobenzenes and anilines (Cai *et al.*, 1992; Turro, 1978).

The reaction of phenyl azide and diethylamine is the most commonly studied photochemical reaction. An azepine should form from this reaction (Figure 1-14) (Leyva *et al.*, 1986; Platz, 1995; Schnapp & Platz, 1993; Schnapp *et al.*, 1993; Schrock, Schuster, 1984; Schuster, 1992) especially when done at room temperature in solvents like cyclohexane, MTHF, hexane or chloroform. In inert solvents intractable polymers have been formed (Degraff *et al.*, 1974). Flash photolysis in the presence of a secondary amines lead to the growth of a secondary intermediate which absorbs strongly in the range of 340-370 nm (Schrock & Schuster, 1984). This system is well understood; therefore, this small molecule model is used in this research as a way to understand the photochemistry behind DAT photoaffinity labels.



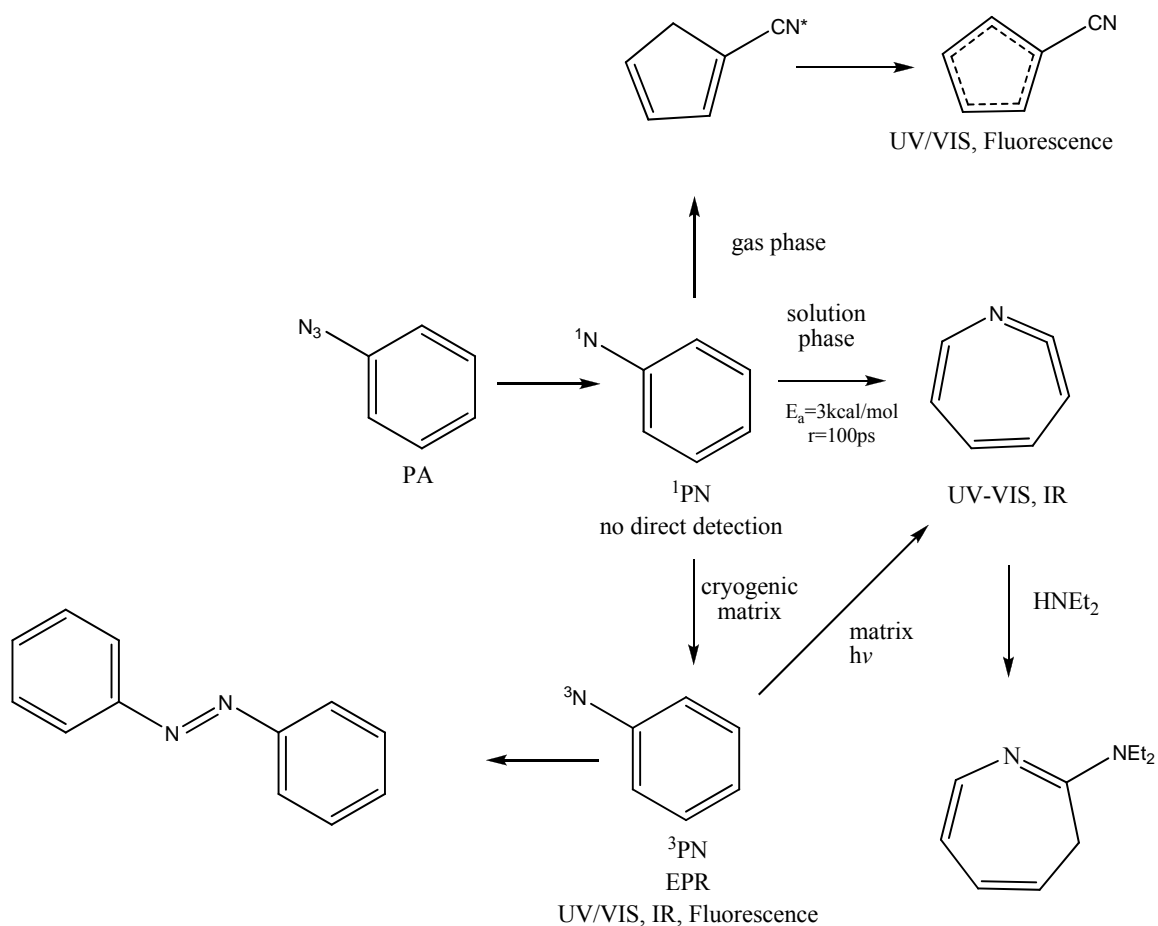


**Figure 1-14. Pathways for Photolysis of Phenyl Azide.** The reaction mechanism of phenyl azide is shown with pathways of both the singlet and triplet states. The common singlet state product, an azepine, from the addition of diethylamine, a ‘trapping reagent’, is also shown (adapted from Platz, 1995).

## Project Overview and Objectives

The overall goal of this dissertation research was to localize the cocaine binding site of the human dopamine transporter protein. Radioiodinated photoaffinity labels (PALs) were used to covalently label hDAT. The radioactivity was tracked through enzymatic and chemical digestions to create smaller labeled peptides. SDS-PAGE, autoradiography, and high performance liquid chromatography (HPLC) were used to separate the labeled radioactive peptides from those that were not. This dissertation aims to sum up the extent this methodology with the GBR analog and PAL, [<sup>125</sup>I]-DEEP. In addition, the photochemical bond that is created during photolysis is unknown. Therefore, solution photoreactions were done to model the photoaffinity label and the target amino acid(s) and/or peptide backbone. The products that were identified and tested for stability in proteolytic conditions.

The specific aims of this dissertation research were to (1) determine whether [<sup>125</sup>I]-DEEP labeled hDAT shared the same site of incorporation as cocaine, (2) to determine whether the [<sup>125</sup>I]-DEEP photolabel would be stable in degradative conditions like CNBr, (3) to determine the reactivity of phenyl azide with amino acid analogs, (4) to identify the products formed from the photoreactions, and (5) to determine the product stability in degradative conditions whether acidic (CNBr) or basic (tryptic).

### **Labeling of the Human Dopamine Transporter (hDAT) with the Photoaffinity Label, [<sup>125</sup>I]-DEEP, a GBR Analog**

Photoaffinity labeling of the human dopamine transporter (hDAT) with [<sup>125</sup>I]-DEEP were aimed at localizing the binding site of cocaine. hDAT has been labeled with inhibitors like DEEP, RTI-82, MFZ 2-24, GA 2-34, JJC 2-24 and AD 96-

129. Although these inhibitors have different types of cocaine pharmacophores, they all possess an aryl azide as the photochemical portion of its structure and a radioactive iodine ( $^{125}\text{I}$ ) (Figure 1-15). These ligands were all shown to label hDAT effectively. Following the labeling of hDAT, proteolytic or chemical digestions followed to yield smaller peptides. The radioactivity was traced on SDS-PAGE and visualized by autoradiography. The radioactive peptide fragment was extracted from the gel and separated by HPLC to isolate the radioabeled peptide. However, there was not a way to further utilize this methodology because there was not enough protein or the results compared to the theoretical peptide retention time using theoretical software was ambiguous. Therefore, another way to discern what peptide or amino acid was most likely being labeled was to develop a small molecule model based on the inhibitor and the amino acids proposed to be involved in the binding site.

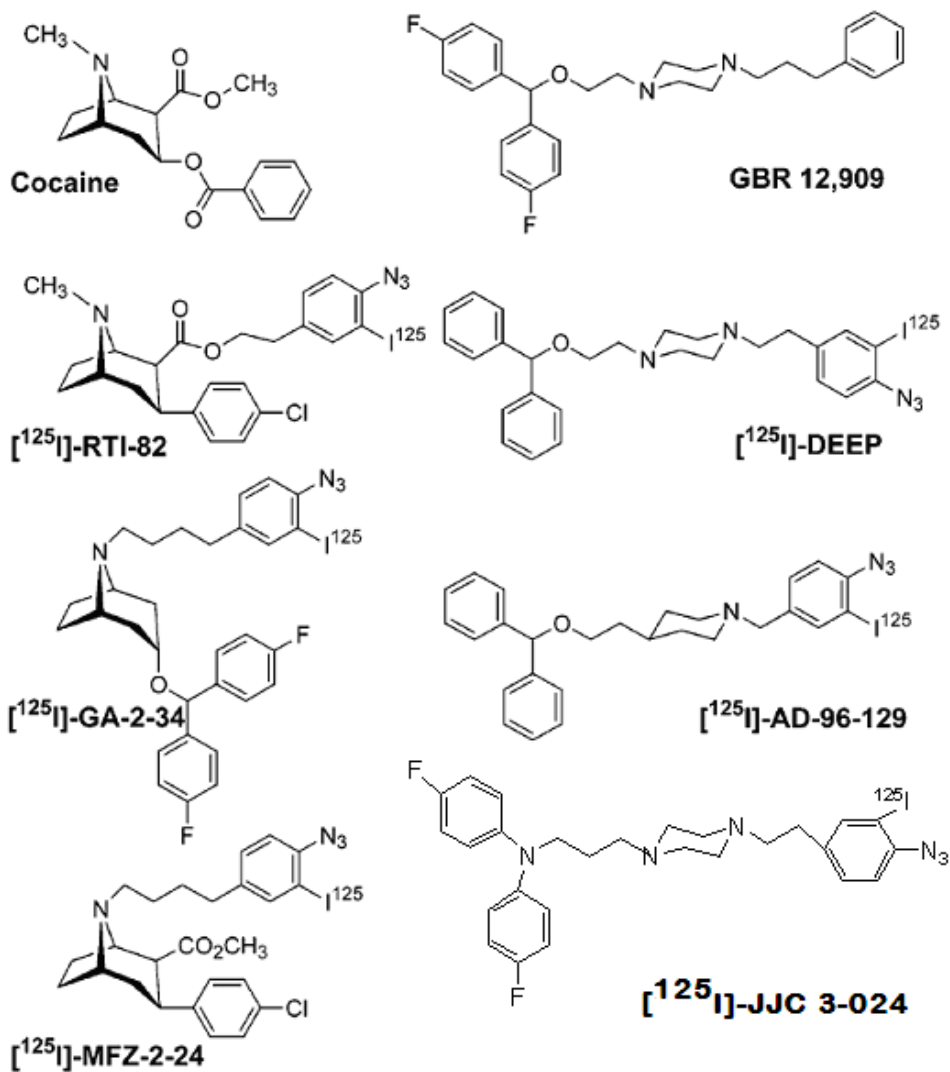
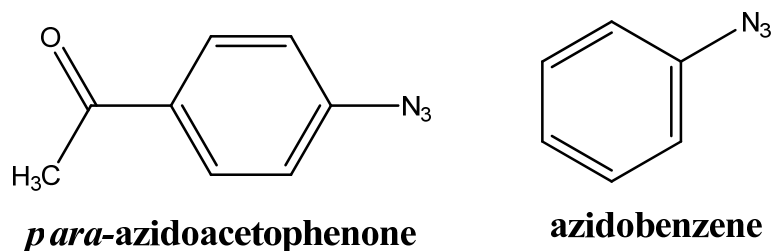


**Figure 1-15. Structures of Cocaine and DAT Photolabels.** [<sup>125</sup>I]DEEP, [<sup>125</sup>I]GA II-34, [<sup>125</sup>I]AD 96-129 [<sup>125</sup>I] RTI-82, [<sup>125</sup>I] JJC 3-024 and [<sup>125</sup>I]MFZ 2-24 contain azide groups and are used for photoaffinity labeling.

## Reactivity of Amino Acid Analogs with Phenyl Azide

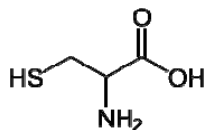
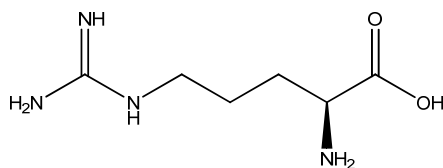
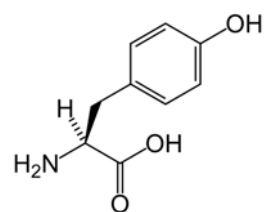
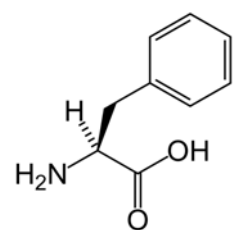
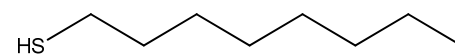
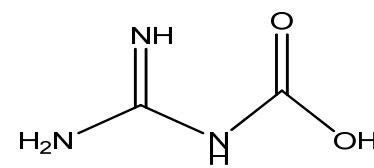
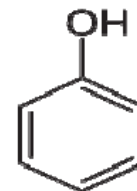
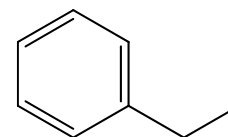
The objective of this research was to determine the rate of reactivity of phenyl azide with amino acid analogs. The DAT photolabels mentioned previously have a phenyl azide moiety, thus making phenyl azide a good analog of DAT photolabels. Compounds that have the same functional group as amino acids were used as analogs. A small molecule model of the photoreactions occurring with hDAT and DAT photolabels was developed. The reactivity of phenyl azide with amino acid analogs was tested.

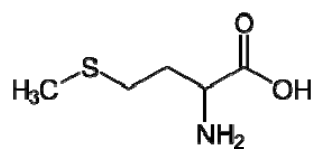
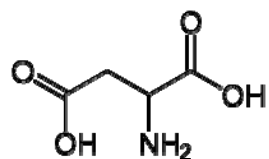
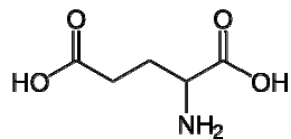
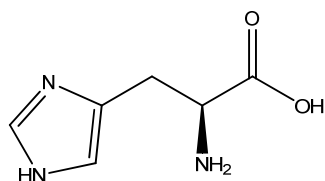
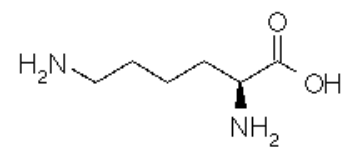
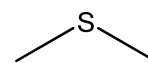
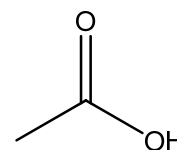
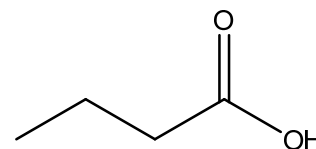
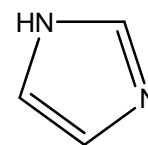
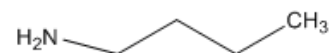
The amino acids that were studied include cysteine, lysine, arginine, phenylalanine, methionine, glutamic acid, histidine, and tyrosine. The amino acid analogs were 1-octanethiol for cysteine, butylamine for lysine, guanidine acetic acid for arginine, butyric acid for glutamic acid, dimethyl sulfide for methionine, imidazole for histidine and phenol for tyrosine. There was also a peptide backbone model, *N*-ethylacetamide to compare to the side chain analogs (Table 1-1).



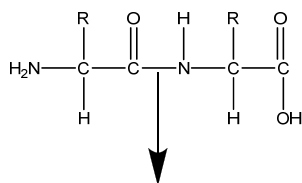
**Figure 1-16. Analogs of DAT Photolabels.** Phenyl azide (synthesized by M. Holmes) and *para*-azidoacetophenone (Toronto Chemicals) were used as analogs of the photochemical portion of the hDAT photoaffinity ligands. These aryl azides were irradiated with the analogs of amino acid side chains or a peptide backbone analog. The reactivity was determined for each model and the dominant product formed in the reaction was determined.

The loss of phenyl azide was determined over time and the rate constant,  $k$ , was derived using the equation  $y=Ae^{-kt}$ . Mass spectra was obtained to confirm the presence of the products. Proton NMR was also attempted for each target but the yields of pure product were very low and only one successful identification was confirmed.

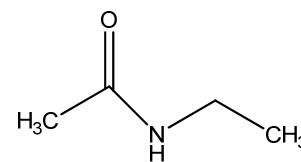
**NATIVE COMPOUND****CYSTEINE****ARGININE****TYROSINE****PHENYLALANINE****MODEL COMPOUND****1-OCTANETHIOL****GUANIDINE ACETIC ACID****PHENOL****ETHYLBENZENE**

**NATIVE COMPOUND****METHIONINE****ASPARTIC ACID****GLUTAMIC ACID****HISTIDINE****LYSINE****MODEL COMPOUND****DIMETHYL SULFIDE****ACETIC ACID****BUTYRIC ACID****IMIDAZOLE****BUTYLAMINE**



**NATIVE COMPOUND****PEPTIDE BACKBONE**

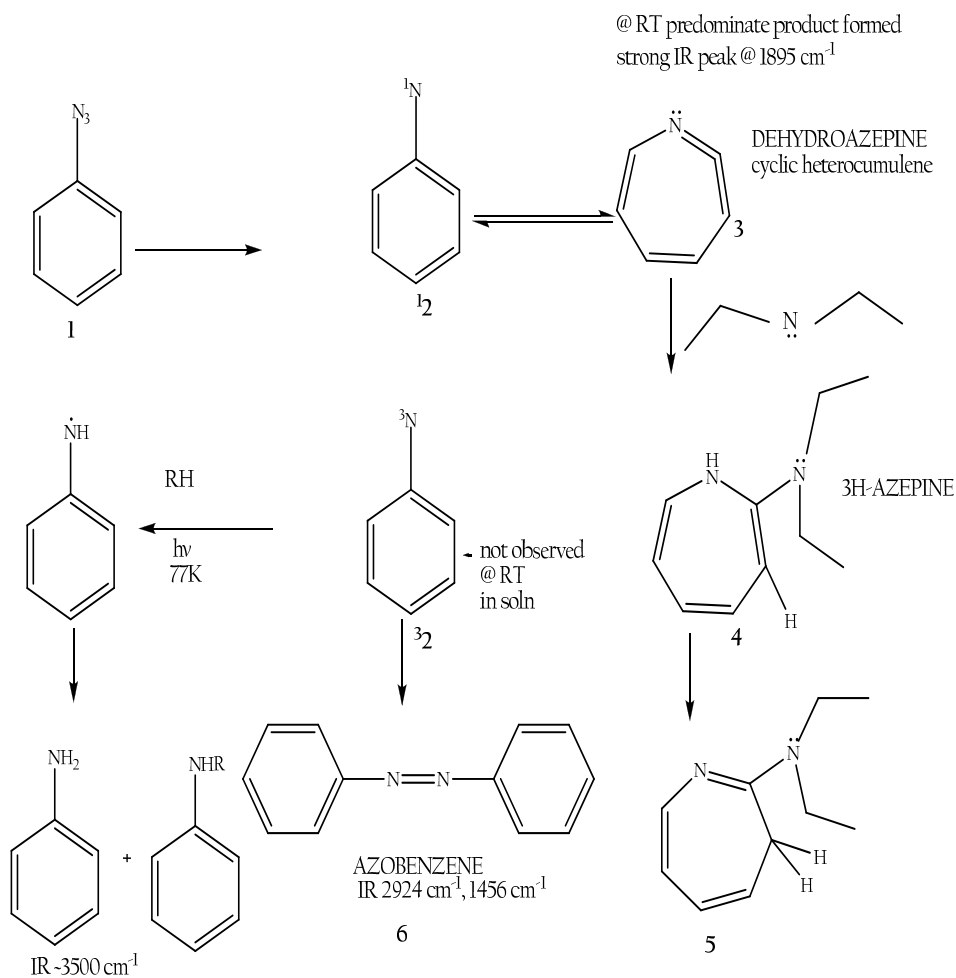
PEPTIDE BOND

**MODEL COMPOUND****N-ETHYLACETAMIDE**

**Table 1-1. Amino Acid Analogs.** Table of the small molecule analogs used in the experiments. The small molecule analogs of cysteine, arginine, lysine, tyrosine, phenylalanine, methionine, glutamic acid, aspartic acid and the peptide bond are listed above. The small molecule used for the aryl azide cocaine analogs like MFZ 2-24, GA 2-34, RTI-82, JJC 2-034, AD 96-129, and DEEP was phenyl azide (Figure 1-15).

### **Identification of Products and Their Stability in Proteolytic Conditions**

The experiments conducted in this research project were aimed at investigating the stability of the covalent bond formed between the aryl azide cocaine analog derivative, the amino acid side chains and the peptide bond. This information will give insight into the stability of the label throughout various sample work-up conditions such as proteolytic digestions. First, the products were identified. Then the products were tested for degradation in basic conditions pH 8.9 over time periods of 4 hours and 24 hours. The basic conditions were used in enzymatic digestions like trypsin for cleavage at lysine and arginine residues. In addition, products were tested in 70% TFA at room temperature for 24 hours in the dark. These acidic conditions at pH 1 were used in conjunction with cyanogen bromide in a solution to cleave residues at methionine during chemical cleavage.



**Scheme 1-1. Photolysis of Phenyl Azide.** This scheme shows the two pathways that can occur during the photolysis of phenyl azide whether alone or in the presence of a target, i.e. diethylamine (adapted from Schrock & Schuster, 1984).

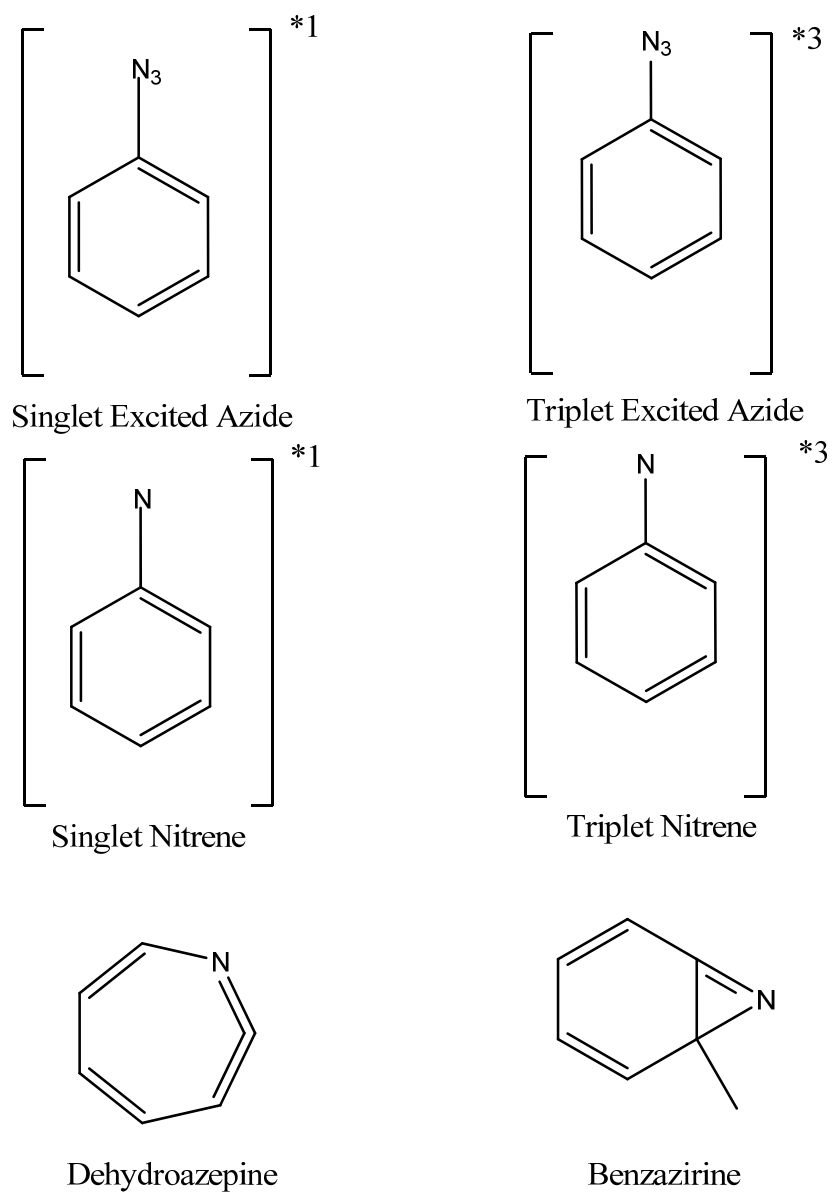


**Figure 1-17. Intermediates of Singlet and Triplet Nitrenes.** Potential reactive intermediates formed on photolysis of phenyl nitrene (adapted from Schuster & Platz, 1992).

In summary, this dissertation will explore the photoaffinity labeling of hDAT with the GBR analog, [<sup>125</sup>I]-DEEP and the proteolysis and peptide mapping that was done in an effort to localize the site of photoincorporation. It will also detail methods that are amenable to identifying the cocaine binding site using the novel DAT photolabel and rimcazole analog, [<sup>125</sup>I]-JJC 3-24. The small molecule research on reaction kinetics of aryl azides was done to determine the reactivity of phenyl azide with amino acid analogs. Furthermore, the stability of the products from the reaction of phenyl azide and amino acid analogs were tested in proteolytic conditions.

**Chapter Two**

**Photoaffinity Labeling**

**of the**

**Human Dopamine Transporter**

**with**

**[<sup>125</sup>I]-DEEP**

“From the first, I made my learning, what little it was, useful every way I could.”

**-Mary McLeod Bethune**

## Introduction

Photoaffinity labeling is a method of identifying binding domains on proteins using photoactivatable ligands targeted at the domain of interest. Most photolabels are aryl azides, diazirines, benzophenones, and diazonium salts (Fleming, 1995). In this research an aryl azide photolabel was used to label the human dopamine transporter (hDAT). There are many dopamine transporter (DAT) inhibitors that have been transformed into photoaffinity labels. There are the GBR analogs, like [ $^{125}\text{I}$ ]-DEEP (Grigoriadis *et al.*, 1989; Vaughan & Kuhar, 1996), rimcazole analogs, [ $^{125}\text{I}$ ]-JJC 3-24 (Cao *et al.*, 2004; Katz *et al.*, 2003; Newman & Kulkarni, 2002), aryl tropane analogs, [ $^{125}\text{I}$ ]-RTI-82 (Vaughan, 1998; Vaughan *et al.*, 1999; Vaughan *et al.*, 2001; Vaughan *et al.*, 2007) and [ $^{125}\text{I}$ ]-MFZ 2-24 (Lever *et al.*, 2005; Parnas *et al.*, 2008), and benztropine analogs, [ $^{125}\text{I}$ ]-GA 2-34 (Desai *et al.*, 2005; Katz *et al.*, 2004; Newman & Kulkarni, 2002; Ukairo *et al.*, 2005) (Figure 2-1). Each DAT photolabel has been shown to label DAT with high affinity.

The DAT photoaffinity labels have a cocaine pharmacophore and a phenyl ring that contains an azido group ( $-\text{N}_3$ ) ortho to a radioactive iodine [ $^{125}\text{I}$ ] (Figure 2-2). This azido group becomes a reactive nitrene following irradiation by ultraviolet (UV) light (Schrock & Schuster, 1984). This reactive nitrene forms a covalent bond with the protein. It is not apparent which amino acid will be labeled with this aryl azide photolabel. Aryl azides can insert into the peptide backbone as well as react with the side chains of the amino acids.

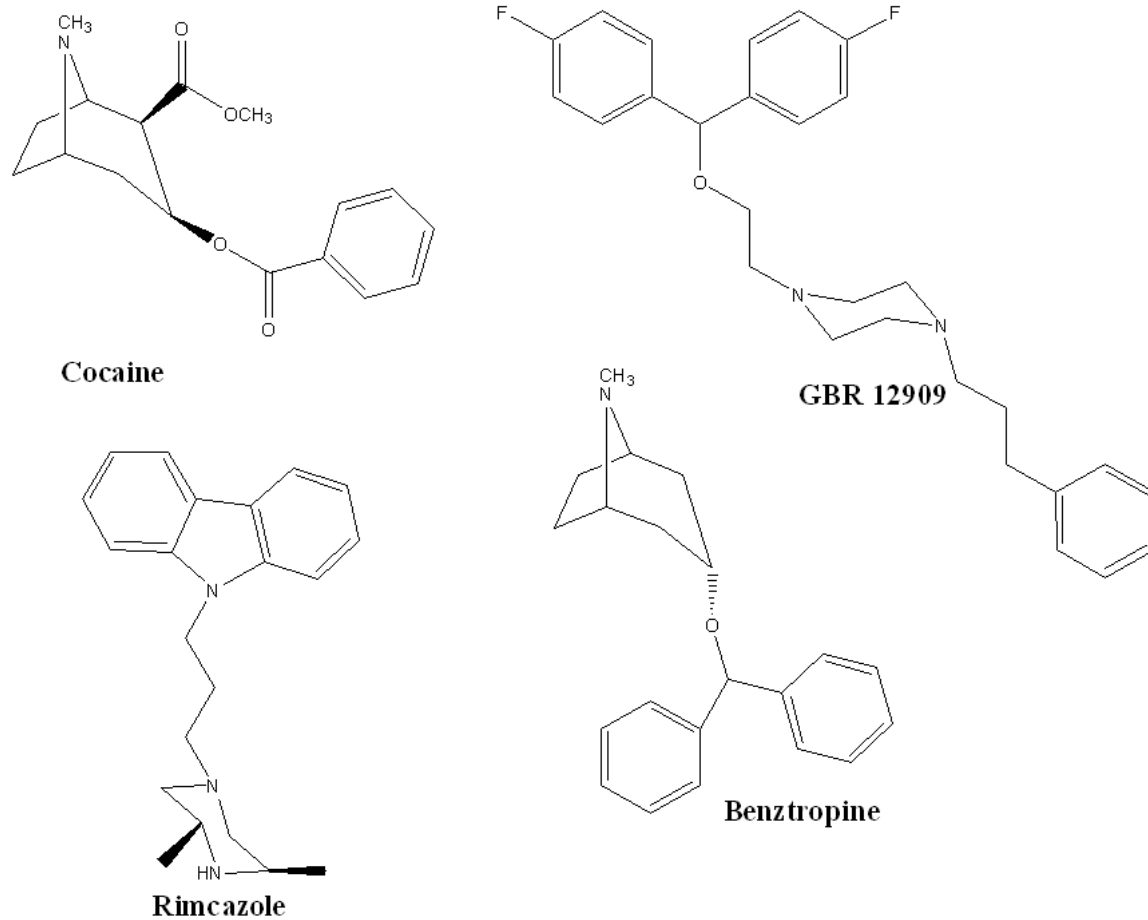


**Figure 2-1. Structures of hDAT Cocaine and hDAT Inhibitors.** Cocaine is an aryl tropane analog that RTI-82 and MFZ 2-24 are based upon. GBR 12909 is the analog from which DEEP is derived. Rimcazole is the compound from which JJC 3-24 was derived. Benztropine is a hybrid of aryl tropane and GBR 12909 in which GA 2-34 is comprised of.



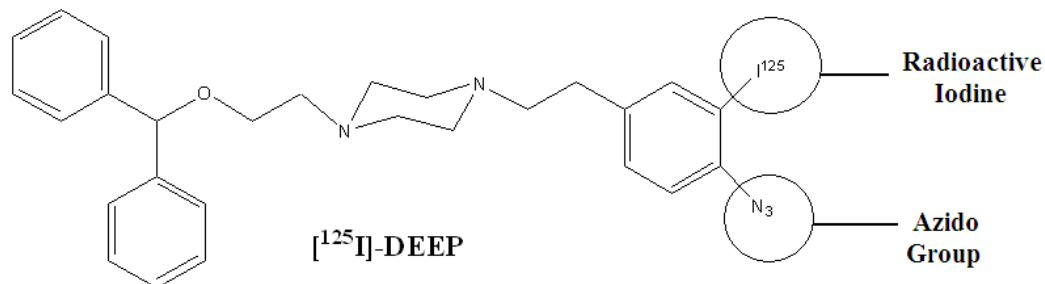


**Figure 2-2. DEEP as an Example of a DAT Photolabel.**  $[^{125}\text{I}]\text{-DEEP}$  is a DAT inhibitor and GBR analog that is used in this dissertation to label hDAT.  $[^{125}\text{I}]\text{-DEEP}$  has been shown to incorporate within TMs 1-2 on hDAT and within the transmembranes but not the loops (Vaughan & Kuhar, 1996)

Photoaffinity labeling has been done with radioactive ligands whether iodinated (Denny & Blobel, 1984) or tritiated (Hanstein *et al.*, 1979) to identify subunits and/or peptide sequences that interact with the ligands (Fleming, 1995). This type of peptide mapping is a good way to identify ligand binding domains without having a three-dimensional picture of the protein. The only example of a sodium chloride dependent transporter (leucine transporter), like hDAT, with an X-ray crystal structure that is available is bacterial in origin (Yamashita *et al.*, 2005). However, the leucine transporter (LeuT<sub>Aa</sub>) gives more insight into the 3D topology of this type of transporter more so than the 2D topology that is based on hydropathy plots.

In this chapter, experiments involving mapping of the human dopamine transporter (hDAT) cocaine binding site by [<sup>125</sup>I]-DEEP, a GBR analog, will be explored. While only a tentative identification was made, it adds a layer of evidence that shapes the picture of how these photolabels work. Every layer of information forwards the effort of identifying the exact amino acid residues that play a role in the binding of cocaine. Preliminary analysis with a novel photolabel that is an analog of rimcazole, [<sup>125</sup>I]-JJC 2-34, and structurally similar to [<sup>125</sup>I]-DEEP was investigated. Suggestions on how it can be used in the future are discussed.

## Methods

## Cell Culture and Photoaffinity Labeling

### Cell Culture

HEK 293 cells stably expressing DAT were obtained as previously described (Chen *et al.*, 1999). The HEK 293-DAT cells were modified by inserting an N-terminal 3xFLAG (Vaughan *et al.*, 2005) and an N-terminal 6xhistidine affinity tag (Reed, 2001). Cells were grown on 150 mm plates or 75 mm flasks in a 37°C, 5% CO<sub>2</sub> incubator. DMEM/F12 50/50 Mix (Cellgro), supplemented with 10% bovine calf serum, 100 µg/mL penicillin-streptomycin, 200 mM l-glutamine, and 0.001% G418, was the medium used for transfected HEK cells. A confluency of cells (90-100%) was achieved from an incubation time of 3-5 days in 75 mm flasks and 150 mm plates, respectively.

### Membrane Preparation

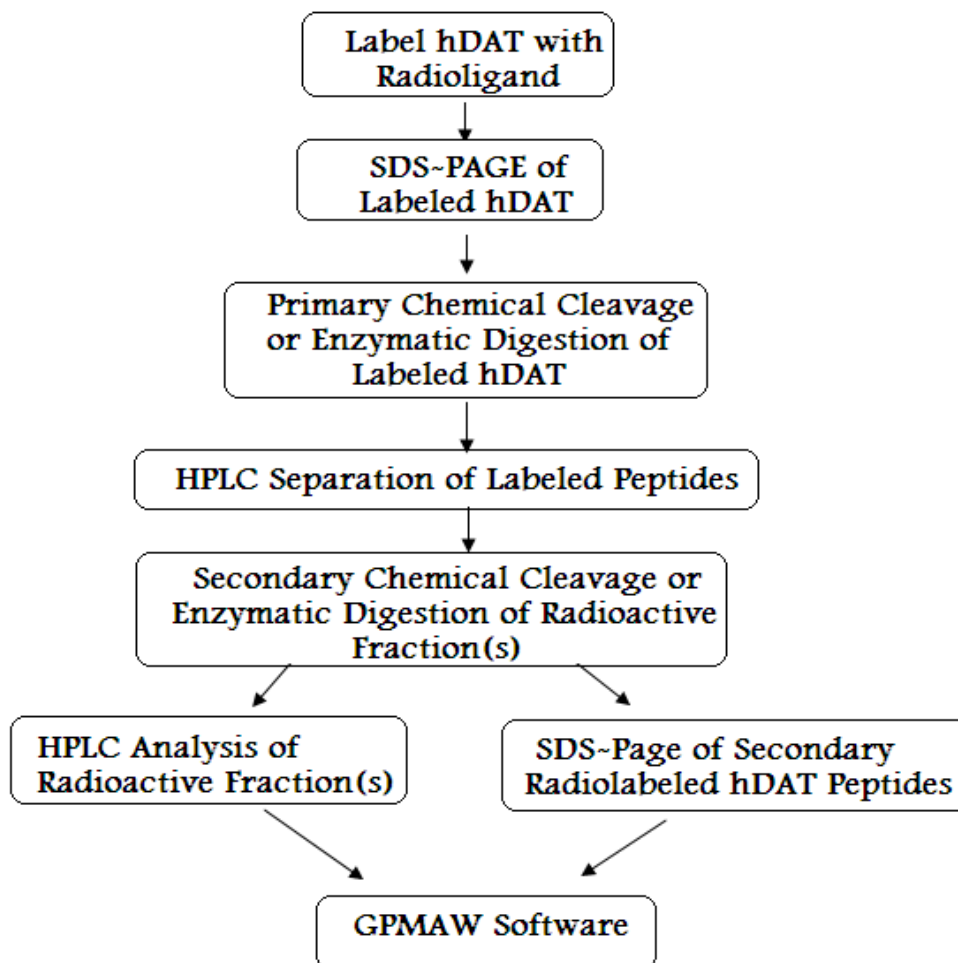
Membranes were prepared from FLAG-his-DAT cells grown on 150 mm tissue culture plates. Results described herein represent an average of 120 plates of cells. Each 150 mm plate of cells grown represent an average of 2 pmol of hDAT protein. Therefore, ~240 pmol DAT protein is the total amount of protein used per experiment. First, cells were washed with Krebs-Ringer-HEPES (KRH) buffer (120mM NaCl, 4.7mM KCl, 2.2mM CaCl<sub>2</sub>, 1.2mM MgSO<sub>4</sub>, 1.2mM KH<sub>2</sub>PO<sub>4</sub>, 10mM glucose, pH 7.4), followed by lysis in 2mM HEPES, 1mM EDTA, for 10 min at 4°C. The lysed cells were scraped (Fisherbrand Disposable Cell Scraper, Handle Length 39 cm), divided between 10 centrifuge tubes and centrifuged at 31,000 x g, 4°C for 20 min. Then, the pellets were combined into 4 centrifuge tubes and membranes were resuspended in 20 mL incubation

buffer (100mM NaCl, 50mM Tris-base, pH 7.0) per tube, sonicated (Heat Systems-Ultrasonics, model W-185F) for 10 sec, and centrifuged as above.

### **Photoaffinity Labeling**

Each pellet was then resuspended by sonicating in either incubation buffer (100mM NaCl, 50 mM Tris base, pH 7.4) or sodium phosphate buffer (300 mM NaCl, 30 mM NaH<sub>2</sub>PO<sub>4</sub>, pH 7.6), to which the radioligands were added. 5nM of [<sup>125</sup>I]-DEEP in incubation buffer or 50nM of [<sup>125</sup>I]-JJC 2-24, 5nM of [<sup>125</sup>I]-RTI-82 in sodium phosphate buffer (amino precursor synthesized by Amy Hauck Newman, Medicinal Chemistry Section, National Institute on Drug Abuse; radioiodinated by J. Lever, University of Missouri-Columbia). The ligand was incubated with membranes for 1 hr on ice with 100 rpm shaking. For protection of hDAT binding experiments, the membranes were incubated with 1mM of WIN 35, 428 for 1 hr on ice first. Then the radioligand was added to the appropriate concentration and allowed to incubate for an additional hour. Two milliliters of the membrane/ligand suspension was transferred to a 60mm x 15mm culture dish (Corning) and irradiated for 4 min with a shortwave (254 nm) UVG-11 Mineralight lamp (UVP). To wash away unreacted label, the preparations were diluted 1:2 in incubation buffer or sodium phosphate buffer, transferred to microcentrifuge tubes (1 mL/tube) and centrifuged (22,000 x g, 4°C, 20 min). Pellets were resuspended in 1 mL sodium phosphate buffer and centrifuged again. The resulting pellets were brought up in 500 µL FLAG solubilization buffer (1% Triton X-100, 1mM EDTA, 150mM NaCl, 50mM Tris-Cl, pH 7.4) and thoroughly resuspended by triterating with a pipette tip. The samples were also vortexed for 5 seconds. Solubilization was carried out overnight at

4°C. The preparation was then centrifuged for 1 hr at 31,000xg, 4°C. The supernatant, containing the solubilized radiolabeled membrane proteins, was removed and saved at 4°C until further use. A scheme for localizing the residues in the cocaine binding site using photoaffinity labels is shown in Scheme 2-1.



**Scheme 2-1. Localization of Photoaffinity Labels.** Details for localizing the amino acid residue of hDAT labeled by DAT photoaffinity ligands are broken down into a step-by-step process. Radiolabeled hDAT is separated on a gel. The labeled hDAT protein is subjected to in-gel primary cleavage or digestion. An HPLC to separate and identify radiolabeled hDAT peptides is done. A secondary digestion of the DAT peptides were done and re-analyzed by HPLC or SDS-PAGE. The results are analyzed against theoretically generated data of primary and secondary DAT digestions using the same HPLC gradient.

## **Purification and Isolation of Radiolabeled hDAT**

### **Immobilized Metal Affinity Chromatography**

Immobilized Metal Affinity Chromatography (IMAC) columns were prepared by applying 0.4 mL of Ni-NTA agarose (Sigma) slurry to 15 mL columns (Qiagen) resulting in a 0.2 mL Ni-NTA column. The resin was equilibrated with 2 column volumes of equilibration buffer (50mM Na<sub>2</sub>PO<sub>4</sub>, 0.3M NaCl, pH 8.0). Solubilized radiolabeled membrane proteins were applied to the column and incubated with the resin up to overnight at 4<sup>0</sup>C on a shaker to allow hDAT to bind completely. The column was washed with 5 column volumes of wash buffer (50mM Na<sub>2</sub>PO<sub>4</sub>, 0.3M NaCl, pH 8.0). The hexahistidine-tagged hDAT was eluted with 10 column volumes of elution buffer (1M imidazole, 50mM Na<sub>2</sub>PO<sub>4</sub>, 0.3M NaCl, pH 8.0) and saved at 4<sup>0</sup>C for further use.

### **Gel Electrophoresis**

Radiolabeled DAT was separated from other solubilized proteins via SDS-PAGE according to Laemmli (1970) on 7.5% polyacrylamide gels for whole proteins and 16.5% gels for peptides, whose dimensions were 16 x 14 x 0.1 cm. 6X sample running buffer (30% glycerol, 70% 50mM Tris-Cl, 0.35M SDS, 0.6M DTT, pH 6.8, with bromphenol blue) was added to the samples in a 1:2 ratio. Afterward, the samples were vortexed and loaded onto the gel. For a 120 plate experiment, 8 gels with 10 wells each were used, and approximately 250 µL of the sample was added to 9 of the 10 wells. ProSieve Color Protein Markers (Cambrex) were used as a high range standard on the 7.5% gels and Rainbow molecular mass markers (Amersham) were used low range standard for the



16.5% gels. 15  $\mu$ L of the standards were added to the 10<sup>th</sup> well as a reference on each gel. Electrophoresis proceeded at 60-90mA for 2-5 hrs, using a Fisher Biotech Electrophoresis System with an EC 250-90 (E-C Apparatus Corporation) power supply.

### **Autoradiography**

Following electrophoresis, gels were transferred to gel drying filter paper. The 7.5% gels were dried at a constant temperature of 80°C while the 16.5% gels were dried at temperatures ranging from 60-80°C under a vacuum with a BioRAD model 583 gel dryer for 2-4 hours, respectively. The dried gel was placed in an exposure cassette with Kodak BioMax MS film and then stored at -80°C. The activity of the ligand determined the amount of autoradiographic exposure time. The exposure times increased as the activity of the ligand decreased. Development was performed manually in a darkroom using Kodak developer and fixer. This film was used as a guide in the cutting of radioactive gel bands that were used in the follow-up experiments.

### **Western Blotting**

Immediately following gel electrophoresis, precast gels were soaked in transfer buffer (39 mM glycine, 40 mM Tris and 10% MeOH) for 15 minutes. A semidry blotting apparatus (Fisher Scientific) was used for the electrotransfer of proteins to polyvinylidene fluoride (PVDF) membranes. Whatman 3M filter paper was cut into the size of the gel and 2x three layers of paper were soaked with transfer buffer. The PVDF membrane was wet thoroughly with methanol and then soaked with transfer buffer. The filter paper, PVDF membrane and gel were assembled. The electrotransfer was carried out for 90

minutes at 60 mA constant current per gel. After the transfer was complete, the PVDF membrane was allowed to air dry. Methanol was used to rehydrate the PVDF membrane. The membranes were washed twice for 5 minutes with TBS buffer (150 mM NaCl, 10mM Tris, pH 7.6) then blocked with blocking buffer (5% nonfat dry milk, 0.1% Tween-20, 150 mM NaCl, 10 mM Tris, pH 7.6) for 1 hour at room temperature on a shaker. The blocked membrane was washed thrice for 10 minutes with TTBS (0.1 Tween-20, 150 mM NaCl, 10 mM Tris, pH 7.6).

Primary antibody directed against the C-terminal of DAT was used at a 1:500 dilution. The antibody was prepared in blocking buffer and applied to the membrane. The PVDF membrane was incubated with the primary antibody mixture overnight at 40C with shaking. The PVDF membrane was washed thrice for 10 minutes with TTBS at room temperature with shaking. A secondary antibody conjugated to alkaline phosphatase was used at a 1:10,000 dilution in blocking buffer. This secondary antibody mixture was applied to the membrane for 1 hour with shaking at room temperature. Following the secondary incubation, the membrane was washed with TTBS thrice while shaking. Then the membrane was developed with NBT/BCIP (Pierce). After the application of the developer, the membranes were visually monitored for development and stopped by rinsing the membranes several times with distilled water. The membrane was allowed to dry and then scanned.

## **Digestion of Radiolabeled hDAT**

### **Enzymatic Digestions of Labeled hDAT**

Trypsin was used to cleave intact labeled hDAT. Trypsin-TPCK (10 mg/mL) is applied directly to chopped gel pieces of labeled hDAT or previously enzymatically digested peptides and incubated at 37°C for 24 hours. Digested peptides were extracted from the chopped gel pieces for 24-48 hours with 60% acetonitrile/0.1% trifluoroacetic acid (TFA) in a sonicating water bath. A final extraction is performed for 4-8 hours with 100% acetonitrile in a sonicating water bath. The extracts are pooled together and dried down with a speedvac. The peptides are reconstituted in 60% acetonitrile/0.1% trifluoroacetic acid (TFA), filtered with Millipore Ultrafree-MC Centrifugal Filter Devices and injected into the HPLC.

### **Chemical Cleavage**

Cyanogen bromide (100mM) in 70% trifluoroacetic acid (TFA) was prepared and stored at room temperature in the dark. Chemical cleavage was done in-gel for both primary and secondary cleavages. On some occasions, secondary cleavages were performed in solution with extracted hDAT peptides dried down. In that case, the extracted peptides were reconstituted with the CNBr solution for 24 hours in the dark at room temperature. Primary in-gel cleavage was done following the 80kDa band being cut out, rehydrated in the CNBr solution and chopped into smaller pieces. Then the chopped gel pieces were placed in an eppendorf tube and filled with CNBr solution. These gel pieces were incubated for 24 hours at room temperature in the dark overnight.

### **Thin Layer Chromatography**

Thin layer chromatography (TLC) analysis was carried out on 5x20 cm Fisherbrand Silica Gel GF plates. The samples were tryptic followed by CNBr or CNBr followed by trypsin radiolabeled digests of hDAT. The development solution was *n*-butanol:H<sub>2</sub>O:acetic acid (70:20:10). The digested radiolabeled peptides were reconstituted in solutions of 60% acetonitrile in water with 0.1% TFA. The radiolabeled peptide digestion was typically performed on a 10-20uL scale. However, the actual amount was dependent upon the radioactivity of the previous digestion. Therefore, less material was necessary for highly radioactive peptides. The digestion was spotted onto the TLC plate 1uL at a time. The sample was allowed to dry completely then 1uL more was applied to the same spot. Once the sample was completely dry, the plate was placed in a development chamber with the development solution. Development was stopped once the solvent front had migrated to approximately 1 inch from the top of the plate. The plate was taken out of the chamber and placed on filter paper. The assembly was placed in a vacuum hood so that it could dry completely. The TLC plate was secured to the filter paper with tape. Plastic wrap was placed on top of the plate. The assembly was placed in an exposure cassette with film on top of it (Kodak Biomax MS). The cassette was placed in the -80°C freezer for 1-2 weeks.

## HPLC

Isocratic reverse phase high pressure liquid chromatography is performed on a Hewlett Packard Series 1100 HPLC. Water/0.1% TFA is phase A and acetonitrile w/ 0.1% TFA is phase B. The flow-rate is 1 mL/min with UV detection at 259 nm. The column type is C18 with the dimensions of 4.6 mm X 25 cm. Fractions are collected every 2 minutes for 146 minutes. 1/5<sup>th</sup> of the fractions are counted with a liquid scintillation counter (LSC) in 5 mL of liquid scintillation fluid (Perkin Elmer). 1/10<sup>th</sup> of the hot fraction(s) are re-injected into the HPLC and counted for a more accurate retention time. The remaining fraction is dried down and re-digested in solution. The sample is re-injected into the HPLC and 1/3<sup>rd</sup> is counted by LSC. Results are graphed by time in minutes versus amount of radioactivity in counts per minute or CPM.

RETENTION TIME	% MOBILE PHASE B
0	0
3	0
93	60
113	90
116	100
126	100
136	0
146	0

**Table 2-1. HPLC Gradient Description of Sara3 Method.** This table shows the gradient used to separate hDAT peptides following primary and secondary enzymatic digestions and chemical cleavages.

### **SDS-PAGE of Extracted hDAT Peptides**

The digestion extracts, which were 1/5<sup>th</sup> of the total peptide content, were separated by low molecular weight SDS-PAGE (BioRad 4-20% Tris-Cl polyacrylamide mini-gels). Rainbow markers (Amersham) were used as a standard to measure low molecular weights. The gradient gels were dried down, placed on film and incubated at 80°C for times depending on the activity of the ligand.

### **Solid-State Photolabeling of hDAT with Radioligands**

Solid-state photolabeling was accomplished in low yield by preparing a solution of the radioligand in methanol or ethanol. The amino acids, tyrosine, leucine and methionine, as well as DAT peptide sequence, PLFYM, were used in a final concentration of 1M. The radioligand was applied directly to the appropriate weight of the amino acid then incubated for 1 hour. The mixture was placed into a 48 well plate and allowed to evaporate to dryness in the dark. Then the thin layer of amino acid and ligand was irradiated for 4 minutes using the same conditions as for the photolabeling of hDAT. 200uL of methanol was added to dissolve the products for HPLC separation and fraction collection. The fractions were collected directly into the liquid scintillation vials and 5 mL of Liquid Scintillation Fluid was added before counting.

### **General Protein/Mass Analysis for Windows (GPMAW)**

The GPMAW program is a tool for mass spectrometric analysis of proteins and peptides. However, other bioinformatics tools have been included. The current program allows sequences to be downloaded from local databases, cleaved by automatic and

manual methods, displayed by mass, HPLC retention time, charge, etc., and hydrophobicity plots and secondary structures can be generated and predicted, respectively (<http://welcome.to/gpmaw/>).

The entire sequence of FLAG-HIS-hDAT is saved into the GPMAW database and retrieved for analysis. Digestions are simulated via automatic or manual cleavages and at least 5-10 missed cleavages are taken into account. For primary digestions, more missed cleavages are taken into account because of the hydrophobic nature of the protein. For secondary digestions, less missed cleavages can be considered because hot hDAT peptides have been separated from the original sample of several mixes of protein and can be more easily accessed by the enzyme.

In table 2-2, the types of enzymes or chemicals that were most commonly used as well as the codes that were inputted into the software are listed. Typically, trypsin digestions were done first followed by a cyanogen bromide cleavage. The software was programmed to omit cleavages of residues next to a proline in the trypsin digestions.

<b>TYPE OF ENZYME/CHEMICAL</b>	<b>CLEAVAGE</b>
<b>TRYPSIN</b>	<b>/K/R-P</b>
Thermolysin	-I/L/F/V
Chymotrypsin	/W/Y/F-P
<b>CNBr</b>	<b>/M</b>

**Table 2-2. GPMAW Codes for Theoretical Proteolytic Digestions.** GPMAW makes simulated cleavages of the protein based on the following codes: “/” denotes that the following residue is necessary for cleavages, “\” denotes that the following residue prohibits cleavage, and “-“ denotes the cleavage position. The bold lettering and grey shading indicates the main proteolysis that were performed in this dissertation.

Once a series of peptides are generated for a particular cleavage mechanism, the retention times from the HPLC gradients can be determined by programming in the solvents. Comparison of HPLC data and GPMAW peptides are done in an attempt to identify the labeled hDAT peptide.



## Results

## Introduction to the Results

The human dopamine transporter (hDAT) was labeled with the GBR analog, [<sup>125</sup>I]-DEEP, the rimcazole analog, [<sup>125</sup>I]-JJC 3-24 and aryltropane cocaine analog, [<sup>125</sup>I]-RTI-82. While an amino acid residue was not identified as being covalently bound to either ligand, significant progress was made with [<sup>125</sup>I]-DEEP. Therefore, the results presented here are a summation of information that was learned while pursuing the localization of the cocaine binding site of the human dopamine transporter by DAT photoaffinity labels.

The human dopamine transporter protein or hDAT was labeled with photoaffinity labels, [<sup>125</sup>I]-DEEP and [<sup>125</sup>I]-RTI-82 in order to determine whether they shared the same binding site as cocaine. Therefore, hDAT was incubated with 10mM WIN 35, 428, a potent cocaine inhibitor, prior to photolabeling with [<sup>125</sup>I]-DEEP or [<sup>125</sup>I]-RTI-82. Both of these radioligands were unable to label the hDAT membranes that were pre-incubated with WIN 35, 428. This suggests that the photoaffinity labels, [<sup>125</sup>I]-DEEP and [<sup>125</sup>I]-RTI-82 are also labeling at or near the cocaine binding site.

[<sup>125</sup>I]-DEEP was used in the generation of smaller peptides of labeled hDAT. Primary digestions of [<sup>125</sup>I]-DEEP labeled hDAT were done with trypsin, followed by secondary digestions of the labeled peptides with CNBr. This secondary digestion suggested that following a tryptic digestion, the [<sup>125</sup>I]-DEEP labeled peptide contained a methionine residue as shown by a shift in the radioactivity using Thin Layer Chromatography (TLC).

Solid-state reactions with amino acids and peptides were performed with [<sup>125</sup>I]-DEEP and [<sup>125</sup>I]-JJC 3-24. This method proved to be a promising technique for

understanding how the hydrophobic photoaffinity ligands of DAT affected the retention times of peptides and amino acids. In order to determine the true retention times of possibly labeled peptide sequences, it was important to know that shifts can occur leading to longer HPLC retention times of small molecules.

The effect of irradiation was tested on [ $^{125}\text{I}$ ]-DEEP. It was determined that the radiolabel was fragmented during the irradiation. The photoreactive portion of the radioligand is an azide which can react with itself to form a dimer upon irradiation (Schrock & Schuster 1984). However, there was also the presence of a highly radioactive molecule at approximately 4 minutes. This 4 minute peak may be the radioactive iodine breaking from the radioligand during irradiation.

The effect of proteolytic conditions was also studied. A 100mM concentration of ammonium bicarbonate (AMBIC), pH 8.9 is used during the enzymatic digestions with trypsin. The application of AMBIC during the digestions to labeled hDAT does not show any cleavage to smaller fragments. However, 70% TFA, v/v, does show a shift of radioactivity on the gel to the lower molecular weight range, signifying that the labeled hDAT protein had been cleaved. An experiment to test the effect of CNBr conditions was done on the radioligands, [ $^{125}\text{I}$ ]-DEEP and [ $^{125}\text{I}$ ]-JJC 3-24. A concentration of 100mM CNBr/70% TFA and 70% TFA was added to the radiologands. It appears that 70% TFA causes the break-up of [ $^{125}\text{I}$ ]-DEEP into fragments as well as produces the 4 minute peak that could be radioactive iodine.

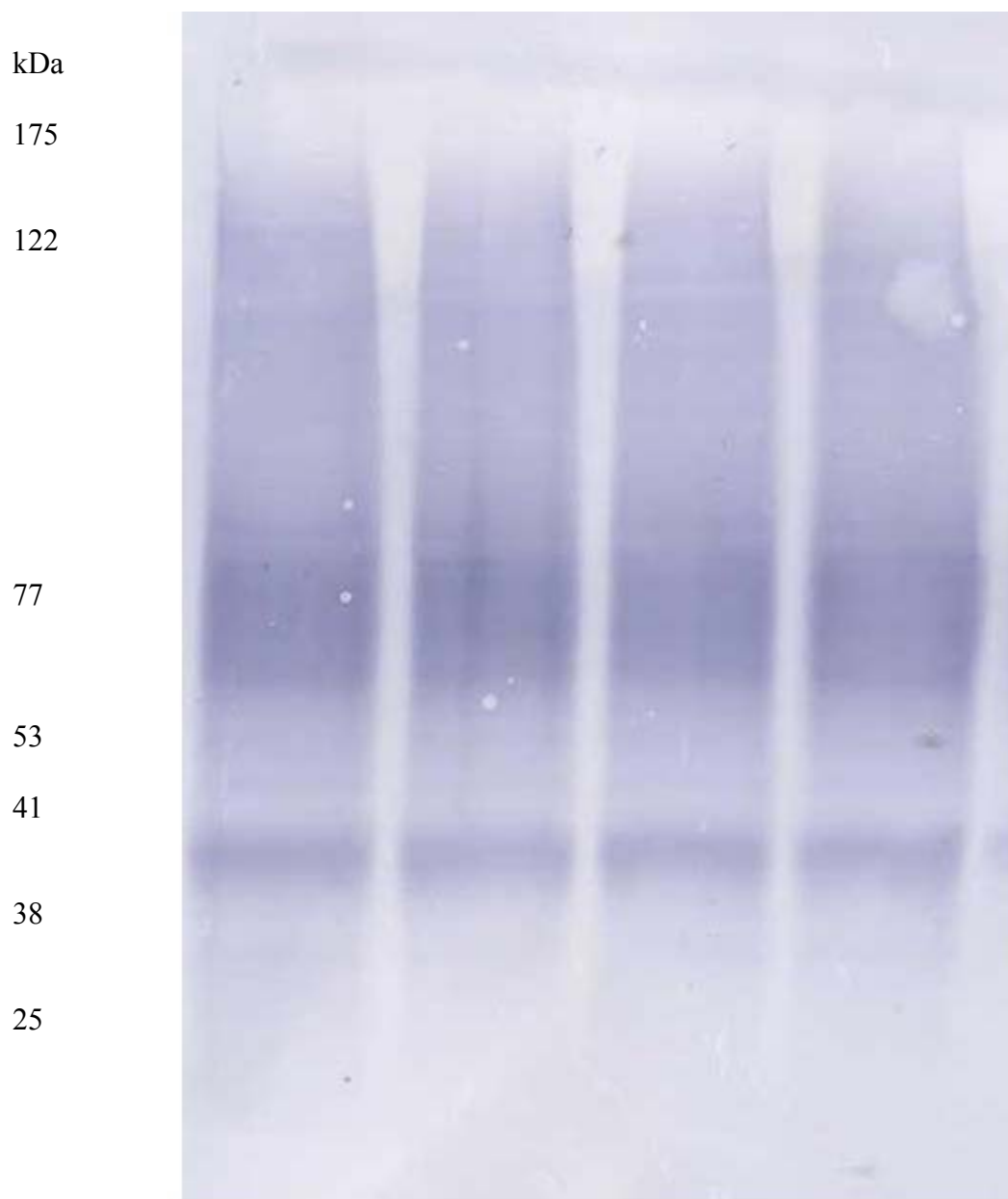
[ $^{125}\text{I}$ ]-JJC 3-24 is a rimcazole analog that is very similar in structure to [ $^{125}\text{I}$ ]-DEEP. It has been shown to label hDAT at a 50 nM concentration. Not much has been published regarding [ $^{125}\text{I}$ ]-JJC 3-24 since its ability to be a DAT photolabel was reported

in 2004 (Cao *et al.*, 2004). However, it fragments into tryptic peptides that are the same size as [<sup>125</sup>I]-DEEP labeled hDAT. It also cleaves into smaller peptides using CNBr as shown by an HPLC of a primary chemical cleavage. Therefore, more information can be obtained using the methodology employed with [<sup>125</sup>I]-DEEP.

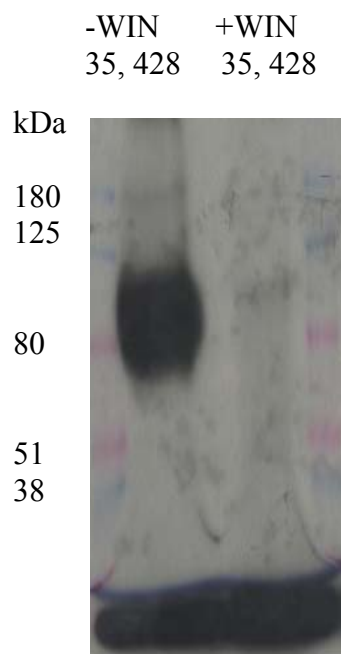
### **Suitability of Photoaffinity Labeling Experimental Conditions**

hDAT was purified with a nickel affinity column. The histidine tag engineered onto the N-terminal end of the protein allowed for the separation of hDAT from other proteins in the membrane preparation by means of immobilized affinity chromatography (IMAC). An antibody directed towards the C-terminal end of hDAT was used to probe the membrane of the western blot. A western blot of the purified elutions from the IMAC column show clearly that hDAT is the ~80 kDa band that is seen on the gels.

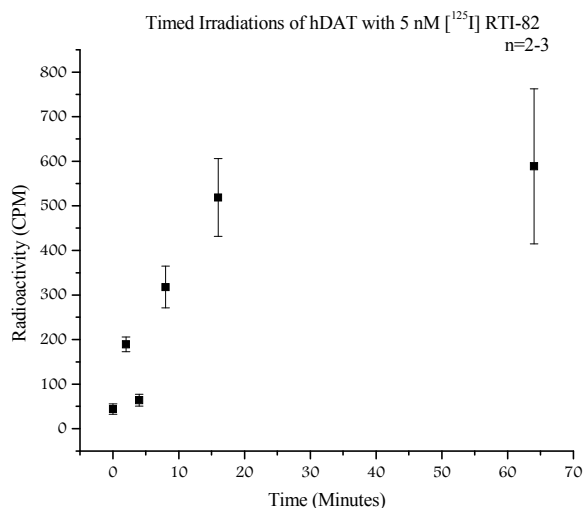
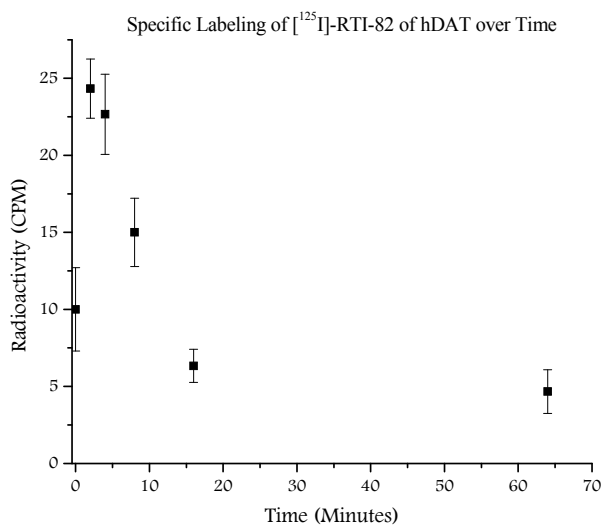
Photolabeling with hDAT radioligands is done via irradiation at 254 nm for four minutes. The optimal time of irradiation was tested with [ $^{125}$ I]-RTI-82, an aryltropane cocaine analog. Total labeling was measured by counting the levels of radioactivity from radiolabeled hDAT over time. Non-specific labeling was measured by irradiating hDAT with [ $^{125}$ I]-RTI-82 following pre-incubation with WIN 35, 428, a potent DAT inhibitor and cocaine analog, over time. The specific labeling of hDAT by [ $^{125}$ I]-RTI-82 was calculated by subtracting the counts of radioactivity of the non-specific labeling from the total labeling. The specific labeling was plotted over time to determine the optimal time for irradiation with DAT photolabels.



**Figure 2-3. Western Blot of Purified hDAT.** Western Blot of hDAT membranes following purification with a nickel column shows that hDAT is ~80 kDa on a 7.5% polyacrylamide gel. All lanes shown above are the same.



**Figure 2-4. [<sup>125</sup>I]-RTI-82 Labels Near the Cocaine Binding Site.** [<sup>125</sup>I]-RTI-82 specifically labels hDAT as shown by the 80 kDa marker. The left side of the gel shows [<sup>125</sup>I]-RTI-82 irradiated with hDAT. The right side of the gel shows [<sup>125</sup>I]-RTI-82's inability to label hDAT in the presence of 10mM WIN 35, 428, an inhibitor of hDAT.

**A.****B.**

**Figure 2-5. Time-Dependent Irradiations with [ $^{125}$ I]-RTI-82.** **A.** Timed irradiations of [ $^{125}$ I]-RTI-82 show that the total labeling of hDAT is increased over time. However, when the amount of total labeling is subtracted by the amount of non-specific labeling as determined by radiolabeling in the presence of 10mM WIN 35, 428, the amount of specific labeling is determined. **B.** The specific labeling of hDAT decreases as the irradiation time increases, although total labeling increases over time. Therefore, 4 minutes is an appropriate time of irradiation for specific labeling of hDAT.



## **Investigations into Localizing the Cocaine Binding Site with the GBR Analog, [<sup>125</sup>I]-DEEP**

[<sup>125</sup>I]-DEEP was used to photolabel hDAT in a means to narrow its region of incorporation on the hDAT protein. Intact hDAT was photolabeled and subjected to an initial digestion with trypsin. The radiolabeled peptide was collected following separation of the peptides by HPLC. A secondary digestion of the tryptic peptides were done with cyanogen bromide (CNBr). These peptides were separated by HPLC and the retention time of the fraction where the radioactivity was located was identified by radioactive counting using a liquid scintillation counter. TLC of the secondary digest was also done to determine the presence of a methionine residue in the primary pool of tryptic peptides.

Initial digestions of [<sup>125</sup>I]-DEEP labeled hDAT was performed with cyanogen bromide. Secondary digestions of the CNBr generated peptides were done and separated using TLC to determine whether there was a tryptic cleavage site within the primary pool of CNBr peptides.

Solid-state labeling with amino acids was done to determine the effect of the hydrophobic [<sup>125</sup>I]-DEEP on the retention time of single amino acids. Methionine, tyrosine and leucine were potential amino acids labeled by [<sup>125</sup>I]-DEEP within the hypothesized labeled peptide based on HPLC results and comparisons with GPMAW software. The shifts of the amino acid retention time were determined by the elution of radioactivity from HPLC separation after the irradiation of the ligand with the amino acids.

The effect of irradiation and proteolytic conditions was tested on the [ $^{125}\text{I}$ ]-DEEP photolabel. There was concern that decomposition of the label could be occurring during the irradiation leading to lower amounts of hDAT being labeled. There was also reason to believe that the proteolytic conditions used after the photolabeling was decomposing the product formed and the radioactive portion of the photolabel. The effects of the irradiation and the solution used in the CNBr cleavages were tested with the photolabel. Probing into the decomposition of product using proteolytic conditions will be explored more in Chapter Three.

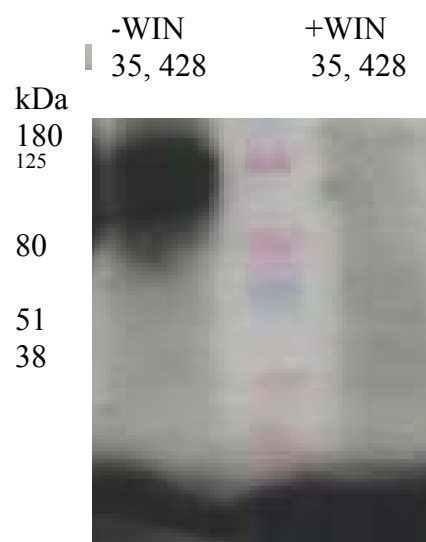


**Figure 2-6. [<sup>125</sup>I]-DEEP Labels Near the Cocaine Binding Site.** [<sup>125</sup>I]-DEEP specifically labels hDAT as shown by the 80 kDa marker. The left side of the gel shows [<sup>125</sup>I]-DEEP irradiated with hDAT. The right side of the gel shows [<sup>125</sup>I]-DEEP's inability to label hDAT in the presence of 10 mM WIN 35, 428, an inhibitor of hDAT.

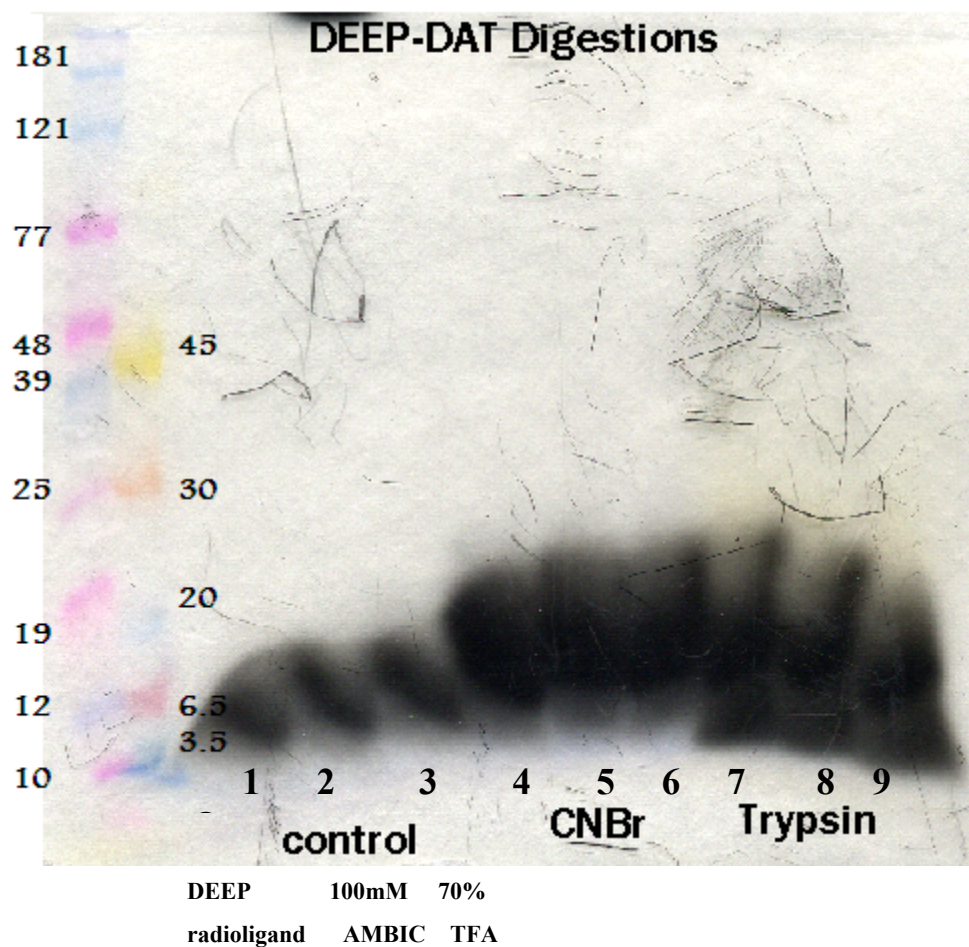


**Figure 2-7. Primary Proteolytic Digestions of [<sup>125</sup>I]-DEEP Labeled hDAT.** Primary CNBr cleavage and tryptic digestion produce nearly the same size peptides with [<sup>125</sup>I]-DEEP labeled hDAT. Trypsin was decided to be the main primary digest used because the peptides proposed to be formed from a CNBr cleavage generated large hydrophobic portions of hDAT which could get stuck on the HPLC column. Lane Assignments: 1- [<sup>125</sup>I]-DEEP alone; 2-[<sup>125</sup>I]-DEEP hDAT treated with 100mM ammonium bicarbonate treated 24 hours at 37<sup>0</sup>C; 3-[<sup>125</sup>I]-DEEP hDAT treated with 70% TFA for 24 hours in the dark at room temperature; 4, 5, 6-CNBr digestion of -[<sup>125</sup>I]-DEEP hDAT; 7, 8, 9- 10mg/mL trypsin digestion of [<sup>125</sup>I]-DEEP hDAT .

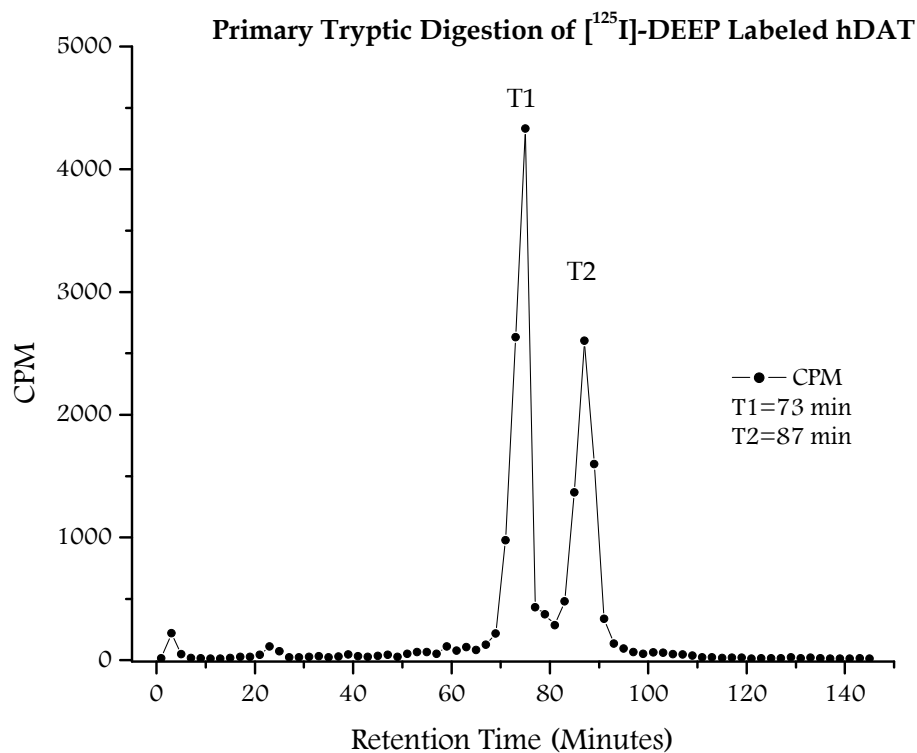


**Figure 2-8. HPLC of Primary Tryptic Digestion of [<sup>125</sup>I]-DEEP hDAT.** Primary trypsin digestion of DEEP labeled hDAT yields two peptides with retention times of 73 (T1) and 87 (T2) minutes. This is one representative spectrum of the tryptic digestions performed on DEEP labeled hDAT. This experiment was performed at least three times with similar results.



**Figure 2-9. TLC Separation of Secondary Digestions of [ $^{125}$ I]-DEEP hDAT.**

Secondary digestions of DEEP labeled hDAT analyzed using Thin Layer Chromatography (TLC). This figure shows that there is the presence of methionine in the primary digested tryptic radioactive fraction (2a) redigested with CNBr (2b) because of the shift on the TLC plate. There are also tryptic cut sites located within the primary cleaved CNBr radioactive fraction (3a) that was redigested with trypsin (3b).

Abbreviations: Con is the control of [ $^{125}$ I]-DEEP hDAT. T-C is the primary tryptic digestion. T-CN is the primary tryptic digestion followed by a cyanogen bromide cleavage. CN-C is the primary cyanogen bromide cleavage of [ $^{125}$ I]-DEEP hDAT. CN-T is the primary cyanogen bromide cleavage followed by a tryptic digestion.

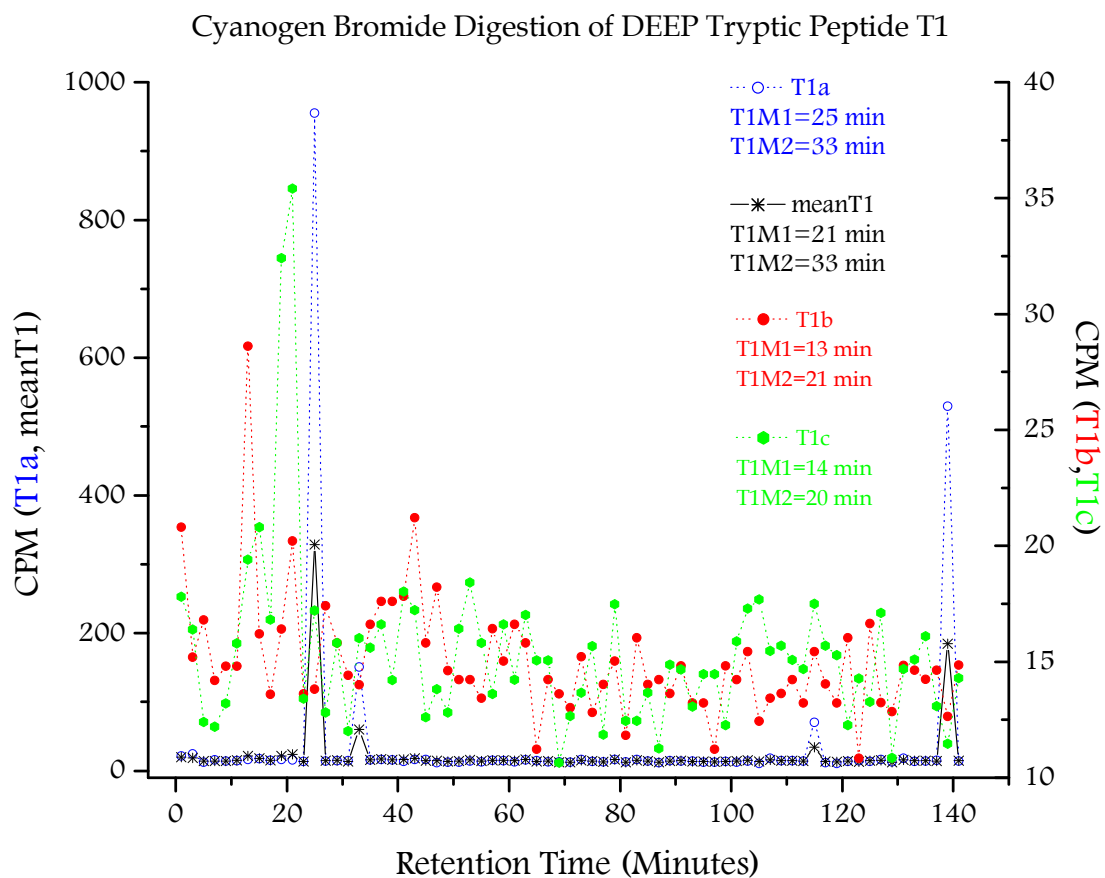


**Figure 2-10. HPLC Analysis of Secondary CNBr Digestion of Tryptic Peptide, T1.**

CNBr cleavage of [ $^{125}$ I]-DEEP tryptic peptide T1 ( $t=73$  min) fragments into two at retention times of 21 (T1M1) and 33 (T1M2) minutes. The nomenclature TXMY means that the ‘T’ is a primary tryptic digestion, ‘X’ is the fragment number based on the original HPLC analysis, ‘M’ in this position means that it was a secondary CNBr digestion, which cleaves methionines, hence the letter M, and ‘Y’ is the fragment number that is being described following CNBr cleavage and HPLC analysis.

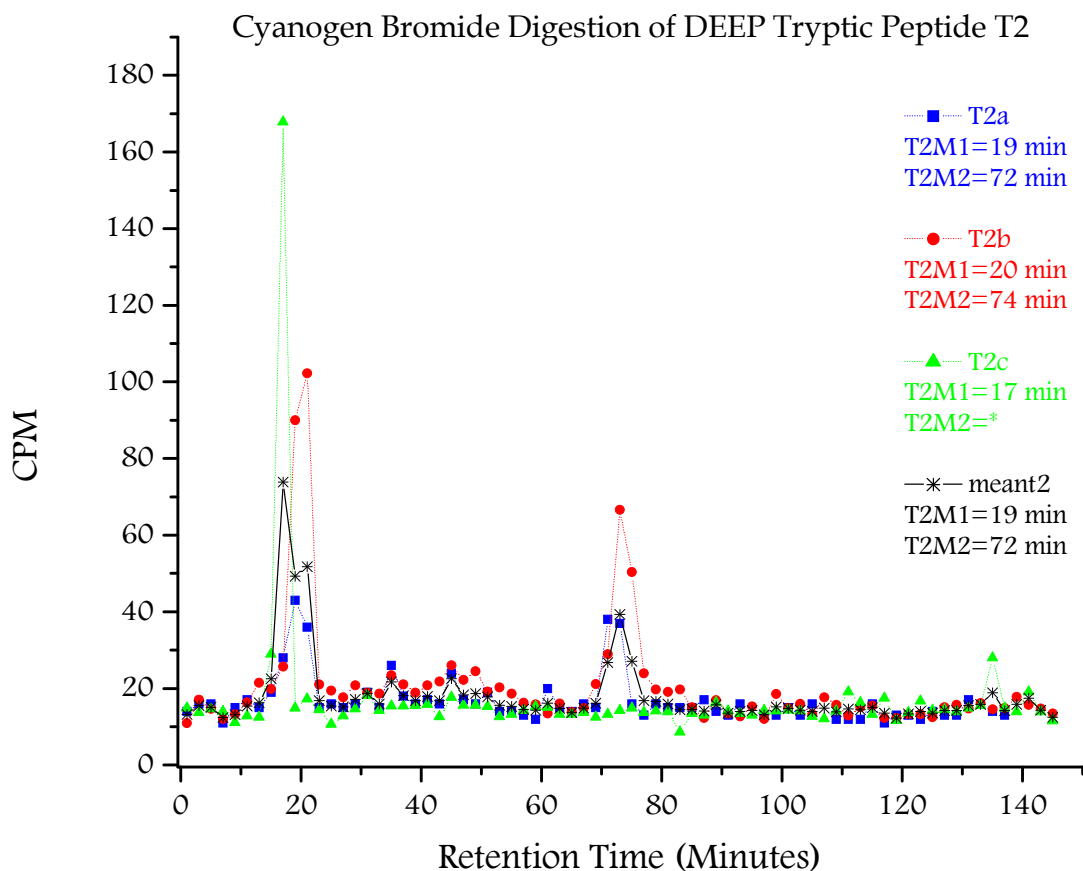


**Figure 2-11. HPLC Analysis of Secondary CNBr Digestion of Tryptic Peptide, T2.**

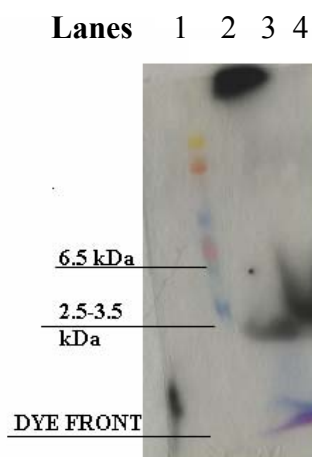
Cyanogen bromide cleavage of [<sup>125</sup>]- DEEP tryptic peptide T2 (87 mins). Tryptic peptide T2 from the primary digestion was cleaved by CNBr yielding peptide fragments eluting from the HPLC at times 19 and 72 minutes. It is possible that this fragment contained peptide T1 (73 min) because T2M2's retention time overlaps that of T1 at time 72 minutes. Therefore, T2 was possibly a longer peptide containing the sequence of T1 within it.



PEPTIDE T=Tryptic M=CNBr cleavage TXMY=Primary Tryptic, Secondary CNBr	EXPERIMENTAL RETENTION TIME (Minutes)
<b>T1</b>	<b>73</b>
T1M1	21
T1M2	33
<b>T2</b>	<b>87</b>
T2M1	19
T2M2	72

**Table 2-3. Summary of Peptides from Primary and Secondary Digestions of [<sup>125</sup>I]-DEEP labeled hDAT.** Primary trypsin digestion of [<sup>125</sup>I]- DEEP labeled hDAT gives two radioactive fragments, T1 and T2. T1 and T2 fragments into two smaller peptides each following CNBr cleavage.

A.



B.

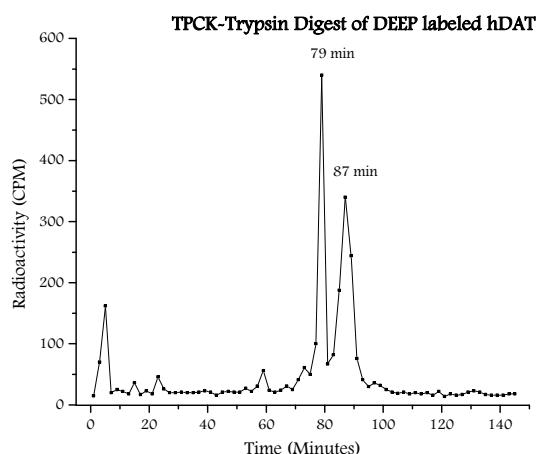


**Figure 2-12. Primary Digestion of [<sup>125</sup>I]-DEEP labeled hDAT with Trypsin-TPCK.**

**A.** 7.5% SDS-PAGE of tryptic-TPCK peptides of DEEP hDAT. The digestion yielded peptides that were 2.5-6.5 kDa in size. Lanes 1-4 are as follows: 1: low molecular weight marker, 2: undigested [<sup>125</sup>I]-DEEP labeled hDAT, 3: [<sup>125</sup>I]-DEEP radiolabel only, 4: Trypsin-TPCK digested [<sup>125</sup>I]-DEEP labeled hDAT. **B.** HPLC Chromatogram of DEEP labeled hDAT primarily digested with 10mg/mL of trypsin-TPCK, an enzyme that eliminates chymotrypsin activity. The retention times of two radiolabeled fragments eluted at retention times 79 and 87 minutes. When compared with the regular tryptic

digestion that was performed, the 79 minute peak from trypsin-TPCK must contain a chymotryptic cut site (W, F, Y) (Table 2-2) because with the regular trypsin, it shifted to 73 minutes.

## Solid-State Photoreactions of [ $^{125}\text{I}$ ]-DEEP and Amino Acids

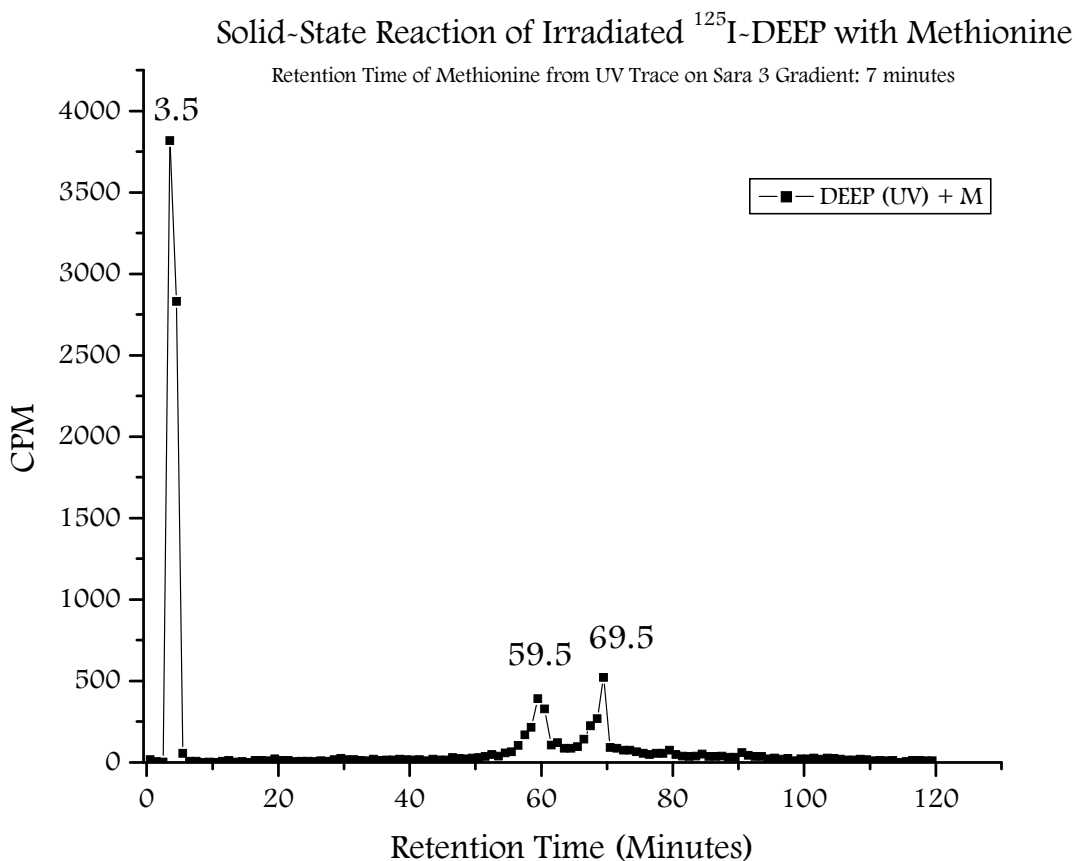


**Figure 2-13. HPLC Radioactive Trace of [ $^{125}\text{I}$ ]-DEEP Irradiated with Methionine.**

Solid-state photolabeling of the amino acid methionine yields hot fractions eluting at retention times 60 and 70 minutes. There is a very hot fraction at 4 minutes that may be the irradiated ligand breaking up into radioactive iodine. Methionine has a retention time of 7 minutes using the same gradient. Therefore, the shift for methionine went from 7 minutes to 60 and 70 minutes, which are closer to the retention times of the ligand reacting with itself upon irradiation. The ligand alone elutes at 71 minutes and breaks into retention times of 61 and 71 minutes upon irradiation. The result may suggest that the ligand has a major effect on the methionine, shifting its retention time to a longer one.

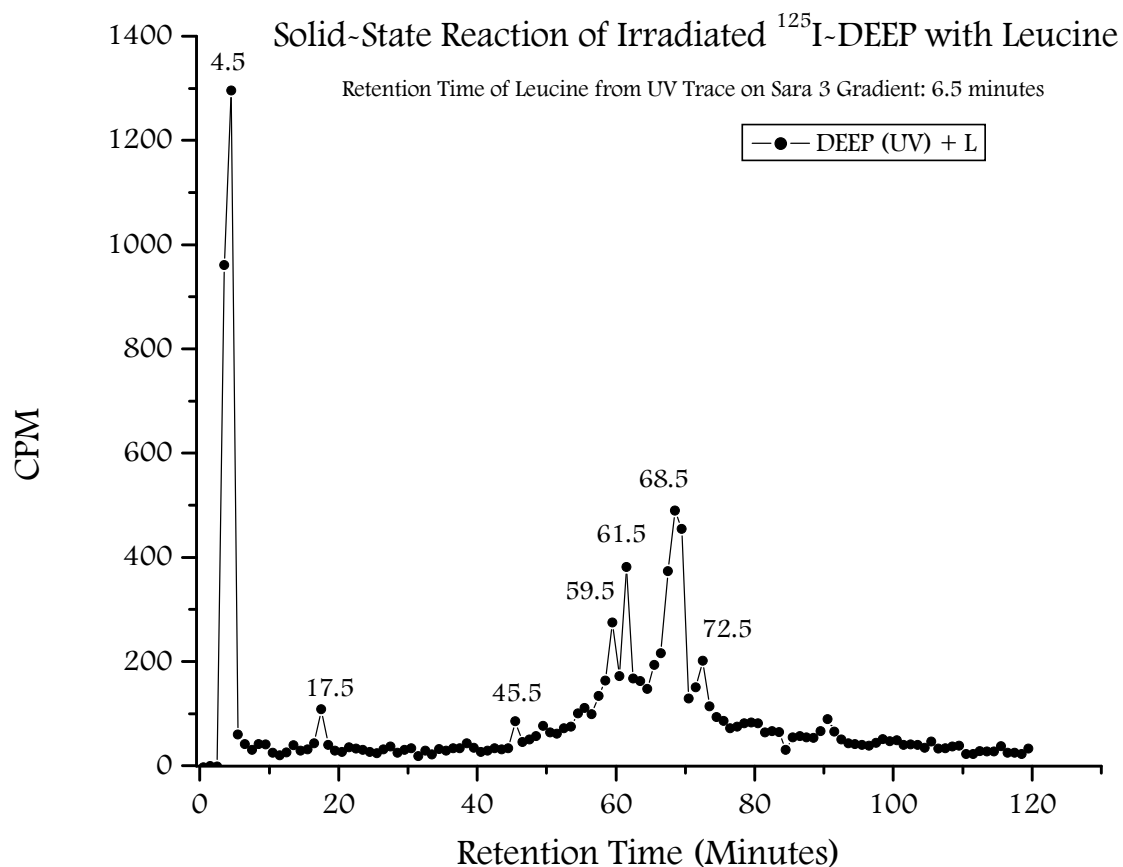


**Figure 2-14. HPLC Radioactive Trace of [ $^{125}\text{I}$ ]-DEEP Irradiated with Leucine.**

Solid state reactions with the amino acid leucine yields fragments that elute at 68.5, 61.5, 59.5, 72.5, 45.5, 17.5, and 4.5 minutes. The 4.5 minute peak is extremely hot and may be radioactive iodine that is cleaved during irradiation of the ligand with the amino acid.

The ligand alone elutes at 71 minutes and breaks into retention times of 61 and 71 minutes upon irradiation.

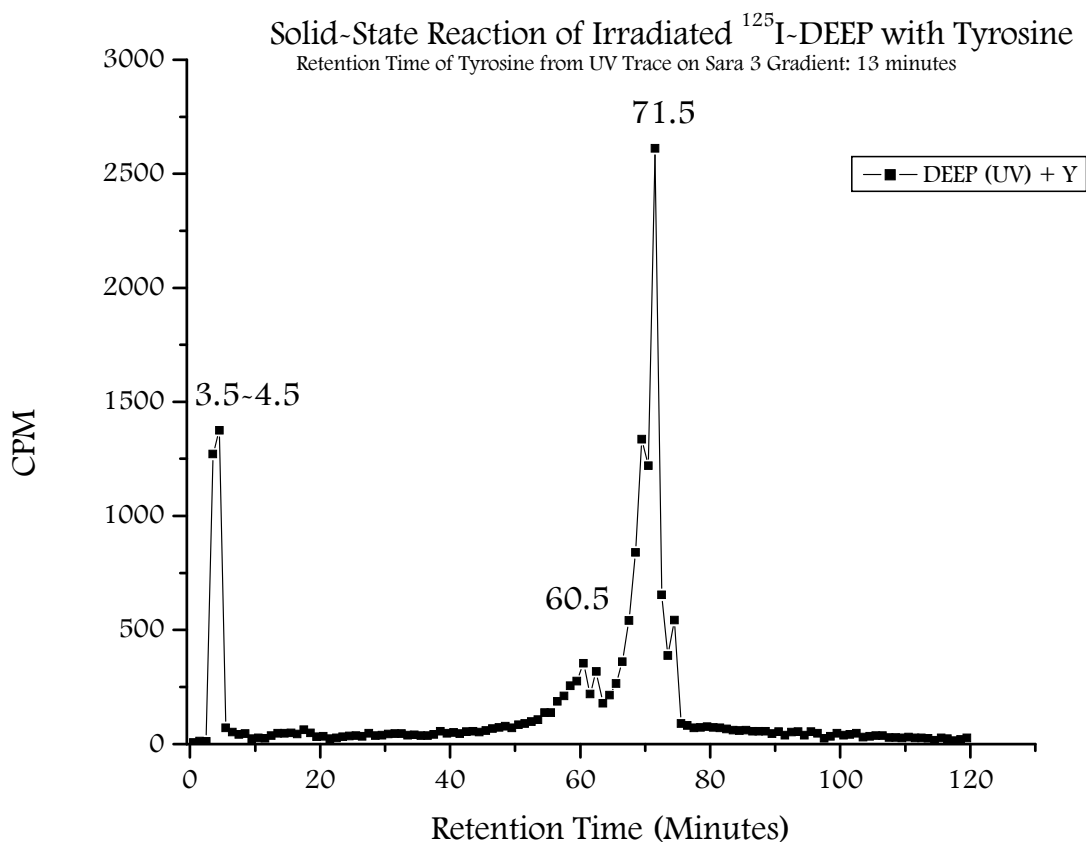
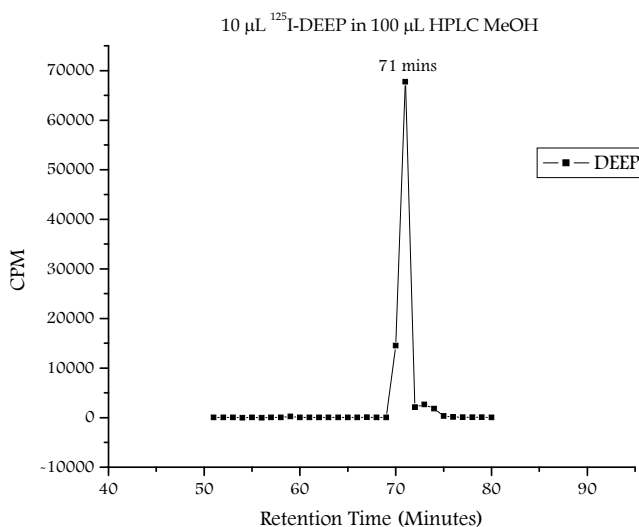


**Figure 2-15. HPLC Radioactive Trace of [ $^{125}\text{I}$ ]-DEEP Irradiated with Tyrosine.**

Solid-state reactions of DEEP with the amino acid tyrosine. This reaction yields hot peaks at 71.5, 60.5 and 3.4-4.5 minutes. The 3.5 minute peak may be the result of instability of the ligand during irradiation. Thereby, cleaving the radioactive iodine from the molecule. Tyrosine, a polar, uncharged amino acid has a retention time of 13 minutes using the same gradient. The ligand alone elutes at 71 minutes and breaks into retention times of 61 and 71 minutes upon irradiation.

## Effect of Photoaffinity Labeling Conditions on [ $^{125}\text{I}$ ]-DEEP

A.



B.

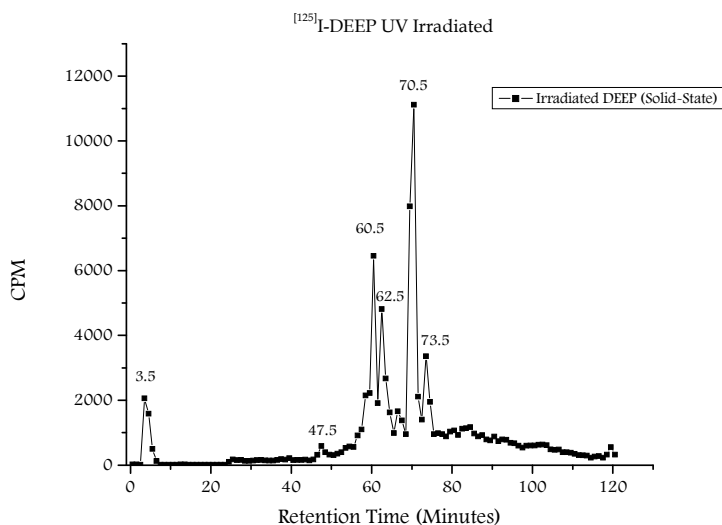


**Figure 2-16. Effect of Irradiation on [ $^{125}\text{I}$ ]-DEEP.** Photoaffinity ligand and radiolabel [ $^{125}\text{I}$ ]-DEEP breaks up upon irradiation. The top graph shows that the retention time of [ $^{125}\text{I}$ ]-DEEP is 71 minutes. Upon irradiation, the major peak of approximately 71 minutes remains but peaks at 61, 62 and 4 minutes are also hot fragments that can play a major role in the labeling of hDAT. These fragments may be decomposition of the radioligand.

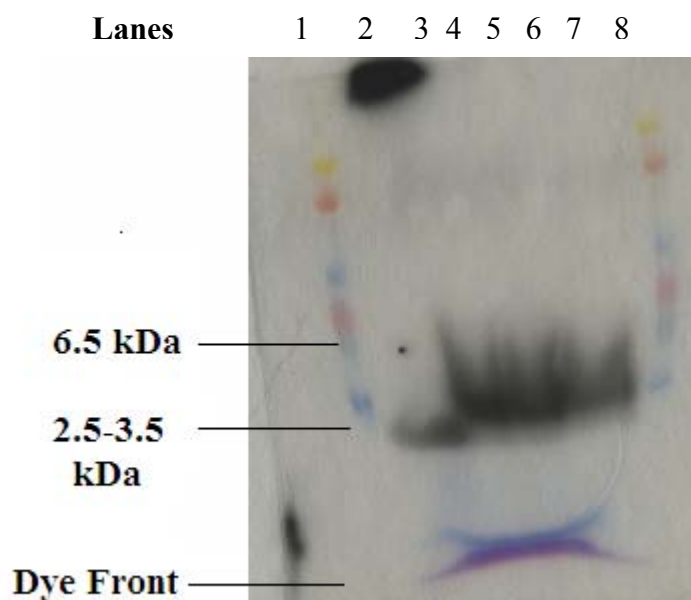
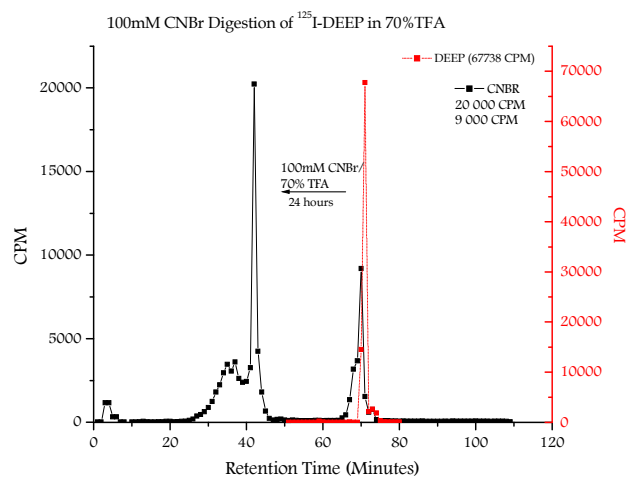


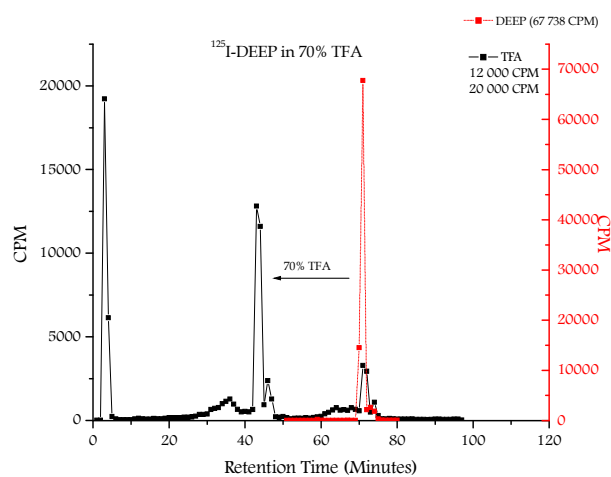
**Figure 2-17. Effect of Tryptic Conditions on [<sup>125</sup>I]-DEEP labeled hDAT.** Digestion of [<sup>125</sup>I]- DEEP labeled hDAT with Trypsin-TPCK, an enzyme with no chymotryptic activity produces more complete peptide fragments between 2.5 to 6.5 kDa in size just as the regular trypsin does. The first lane on the left is labeled hDAT incubated for 24 hours at 37°C with 100 mM ammonium bicarbonate (AMBIC). No cleavage of the labeled hDAT was seen. However, excess radioactivity was seen above the dye front, which can result from the decomposition of the ligand. Lanes 1 & 8: Low molecular weight markers, 2: Undigested [<sup>125</sup>I]-DEEP labeled hDAT, 3-7: TPCK-Trypsin digested [<sup>125</sup>I]-DEEP labeled hDAT.



A.

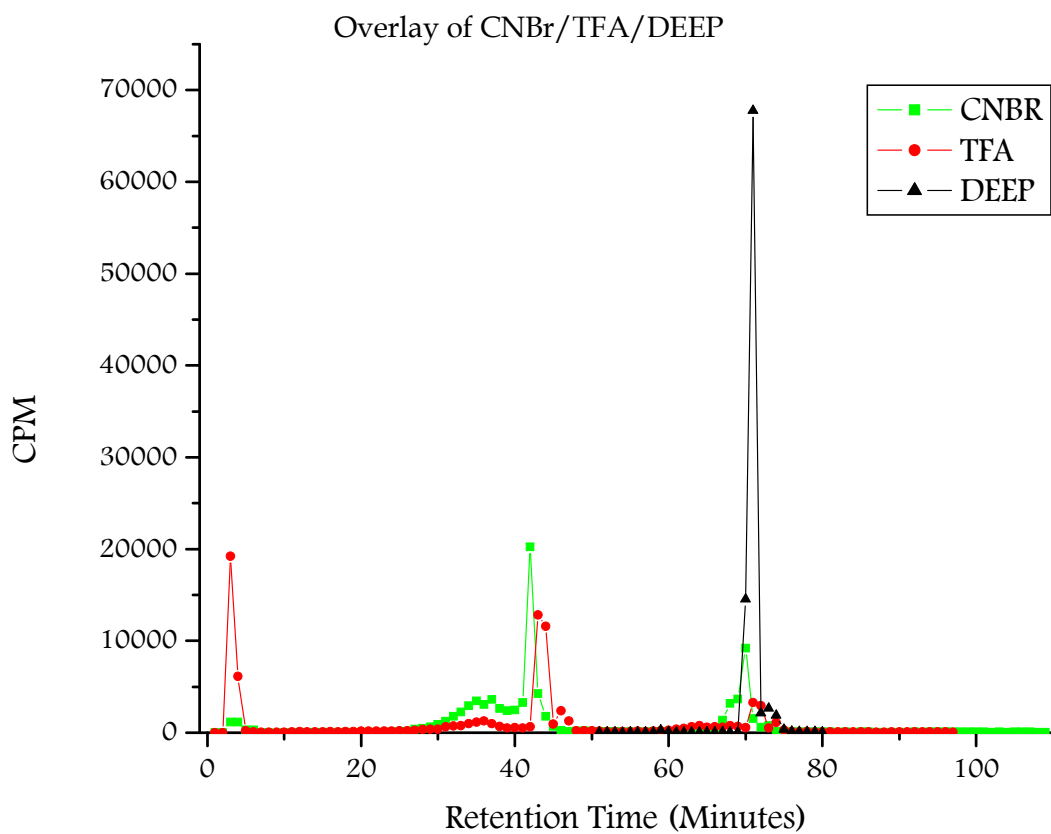


B.



**Figure 2-18. Effect of CNBr/TFA Solution on the Photoaffinity Label [ $^{125}\text{I}$ ]-DEEP.**

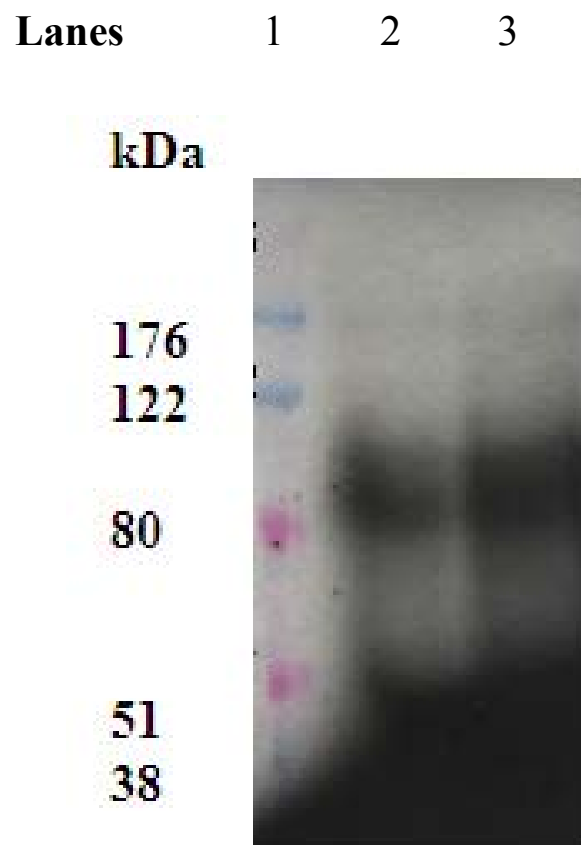
The top graph (A) shows [ $^{125}\text{I}$ ]- DEEP following application of CNBr/70% TFA for 24 hours at 25<sup>0</sup>C. The bottom graph (B) shows [ $^{125}\text{I}$ ]- DEEP following the application of 70% TFA. The radioactivity of the ligand along with the retention time of the ligand is compromised following both applications. Thereby suggesting that the shift of the label's retention time is due to the 70% TFA.



**Figure 2-19. TFA causes Decomposition of [ $^{125}\text{I}$ ]-DEEP Photolabel.** Overlay of the CNBr/TFA/DEEP chromatograms. The shift in retention time of DEEP seems to be due to the trifluoroacetic acid (TFA) and not necessarily the CNBr.

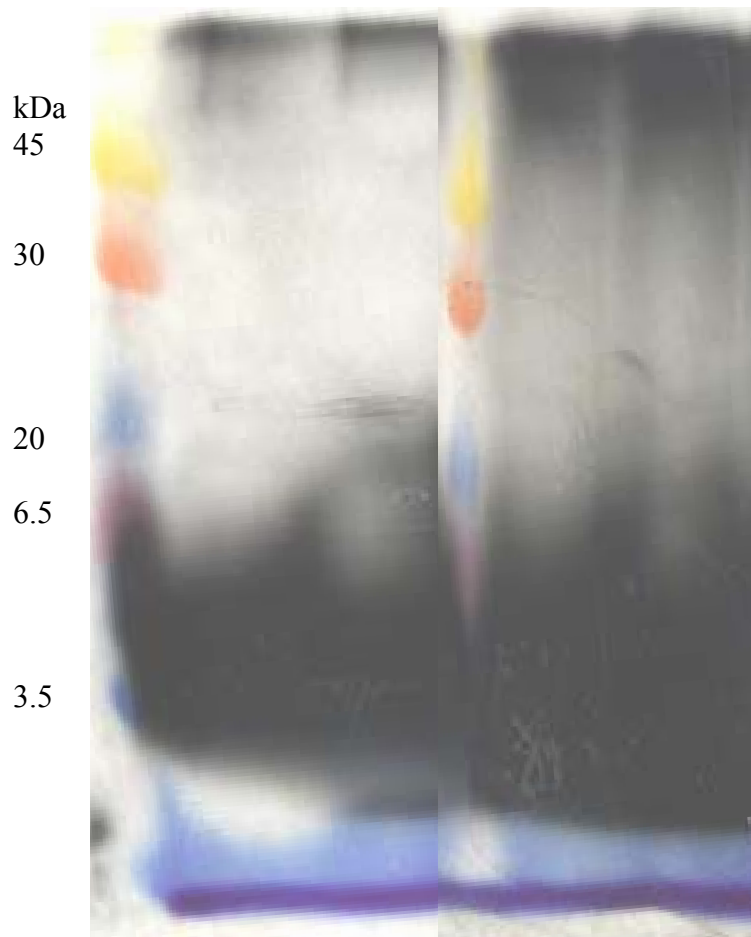
### **Preliminary Investigations of [<sup>125</sup>I]-JJC 3-24, a Rimcazole Photolabel of DAT**

[<sup>125</sup>I]-JJC 3-24, a rimcazole analog and inhibitor of hDAT was synthesized by Amy Hauk Newman of the Medicinal Division of NIDA in an effort to identify other inhibitors of DAT that may be useful for exploring the cocaine binding site of the human dopamine transporter (hDAT) (Newman & Kulkarni, 2002). Rimcazole has been shown to reduce the effects of cocaine (Katz *et al.*, 2003) and in animal models, analogs of rimcazole have been shown to be extremely effective at blocking the convulsions caused by cocaine overdose (Matsumoto *et al.*, 2001), characteristics that make it an analog worth pursuing as a photoaffinity ligand of hDAT. M. Holmes and Dr. A. Pham applied the techniques used in this research to determine that [<sup>125</sup>I]-JJC 3-24 labels hDAT (Cao *et al.*, 2004). In this section are the follow-up experiments that were performed to further determine the usefulness of the photolabeling techniques applied to [<sup>125</sup>I]-DEEP on this DAT rimcazole analog and photolabel, [<sup>125</sup>I]-JJC 3-24.

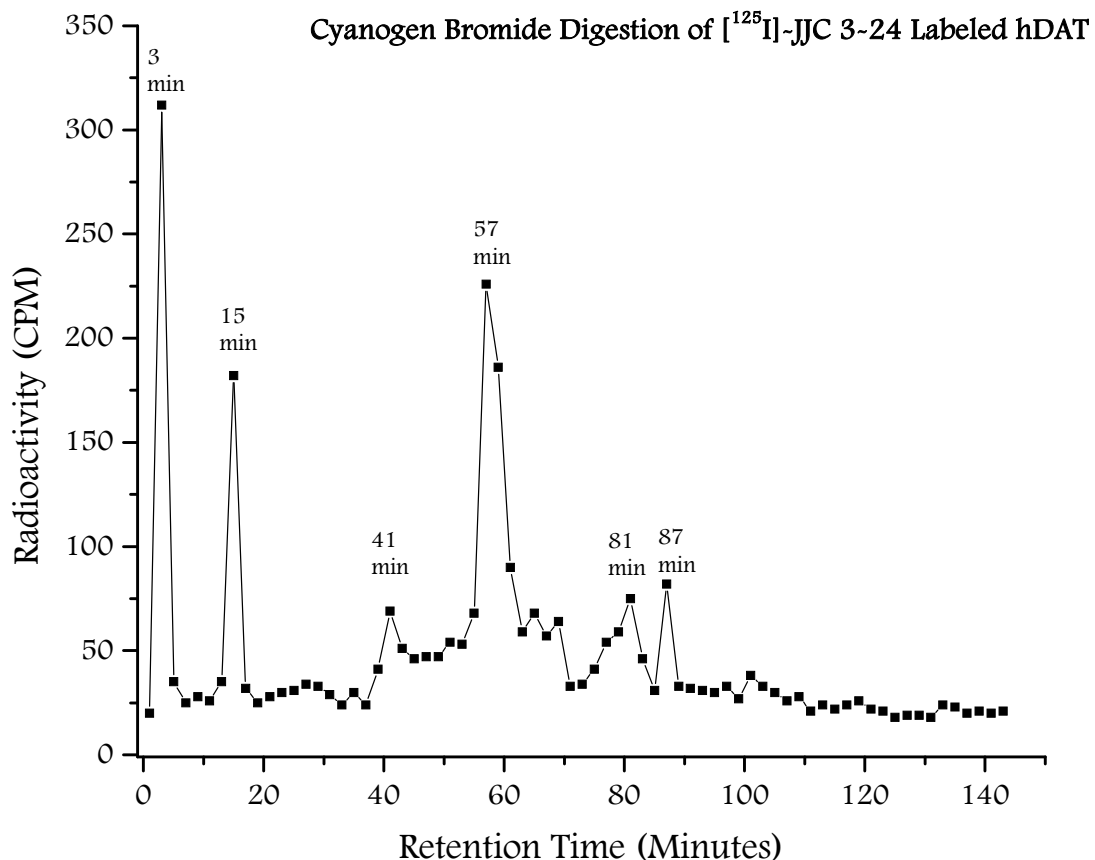


**Figure 2-20. High Concentration of [<sup>125</sup>I]-JJC3-24 Label hDAT.** [<sup>125</sup>I]-JJC 3-24 labels hDAT at a concentration of 50 nM as opposed to the 5 nM needed to label hDAT with [<sup>125</sup>I]-RTI-82 (performed by Muhsinah Holmes). This 80 kDa band was determined to be hDAT based on Western Blotting and visualization after immunoreacting with an antibody directed towards the FLAG tag on the N-terminal end of hDAT (performed by Anh Pham) (Cao *et al.*, 2004). Lanes are as follows: 1: High molecular weight marker, 2 & 3: 50 nM [<sup>125</sup>I]-JJC 3-24 labeled hDAT.

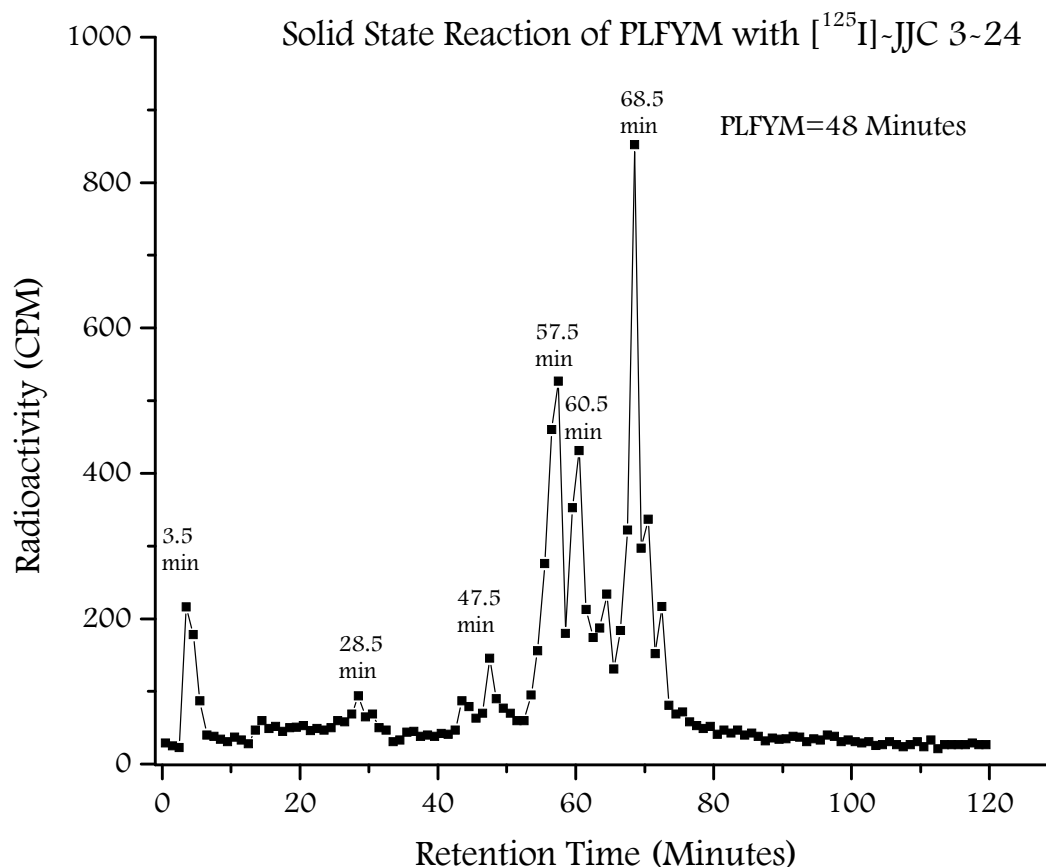
Lanes      1                      **DEEP**                      3                      4                      **JJC 3-24**                      5                      6



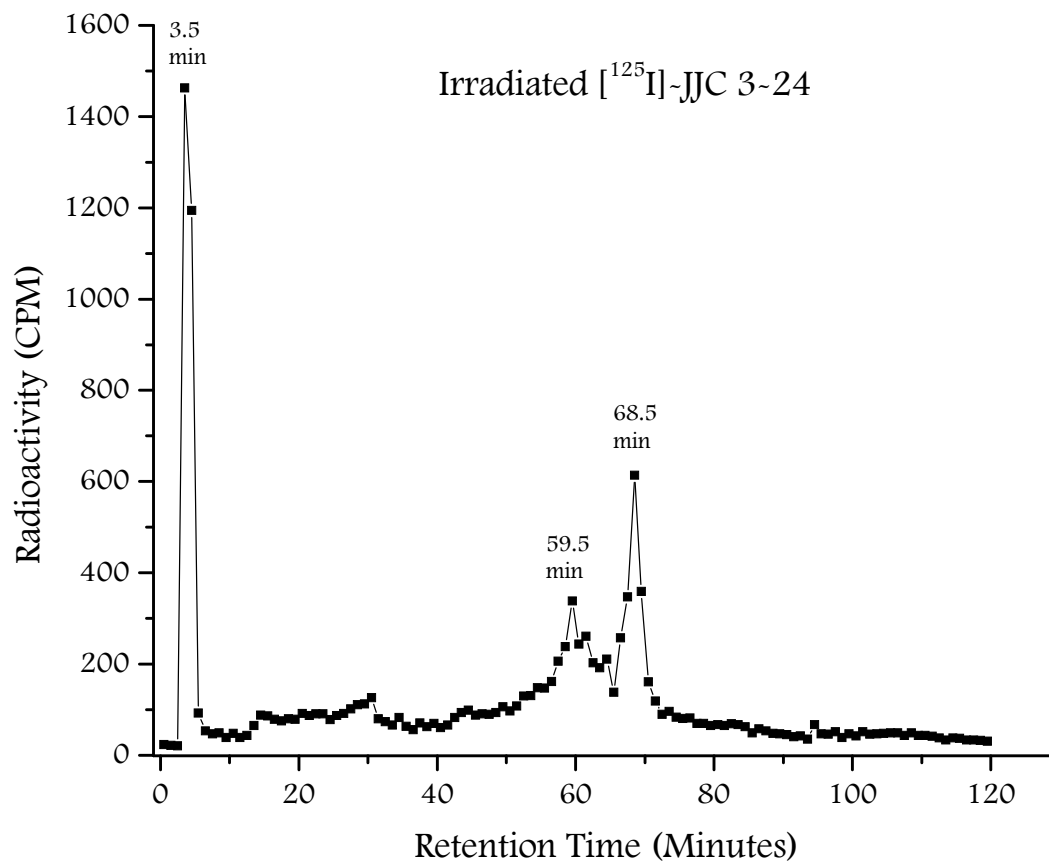
**Figure 2-21. SDS-PAGE of Primary Tryptic Digestion of hDAT Labeled with [<sup>125</sup>I]-DEEP and [<sup>125</sup>I]-JJC 3-24.** Tryptic digestion of [<sup>125</sup>I]-DEEP labeled hDAT is on the left and [<sup>125</sup>I]-JJC 3-24 labeled hDAT is on the right. The tryptic fragments of these photolabels that share the same pharmacophore as GBR analogs appear to be the same size between 3.5-6.5 kDa. There appears to be more of a less complete digestion of [<sup>125</sup>I]-JJC 3-24 labeled hDAT as shown by the streaking and the heavy band at the top of the gel. Lanes are as follows: 1 & 4: Low molecular weight markers, 2 & 3: Trypsin digested [<sup>125</sup>I]-DEEP labeled hDAT, 5 & 6: Trypsin digested [<sup>125</sup>I]-JJC 3-24 labeled hDAT.



**Figure 2-22. Primary CNBr Cleavage of [<sup>125</sup>I]-JJC 3-24 Labeled hDAT.** [<sup>125</sup>I]-JJC 3-24 has been shown to effectively label hDAT in an efficient manner. The digestion of the labeled protein with CNBr yielded several radioactive fragments at 3, 15, 41, 57, 81 and 87 minutes. Besides the extremely hot peak at a retention time of 3 minutes (300 CPM), there is another significantly hot peak at 57 minutes (225 CPM). Solid-state reactions with synthetic peptide PLFYM and [<sup>125</sup>I]-JJC 3-24 have also yielded a hot peak at 57.5 minutes that does not correspond with the irradiated label (Figure 2-25) (68.5 and 59.5 min) or the peptide (51.2 min) retention time. Besides the hot peaks at 3 and 57, there are 4 others with 15 min at 190 CPM, being the third most radioactive.

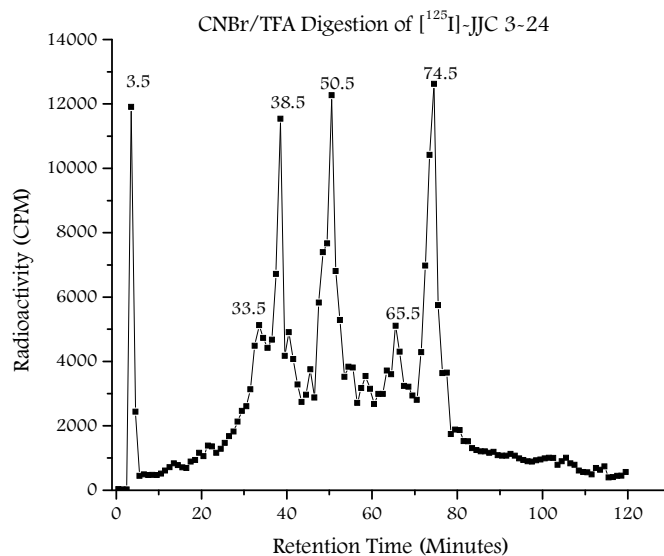
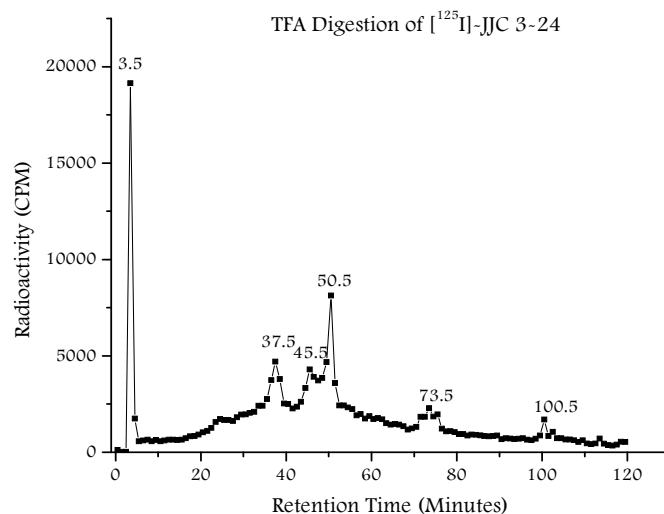


**Figure 2-23.** [ $^{125}$ I]-JJC 3-24 Labels hDAT Peptide PLFYM. hDAT transmembrane 2 peptide PLFYM was reacted with [ $^{125}$ I]-JJC 3-24 to determine how much this ligand shifts a peptide that is relevant to the protein. The peaks that were radioactive eluted at times 69, 61, 58, 48, 29, and 3.5 minutes. The three peaks that can be attributed to the ligand and irradiated ligand are at 69, 61 and 3.5 minutes. The major hot peak at 58 minutes may be a shift to the peptide, which has a retention time of 48 minutes.



**Figure 2-24. Effect of Irradiation on [<sup>125</sup>I]-JJC 3-24.** Irradiation of [<sup>125</sup>I]-JJC 3-24 fragments the label. The original retention time of [<sup>125</sup>I]-JJC 3-24 is 69 minutes. The irradiated label breaks up into 69, 60 and 4 minute peaks.



**A.****B.**

**Figure 2-25. Effect of CNBr Digestion Conditions on [<sup>125</sup>I]-JJC 3-24.** The decomposition of the rimcazole ligand, [<sup>125</sup>I]-JJC 3-24, during CNBr cleavage appears to be caused by the TFA solution. **A.** CNBr (100mM) is added to [<sup>125</sup>I]-JJC 3-24 at 25<sup>0</sup>C in the dark for 24 hours in 70% TFA. **B.** 70% TFA is applied to [<sup>125</sup>I]-JJC 3-24 at 25<sup>0</sup>C for 24 hours in the dark.

## **Discussion**

## Introduction to the Discussion

The photolabel and GBR analog, [ $^{125}\text{I}$ ]-DEEP was used to narrow its site of incorporation on hDAT. [ $^{125}\text{I}$ ]-DEEP was previously characterized (Vaughan & Kuhar, 1996) but its labeling site is unknown. In the present work, photoaffinity labeling was used in conjunction with proteolytic digestions, gel and HPLC separations to narrow the site of incorporation of [ $^{125}\text{I}$ ]-DEEP in hDAT.

The suitability of the photolabeling conditions was determined with a tropane-like cocaine analog and photolabel, [ $^{125}\text{I}$ ]-RTI-82. The analysis of this result provided the optimum time of irradiation for specific labeling of hDAT. The location of hDAT on gels was identified by directing DAT antibodies towards it.

Photolabeling of hDAT with [ $^{125}\text{I}$ ]-DEEP was followed by gel separation and then proteolysis. The hDAT peptides were separated by HPLC. The radioactivity profiles of the runs allowed determination of the retention times for the radioactively labeled hDAT peptides. The labeled peptides were collected and subjected to a secondary CNBr digestion to investigate the possible changes of the retention time of the labeled peptide. Changes in the retention time suggest that specific CNBr cut sites are present in the peptide.

Cyanogen bromide cleavage followed by a tryptic digest would indicate a tryptic cleavage site, an arginine or a lysine, in the midst of the cyanogen bromide peptide if there was a shift in the radioactivity profile. While an initial trypsin digestion followed by a CNBr cleavage would indicate the presence of a methionine residue within the tryptic peptide if there was a shift in radioactivity profile.

Photolabeling of amino acids with [ $^{125}\text{I}$ ]-DEEP was done to determine the effect of the label on the retention times of the amino acids. The label is hydrophobic and could change the retention time when attached to a single amino acid. The shifts by the label are analyzed in this discussion.

The methodology employed with [ $^{125}\text{I}$ ]-DEEP to localize the site of photoincorporation was applied to the rimcazole analog, [ $^{125}\text{I}$ ]-JJC 3-24. There are complications with [ $^{125}\text{I}$ ]-JJC 3-24 that limit its use as a photolabel of DAT, including its low affinity to hDAT compared to other DAT ligands like [ $^{125}\text{I}$ ]-DEEP and [ $^{125}\text{I}$ ]-RTI-82.

The effect of CNBr cleavage conditions were tested on the ligands, [ $^{125}\text{I}$ ]-DEEP and [ $^{125}\text{I}$ ]-JJC 3-24. Irradiation of the photolabels and treatment with CNBr in 70% TFA and 70% TFA was applied to determine if decomposition of the photolabel occurred.

In this discussion, the interpretation of results will be presented and supported by information from the experimental data and the literature. Based on the information obtained from trypsin and CNBr digests of hDAT, the labeled peptide will be tentatively identified.

## **Investigation of Photoincorporation Site of [ $^{125}\text{I}$ ]-DEEP on hDAT**

### **Suitability of Photoaffinity Labeling Experiment Conditions**

hDAT was identified as being the 80 kDa band on the gels using Western blotting with an antibody that recognizes the C-terminal end of DAT. The result confirmed that hDAT would appear on the gels at around 80 kDa (Figure 2-3).

The irradiation time for photolabeling of hDAT was chosen as 4 minutes. The confirmation that this irradiation time was optimum was done by photolabeling hDAT with

[<sup>125</sup>I]-RTI-82 at t=0, 2, 4, 8, 16, and 64 minutes in the presence and absence of WIN 35, 428 (Figure 2-5).

It was necessary to get the most labeling accomplished with minimum time because irradiation at 254 nm wavelength causes damage to proteins (Schaich, 1980). UV wavelength ranges from 100 to 400 nm, while UV-C, which is from 100 to 280 nm, causes gross alterations in protein thiol reactivity, indicative of oxidative damage (Chan *et al.*, 2006). Therefore, the least amount of time with the maximum amount of specific labeling is optimal for photolabeling studies with hDAT.

While total labeling increased over 64 minutes of irradiation, non-specific labeling also increased. Thus the best time to irradiate was either 2 or 4 minutes for the highest amount of specific labeling. There was not a significant difference in the amounts of specific labeling at 2 or 4 minutes. Four minutes was chosen as an irradiation time for all DAT photolabels.

### **WIN 35, 428 Protection Experiment**

The WIN 35, 428 protection experiment helps to establish the relationship between [<sup>125</sup>I]-DEEP and the cocaine binding site of hDAT. [<sup>125</sup>I]-DEEP is a DAT inhibitor that is an analog of the highly potent DAT inhibitor, GBR 12909. The cocaine analog WIN 35,428 is used as a substitute for cocaine in the protection experiment because of its higher affinity ( $K_i = 43$  nM) compared to cocaine ( $K_i = 278$  nM) (Madras *et al.*, 1989). The affinity ( $K_i$ ) of [<sup>125</sup>I]-DEEP is 10-20 nM compared to that of GBR 12909, which is 36.3 nM (Grigoriadis *et al.*, 1989). The effect of WIN 35, 428 on the ability of [<sup>125</sup>I]-DEEP to photolabel hDAT was visualized by autoradiography (Figure 2-6). Incubation of hDAT with WIN 35, 428 prior to

labeling with [<sup>125</sup>I]-DEEP resulted in nearly total inhibition of photolabeling. The results suggest that [<sup>125</sup>I]-DEEP has the same binding site as WIN 35, 428. Therefore implying that [<sup>125</sup>I]-DEEP photolabeling occurs close to the cocaine binding site on hDAT.

### **Analysis of [<sup>125</sup>I]-DEEP Labeled Peptides Resulting from Proteolytic Digestions:**

#### **Primary CNBr Digestion followed by Secondary Trypsin Digestion**

Primary CNBr digestion gave hDAT peptides ranging in size from 3.5 kDa to 20 kDa on a 16.5% SDS-PAGE. There are 13 methionine residues in the hDAT protein (Figure 2-26). [<sup>125</sup>I]-DEEP has been shown previously to be incorporated within the membranes of hDAT and between TMs 1-2 (Vaughan & Kuhar, 1996). There are three methionines in TM2 alone. There are none in TM1. A primary CNBr digestion of hDAT does produce a fragment of 10.5 kDa size from S12 (N-terminus) to M106 (TM2). This is within the range of radiolabeled peptides obtained experimentally from primary a CNBr digestion.

The CNBr peptides obtained were subjected to trypsin which cleaves on the C-terminal end of arginine and lysine residues. Following this, the digest was separated on a TLC plate. The primary CNBr peptides were spotted alongside the CNBr peptides with trypsin. A shift in radioactivity in the CNBr peptide with trypsin would indicate tryptic cleavage sites within the CNBr peptide. A shift was observed so there are tryptic cut sites within the CNBr peptide. There are 5 peptides formed from this digest, in which only 3 have tryptic cut sites. There are seven tryptic cut sites within the suspected 10 kDa peptide (S12 to M106) (Figure 2-25). Two other hDAT peptides from S2 to M10 and E117 to M272 that have tryptic cleavage sites have been ruled out based on the immunoprecipitation studies done by Vaughan and Kuhar (1996). S2-M10 is located at the N-terminal end of hDAT and

was ruled out as possible labeling sites in the previous study (Vaughan & Kuhar, 1996). E117-M272 is a large peptide that spans well into TMs 3, 4, and 5. This peptide has been eliminated because the DEEP labeled peptide did not immunoprecipitate with antibodies directed towards TMs 4-7 (Vaughan & Kuhar, 1996). Also, E117 to R125 falls within the loops, which were also ruled out to be the place of incorporation by Vaughan & Kuhar (1996). This leaves S12 to M106 as being the most likely site of [<sup>125</sup>I]-DEEP incorporation on hDAT.

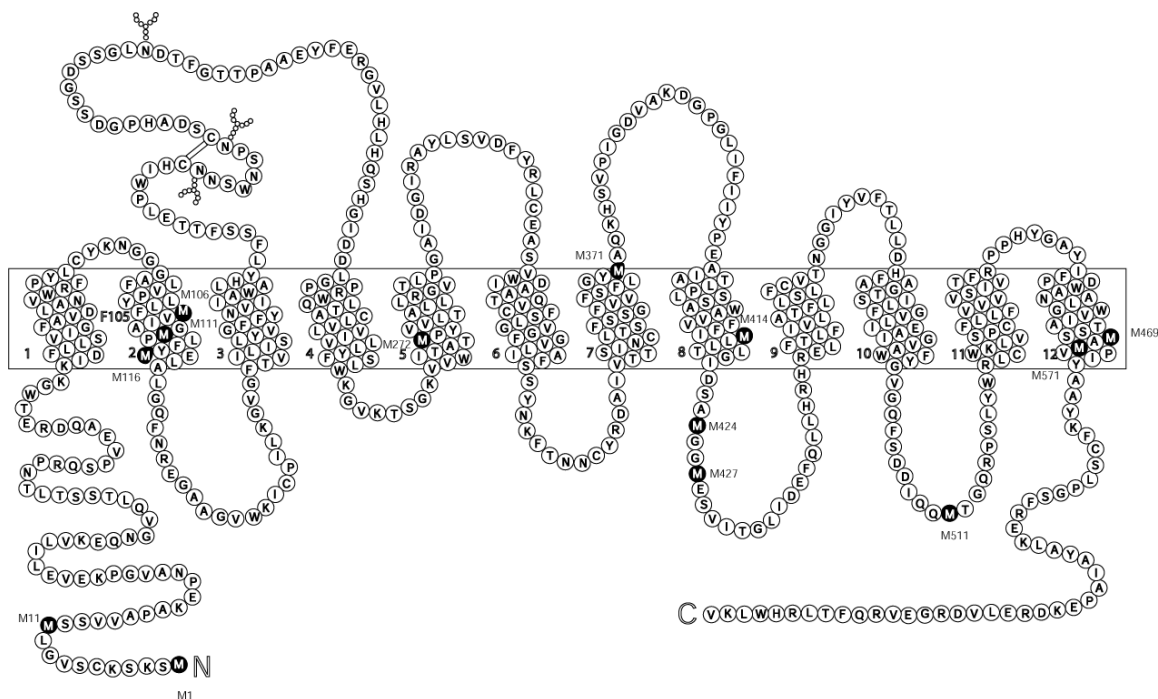
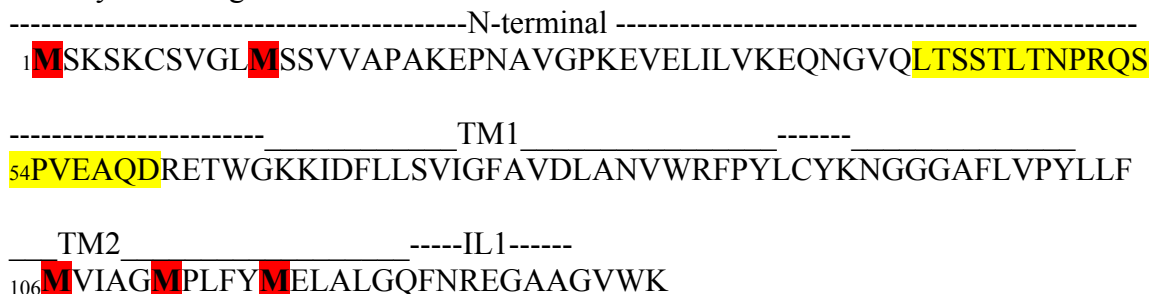


**Figure 2-26. CNBr cleavage sites of hDAT**

Methionine residues are shown as black circles with white letters. hDAT contains 13 methionines. Three methionines are located in TM2 region (adapted from Giros & Caron, 1993).



Primary CNBr digest:



Secondary Trypsin digest:

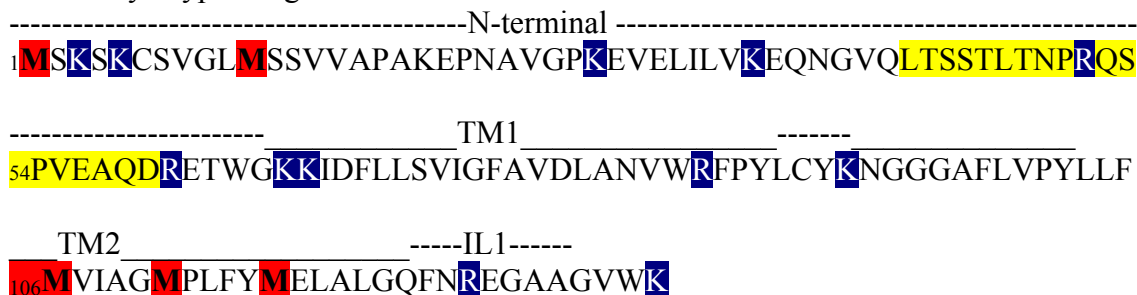
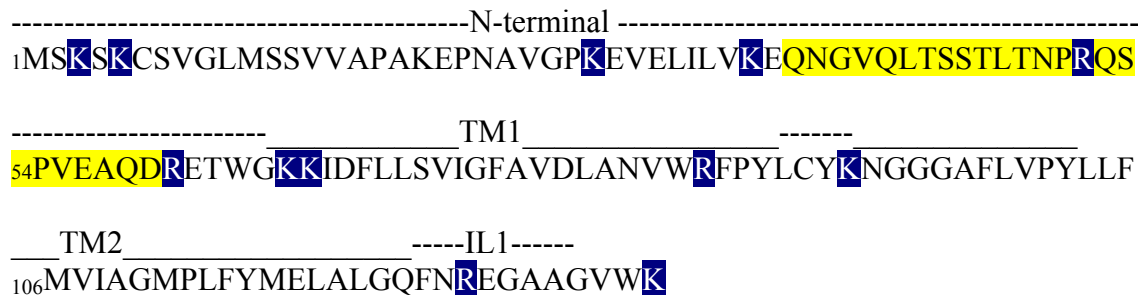


**Figure 2-27. Primary CNBr and Secondary Tryptic Digestion Cleavage Sites.** The CNBr cleavage of transmembrane domains 1 and 2 produces 5 hDAT peptides. One of particular interest was the 10kDa peptide from S12 to M106. Blue highlights indicate tryptic cut sites, red indicates CNBr cut sites, and the yellow highlights indicate the peptide sequence that the antibodies were directed towards and used in the immunoprecipitation studies with [ $^{125}$ I]-DEEP (Vaughan & Kuhar, 1996).

Primary Trypsin digest:



Secondary CNBr digest:

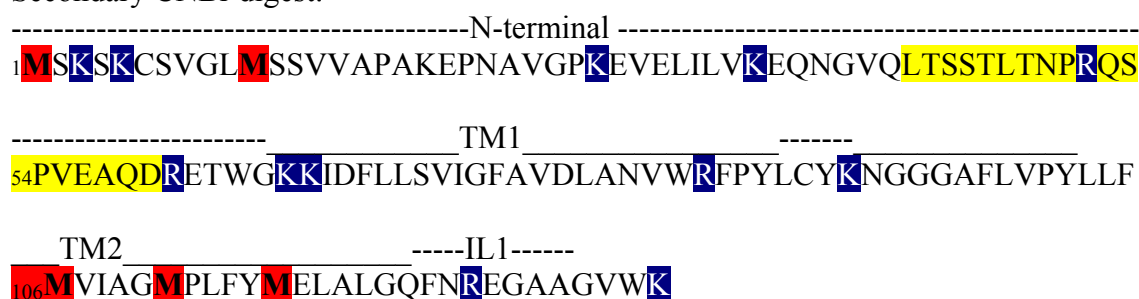


**Figure 2-28. Primary Tryptic and Secondary CNBr Digestion Cleavage Sites.**

The trypsin digest of the transmembrane domains 1 and 2 produces a 2149 Da peptide from I67 to R85 and a 3652 Da peptide from N93 to R125. The latter peptide contains 3 CNBr cleavage sites as opposed to none in the former one. Both are hydrophobic peptides. Blue highlights indicate tryptic cut sites, red indicates CNBr cut sites, and the yellow highlights indicate the peptide sequence that the antibodies were directed towards and used in immunoprecipitation studies with [<sup>125</sup>I]-DEEP (Vaughan & Kuhar, 1996).

## **Primary Trypsin Digestion followed by Secondary CNBr Cleavage: Gel and TLC**

### **Analysis**

Primary tryptic digestion of [ $^{125}$ I]-DEEP hDAT gave peptides ranging from 3.5 to 20 kDa in size. This range of labeled peptides is due to partial cleavages by the trypsin enzyme. Although the intact labeled protein was incubated with trypsin for 24 hours, missed cleavages are common (Keil, 1992; Siepen *et al.*, 2007), especially at K-P or R-P bonds (Olsen *et al.*, 2004; Siepen *et al.*, 2007) and within hydrophobic, unexposed transmembrane domains (Fischer & Poetsch, 2006). Expected analysis of hDAT tryptic peptides are 2149 Da and 3652 Da sized peptides in the TM 1 and 2 regions (Figure 2-28).

The radiolabeled tryptic peptides were subjected to CNBr and spotted on a TLC plate. A shift in the radioactivity suggested that there was a CNBr cleavage site within the tryptic peptides. TM2 contains three methionine residues as opposed to none in TM1. TM 2 appears to be the likely site of incorporation of [ $^{125}$ I]-DEEP.

### **HPLC of [ $^{125}$ I]-DEEP Labeled hDAT**

Trypsin was used as the primary digestion for [ $^{125}$ I]-DEEP hDAT because a primary CNBr digestion gave larger peptides, which could be strongly retained on the HPLC column because of the hydrophobicity of the transmembrane domains. A primary tryptic digestion of hDAT labeled with [ $^{125}$ I]-DEEP was separated on the HPLC with fractions collected and counted. The radioactive fragments were pooled, digested with CNBr (in-solution), and injected into the HPLC. The radioactive fractions were identified by liquid scintillation counting.

The primary tryptic digest gave radioactive peptides that eluted with a retention time of 73 and 87 minutes, named T1 and T2, respectively. It is possible that two peptides that were labeled may be the same sequence with one having uncleaved sites within. For example, the 87 minute fraction may contain the 73 minute fraction sequence buried within it. There may also be two different labeling sites. The 73 minute fraction was subjected to CNBr digestion and the hot fractions eluted at 21 and 33 minutes, named T1M1 and T1M2, respectively (Figure 2-10). T2 (87 min) was subjected to CNBr cleavage and the hot fractions eluted with a retention time of 19 and 72 minutes, named T2M1 and T2M2 respectively (Figure 2-11).

### **Solid-state photolabeling of TM2 Amino Acids**

The suspected hDAT peptide that is being labeled by [<sup>125</sup>I]-DEEP is N93 to M106. This peptide, NGGGAFVLPYLLFM, according to GPMW, does not elute at 19 (T2M2), 21 (T1M1), 33 (T1M2), or 72 (T2M2) minutes. The label itself causes a shift in the retention time of the labeled peptide or amino acid. Therefore, single amino acids were labeled with [<sup>125</sup>I]-DEEP to determine the amount of shift that occurs because of the hydrophobic ligand. Methionine, leucine and tyrosine are all amino acids found within the suspected peptide. When labeled with [<sup>125</sup>I]-DEEP, methionine's retention time shifted from 7 minutes to 60 and 70 minutes (Figure 2-13). These retention times are closer to that of the ligand itself (71 minutes with no irradiation and 69, 62, 60 and 5 minutes upon irradiation for 4 minutes). Irradiation of [<sup>125</sup>I]-DEEP with leucine (6.5 minute retention time) gave retention times that correspond with the irradiation of the ligand (69, 62, 60, and 5 minutes) (Figure 2-14). There are hot peaks eluting with retention times of 18 and 46 minutes. Tyrosine (13 minutes

retention time) shifted to 72 minutes when irradiated with [ $^{125}\text{I}$ ]-DEEP (Figure 2-15). It is a polar amino acid that shifts less when labeled than the other two amino acids (Figure 2-29).

### **Effect of Photoaffinity Labeling Conditions on [ $^{125}\text{I}$ ]-DEEP**

Irradiation of the aryl azide photolabel, [ $^{125}\text{I}$ ]-DEEP causes dimerization of the label into an azobenzene as well as decomposition of the label. When [ $^{125}\text{I}$ ]-DEEP is not irradiated, it has a retention time of 71 minutes. However, upon irradiation for 4 minutes, there is a break up of the ligand into 5 fragments. Each piece still contains the radioactive iodine because they are identified as radioactive by the liquid scintillation counter. These 5 fragments elute at 71, 61, 63, 74 and 4 minutes. The hottest fraction at 71 minutes still corresponds with the original ligand. Therefore, not all of the ligand decomposes upon irradiation at 4 minutes (Figure 2-16). This may mean that when interacting with the protein, the reactive nitrene that causes phenyl azide to react with either itself or an amino acid side chain, is not fully activated thus causing less labeling of the protein. This is in agreement with literature that talks about the low labeling efficiency of aryl azides (Brunner, 1993).

After photolabeling of hDAT with [ $^{125}\text{I}$ ]-DEEP, a tryptic digest is performed in 100 mM ammonium bicarbonate (AMBIC). AMBIC was applied to the labeled protein and run alongside the tryptic treated protein on a gel. According to the intact hDAT at the top of the gel, it appears as though AMBIC has no effect on the covalently bound [ $^{125}\text{I}$ ]-DEEP (Figure 2-17). This is not so with CNBr (Figure 2-7) where 70% TFA causes cleavage of labeled hDAT just as CNBr does. The effect of CNBr/TFA was tested on [ $^{125}\text{I}$ ]-DEEP. The outcome of this experiment was that 70% TFA causes more decomposition of the label than CNBr

with TFA. It appears as though CNBr actually buffers the effect of TFA on the decomposition of [ $^{125}$ I]-DEEP (Figure 2-18 and Figure 2-19).

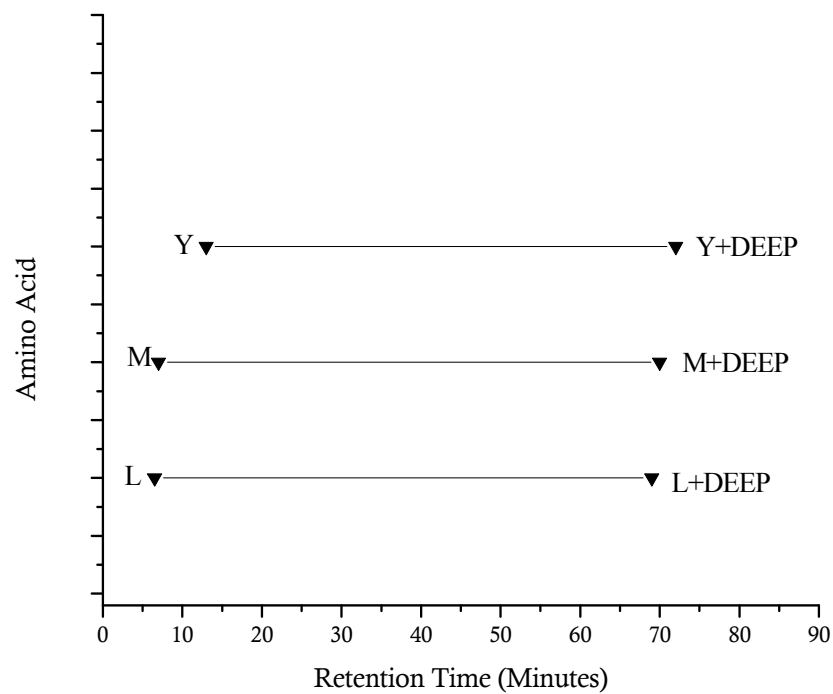


**Figure 2-29. Effect of [<sup>125</sup>I]-DEEP on the Retention Time of Amino Acids.**

Amino acids that are found within TM2 of hDAT where [<sup>125</sup>I]-DEEP is proposed to be incorporated were photolabeled with [<sup>125</sup>I]-DEEP. Retention times of the amino acids are shown together with retention times of the products of photolysis with [<sup>125</sup>I]-DEEP.

### **Analysis of Photolabeling of hDAT with [<sup>125</sup>I]-JJC 3-24**

[<sup>125</sup>I]-JJC 3-24 is a novel DAT inhibitor and photolabel. It is one of the first photoaffinity labels for DAT that is an analog of rimcazole. The results that are presented as well as the discussion of the results are of preliminary studies on the efficacy of the photolabel with hDAT. This rimcazole analog was used as a DAT inhibitor and photolabel because of its structural similarity to [<sup>125</sup>I]-DEEP.

Concentration dependent photolabeling of [<sup>125</sup>I]-JJC 3-24 was done to determine the concentration necessary for the labeling of hDAT. It was found that 50 nM concentration of [<sup>125</sup>I]-JJC 3-24 was needed to label hDAT (Figure 2-20). This is a high concentration compared to the 5 nM [<sup>125</sup>I]-DEEP that is needed to label hDAT. The  $K_i$  of [<sup>125</sup>I]-DEEP to hDAT is 10-20 nM as opposed to a  $K_i$  of 224 nM for rimcazole. SDS-PAGE analysis of a tryptic digestion of [<sup>125</sup>I]-JJC 3-24 labeled hDAT yields incompletely cleaved peptides that range from 3.5 to 20 kDa (Figure 2-21). This size range of peptides is the same as that of the tryptic peptides from [<sup>125</sup>I]-DEEP labeled hDAT. A primary CNBr cleavage of [<sup>125</sup>I]-JJC 3-24 labeled hDAT showed two radioactive peaks at 15 and 57 minutes (Figure 2-22). Solid-state labeling of [<sup>125</sup>I]-JJC 3-24 with PLFYM, a peptide in TM2 of hDAT, gave a peak that does not correspond to the label alone (58 minutes) (Figure 2-23). The shift of PLFYM with this peptide was 10 minutes from 48 minutes to 58 minutes. The CNBr/TFA digestion conditions were applied to the label to test the sensitivity of the rimcazole analog to the proteolytic conditions (Figure 2-25). The CNBr/TFA and the 70% TFA both caused the label to decompose into fragments and the hottest fraction eluted at 4 minutes. This same pattern is seen with [<sup>125</sup>I]-DEEP, whose structure is very similar to [<sup>125</sup>I]-JJC 3-24.



There is a structural similarity between [ $^{125}\text{I}$ ]-DEEP and [ $^{125}\text{I}$ ]-JJC 3-24. However, the use of [ $^{125}\text{I}$ ]-JJC 3-24 as a photolabel for localizing the site of incorporation on hDAT is not as effective a label as [ $^{125}\text{I}$ ]-DEEP. First, it takes a high concentration of the label to effectively label the protein. Second, it is not stable under proteolytic conditions like CNBr/TFA. It also decomposes upon irradiation, possibly losing some of its radioactive iodine that can non-specifically label hDAT. Finally, there are other DAT photolabels that are acceptable for mapping the cocaine binding site of hDAT and currently there is not enough information about the binding site of hDAT using them. Therefore, older, more studied photolabels should be explored instead of focusing on the newer, less investigated photolabels like [ $^{125}\text{I}$ ]-JJC 3-24.

### **Future Studies**

There are some follow-up experiments that can be done with [ $^{125}\text{I}$ ]-DEEP to further the identification of the cocaine binding site of hDAT. Edman sequencing of the labeled peptide from a CNBr digest would help to identify which position in the peptide sequence is being labeled. The cycles of radioactivity would be counted and the hottest fraction identified as where the label is on the peptide. The sequential removal of amino acids will not tell exactly which amino acid is labeled but it will identify the placement of the label in the peptide sequence.

Mutagenesis of the proposed labeled amino acid(s) can be done and followed with [ $^{125}\text{I}$ ]-DEEP photolabeling. If [ $^{125}\text{I}$ ]-DEEP continues to label the protein, then either this amino acid is not being reacted with the label or there is no specification of which amino

acid is being labeled by the photolabel. The label could just label the same mutant amino acid or the next reactive amino acid.

The follow-up experiments with [<sup>125</sup>I]-JJC 3-24 would be to narrow its region of incorporation through immunoprecipitation experiments to determine which region it is being incorporated in on hDAT. In situ proteolysis should be done to determine whether [<sup>125</sup>I]-JJC 3-24 labels in the membrane or in the loops of hDAT. Additionally, more proteolysis followed by Edman sequencing, solid-state labeling of amino acids, then mutagenesis studies of proposed amino acid followed by photolabeling should all be explored. It is not recommended to use [<sup>125</sup>I]-JJC 3-24 as a DAT photolabel until more is known with others because of its low affinity to hDAT.

## **Chapter Three**

### **Photoreactions of Phenyl Azide**

**with**

### **Amino Acid Analogs**

“Imagination is more important than knowledge. For while knowledge defines all we currently know and understand, imagination points to all we might yet discover and create.”

**-Albert Einstein**

## Introduction

The photochemistry of phenyl azide is complex. The intermediates formed upon irradiation of phenyl azide have been studied (Doering & Odum, 1966; Schrock & Schuster, 1984; Schuster, 1992) since its inception as a photoaffinity label. The products that are formed from either a singlet or triplet pathway have also been investigated. Upon photolysis of phenyl azide, a reactive phenyl nitrene is formed (Scheme 3-1). This phenyl nitrene can react with nucleophiles, electrophiles and acids through the singlet state to form *3H*-azepines (Schrock & Schuster, 1984; Takeuchi, 1981). The singlet phenyl nitrene can also undergo intersystem crossing (ISC) to the triplet phenyl nitrene and dimerize to form azobenzene (Gritsan & Pritchina, 1992; Leyva *et al.*, 1986; Wang *et al.*, 2007). Phenyl azide undergoes these steps whether reacting in organic solvents (Schrock & Schuster, 1984) or aqueous conditions (Rizk *et al.*, 2006).

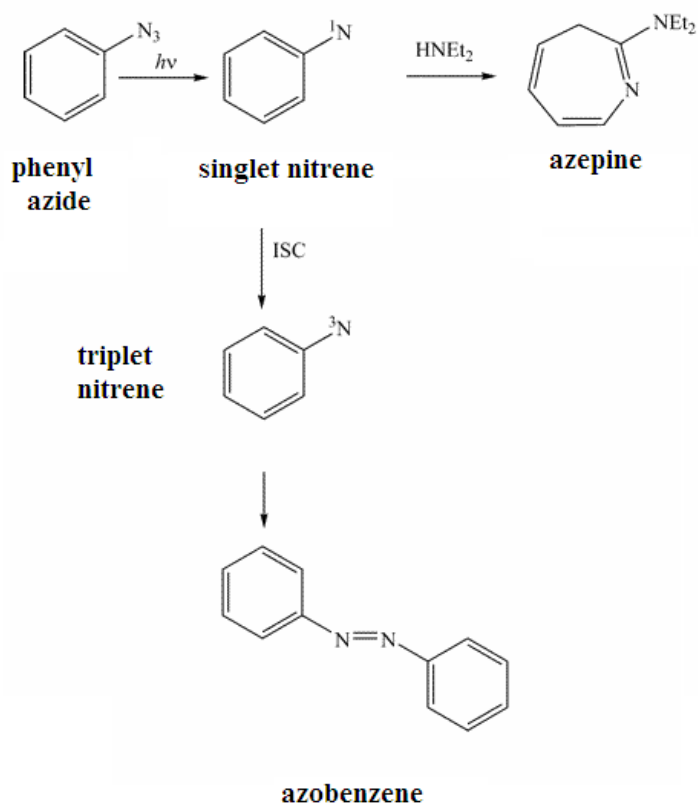
The singlet state pathway is of importance for its implications in photoaffinity labeling. The product that is formed by the stable, covalent bond that is formed with the amino acid side chains from irradiation of an aryl azide photolabel is the singlet state product, which is a *3H*-azepine. *3H*-Azepines are more thermodynamically stable than *1H*-azepines, *2H*-azepines and *4H*-azepines (Satake *et al.*, 1988; Vogel, 1980). *1H*-Azepine can rearrange to form the more stable *3H*-azepine (Satake *et al.*, 1991). The stability of azepine is important to understand because photoaffinity labeling experiments rely on the stability of the covalent bond formed between the label and the protein.

Prolonged exposure to ultraviolet radiation can cause damage to the proteins that are being photolabeled (Chan *et al.*, 2006). Irradiation beyond the time needed for photolabeling can also cause the *3H*-azepine to isomerize to 3-substituted 2-azabicyclo-

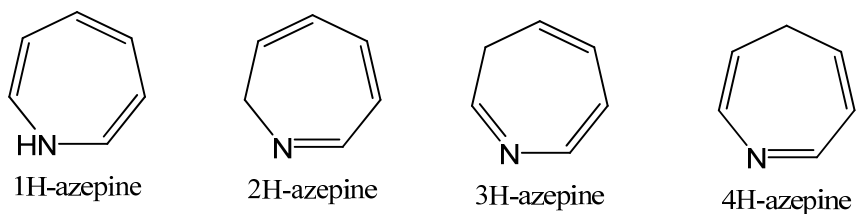
[3.2.0]hepta-2,6-dienes (Odum, 1997). This reaction is reversible with 3*H*-azepine being the more stable tautomer. Stability of 3*H*-azepines in proteolytic conditions is also important because proteolysis is often used in conjunction with photolabeling in order to narrow the region of incorporation of the photolabel. The conditions used for proteolysis range from acidic to basic in terms of chemical cleavages (CNBr/trifluoroacetic acid, CNBr/formic acid, formic acid, and HCl) and enzymatic digestions (trypsin, thermolysin, and chymotrypsin), respectively. Hydrolysis of azepine occurs from treatment with acid (Noskov *et al.*, 1997). Tautomerization to either 1*H*-azepine (Kubota, 2003) or to 2*H*-azepine (Cordonier *et al.*, 2005) has been seen upon addition of bases to 3*H*-azepine. Both acids and bases affect the stability of 3*H*-azepine leading to the formation of less stable compounds.

It is the aim of this chapter to test the reactivity of different classes of amino acid analogs with phenyl azide in an attempt to shed greater light on the usefulness of aryl azides as photoaffinity labels. The amino acid analogs imidazole, phenol and guanidine acetic acid were irradiated with phenyl azide in polar conditions. The amino acid analogs ethylbenzene, butylamine, *N*-ethylacetamide, dimethyl sulfide, butyric acid, 1-octanethiol were irradiated with phenyl azide in nonpolar conditions. In addition, the identification of 3*H*-azepine was made and the stability of the products in proteolytic conditions was tested. The proteolytic conditions that were of importance to the research contained in this dissertation were those conditions used in trypsin digestions (basic) and CNBr cleavages (acidic).

A.



B.



**Scheme 3-1. Irradiation of Phenyl Azide forms 3H-Azepine and Azobenzene. A.**

Phenyl azide reacts with itself through the triplet state forming azobenzene, while it reacts with diethylamine, a nucleophile, through the singlet state forming *N,N*-diethyl-

3*H*-azepin-2-amine (adapted from Schrock & Schuster, 1984). **B. Azepine Isomers.** Of

all of the azepine isomers, 3*H*-azepine is the most stable (adapted from Satake *et al.*, 1991).

## **Methods**

## **Photoreactions of Phenyl Azide/*Para*-azidoacetophenone with Amino Acid Analogs**

### **General Notes**

Unless otherwise noted, all reagents were obtained from commercial suppliers and used without further purification. Specific reactions were performed in 10 mL glass beakers in a Rayonet Reactor (254 nm). All solvents were used as supplied by the company. Infrared spectra were recorded on Nicolet Avatar 370 DTGS FT-IR spectrometer as thin films on sodium chloride plates.  $^1\text{H}$  NMR,  $^{13}\text{C}$  NMR spectra were recorded on a Mercury 300 MHz, Varian 400 MHz or Varian 600 MHz spectrometer. Unless otherwise stated, all NMR spectra were recorded in deuterated chloroform ( $\text{CDCl}_3$ ) and referenced to the residual peak; chemical shifts ( $\delta$ ) are reported in parts per million, and the coupling constants (J) are reported in Hertz (Hz). Mass spectra were obtained using a FT-ICR LTQ-FT high resolution mass spectrometer. Isocratic reverse phase high pressure liquid chromatography was performed on a Hewlett Packard Series 1100 HPLC. Water/0.1% TFA (v/v) is phase A and acetonitrile w/ 0.1% TFA (v/v) is phase B. The flow-rate was 1 mL/min with UV detection at 254 nm. The column type was C18 with the dimensions of 4.6 mm X 25 cm.

### **Synthesis of Phenyl Azide**

A molar concentration of 16.3 mmol of  $\text{NaNO}_3$  was added drop-wise to a solution of 18.10 mmol aniline in 2N HCl at  $-5^\circ\text{C}$  and stirred for 30 minutes. A solution of 17.54 mmol of  $\text{NaN}_3$  was subsequently added drop-wise to this reaction and stirred for one hour



at  $-5^{\circ}\text{C}$ . The reaction mixture was brought to room temperature. Then, the pH was brought up to 10 using KOH. The product was extracted three times using dichloromethane (DCM), washed with water, and dried using  $\text{MgSO}_4$ . The product was filtered and the solvent was removed via rotovap.

### **Purification of Phenyl Azide**

The solvent used for purification of phenyl azide was 5:95 acetone:pentane. TLC of the crude mixture resulted in better separation of each of the products. There were 3 yellow spots and 1 UV detectable spot visualized. A 1.5 inch diameter column was used for the purification and  $\sim 6$  inches of silica was added to the column. The first fractions collected were the phenyl azide. It was the UV detectable spot. The IR clearly shows  $\sim 2100\text{ cm}^{-1}$  peak for the azide. The  $^1\text{H}$  and  $^{13}\text{C}$  NMR spectrums show the phenyl ring. The HPLC at 50:50 dH<sub>2</sub>O with 0.1%TFA:acetonitrile with 0.1%TFA gives a sharp peak for phenyl azide at 10 minutes. The crude mixture of phenyl azide gave the following results: IR showed  $\sim 2100\text{cm}^{-1}$  peak of the azide, NMR showed the phenyl ring, and the TLC showed three spots 2 yellow, 1 orange-red, and 1 UV detectable spot at the end of the solvent front (80:20 petroleum ether:ethyl acetate). Better separation was achieved with 5:95 acetone:pentane. Following column purification, 3g of phenyl azide was made with 85% yield.

## Irradiations of Phenyl Azide with Amino Acid Analogs

### Sample Preparation

Phenyl azide was synthesized by M. Holmes and stored at  $-20^{\circ}\text{C}$  in the dark. Solutions of 1M were made of butylamine, 1-octanethiol, ethylbenzene, butyric acid, dimethyl sulfide, and *N*-ethylacetamide in cyclohexane and were prepared fresh each time.

Solutions of 1M were made of phenol, guanidine acetic acid, and imidazole in 10% methanol and 90% PBS buffer (v/v) (138 mM NaCl, 2.7 mM KCl, 1.5 mM  $\text{KH}_2\text{PO}_4$ , 9.6 mM  $\text{NaH}_2\text{PO}_4 \cdot \text{H}_2\text{O}$ ) pH 7.4 and were prepared in distilled water, made fresh each time.

All irradiations were performed at room temperature in 10 mL glass beakers in a Rayonet Reactor at 254 nm. 100mM ammonium bicarbonate (AMBIC) was prepared and stored at room temperature. Trifluoroacetic acid (TFA) (70% v/v) was prepared and stored at room temperature.

### High Pressure Liquid Chromatography Analysis

Samples were loaded into a  $20\mu\text{L}$  loop and injected into a Hewlett Packard series 1100 reverse phase High Pressure Liquid Chromatography spectrometer. The column used was a Zorbex  $5\mu\text{m}$  C18 column with dimensions of  $4.6 \times 150$  mm. Separation was achieved using a gradient (see Tables 3-1 & 3-2) where mobile phase A was  $\text{H}_2\text{O} + 0.1\%$  trifluoroacetic acid (TFA), and mobile phase B was acetonitrile +  $0.1\%$  TFA. All mobile phases were filtered, and degassed with helium before use. The flow rate through the column was 1 mL/min. A UV detector measured UV absorbance at  $\lambda = 254$  nm.

RETENTION TIME	% MOBILE PHASE B
0	0
20	100
40	100
45	0

**Table 3-1. HPLC Gradient Description for Method SHORT1.** This table shows the SHORT1 method gradient that was used to separate the products following the photochemical reactions. Mobile phase A was 100% H<sub>2</sub>O/0.1% trifluoroacetic acid (TFA) (v/v) and mobile phase B was 100% acetonitrile/0.1% TFA (v/v). The mobile phase increased from 0 to 100% acetonitrile/0.1% TFA by 5% every minute.

RETENTION TIME	% MOBILE PHASE B
0	0
10	100
15	100
20	0

**Table 3-2. HPLC Gradient Description for Method 16.** This table shows the gradient that was used in some cases to separate the products following the photochemical reactions. Mobile phase A was 100% H<sub>2</sub>O/0.1% trifluoroacetic acid (TFA) (v/v) and mobile phase B was 100% acetonitrile/0.1% TFA (v/v). The mobile phase increased from 0 to 100% acetonitrile/0.1% TFA by 10% every minute.

### **Irradiation of Phenyl Azide and Amino Acid Analogs for HPLC and Mass Spectral Analysis**

Phenyl azide (100uM) and 1M of the amino acid analogs in appropriate solvents were irradiated over time for 0, 10, 30, 60, 120, and 240 seconds. The irradiated products were immediately injected into the HPLC for analysis. The non-irradiated solution of 100uM phenyl azide and 1M amino acid analog and the 100uM phenyl azide in solvents were injected as a control and used to overlay chromatograms for the identification of the suggested product peak(s). This procedure was repeated three times for quantitation of the phenyl azide and product peak heights. The mass spectral analysis of the products were performed using APCI or ESI mass spectrometry from a 4 minute irradiation of phenyl azide with the amino acid analogs.

### **Irradiation of *para*-azidoacetophenone (PAAP) and Amino Acid Analogs for HPLC and Mass Spectral Analysis**

*Para*-azidoacetophenone (100uM) and 1M of the amino acid analogs in acetonitrile were irradiated for 4 minutes. The irradiated products were immediately injected into the HPLC for analysis. The non-irradiated solution of 100uM *para*-azidoacetophenone with 1M amino acid analog and the 100uM *para*-azidoacetophenone in acetonitrile were injected as controls and used to overlay chromatograms for the identification of the suggested product peak(s). This procedure was repeated three times. The mass spectral analysis of the products were performed using APCI or ESI mass spectrometry from a 4 minute irradiation of *para*-azidoacetophenone with the amino acid analogs.

### **Irradiation of Phenyl Azide and Amino Acid Analogs for $^1\text{H}$ Nuclear Magnetic Resonance (NMR)**

Phenyl azide (1M) was irradiated under NEAT conditions with the amino acid analogs for 4 minutes. The sample was dried down and reconstituted in deuterated chloroform for  $^1\text{H}$  NMR. Phenyl azide (1M) in cyclohexane and 10% methanol/90% PBS Buffer (v/v), pH 7.4 was also irradiated. The products were dried down and reconstituted in deuterated chloroform for  $^1\text{H}$  NMR.

### **Collection of the Product from the Reaction between Phenyl Azide and the Amino Acid Analogs**

A 200  $\mu\text{L}$  sample was injected into the HPLC. A fraction was collected of the product as it came out of the column. This fraction was then dried down and submitted to the high resolution mass spectrometry laboratory. The submitted samples were run on an FT-ICR LTQ-FT high resolution mass spectrometer.

## **Stability of Products**

### **Stability of the Products of Phenyl Azide and the Amino Acid Analogs at pH 8.9 in Ammonium Bicarbonate**

Phenyl azide (100 $\mu\text{M}$ ) and 1M concentrations of the amino acid analogs were prepared in the appropriate solvents (10% methanol/90% PBS Buffer (v/v), pH 7.4 or cyclohexane). The solutions were irradiated at 254 nm for 4 minutes. The solution was dried down and 300 $\mu\text{L}$  of 100mM ammonium bicarbonate was added and kept at 25 $^{\circ}\text{C}$  for 24 hours. The products were dried down and reconstituted with 100% mobile phase B (100%

acetonitrile with 0.1% TFA, (v/v)) prior to HPLC injection. The samples were analyzed at 4 hours and at 24 hours. The samples were injected into the HPLC for analysis of the products and starting materials. The HPLC was monitored for product loss and the emergence of new products.

### **Stability of the Products of Phenyl Azide and the Amino Acid Analogs at 25<sup>0</sup>C in Trifluoroacetic Acid (TFA), pH 1**

Phenyl azide (100uM) and 1M concentrations of the amino acid analogs were prepared in the appropriate solvents (10% methanol/90% PBS Buffer (v/v), pH 7.4 or cyclohexane). The solutions were irradiated at 254 nm for 4 minutes. The products were dried down and 300uL of 70% trifluoroacetic acid (TFA), pH 1, was added to the products. The acid was quenched with dH<sub>2</sub>O and then dried down. The products were reconstituted in HPLC mobile phase B (100% Acetonitrile with 0.1% TFA (v/v)) and injected into the HPLC for analysis.

### **Data Analysis**

All the data collected from the experiments detailed in the Methods section were graphed and analyzed in ORIGIN 6.1 software. Means and error values were obtained and illustrated in the graphs. The error values used were the standard error of the mean (SEM). For each trial, a graph was made of these mean values and their error bars.

### First-Order Rate Constants

The data were fit to an equation of the form shown below in eq. 1:

$$[\text{phenyl azide}] = Ae^{-k_1't/M} + B \quad (\text{Eq. 1})$$

where:

A = initial relative peak height in %

$k_1'$  = rate constant in  $\text{sec}^{-1}$

t = time in seconds

M = molar concentration of the target amino acid analogs

B = y offset to account for nonzero baseline that sometimes remained at the end of the reaction

The purpose of fitting the data to this equation was to get values for the first order rate constant,  $k_1'$ . The data collected were fit to this equation because the reactions were pseudo first order. A pseudo first order reaction is when the concentration of one of the reactants remains constant (it is in great excess with respect to the other reactants). If the amino acid analog is the reactant whose concentration is constant then  $rate = k_1[\text{phenyl azide}][\text{amino acid analogs}] = k_1'[\text{phenyl azide}]$ . The second order rate equation has been reduced to a pseudo first order rate equation. In these series of reactions, the amino acid analogs were ten thousand times in excess of phenyl azide. Therefore, the each reaction was a pseudo first order reaction.

### Double Exponential Decay Curve Fit

The data were fit to a double exponential rate equation because the single exponential first-order rate equation did not always fit the data. A double exponential rate equation can be used to explain two parallel reactions. The rate constant,  $k_{AA}$  describes the loss of phenyl azide when reacting with the amino acid analog while the rate constant,  $k_{PA}$  describes the loss of phenyl azide when reacting without an amino acid analog in the appropriate solvent. The rate constant,  $k_{PA}$  was obtained by following the loss of phenyl azide irradiated in cyclohexane or aqueous conditions over a 4 minute time period. The rate constant,  $k_{PA}$ , was found to be  $4.27 \cdot 10^{-2} \pm 0.27 \cdot 10^{-2} \text{ sec}^{-1}$  in cyclohexane and  $14.8 \cdot 10^{-2} \pm 1.3 \cdot 10^{-2} \text{ sec}^{-1}$  in aqueous conditions. The rate constant,  $k_{AA}$ , which describes the loss of phenyl azide irradiated with amino acid analogs was unknown. All variables in the equation were fixed except for  $k_{AA}$ , which varied. The data were fit to an equation of the form:

$$[\text{phenyl azide}] = A(e^{-k_{AA} t/M} + e^{-k_{PA} t}) \quad (\text{Eq. 2})$$

*where:*

A = initial relative peak height in %

$k_{AA}$  = rate constant of the loss of phenyl azide when reacting with the amino acid analogs,  $\text{sec}^{-1}$

M = molar concentration of the amino acid analogs

$k_{PA}$  = rate constant of the loss of phenyl azide reacting without amino acid analogs in cyclohexane or aqueous conditions,  $\text{sec}^{-1}$

t = time in seconds



### Second-Order Rate Equation

The rate constant of the dimerization of phenyl azide can be determined by applying the second-order rate equation (Eq. 3) to  $1/[PA]$  over time.

$$1/[PA] = 1/[PA]_0 + k_2t \quad (\text{Eq. 3})$$

where:

$[PA]_0$  = the initial concentration of phenyl azide or 100uM

$k_2$  = the second-order rate constant in  $(M \cdot \text{sec})^{-1}$

$t$  = time in seconds.

### Determining the Total Rate of Reaction

In order to examine the effect that phenyl azide dimerization has on the total rate of reaction, the dimerization reaction rate was added to the target reaction rate. The total reaction rate accounts for the inclusion of the phenyl azide self-reaction which can be described as:

$$\text{Total Rate} = \text{Target Reaction Rate} + \text{Dimerization Reaction Rate} \quad (\text{Eq. 4a})$$

$$\text{Total Rate} = k_1'[PA] + k_2[PA][PA] \quad (\text{Eq. 4b})$$

where:

$k_1'$  = pseudo first-order rate constant of phenyl azide reacting with the amino acid analog

$k_2$  = rate constant from the second-order rate equation describing the dimerization of phenyl azide

[PA] = molar concentration of phenyl azide in the reactions, which is 100 $\mu$ M.

### **Product Formation Rate Constants**

The data for the formation of the product in the photoreactions of phenyl azide and amino acid analogs were fit to an equation of the form:

$$\text{rate of product formation} = A(1 - e^{-kt}) \quad (\text{Eq. 5})$$

where:

A = maximum UV absorbance of product peak height in mV

$k$  = rate constant in  $\text{sec}^{-1}$

t = time in seconds.

## Results

## Introduction to the Results

In order to better understand the photoreaction between DAT photoaffinity ligands and the hDAT protein, a small molecule model of the photoreaction was examined. Phenyl azide (PA) was irradiated with various amino acid analogs and the kinetics of the reaction determined for each analog. The products from the irradiation of phenyl azide and each nucleophile were identified by HPLC,  $^1\text{H}$  NMR and/or mass spectrometry.

Proteolysis of photolabeled hDAT with [ $^{125}\text{I}$ ]-DEEP was done to generate labeled peptides that could be localized to a particular region (see Chapter 2). Enzymatic proteolysis with trypsin occurred in basic conditions, pH 8.9, and chemical cleavage by CNBr was performed in acidic conditions, pH 1. The product from the developed small molecule model was subjected to the proteolytic conditions of photoaffinity labeled hDAT and the amount of decomposition was measured.

*Para*-azidoacetylphenone (PAAP) was used as a model for the photoaffinity labels because it represents the photoactive part of the photoaffinity label. In addition, it mimics the hDAT photoaffinity ligands by having a substituent para to the azido group on the phenyl ring. Irradiations of PAAP were done with the amino acid analogs. The products were identified by mass spectrometry.

Amino acid analogs butylamine and 1-octanethiol are highlighted as models in this results section. The reactivity of lysine and cysteine in proteins is exploited in order to probe the binding pocket of enzymes, receptors, and transporters. It is possible that DAT photoaffinity labels are labeling a cysteine or a lysine residue. For that reason, it was reasonable to study in depth the reactivity of phenyl azide with butylamine (lysine

analog) and 1-octanethiol (cysteine analog). The photoreactivity of these amino acid analogs are presented first followed by other amino acid analogs spanning the different classes of amino acids.

The reactivity of each amino acid analog when irradiated with phenyl azide was determined. The primary product and the stability of that product in proteolytic conditions were also established. Comparisons are made between the amounts of products detected by HPLC for each amino acid analog in various solvent conditions. This section reports the reactivity of amino acid analogs with phenyl azide irradiated in hydrophobic and hydrophilic conditions. Products formed were also determined and product stability examined under conditions applicable to hDAT photoaffinity labeling studies.

## Photoreactions with Phenyl Azide and Butylamine as a Model for Lysine

### *Phenyl Azide Photoreactivity with Butylamine as a Model for Lysine*

The exploration of phenyl azide reactivity in the presence of compounds that have similar functionality as the amino acid side chains was performed. Lysine is one of the most reactive amino acids with aryl azides (Schwartz, 1989). Butylamine was used as a model of lysine. Butylamine has a primary amine as the functional group just as lysine does. Phenyl azide (100 $\mu$ M) was irradiated in the presence of 1M butylamine in cyclohexane over time, where t is equal to 0, 10, 30, 60, 120, and 240 seconds. The first-order rate constant,  $k_1'$ , was determined based on the rate of loss of phenyl azide. The rate constant for phenyl azide loss,  $k_1'$ , was determined to be  $4.52 \cdot 10^{-2} \pm 0.2 \cdot 10^{-2} \text{ sec}^{-1}$ , which is one of the larger rate constants compared to the other amino acid analogs. The product was identified using mass spectrometry and proton NMR.

In addition, the effect of proteolytic conditions was tested on the product formed from phenyl azide and butylamine, *N*-butyl-3*H*-azepin-2-amine. Incubation of the butylazepine product in basic conditions, pH 8.9 showed a 91% reduction in the product after 4 hours. After incubation in acidic conditions, pH 1, there was a 100% reduction in the product after 24 hours at room temperature. Therefore, lysine is a reactive target for phenyl azide but the product formed is unstable under the proteolytic conditions used to digest photoaffinity labeled proteins into smaller peptides.

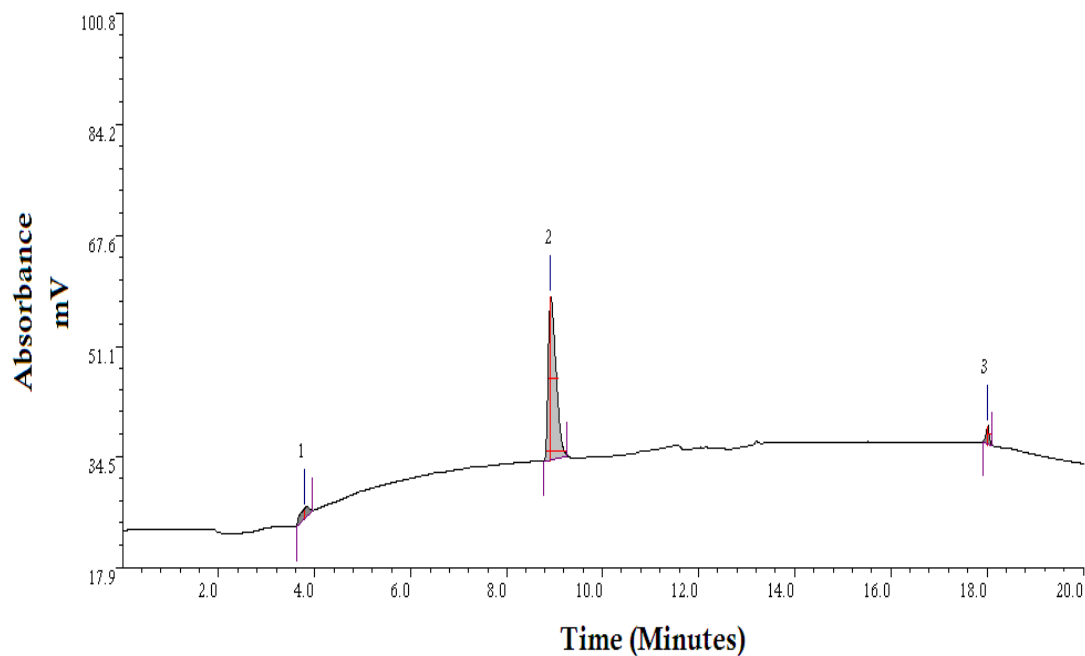
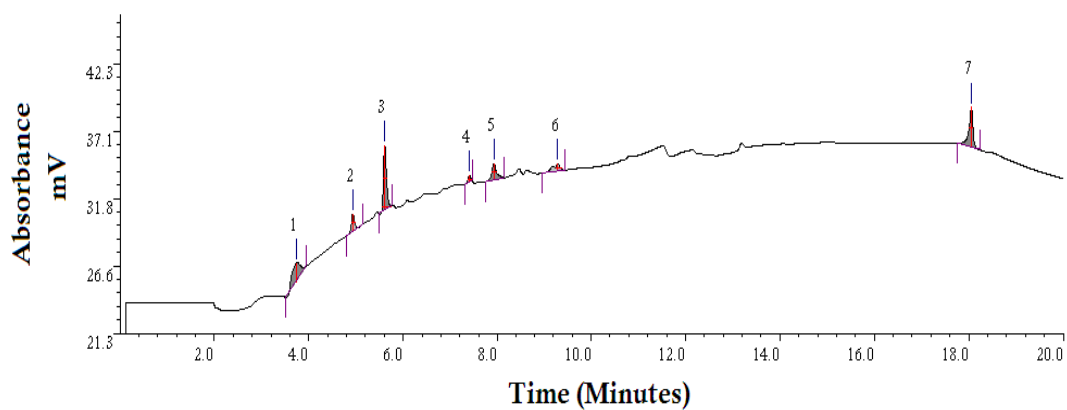


**Figure 3-1. Phenyl Azide and Butylamine in Cyclohexane Before Irradiation.** The HPLC chromatogram of 100 $\mu$ M phenyl azide + 1M butylamine in cyclohexane show that phenyl azide (peak 2) elutes at an 8.9 minute retention time. This coincides with the retention time of phenyl azide alone in cyclohexane. No reaction has begun at the irradiation time of 0 for phenyl azide and butylamine. The gradient used to record this data was Method 16 described in the Methods section.



Peak	RT	Area	%Ar	Height
1	3.733	17.582	22.03	1.449
2	4.938	5.598	7.01	1.347
3	5.612	21.589	27.05	4.971
4	7.404	1.525	1.91	0.466
5	7.921	8.537	10.70	1.227
6	9.296	5.492	6.88	0.509
7	18.058	19.500	24.43	3.128

**Figure 3-2. Phenyl Azide and Butylamine in Cyclohexane After Irradiation.** The HPLC chromatogram of 100 $\mu$ M phenyl azide + 1M butylamine in cyclohexane is shown after a 4 minute irradiation at 254 nm. The phenyl azide has disappeared from the chromatogram as shown by no peak at 8.9 minutes. There is the emergence of several small new peaks, one of which is a major peak at 5.6 minutes.



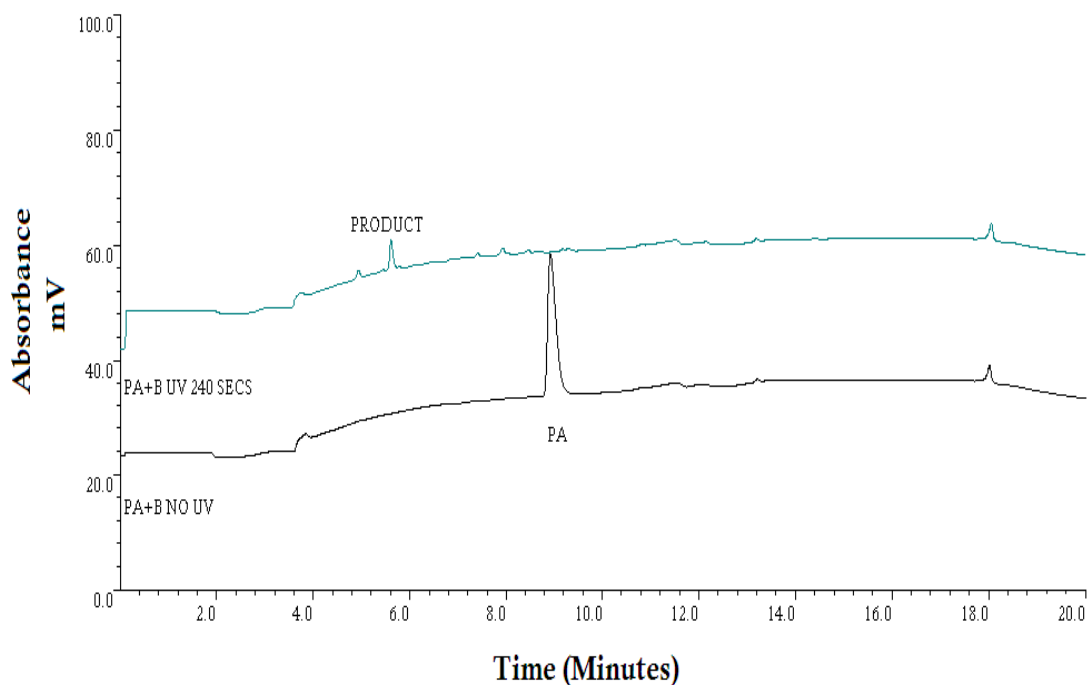


**Figure 3-3. Phenyl Azide and Butylamine in Cyclohexane Before and After Irradiation.** The lower curve is the phenyl azide and butylamine in cyclohexane with no irradiation. The upper curve is the phenyl azide and butylamine in cyclohexane after four minutes of irradiation. The abbreviations in the figure are as follows: PA is phenyl azide, B is butylamine, NO UV is no irradiation time, and UV 240 secs is the irradiation time of 4 minutes. It is clear from this overlay that there is a complete loss of phenyl azide at an irradiation time equal to 240 seconds.

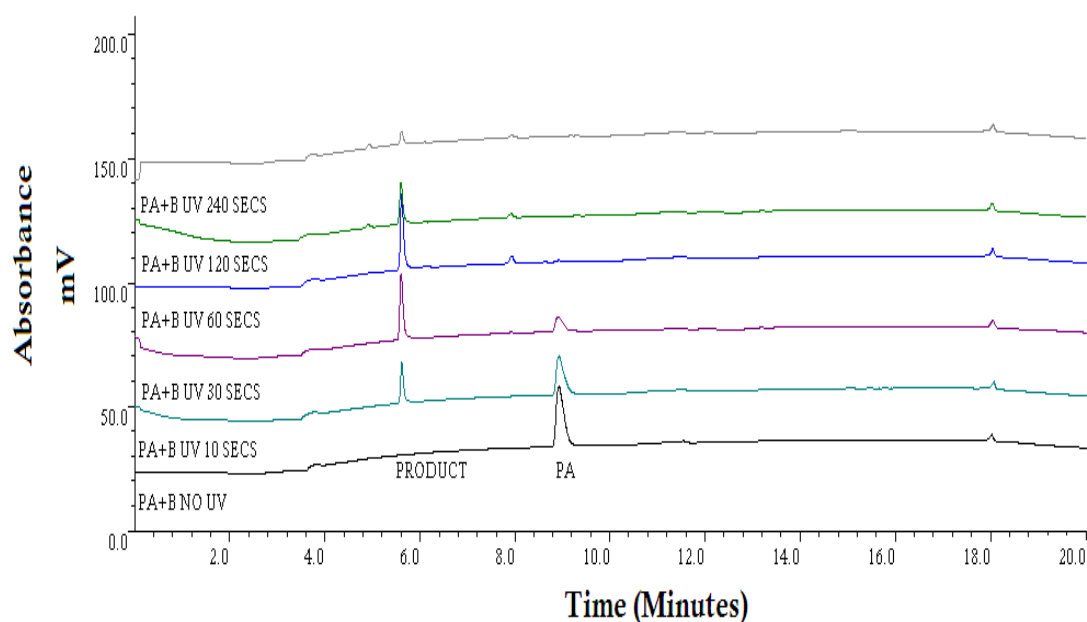


**Figure 3-4. Phenyl Azide and Butylamine in Cyclohexane Irradiated over Time.**

HPLC chromatograms for 100 $\mu$ M phenyl azide + 1M butylamine in cyclohexane over time, where  $t=0, 10, 30, 60, 120$  and 240 seconds. In the control with no irradiation, the phenyl azide peak (PA) from Figure 3-1 can be seen. In the 240 seconds chromatogram, the 5.6 minute peak from Figure 3-2 is shown. A trend that can be observed from the chromatograms is that the 5.6 minute peak decreases after 60 seconds of irradiation and may represent decomposition.

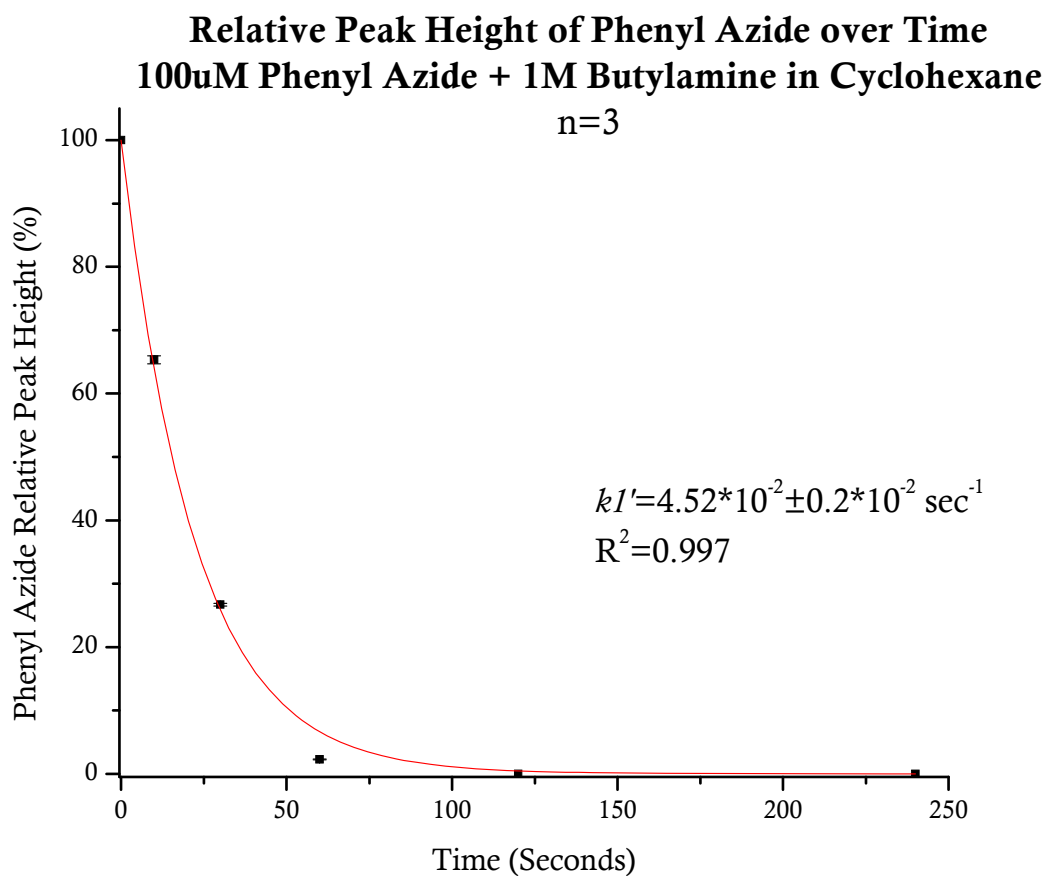


**Figure 3-5. Single First-Order Exponential Decay Curve Fit for Phenyl Azide and Butylamine in Cyclohexane.** The equation,  $B + Ae^{-k1't}$ , was used for the determination of the rate constant,  $k1'$ . B and A are fixed values, where B is 0, the y offset when the baseline did not go to zero, A is 100, the initial relative peak height in %,  $k1'$  is the rate constant in  $\text{sec}^{-1}$  and t is time in seconds. Some error bars (SEM) fall within the designated symbol.  $k1'$  is  $4.52 \cdot 10^{-2} \pm 0.2 \cdot 10^{-2} \text{ sec}^{-1}$  and  $R^2$  is 0.997 for this data.

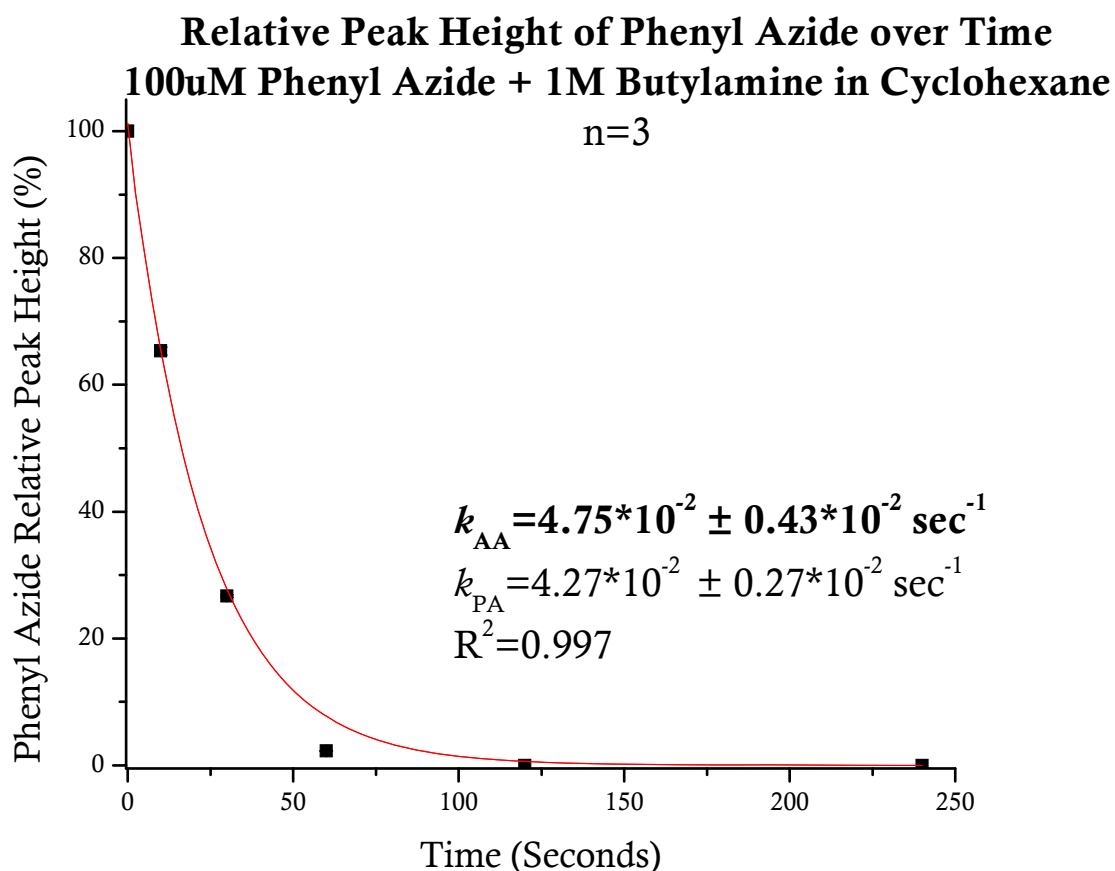
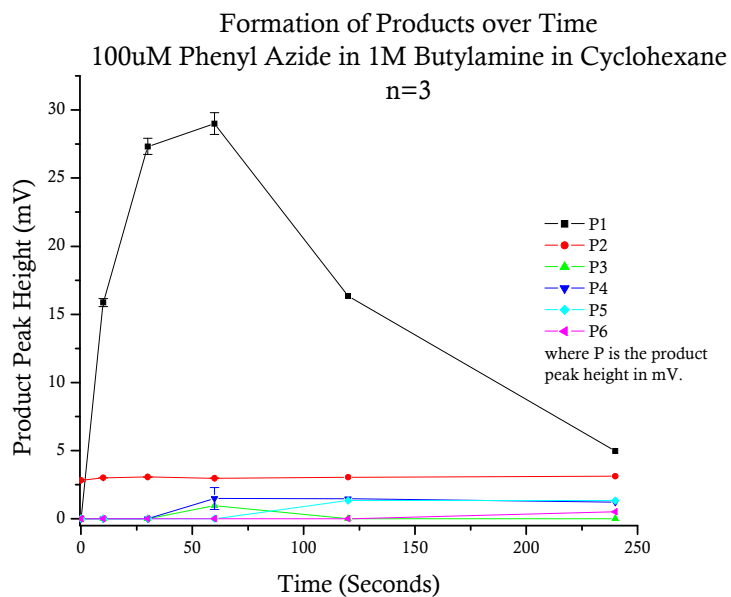


**Figure 3-6. Double First-Order Exponential Decay Curve Fit for Phenyl Azide and Butylamine in Cyclohexane.**  $k_{AA}$  is the rate constant for the amino acid analog reacting with phenyl azide in cyclohexane, where AA means amino acid analog. The equation used to fit the data was  $A(e^{-k_{AA} t/M} + e^{-k_{PA} t})$ , where A is the initial phenyl azide relative peak height (%),  $k_{PA}$  is the rate constant for the loss of phenyl azide in cyclohexane,  $4.27 \cdot 10^{-2} \pm 0.27 \cdot 10^{-2} \text{ sec}^{-1}$  (Figure 3-41), M is the molar concentration of butylamine (1M),  $k_{AA}$  is the rate constant of the loss of phenyl azide when reacting with butylamine, and t is time in seconds. All constants were fixed values, while  $k_{AA}$  varied.  $k_{AA}$  is  $4.75 \cdot 10^{-2} \pm 0.43 \cdot 10^{-2} \text{ sec}^{-1}$  and  $R^2 = 0.997$ .

A.



B.

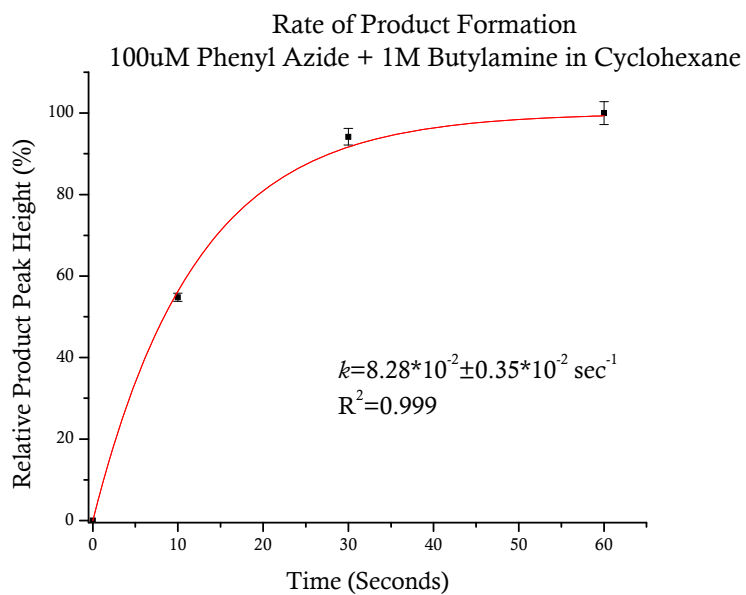


**Figure 3-7. Product Formation for Phenyl Azide and Butylamine in Cyclohexane.**

A. 100 $\mu$ M phenyl azide and 1M butylamine irradiated in cyclohexane show a major product, P1 that begins to decompose the instant that it is formed. The possibility exists

that P1 may decompose into these products. **B.** The equation,  $A(1-e^{-kt})$  was used to determine the rate constant for the butylazepine product formation of P1 from (A.). A is the maximum relative product peak height (%),  $k$  is the rate constant and  $t$  is time in seconds.  $k$  is  $8.28 \times 10^{-2} \pm 0.35 \times 10^{-2} \text{ sec}^{-1}$  and  $R^2$  is 0.999 for this data.  $N=3$ .

## Phenyl Azide Photoreactivity with Butylamine as a Model for Lysine under NEAT Conditions

The irradiation of 100 $\mu$ M phenyl azide and 15M butylamine (NEAT) was performed. The rate of the loss of phenyl azide, the rate of product formation and the identification of the butylazepine product was determined. The rate constant,  $k_1'$ , for the loss of phenyl azide is  $6.17 \times 10^{-2} \pm 0.31 \times 10^{-2} \text{ sec}^{-1}$ . The rate constant,  $k$ , for the formation of product is  $6.31 \times 10^{-2} \pm 1.31 \times 10^{-2} \text{ sec}^{-1}$ . The rate of phenyl azide loss is faster in NEAT conditions than in cyclohexane ( $k_1'_{\text{NEAT}} = 6.17 \times 10^{-2} \pm 0.31 \times 10^{-2} \text{ sec}^{-1}$  vs.  $k_1'_{\text{cyclohexane}} = 4.52 \times 10^{-2} \pm 0.2 \times 10^{-2} \text{ sec}^{-1}$ ). The amount of product formed is slightly more in NEAT conditions (NEAT~36 mV and Cyclohexane~29 mV). The profile of the product formation under NEAT conditions mimics that of the cyclohexane irradiation, where the product increases until time=60 seconds, then begins to decompose.

The product *N*-butyl-3*H*-azepin-2-amine (Scheme 3-1) was produced during the irradiation of 1M phenyl azide with 15M butylamine as determined by  $^1\text{H}$  NMR and confirmed by ESI-MS (165.13854 m/z). The butylazepine product was expected (Schrock & Schuster, 1984) but it begins to decompose upon irradiation beyond  $t=60$  seconds. The butylazepine product forms at a rate near that of the rate for the loss of phenyl azide.

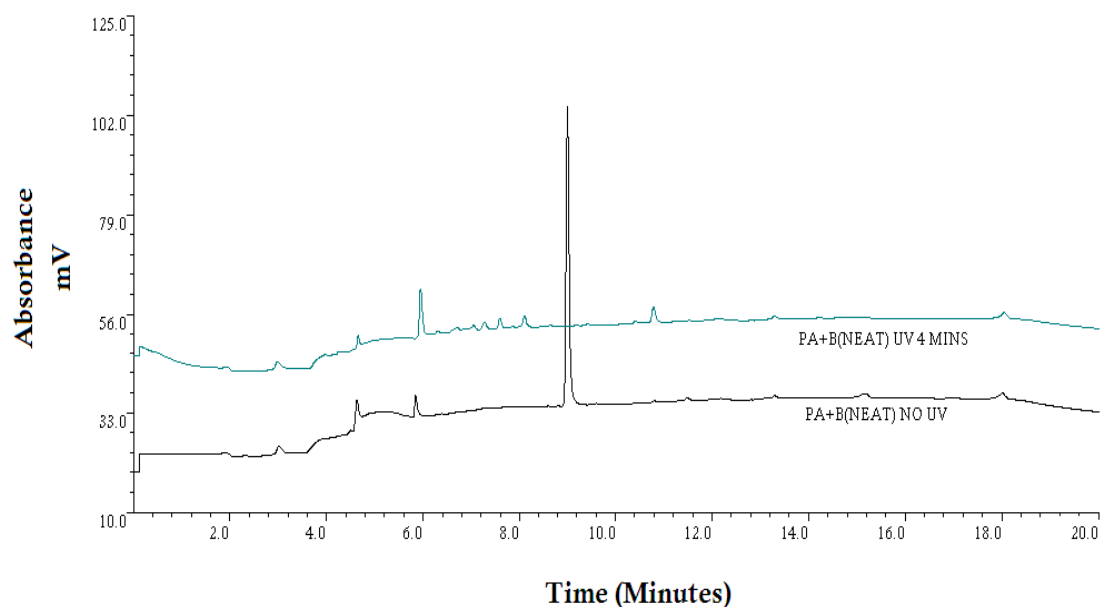


**Figure 3-8. Phenyl Azide and Butylamine (NEAT) Before and After Irradiation.**

HPLC chromatograms for 100 $\mu$ M phenyl azide in 15M butylamine prior to and following 4 minutes of irradiation. The phenyl azide elutes at a retention time of 8.9 minutes using the method 16 gradient (see Methods). The lower curve is the phenyl azide in butylamine with no irradiation. The upper curve is phenyl azide in butylamine after 4 minutes of irradiation. The abbreviations in the figure are as follows: PA is phenyl azide, B(NEAT) is 15M butylamine, and UV is the irradiation followed by the time of irradiation. There is a complete loss of phenyl azide at an irradiation time equal to 240 seconds.



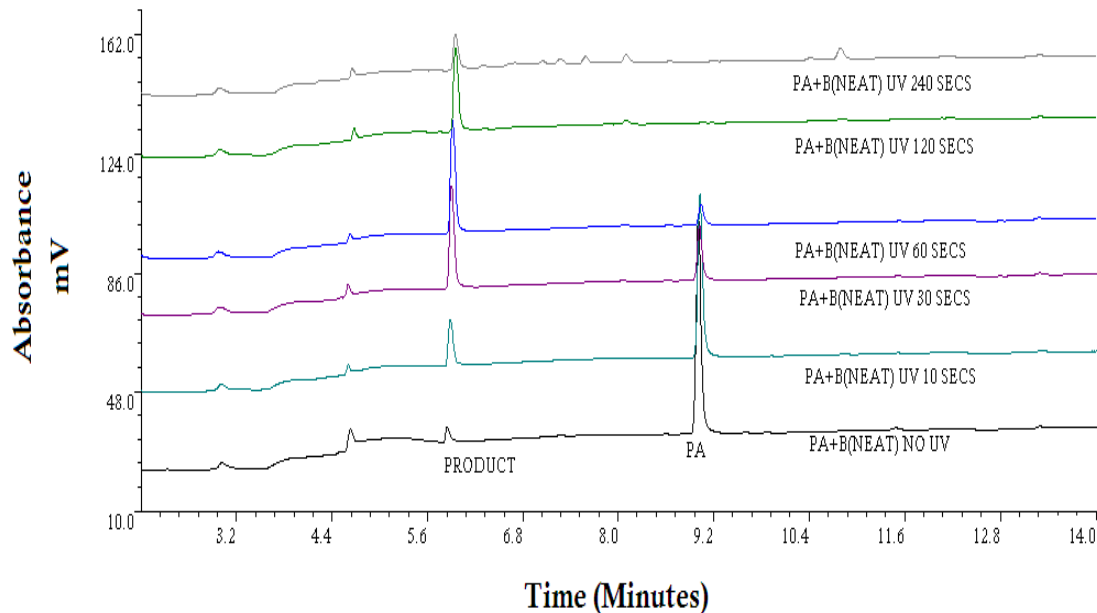


**Figure 3-9. Phenyl Azide and Butylamine (NEAT) Irradiated over Time.** HPLC chromatograms for 100 $\mu$ M phenyl azide in 15M butylamine irradiated over time, where  $t=0, 10, 30, 60, 120,$  and  $240$  seconds. Phenyl azide elutes at 8.9 minutes and the major product elutes at 6 minutes. A trend that can be observed from the chromatograms is that the 6 minute peak decreases after 60 seconds of irradiation and may represent decomposition.

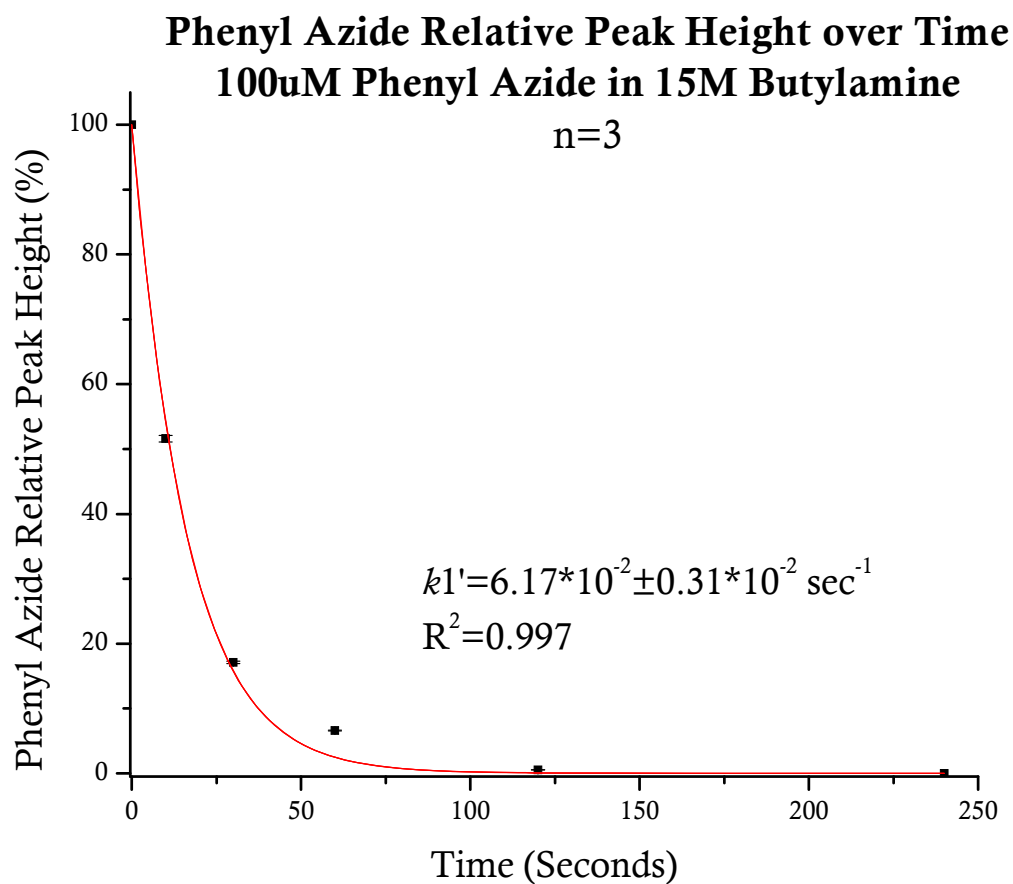
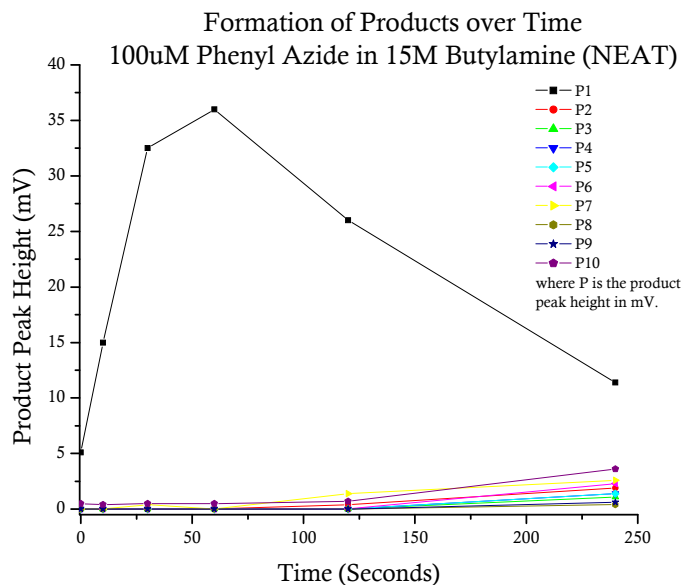


**Figure 3-10. Single First Order Exponential Decay Curve Fit Phenyl Azide and Butylamine (NEAT).** The rate constant of the loss of phenyl azide was determined via time dependent irradiations in the presence of pure (15M) butylamine. The rate constant,  $k1'$ , is  $6.17 \cdot 10^{-2} \pm 0.31 \cdot 10^{-2} \text{ sec}^{-1}$ , where  $R^2$  is equal to 0.997. Some error bars are within the designated symbol.

A.



B.

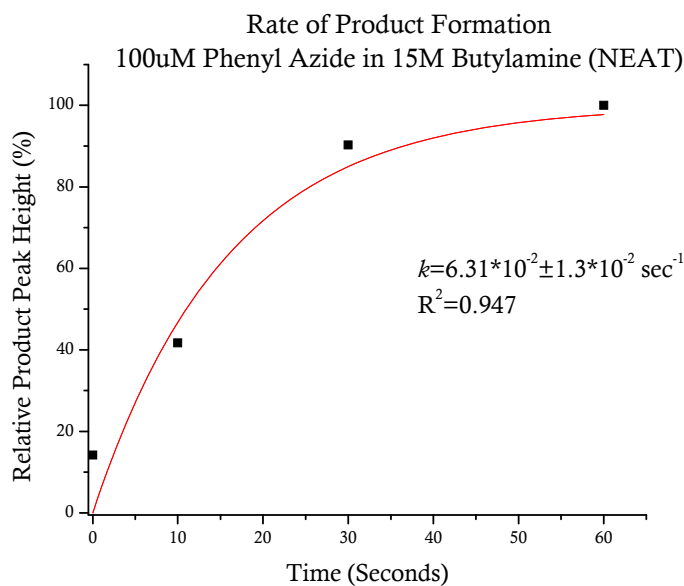
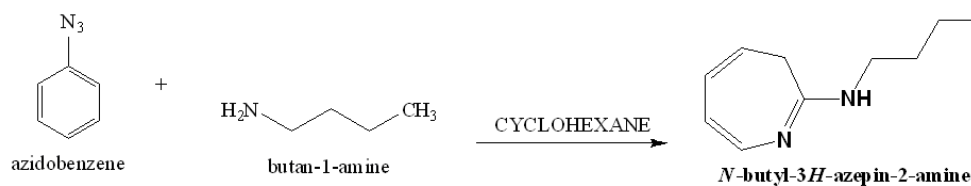


**Figure 3-11. Phenyl Azide and Butylamine (NEAT) Product Formation.** **A.** Phenyl azide (100 $\mu$ M) in 15M butylamine irradiated over time show a major product, P1. The major product reaches a maximum concentration at about 1 minute of irradiation and begins to decompose, possibly into the minor products, thereafter. **B.** The rate constant,

$k$ , for the formation of this product is  $6.31 \cdot 10^{-2} \pm 1.31 \cdot 10^{-2} \text{ sec}^{-1}$ . This product formation profile mimics that of the product formation of butylamine and phenyl azide in cyclohexane.  $N=1$ .

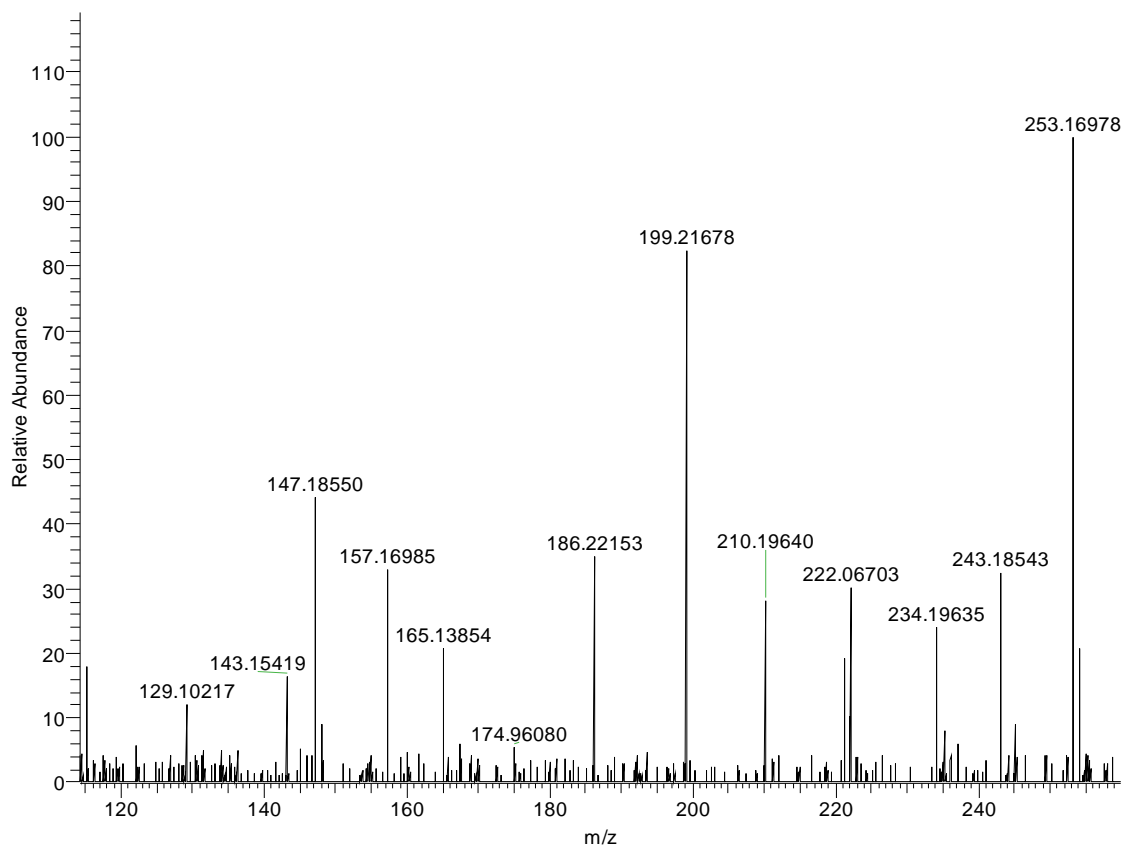
**The Identification of *N*-butyl-3*H*-azepin-2-amine by Electrospray Ionization (ESI) Mass Spectrometry (MS) and Proton Nuclear Magnetic Resonance (<sup>1</sup>H NMR )**

The product from the photoreaction of phenyl azide and butylamine was separated via HPLC and collected for analysis by mass spectrometry. The experimental chemical formula of *N*-butyl-3*H*-azepin-2-amine for (M+H)<sup>+</sup> was C<sub>10</sub>H<sub>17</sub>N<sub>2</sub> and the experimental mass was 165.13854, which was within 5 ppm of the theoretical mass



**Scheme 3-2. Reaction Scheme for Butylamine and Phenyl Azide.** The product formed from this reaction at an irradiation time of 4 minutes and at room temperature is *N*-butyl-3*H*-azepin-2-amine. This azepine product is expected from these reaction conditions (Degraff *et al.*, 1974; Doering & Odum, 1966; Schrock & Schuster, 1984).

butylamine\_080424155138 #1-3 RT: 0.01-0.09 AV: 3 NL: 3.31E5  
T: FTMS + p ESI Full ms [50.00-400.00]



m/z	Intensity	Relative
143.15419	56573.7	20.58
147.18550	150035.2	54.59
148.04532	29820.6	10.85
148.04645	22808.6	8.30
157.16985	109288.2	39.76
<b>165.13854</b>	<b>70257.7</b>	<b>25.56</b>
167.47548	20031.0	7.29
186.21997	20394.6	7.42
186.22153	117261.6	42.66
199.21678	274862.3	100.00
210.19640	96256.9	35.02
221.20109	63740.0	23.19
222.01233	29830.3	10.85
222.01306	19245.6	7.00
222.06633	28926.4	10.52
222.06703	102888.7	37.43
222.12332	23205.3	8.44

234.19635    79983.2    29.10  
 235.18045    26237.6    9.55  
 237.19608    20081.1    7.31

Elemental composition search on mass 165.13854

m/z= 160.13854-170.13854

m/z	Theo. Mass	Delta (ppm)	RDB equiv.	Composition
165.13854	165.13863	-0.52	3.5	C <sub>10</sub> H <sub>17</sub> N <sub>2</sub>
	165.13595	15.71	-1.0	C <sub>7</sub> H <sub>19</sub> O <sub>3</sub> N <sub>1</sub>
	165.13460	23.84	-0.5	C <sub>5</sub> H <sub>17</sub> O <sub>2</sub> N <sub>4</sub>
	165.13326	31.97	0.0	C <sub>3</sub> H <sub>15</sub> O <sub>1</sub> N <sub>7</sub>
	165.14449	-36.05	0.0	C <sub>2</sub> H <sub>15</sub> N <sub>9</sub>
	165.13192	40.10	0.5	C <sub>1</sub> H <sub>13</sub> N <sub>10</sub>
	165.14584	-44.18	-0.5	C <sub>4</sub> H <sub>17</sub> O <sub>1</sub> N <sub>6</sub>
	165.14718	-52.31	-1.0	C <sub>6</sub> H <sub>19</sub> O <sub>2</sub> N <sub>3</sub>

**Figure 3-12. Mass Spectrometry of the Butylazepine Product.** The chemical formula of *N*-butyl-3*H*-azepin-2-amine is C<sub>10</sub>H<sub>16</sub>N<sub>2</sub>. The theoretical monoisotopic mass is 164.13134. The experimental chemical formula for (M+H)<sup>+</sup> was C<sub>10</sub>H<sub>17</sub>N<sub>2</sub> and the experimental mass was 165.13854, which was within 5 ppm of the theoretical mass.

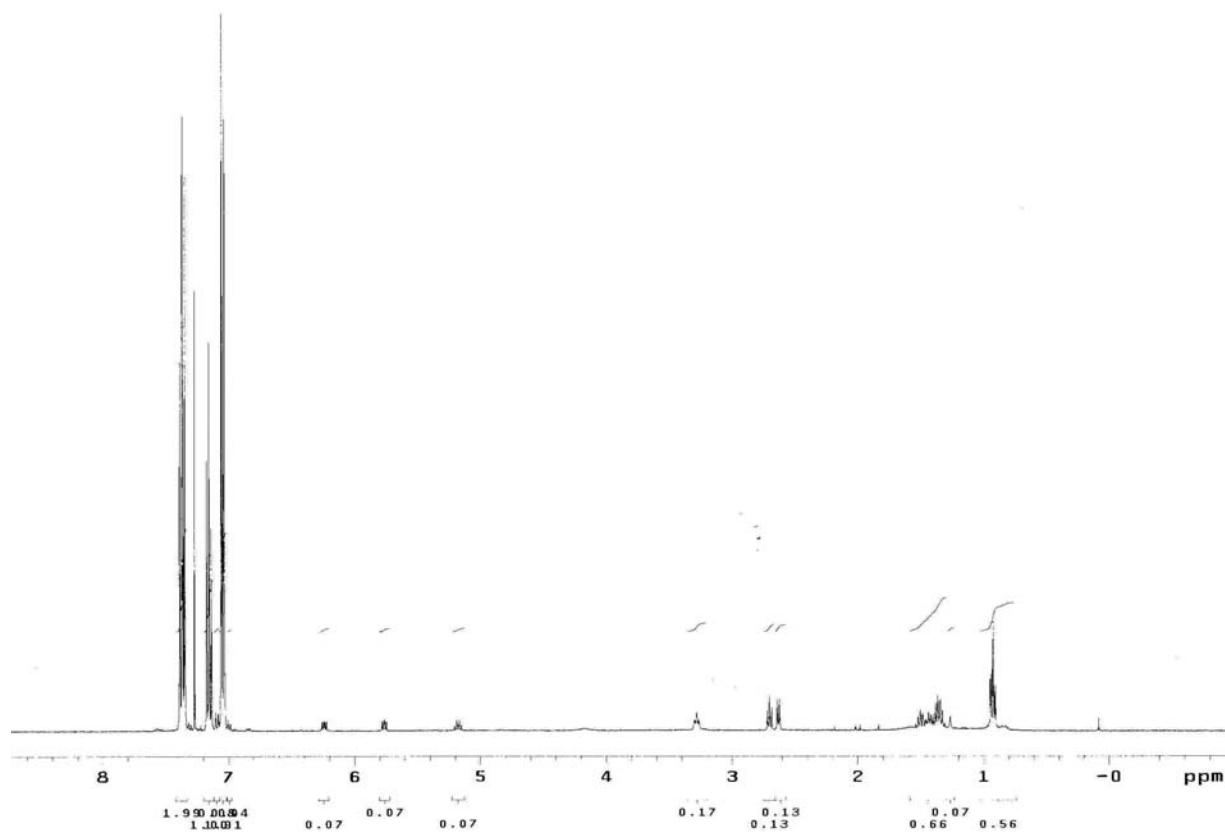


**Figure 3-13. Experimental Proton NMR of *N*-butyl-3*H*-azepin-2-amine.** There was 3 mg of product formed, which contained some impurities. A Varian 400 MHz spectrometer was used to obtain the NMR.



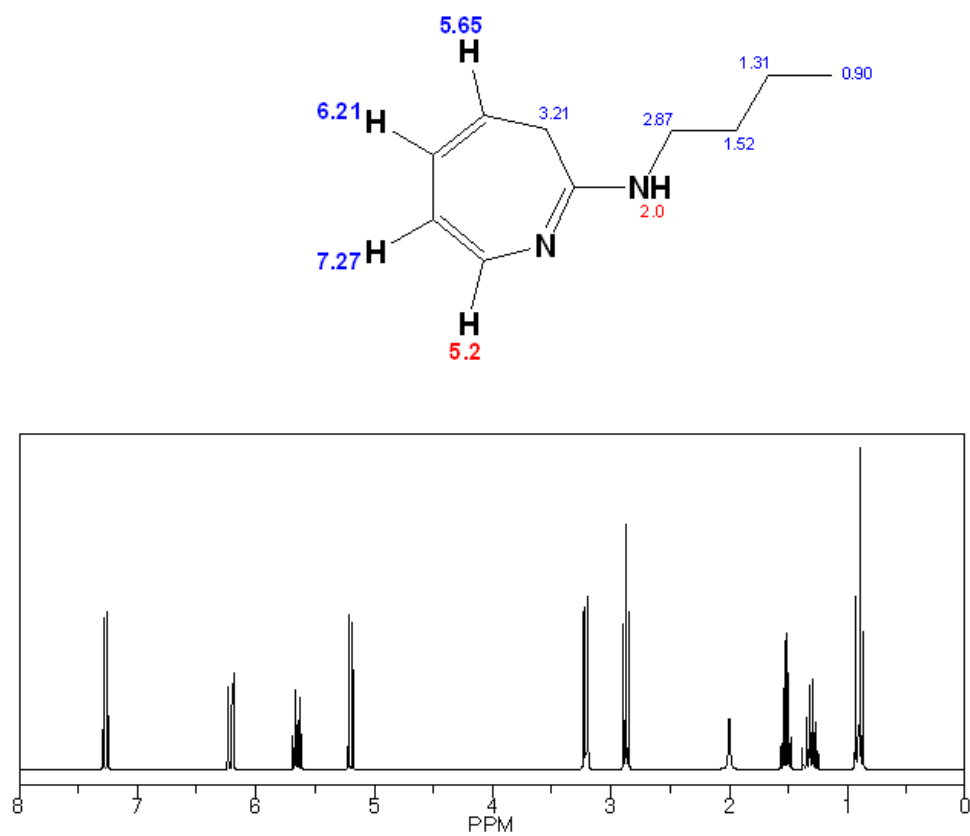


**Figure 3-14. Theoretical Proton NMR of *N*-butyl-3*H*-azepin-2-amine.** This figure shows the shifts of a theoretical proton NMR for the expected product of butylamine and phenyl azide after irradiation. The structure is *N*-butyl-3*H*-azepin-2-amine. <sup>1</sup>H NMR from ChemDraw.

### **Product Stability of Butylazepine under Proteolytic Conditions**

Following the photoaffinity labeling of hDAT, enzymatic digestions and chemical cleavages are performed to form smaller labeled DAT peptides. The product formed between the photoaffinity ligand, which is an aryl azide and the site of incorporation on an amino acid side chain is unknown. It is certain that a covalent bond is formed and attached to hDAT as seen in Chapter Two with [<sup>125</sup>I]-DEEP. For cyanogen bromide cleavage of labeled hDAT, 100 mM CNBr in 70% trifluoroacetic acid (TFA) is used and for enzymatic digestions, the enzyme, trypsin or thermolysin, is reconstituted in 100 mM ammonium bicarbonate (AMBIC). While the protein is still labeled these basic and acidic conditions, less is detected. Therefore, 70% TFA, pH 1 and 100 mM AMBIC, pH 8.9 were used to test the stability of the butylazepine product. 92% of the butylazepine product is decomposed following the application of basic conditions after 4 hours and 100% of the butylazepine product decomposed following the application of both basic and acidic conditions after 24 hours.

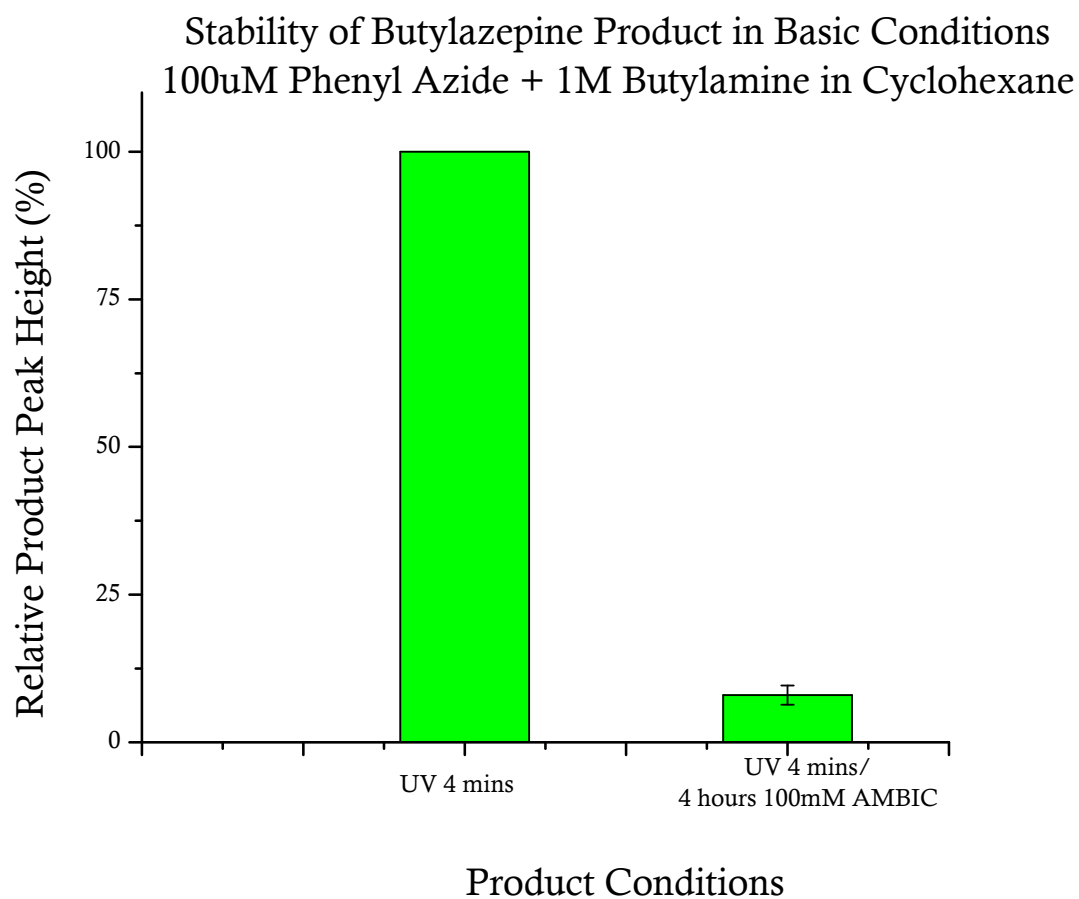


**Figure 3-15. Stability of Butylazepine in Basic Conditions.** After incubation in 100 mM ammonium bicarbonate (AMBIC), pH 8.9 for 4 hours, there is the decomposition of the product. The butylazepine product is reduced by 90% under basic conditions. N=3.

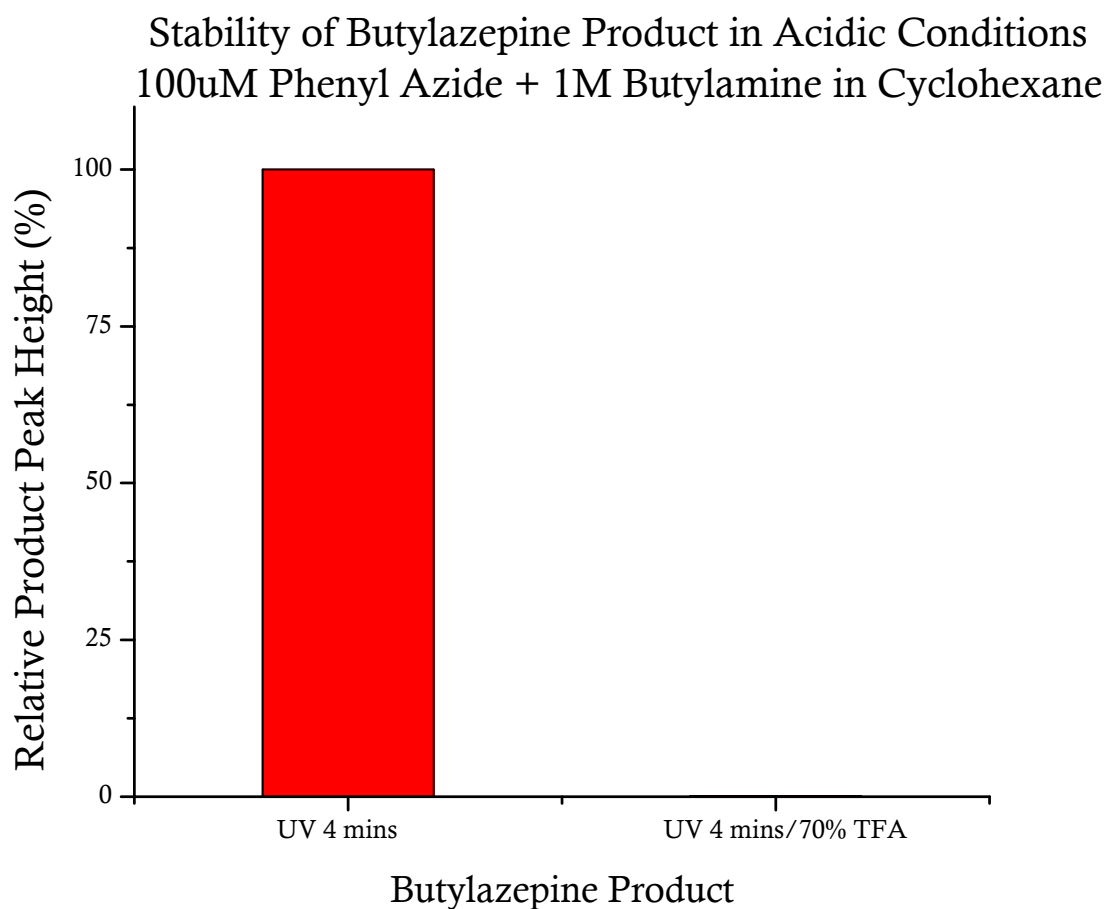


**Figure 3-16. Stability of Butylazepine in Acidic Conditions.** After 24 hours of incubation of the butylazepine product with 70% TFA (v/v) at room temperature in the dark, the entire product decomposes. This suggests that the product formed upon irradiation of phenyl azide with butylamine is not stable under acidic conditions, such as those used for CNBr digests. N=3.

## **Photoreactions with Phenyl Azide and 1-Octanethiol as a Model for Cysteine**

### ***Phenyl Azide Photoreactivity with 1-Octanethiol as a Model for Cysteine***

1-Octanethiol was used to model the amino acid cysteine. Cysteine is typically one of the most reactive amino acids in proteins. Schwartz showed that cysteine was far more reactive with phenyl nitrenes than lysine (Schwartz, 1989). It was important to study the thiol functionality because many people base their research on the reactivity of cysteine (Dayon *et al.*, 2006; Javitch, 1998; Javitch *et al.*, 1994; Liapakis *et al.*, 2001; Lutolf *et al.*, 2001).

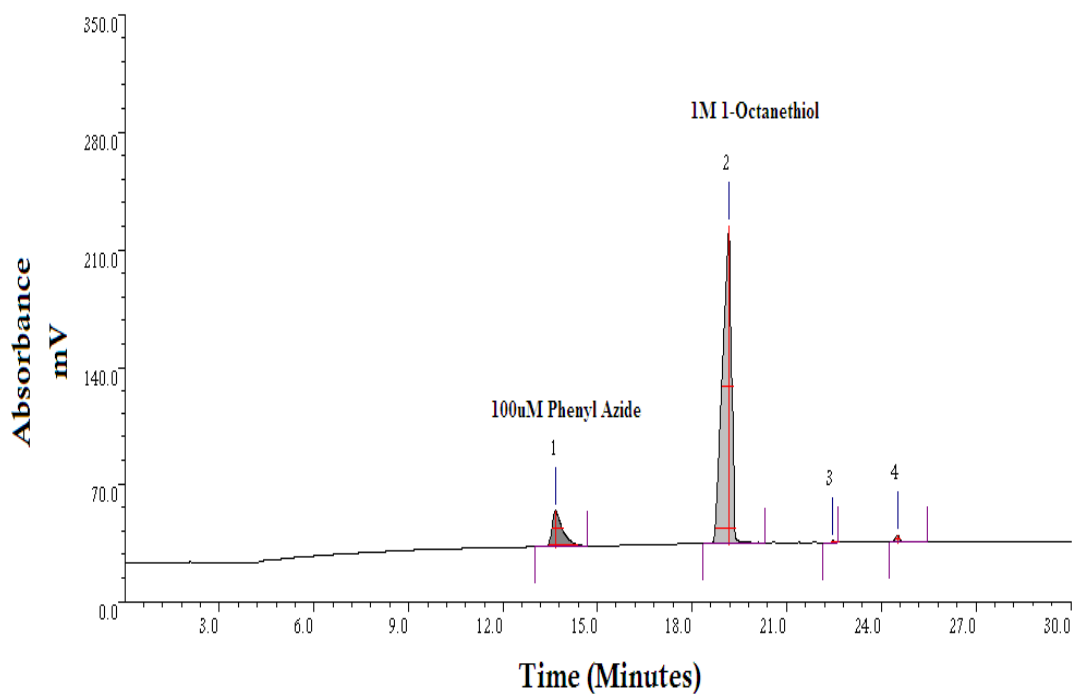


**Figure 3-17. Phenyl Azide and 1-Octanethiol in Cyclohexane Before Irradiation.**

This is an HPLC chromatogram of 100µM phenyl azide +1M 1-octanethiol in cyclohexane before irradiation. Peak 1, which is the phenyl azide, elutes at 13.2 minutes for this gradient (SHORT1). Two new peaks (peaks 3 and 4) at retention times of 23 and 24.5 minutes result from the combining of 100µM phenyl azide with 1M 1-octanethiol in cyclohexane for  $t=0$ . The peaks are not initially present in solvent or either reactant. This could be a dark reaction that occurs regardless of any effect from UV light (Fleming, 1995).

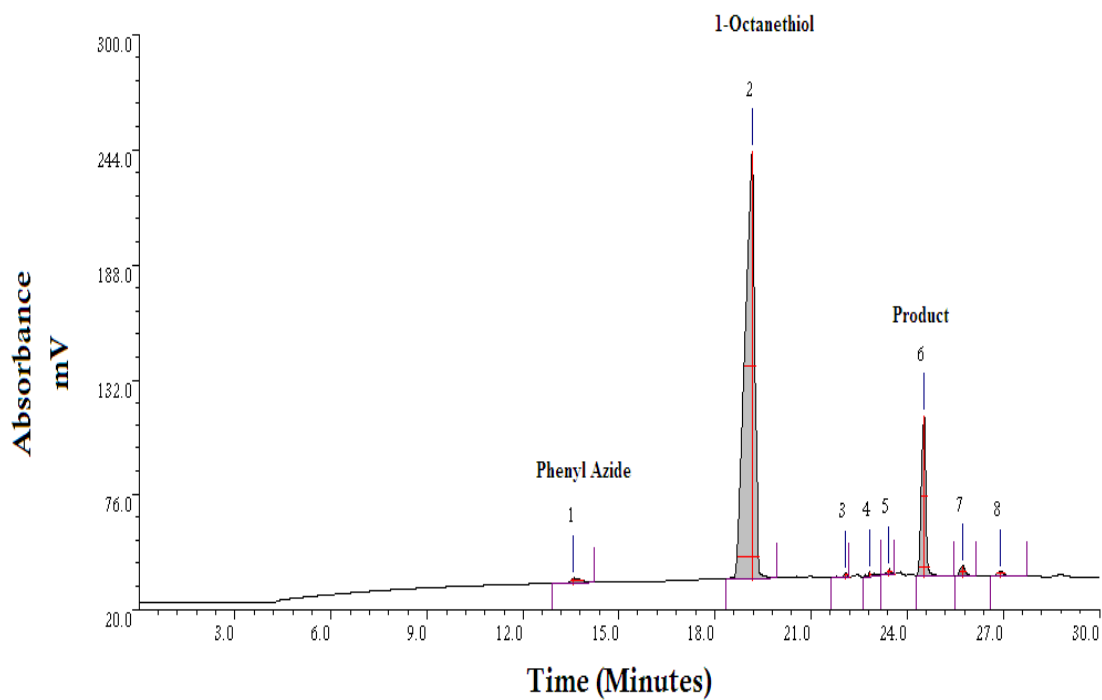


**Figure 3-18. Phenyl Azide and 1-Octanethiol in Cyclohexane After Irradiation.**

This is an HPLC chromatogram of 100 $\mu$ M phenyl azide + 1-octanethiol in cyclohexane after 4 minutes of irradiation. The major product of the reaction is 2-(octylthio)-3*H*-azepine. It elutes at approximately 25 minutes using the gradient method SHORT 1.

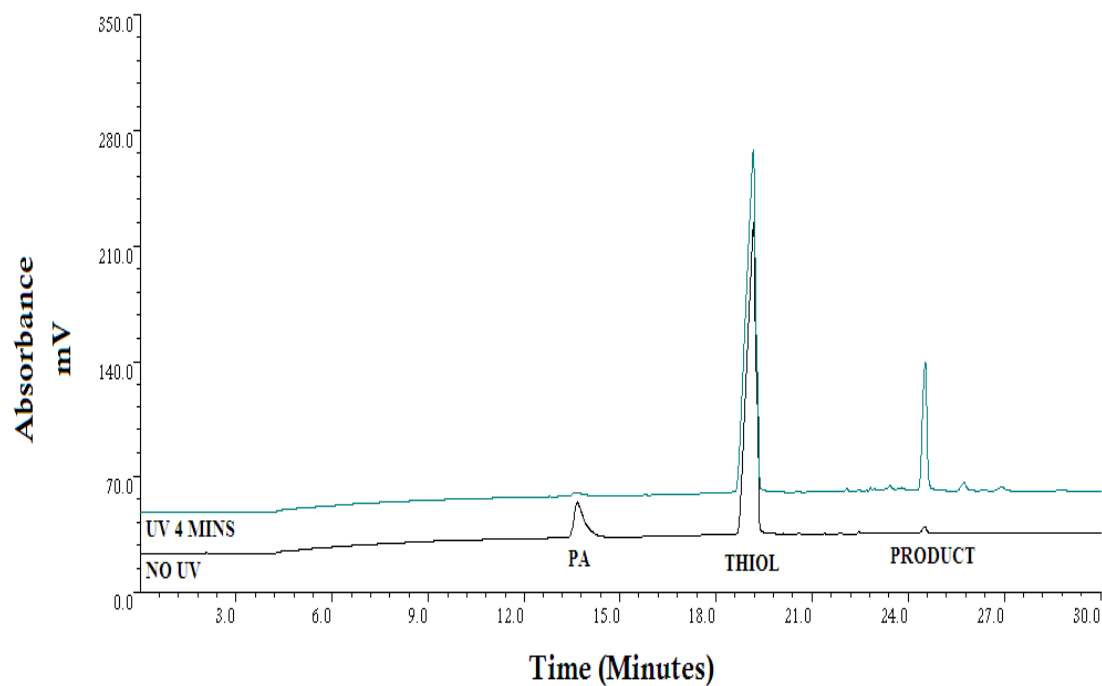


**Figure 3-19. Phenyl Azide and 1-Octanethiol in Cyclohexane Before and After Irradiation.** The lower curve is the phenyl azide and 1-octanethiol in cyclohexane with no irradiation. The upper curve is the phenyl azide and 1-octanethiol in cyclohexane after four minutes of irradiation. Abbreviations: PA is phenyl azide, THIOL is the 1-octanethiol, NO UV is the data before irradiation, and UV 4 MINS is the irradiation at  $t=4$  minutes. The product elutes at approximately 25 minutes. The phenyl azide, which has a retention time of approximately 13 minutes, is diminishing as the product is increasing.



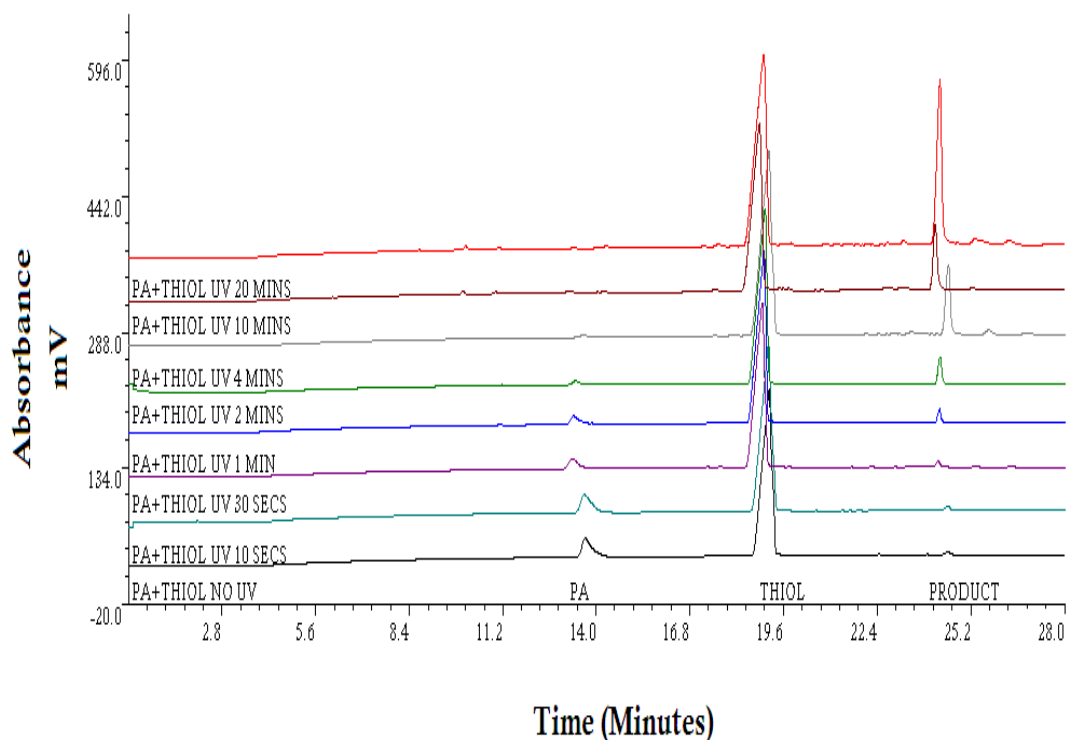
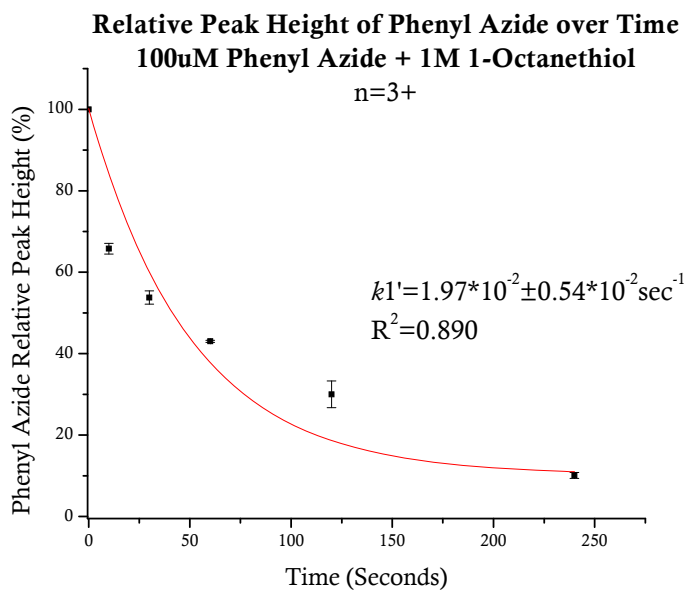


**Figure 3-20. Phenyl Azide and 1-Octanethiol in Cyclohexane Irradiated over Twenty Minutes.** HPLC chromatograms for 100 $\mu$ M phenyl azide + 1M 1-octanethiol in cyclohexane irradiated over time, where  $t=0, 10, 30, 60, 120, 240, 600,$  and  $1200$  seconds. The loss of phenyl azide over time is seen by the loss of a peak at 13 minutes. The emergence of product is also shown at a retention time of approximately 25 minutes.

A.



B.

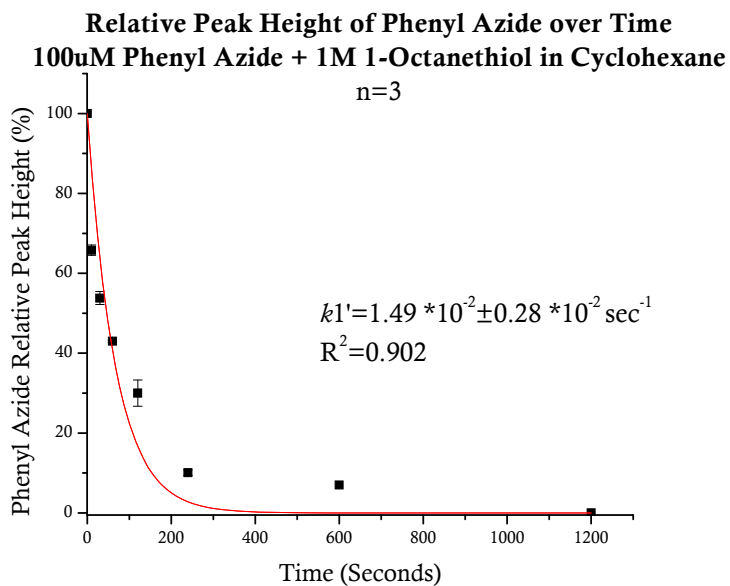


**Figure 3-21. Single Exponential First-Order Decay Curve Fit for Phenyl Azide and 1-Octanethiol in Cyclohexane. A. Kinetic Analysis of Data for Four Minutes of Irradiation.** The first-order kinetic analysis of this data gave a rate constant,  $k1'$  that is

equal to  $1.97 \times 10^{-2} \pm 0.54 \times 10^{-2} \text{ sec}^{-1}$  with an  $R^2$  equal to 0.890. The single first-order exponential fit did not fit the data as well as the double first-order exponential fit, which is not shown here. However, this suggests that the possibility that two parallel processes may be going on during the irradiation of phenyl azide with 1-octanethiol. **B. Kinetic Analysis of Data for 20 Minutes of Irradiation.** Further irradiation of phenyl azide with 1M 1-octanethiol beyond 4 minutes gives a rate constant,  $k_1'$ , of  $1.49 \times 10^{-2} \pm 0.28 \times 10^{-2} \text{ sec}^{-1}$ .

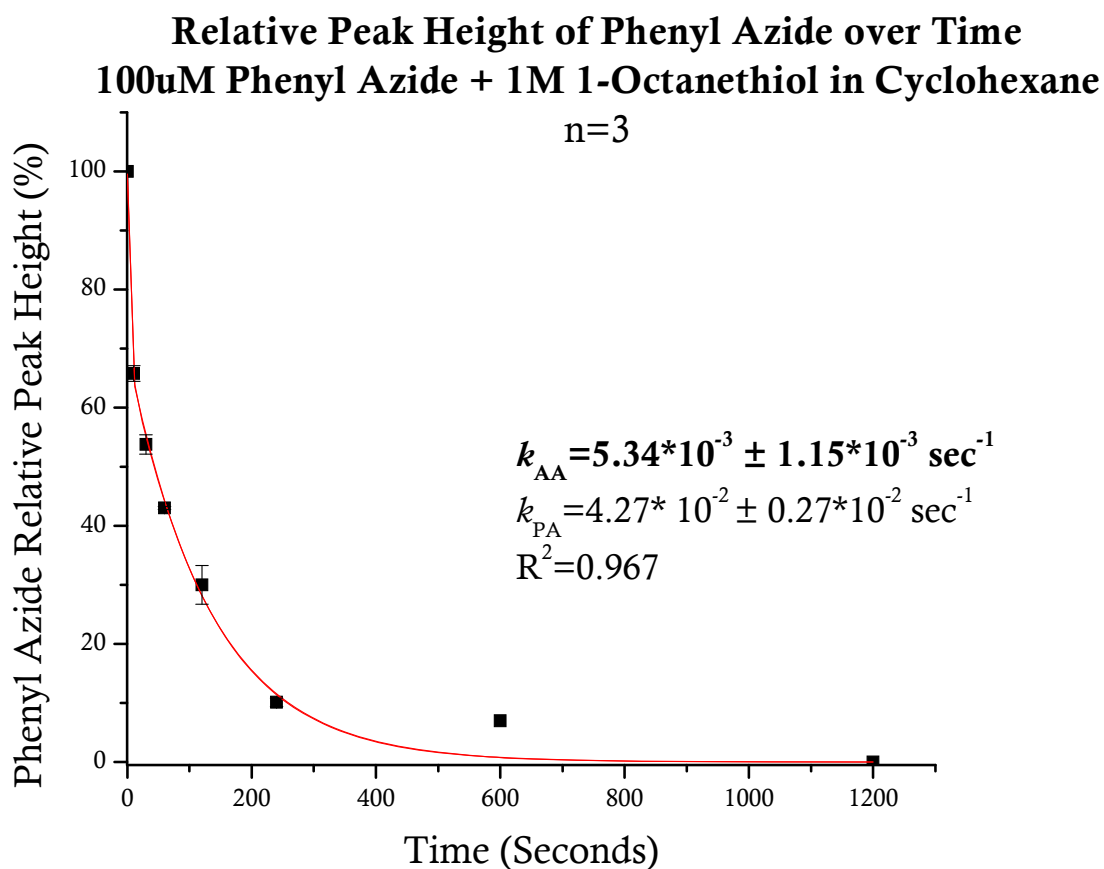


**Figure 3-22. Double Exponential Decay Curve Fit for Phenyl Azide and 1-Octanethiol in Cyclohexane.**  $k_{AA}$  is the rate constant for the amino acid analog reacting with phenyl azide in cyclohexane, where AA means amino acid analog. The equation used to fit the data was  $A(e^{-k_{AA} t/M} + e^{-k_{PA} t})$ , where A is the initial phenyl azide relative peak height (%),  $k_{PA}$  is the rate constant for phenyl azide loss when reacting alone in cyclohexane,  $4.27 \cdot 10^{-2} \pm 0.27 \cdot 10^{-2} \text{ sec}^{-1}$ , M is the molar concentration of 1-octanethiol (1M),  $k_{AA}$  is the rate constant based on the loss of phenyl azide when reacting with 1-octanethiol, and t is time in seconds. All constants except  $k_{AA}$  were fixed values.  $k_{AA}$  was found to be  $5.34 \cdot 10^{-3} \pm 1.15 \cdot 10^{-3} \text{ sec}^{-1}$  and  $R^2 = 0.967$ .

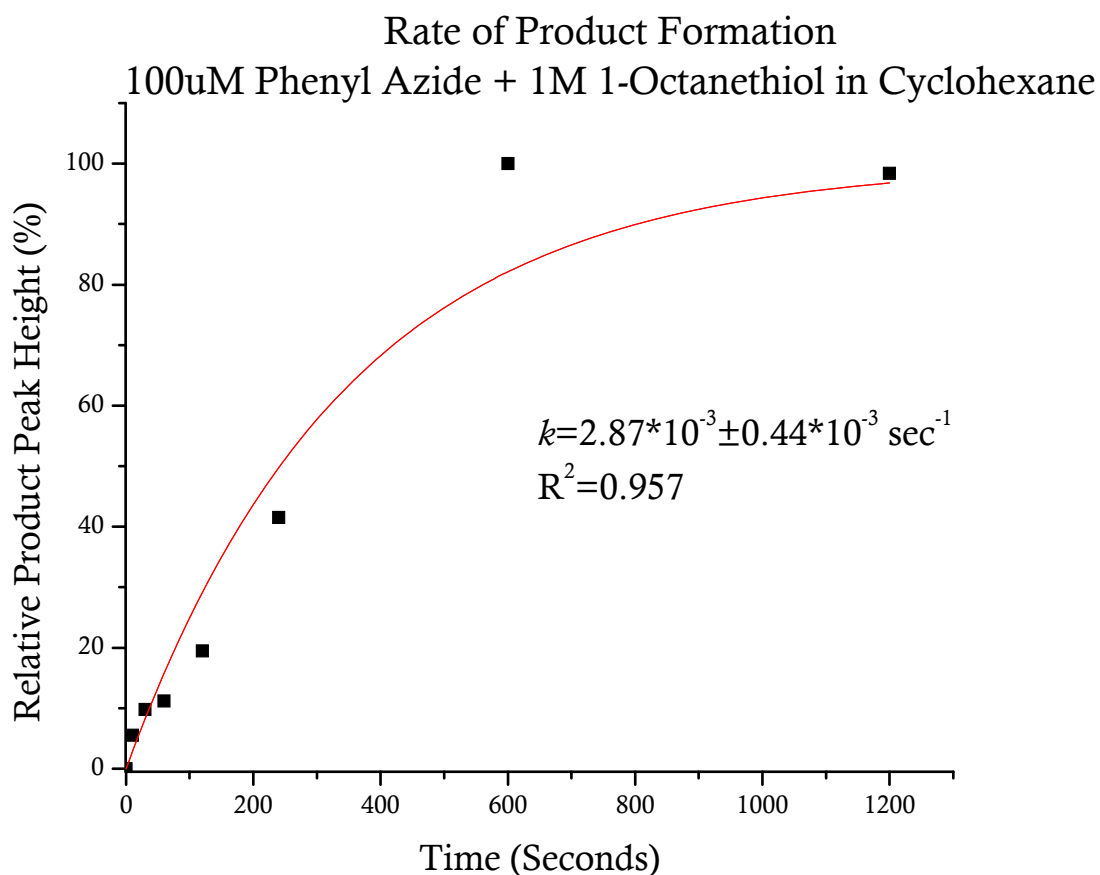


**Figure 3-23. Product Formation for Phenyl Azide and 1-Octanethiol in**

**Cyclohexane.** Phenyl azide (100 $\mu$ M) and 1M 1-octanethiol irradiated in cyclohexane

show a major product, P1 (Figure 3-20). The equation  $A(1-e^{-kt})$  was used to determine

the rate constant for the product formation. The rate constant,  $k$ , is  $2.87 * 10^{-3} \pm 0.44 * 10^{-3}$

$\text{sec}^{-1}$ , which is slower than the butylazepine product formation ( $k_{\text{cyclohexane}}=8.28*10^{-$

$2 \pm 0.35*10^{-2}$  and  $k_{\text{NEAT}}=6.31*10^{-2} \pm 1.31*10^{-2} \text{ sec}^{-1}$ ).  $A$  is the maximum relative product

peak height (%),  $k$  is the rate constant in  $\text{sec}^{-1}$ , and  $t$  is the time in seconds.  $N=1$ .

**Phenyl Azide Photoreactivity with 1-Octanethiol as a Model  
for Cysteine in NEAT Conditions**

The irradiation of 100 $\mu$ M phenyl azide and 1-octanethiol was performed under neat conditions (5.6M 1-octanethiol). The first order rate constant of phenyl azide loss, the rate constant for the product formation and the identification of the octylazepine product was determined. The single exponential first-order rate constant,  $k_1'$ , was  $3.34 \times 10^{-3} \pm 0.16 \times 10^{-3} \text{ sec}^{-1}$  for the loss of phenyl azide in 5.6M 1-octanethiol over a 4 minute time period. However, the reaction had not gone to completion and was carried out over a 60 minute time period. The single first-order exponential rate constant,  $k_1'$ , was  $2.98 \times 10^{-3} \pm 0.58 \times 10^{-3} \text{ sec}^{-1}$  for phenyl azide loss in 5.6M 1-octanethiol over a 60 minute time period. The rate constant,  $k$ , for the formation of the octylthioazepine product was  $1.27 \times 10^{-3} \pm 0.38 \times 10^{-3} \text{ sec}^{-1}$ .

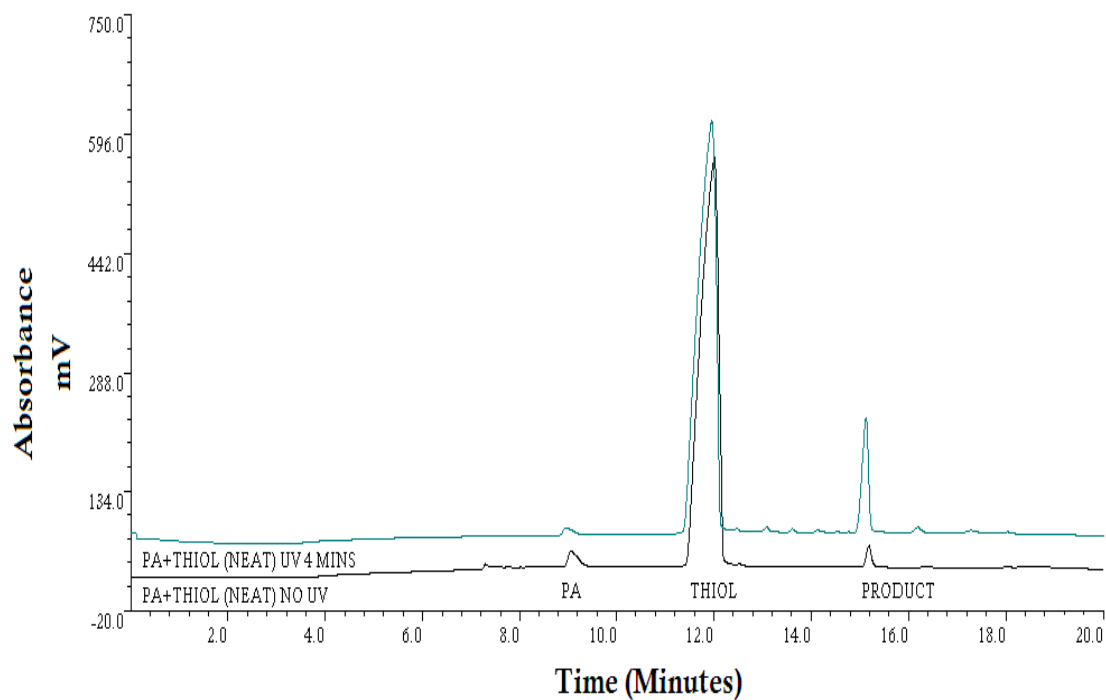


**Figure 3-24. Phenyl Azide and 1-Octanethiol (NEAT) Before and After Irradiation.**

HPLC Chromatograms of 100 $\mu$ M phenyl azide in 5.6M 1-Octanethiol. The phenyl azide has a retention time of 8.9 minutes using a gradient named method 16 (see methods).

The formation of products began with no irradiation, possibly signifying a dark reaction of the aryl azide (Fleming, 1995). The phenyl azide has been reduced to 44% of its original peak height following 4 minutes of irradiation with 1-octanethiol in no solvent.

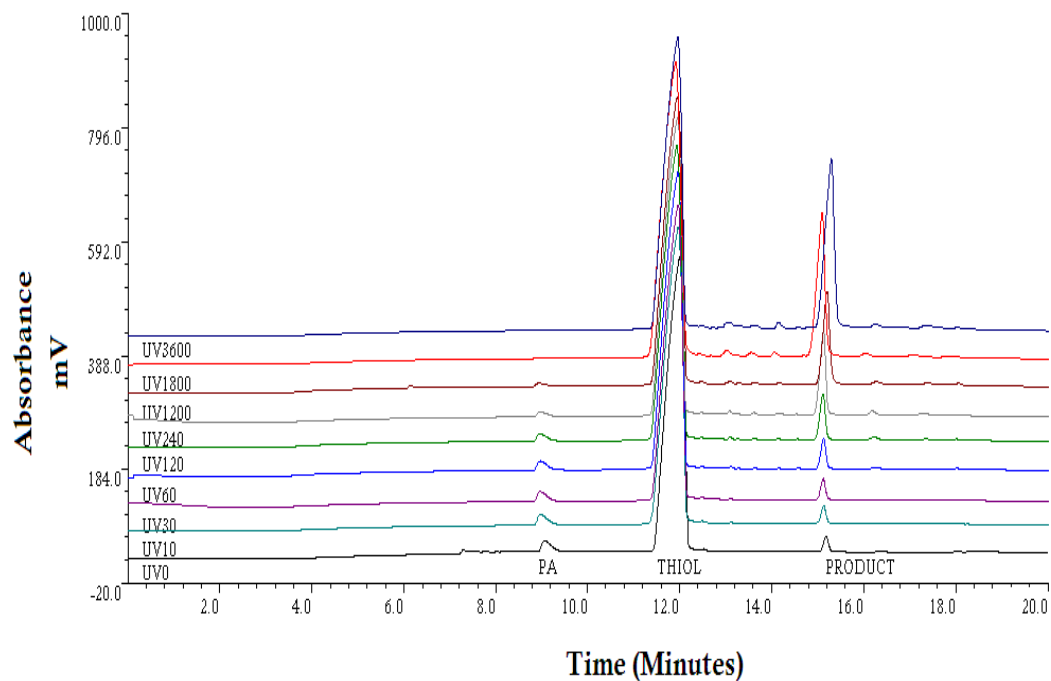
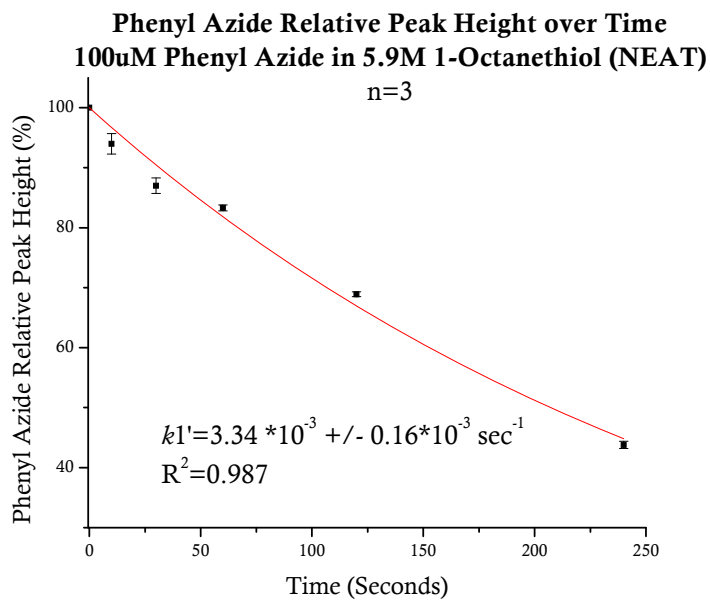


**Figure 3-25. Phenyl Azide and 1-Octanethiol (NEAT) Irradiated over Sixty Minutes.** The loss of phenyl azide over time is seen by the loss of a peak at the 8.9 minute retention time. The emergence of product is shown at a retention time of approximately 15 minutes. The gradient used was method 16 (see methods).



A.



B.

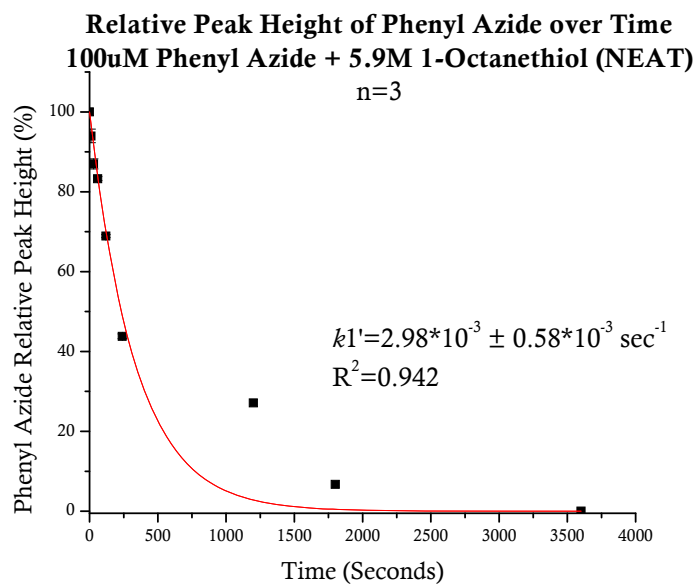


**Figure 3-26. Single First-Order Exponential Decay Curve Fit for Phenyl Azide and 1-Octanethiol (NEAT). A. Kinetic Analysis of Data for 4 Minutes of Irradiation.**

The first-order kinetic analysis of this data over a 4 minute time period gave a rate constant,  $k1'$ , equal to  $3.34 \cdot 10^{-3} \pm 0.16 \cdot 10^{-3} \text{ sec}^{-1}$  with an  $R^2$  equal to 0.987. **B. Kinetic**

**Analysis of Data for 60 Minutes of Irradiation Time.** With longer irradiation times, the rate constant,  $k_1'$ , was  $2.98 \times 10^{-3} \pm 0.58 \times 10^{-3} \text{ sec}^{-1}$  with an  $R^2$  equal to 0.942. This rate was smaller than the rate constant of 1-octanethiol irradiated with phenyl azide in cyclohexane, which was  $1.97 \times 10^{-2} \pm 0.54 \times 10^{-2} \text{ sec}^{-1}$ .

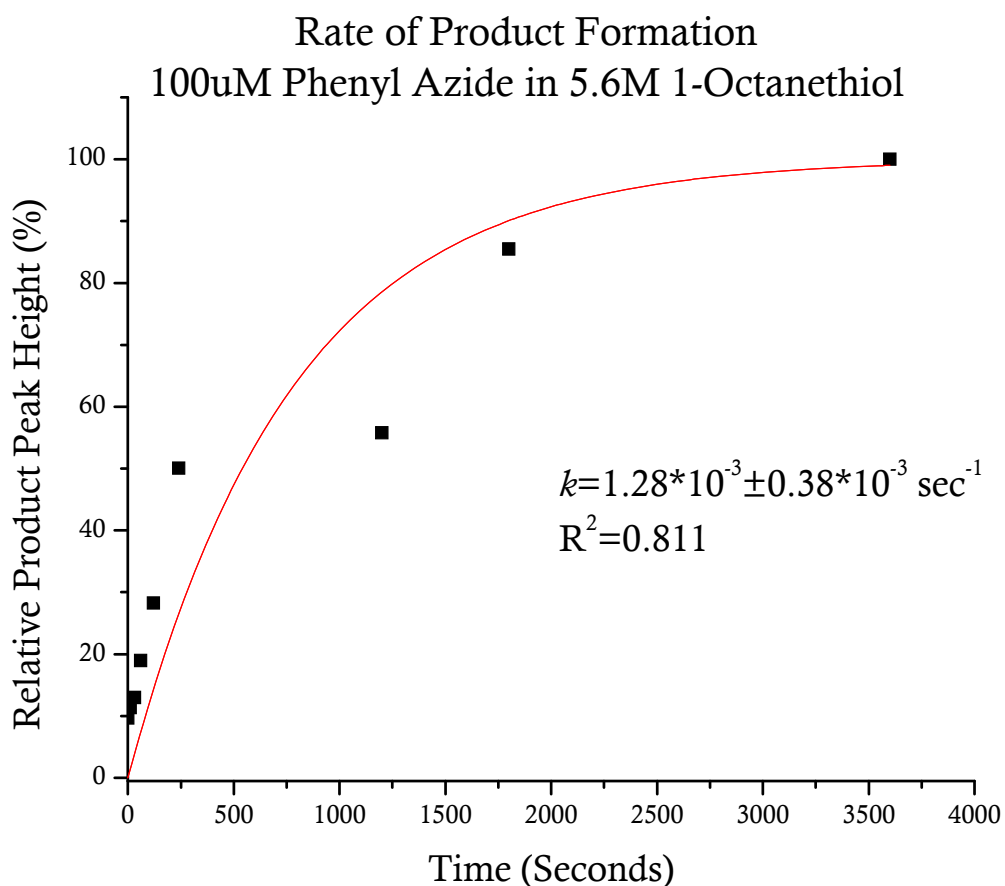
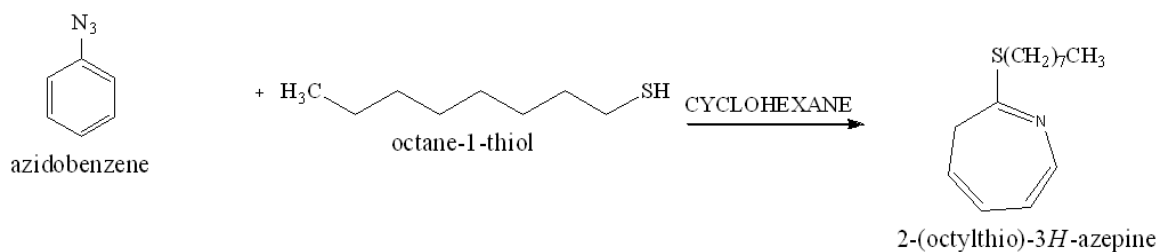


**Figure 3-27. Rate of Product Formation for Phenyl Azide and 1-Octanethiol**

(NEAT). 100 $\mu$ M phenyl azide in 5.6M 1-octanethiol irradiated over time show a major product. The rate constant,  $k$ , for the formation of product is  $1.28*10^{-3}\pm 0.38*10^{-3}\text{ sec}^{-1}$ . At time zero, there is the formation of product being formed which could be caused by dark reactions that have been known to occur with aryl azides (Fleming, 1995). Thiols also cause the reduction of azides to amines (Handlon & Oppenheimer, 1988; Staros *et al.*, 1978). N=1.

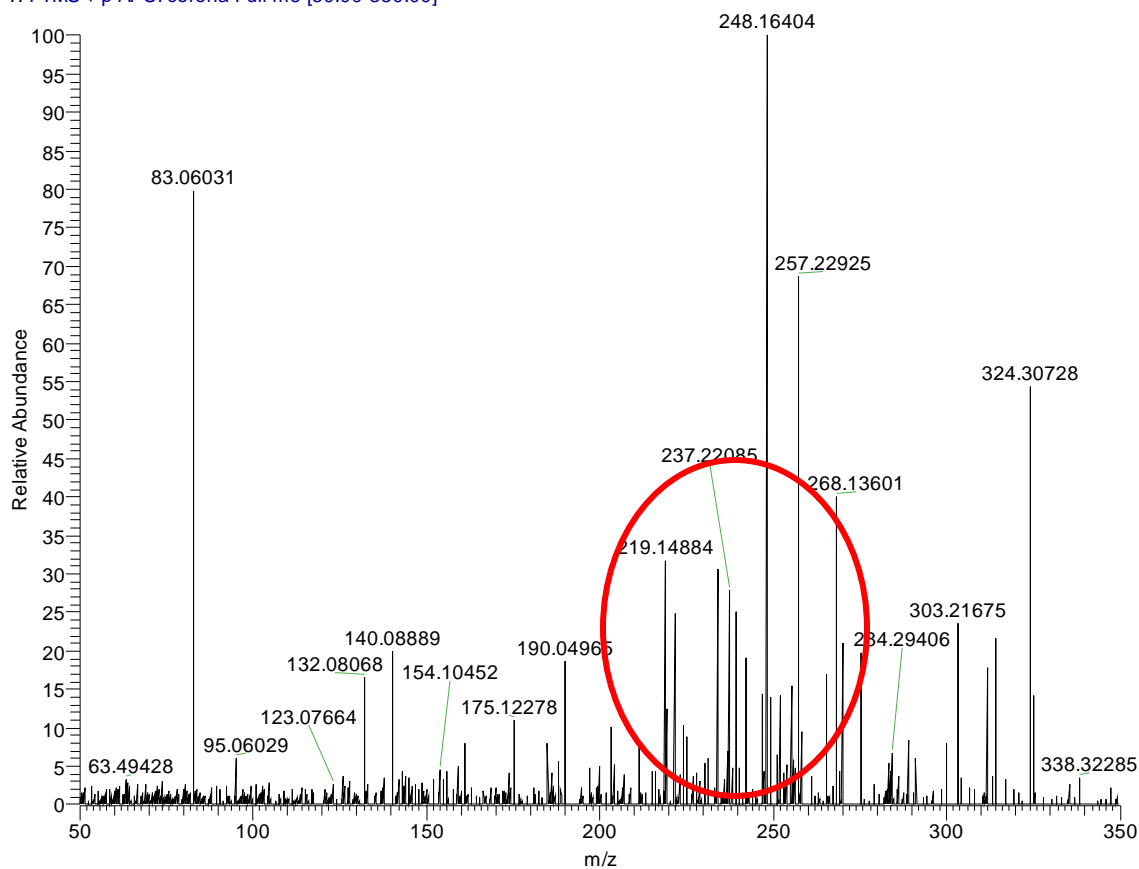
**The Identification of 2-(octylthio)-3*H*-azepine by  
Atmospheric Pressure Chemical Ionization (APCI)  
Mass Spectrometry (MS)**

The product from the photoreaction of phenyl azide and 1-octanethiol was separated via HPLC and collected for analysis by mass spectrometry. The experimental chemical formula was C<sub>14</sub>H<sub>23</sub>NS and the experimental mass was 237.15421, which was within 5 ppm of the theoretical mass.



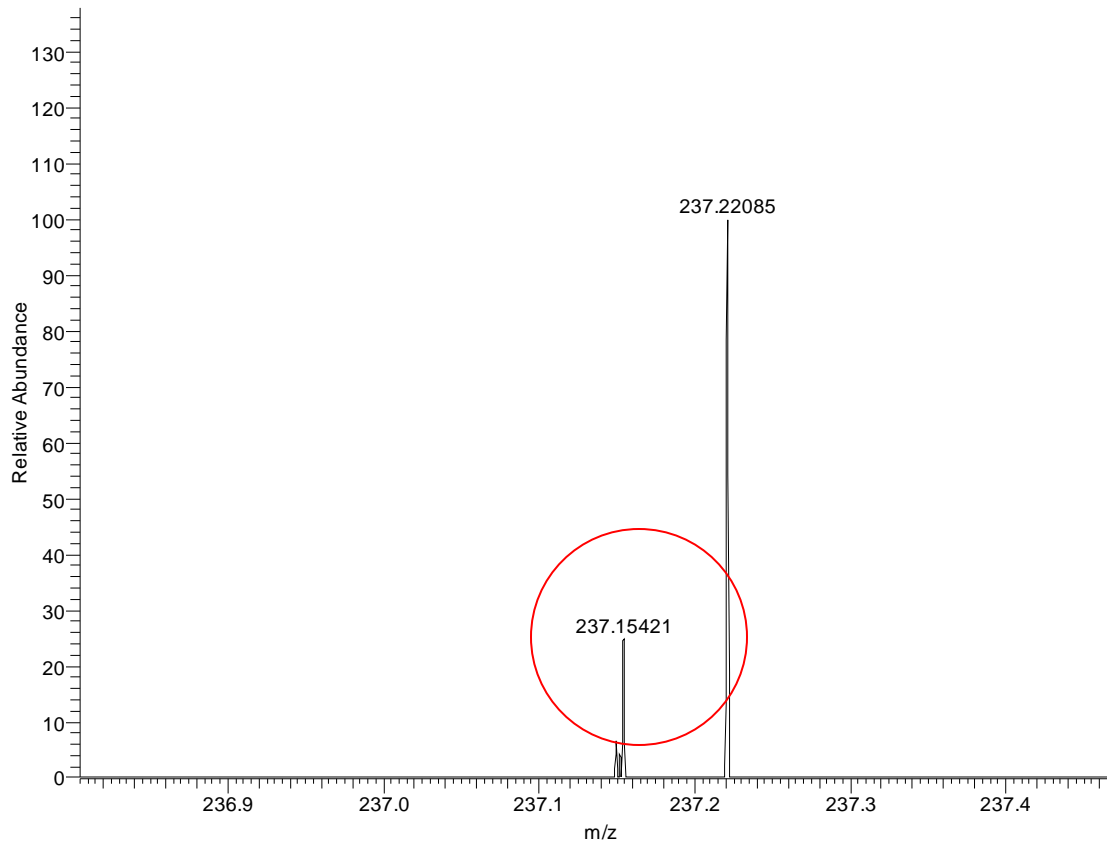
**Scheme 3-2. Reaction Scheme for 1-Octanethiol and Phenyl Azide.** The product formed from this reaction is 2-(octylthio)-3*H*-azepine. In fraction 25 at a retention time of 25 minutes using gradient SHORT1, this product was collected and submitted for mass spectrometry analysis. The product was identified using APCI-MS.

25thiol\_080513141059 #1-2 RT: 0.02-0.11 AV: 2 NL: 1.87E4  
T: FTMS + p APCI corona Full ms [50.00-350.00]



m/z	Intensity	Relative
83.06031	15272.7	81.38
132.08068	3094.1	16.49
140.08889	3774.7	20.11
190.04965	3516.5	18.74
219.14884	5943.5	31.67
221.89173	4772.9	25.43
234.14848	5787.4	30.84
239.23652	4911.5	26.17
242.07246	3641.3	19.40
248.16404	18767.8	100.00
257.22925	13178.1	70.22
265.25204	3228.6	17.20
268.13601	7519.3	40.07
270.13392	3975.9	21.18
275.23973	3755.8	20.01
303.21675	4458.7	23.76
312.03751	3376.0	17.99
314.03545	4105.0	21.87
324.30728	10509.0	55.99

25thiol\_080513141059 #1-2 RT: 0.02-0.11 AV: 2 NL: 5.23E3  
T: FTMS + p APCI corona Full ms [50.00-350.00]



m/z	Intensity	Relative
237.14951	350.7	6.67
237.15196	221.8	4.22
<b>237.15421</b>	<b>1342.5</b>	<b>25.53</b>
237.22085	5259.4	100.00

Elemental composition search on mass 237.15421

m/z= 232.15421-242.15421

m/z	Theo. Mass	Delta (ppm)	RDB equiv.	Composition
237.15421	237.15439	-0.76	1.0	C <sub>8</sub> H <sub>19</sub> O <sub>3</sub> N <sub>7</sub>
	237.15457	-1.53	4.0	C <sub>14</sub> H <sub>23</sub> N <sub>1</sub> <sup>32</sup> S <sub>1</sub>
	237.15305	4.91	1.5	C <sub>4</sub> H <sub>17</sub> O <sub>2</sub> N <sub>10</sub>
	237.15573	-6.42	0.5	C <sub>8</sub> H <sub>21</sub> O <sub>4</sub> N <sub>4</sub>
	237.15189	9.77	-0.5	C <sub>11</sub> H <sub>25</sub> O <sub>3</sub> <sup>32</sup> S <sub>1</sub>
	237.15707	-12.06	5.5	C <sub>9</sub> H <sub>17</sub> N <sub>8</sub>
	237.15707	-12.08	0.0	C <sub>10</sub> H <sub>23</sub> O <sub>5</sub> N <sub>1</sub>
	237.15120	12.69	9.0	C <sub>17</sub> H <sub>19</sub> N <sub>1</sub>
	237.15055	15.43	0.0	C <sub>9</sub> H <sub>23</sub> O <sub>2</sub> N <sub>3</sub> <sup>32</sup> S <sub>1</sub>
	237.15841	-17.72	5.0	C <sub>11</sub> H <sub>19</sub> O <sub>1</sub> N <sub>5</sub>
	237.14921	21.09	0.5	C <sub>7</sub> H <sub>21</sub> O <sub>1</sub> N <sub>6</sub> <sup>32</sup> S <sub>1</sub>
	237.15975	-23.38	4.5	C <sub>13</sub> H <sub>21</sub> O <sub>2</sub> N <sub>2</sub>
	237.14852	23.99	4.5	C <sub>14</sub> H <sub>21</sub> O <sub>3</sub>
	237.16044	-26.28	0.5	C <sub>6</sub> H <sub>21</sub> N <sub>8</sub> <sup>32</sup> S <sub>1</sub>
	237.14787	26.75	1.0	C <sub>8</sub> H <sub>19</sub> N <sub>9</sub> <sup>32</sup> S <sub>1</sub>
	237.14718	29.65	5.0	C <sub>12</sub> H <sub>19</sub> O <sub>2</sub> N <sub>3</sub>
	237.16178	-31.94	0.0	C <sub>8</sub> H <sub>23</sub> O <sub>1</sub> N <sub>5</sub> <sup>32</sup> S <sub>1</sub>
	237.14584	35.31	5.5	C <sub>10</sub> H <sub>17</sub> O <sub>1</sub> N <sub>6</sub>
	237.16313	-37.60	-0.5	C <sub>10</sub> H <sub>25</sub> O <sub>2</sub> N <sub>2</sub> <sup>32</sup> S <sub>1</sub>
	237.16378	-40.34	8.5	C <sub>18</sub> H <sub>21</sub>

**Figure 3-28. Mass Spectrometry of the Octylthioazepine Product.** The chemical formula of 2-(octylthio)-3*H*-azepine is C<sub>14</sub>H<sub>23</sub>NS. The theoretical monoisotopic mass is 237.15511. The experimental chemical formula found was C<sub>14</sub>H<sub>23</sub>NS and the experimental mass was 237.15421, which was within 5 ppm of the theoretical mass.

### **Product Stability of Octylthioazepine in Proteolytic Conditions**

The product from phenyl azide and 1-octanethiol was incubated for 4 hours and 24 hours with 100mM ammonium bicarbonate, pH 8.9 at room temperature in the dark. After 4 hours of treatment with ammonium bicarbonate, there was 28% of the product remaining. After 24 hours of incubation, the product completely decomposed. The octylthioazepine product was also treated with 70% trifluoroacetic acid (TFA), pH 1, for 24 hours at room temperature in the dark. 67% of the octylthioazepine product remained following the 24 hour incubation with TFA. The octylthioazepine product was the most stable product in acidic conditions.



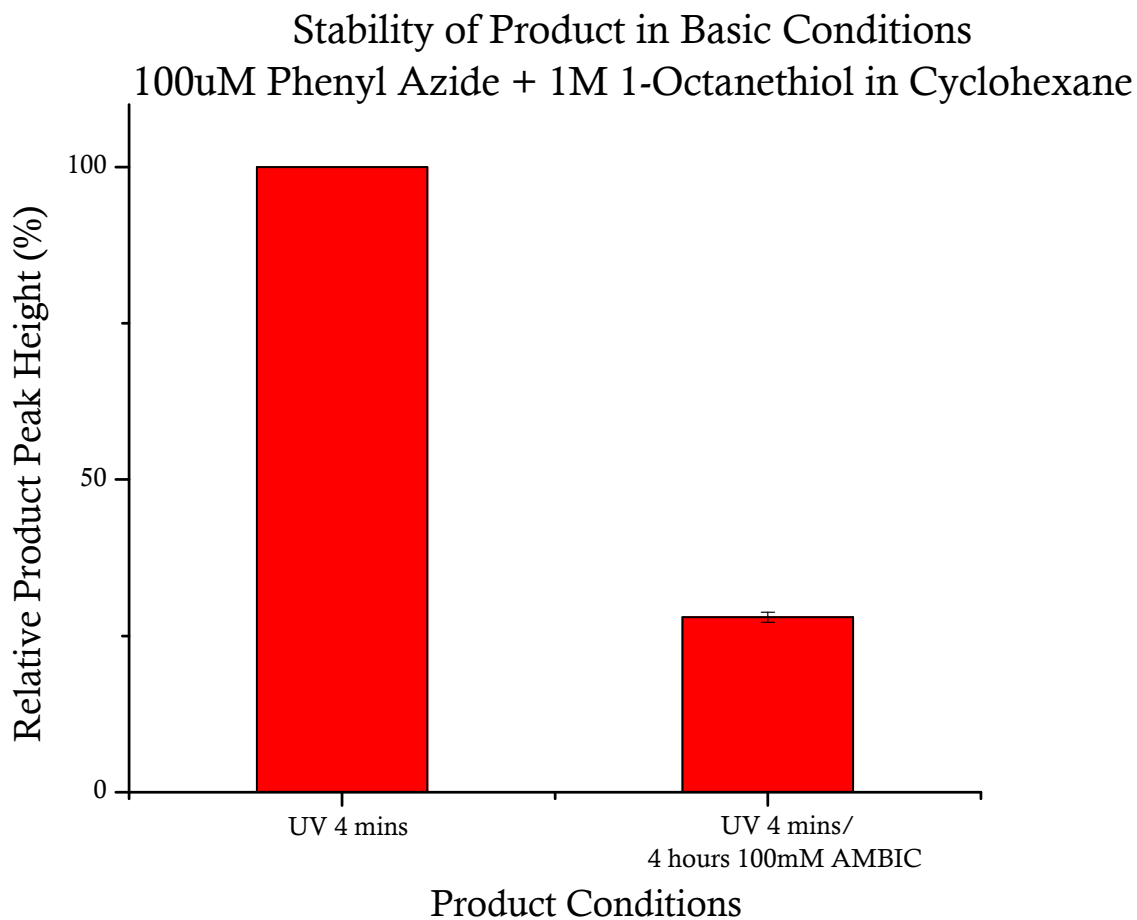


**Figure 3-29. Stability of Octylthioazepine in Basic Conditions.** There is approximately 28% of the octylthioazepine product left after incubation in 100mM ammonium bicarbonate for 4 hours (pH=8.9). After 24 hours, the entire product had decomposed (results not shown here). N=3.

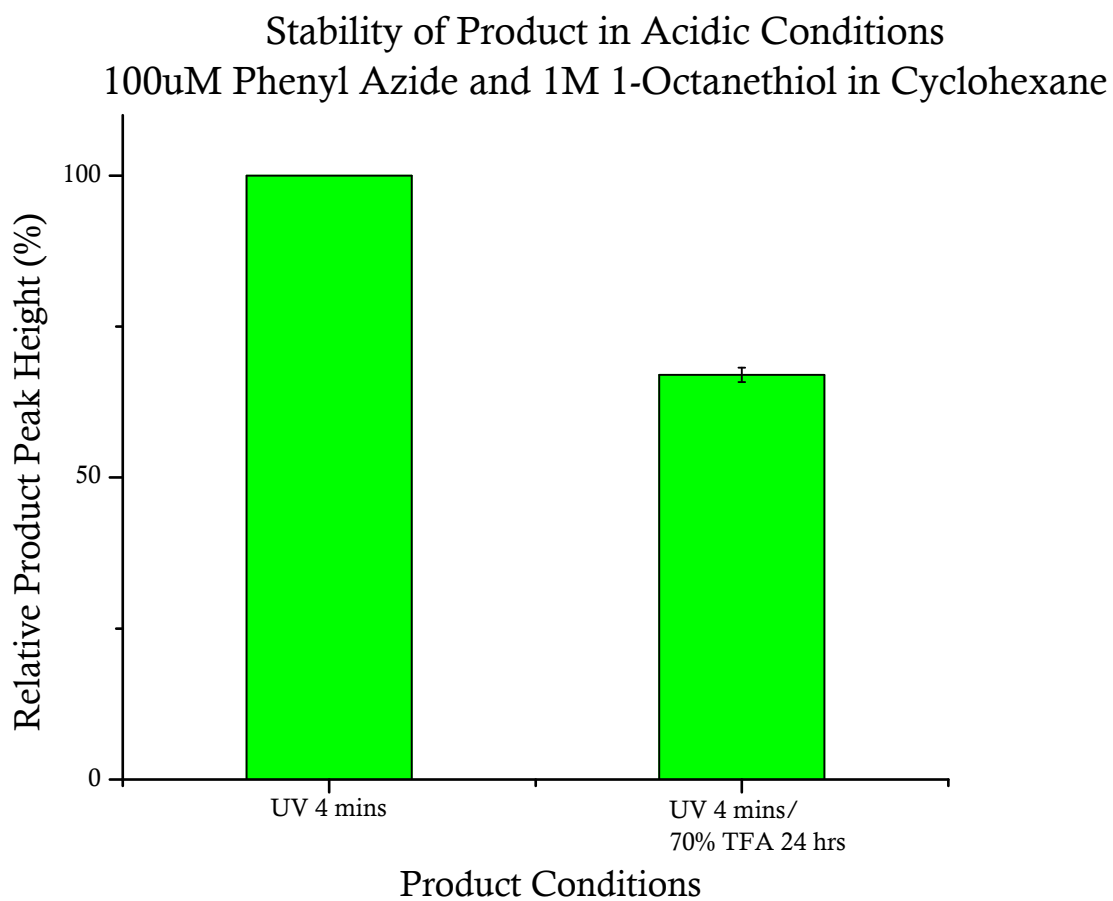


**Figure 3-30. Stability of Octylthioazepine in Acidic Conditions.** After incubation with 70% trifluoroacetic acid (TFA) for 24 hours in the dark at room temperature, 67% of the product remains. N=3.

### **Single Exponential First-Order Rate Constants for Phenyl Azide Irradiated with Amino Acid Analogs**

In addition to butylamine and 1-octanethiol, additional compounds were irradiated with phenyl azide that model amino acids or the peptide backbone. These compounds were irradiated with phenyl azide over time to determine the rate constant,  $k_1'$ , for each amino acid analog. Some of the models were done in aqueous conditions mimicking a polar environment at a physiological pH of 7.4, while others were done in the nonpolar solvent cyclohexane mimicking a hydrophobic environment. The compounds irradiated in a hydrophilic environment were imidazole, a model for histidine, phenol for tyrosine and guanidine acetic acid for arginine. The compounds irradiated in a hydrophobic environment were *N*-ethylacetamide for the peptide backbone, ethylbenzene for phenylalanine, butyric acid for glutamic acid, and dimethyl sulfide for methionine. Phenyl azide, which models the DAT photolabels, [ $^{125}\text{I}$ ]-DEEP, [ $^{125}\text{I}$ ]-MFZ 2-24, and [ $^{125}\text{I}$ ]-RTI-82, was irradiated by itself in both environments and a rate constant was determined for each environment.

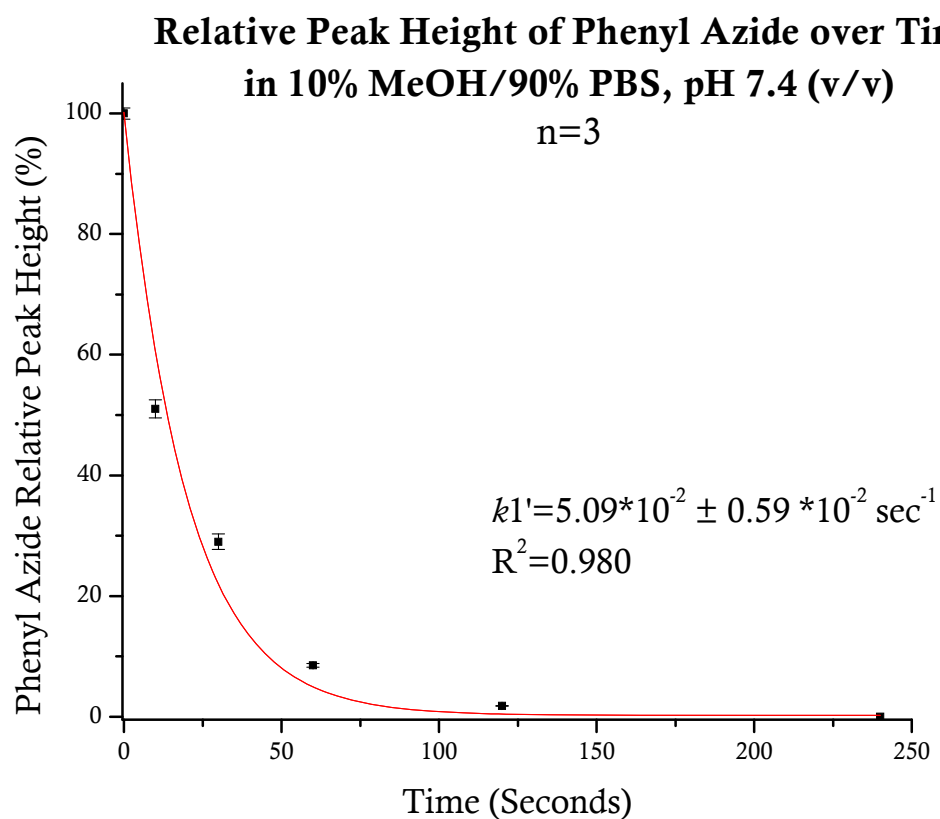


**Figure 3-31. Single Exponential First-Order Curve Fit for Phenyl Azide and Imidazole.** The rate constant,  $k1'$ , was determined to be equal to  $5.09 * 10^{-2} \pm 0.59 * 10^{-2} \text{ sec}^{-1}$  with  $R^2$  equal to 0.980 using a single exponential first-order decay curve fit.

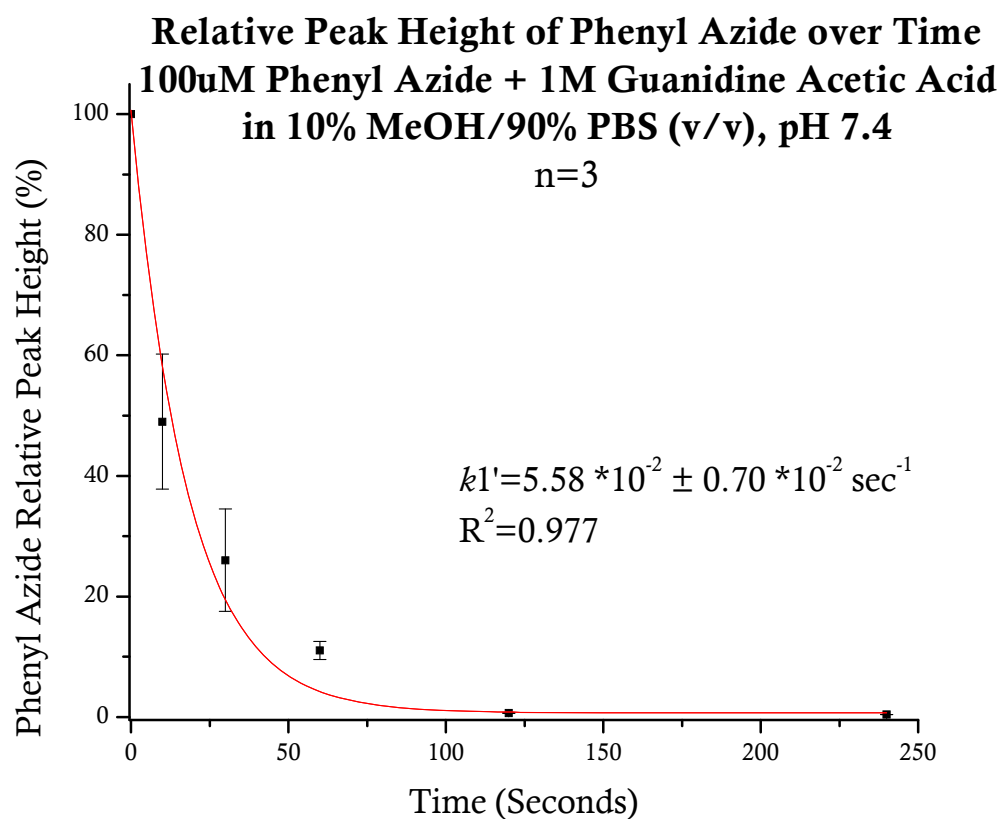


**Figure 3-32. Single Exponential First-Order Curve Fit for Phenyl Azide and Guanidine Acetic Acid.** The rate constant,  $k1'$ , was determined to be equal to  $5.58 * 10^{-2} \pm 0.70 * 10^{-2} \text{ sec}^{-1}$  with  $R^2$  equal to 0.977 using a single exponential first-order decay curve fit.

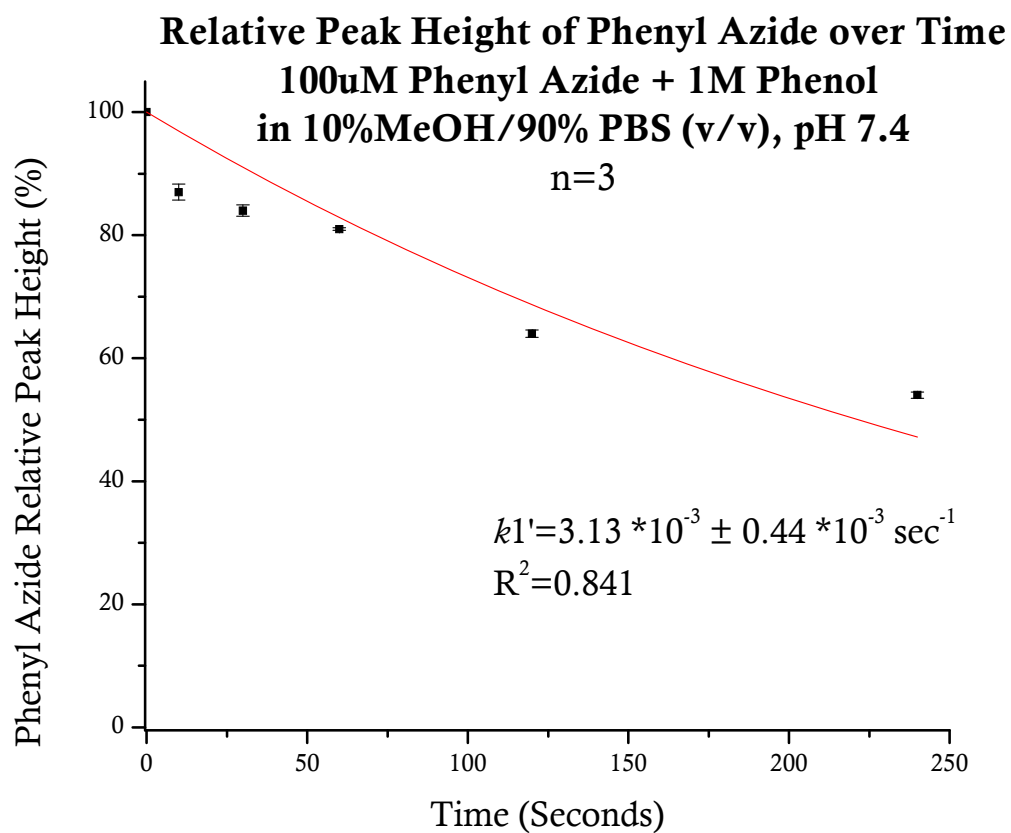


**Figure 3-33. Single Exponential First-Order Curve Fit for Phenyl Azide and**

**Phenol.** The rate constant,  $k_1'$ , was determined to be equal to  $3.13 \cdot 10^{-3} \pm 0.44 \cdot 10^{-3} \text{ sec}^{-1}$  with  $R^2$  equal to 0.841 using a single exponential first-order decay curve fit.

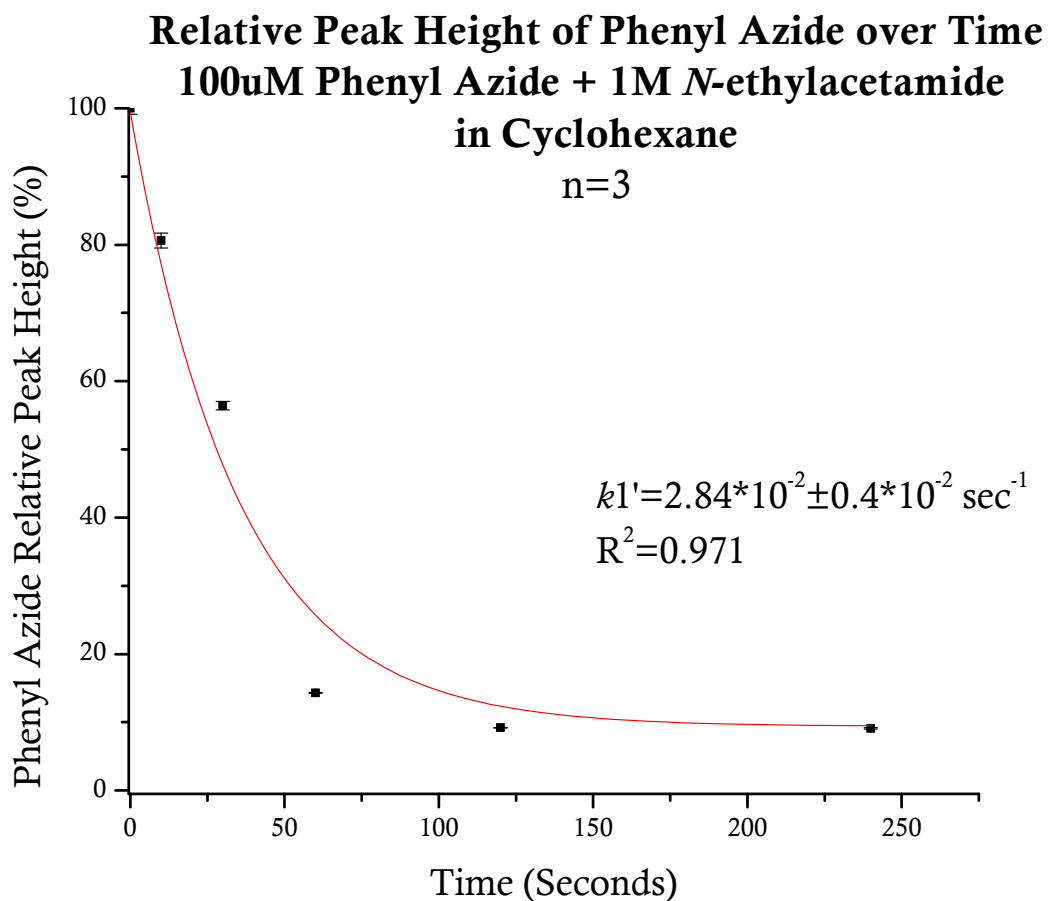


**Figure 3-34. Single Exponential First Order Curve Fit for Phenyl Azide and *N*-Ethylacetamide.** The rate constant,  $k1'$ , was determined to be equal to  $2.84 \cdot 10^{-2} \pm 0.4 \cdot 10^{-2} \text{ sec}^{-1}$  with  $R^2$  equal to 0.971 using a single exponential first-order decay curve fit.

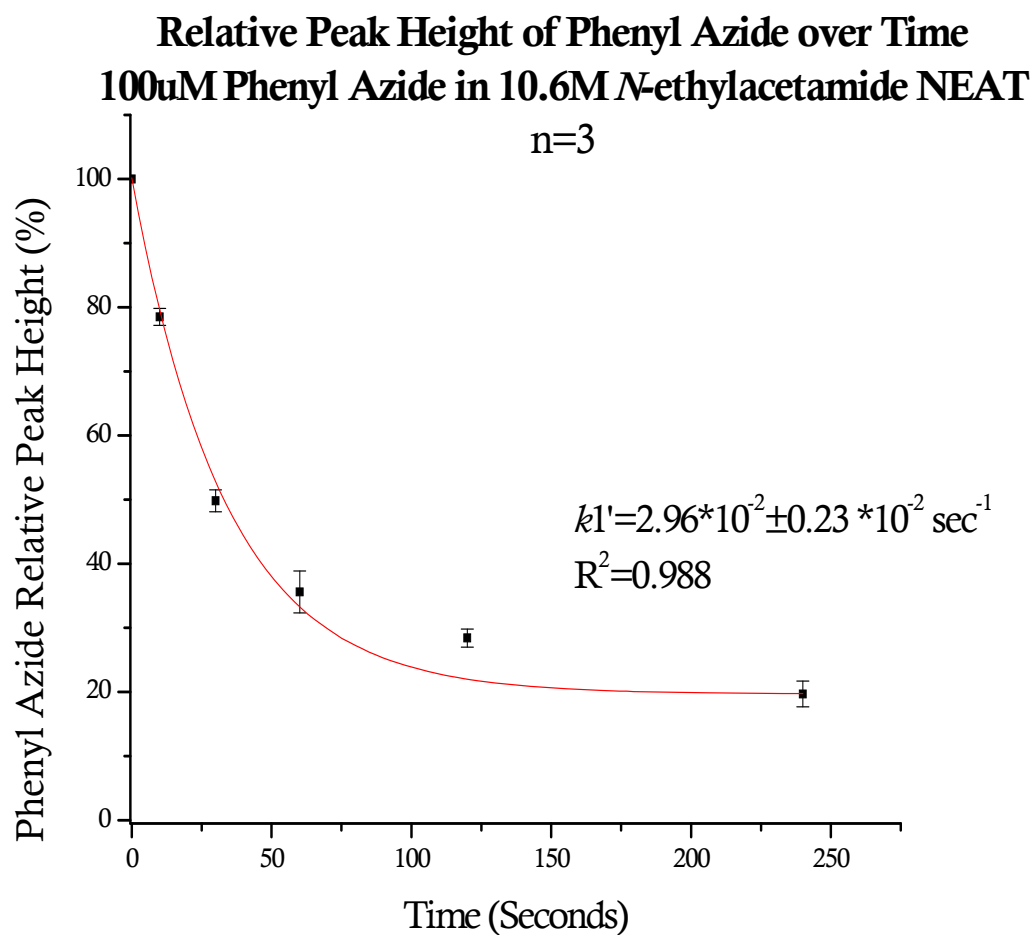


**Figure 3-35. Single Exponential First-Order Curve Fit for Phenyl Azide and *N*-ethylacetamide (NEAT).** The rate constant,  $k_1'$ , was determined to be equal to  $2.96 \times 10^{-2} \pm 0.23 \times 10^{-2} \text{ sec}^{-1}$  with  $R^2$  equal to 0.991 using a single exponential first-order decay curve fit.



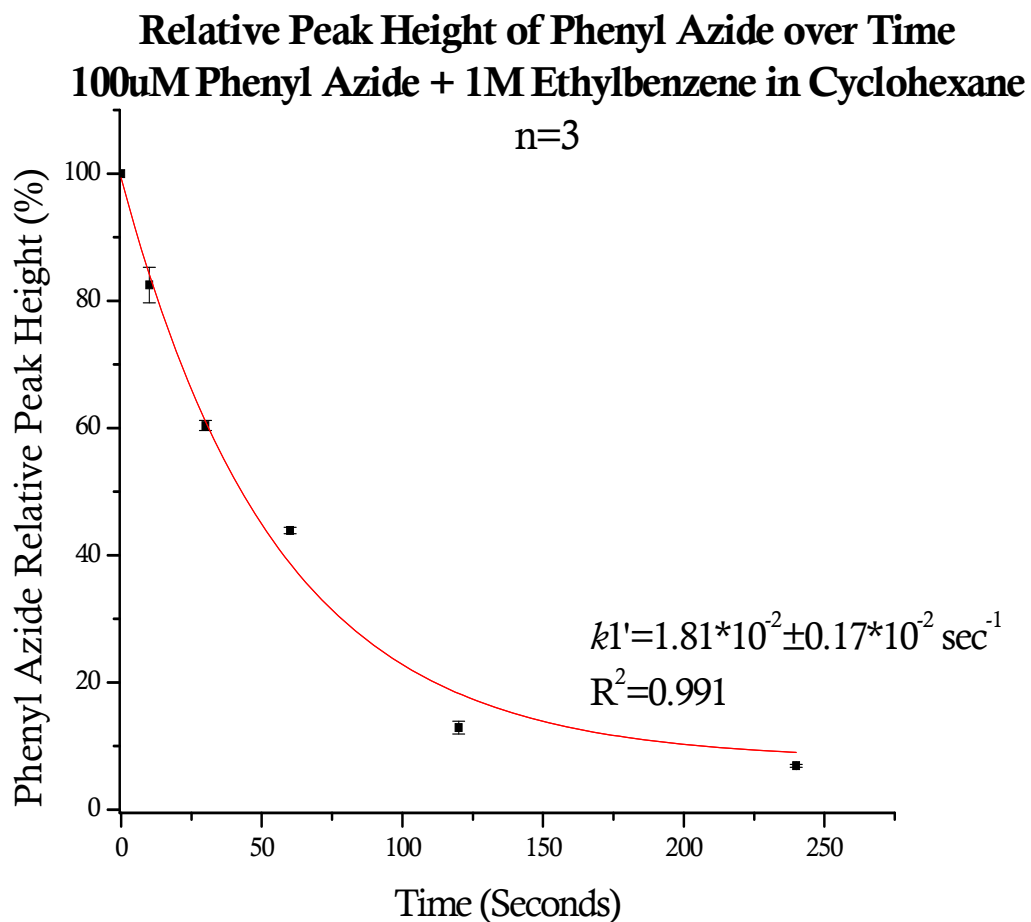


**Figure 3-36. Single Exponential First-Order Curve Fit for Phenyl Azide and Ethylbenzene.** The rate constant,  $k1'$ , was determined to be equal to  $1.81 * 10^{-2} \pm 0.17 * 10^{-2} \text{ sec}^{-1}$  with  $R^2$  equal to 0.991 using a single exponential first-order decay curve fit.

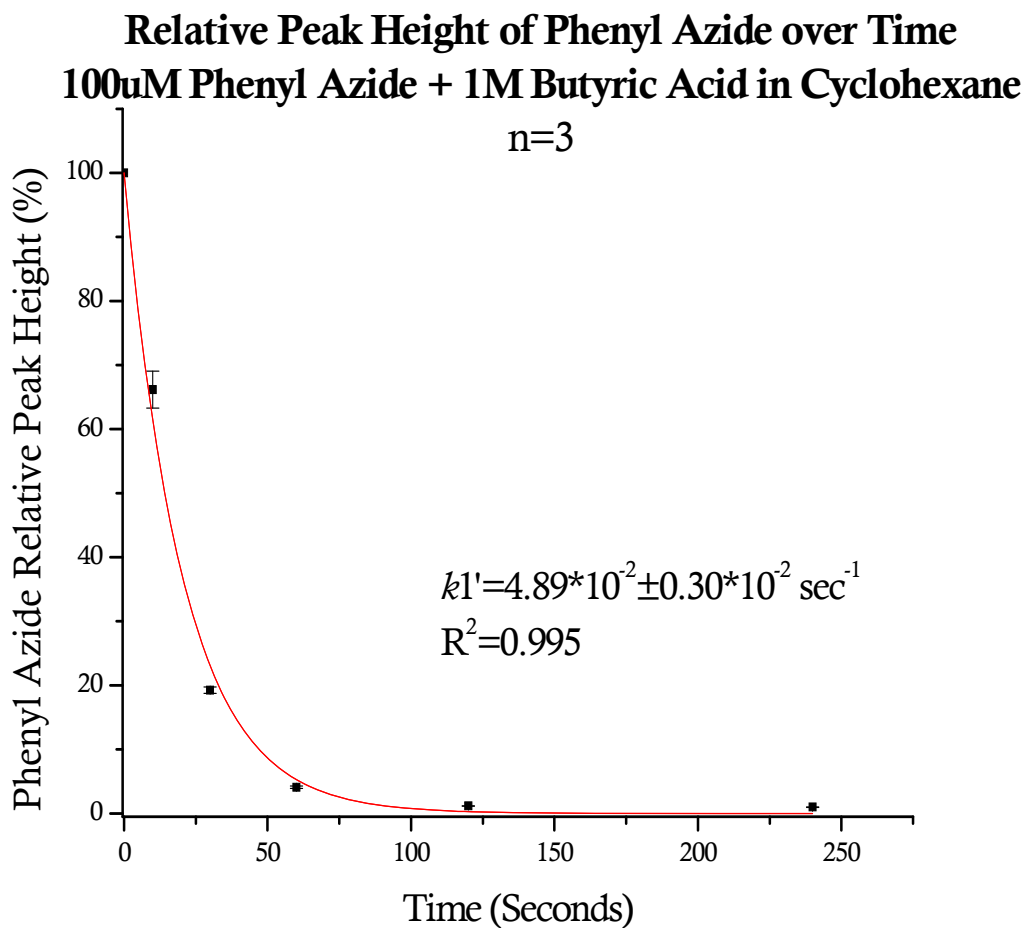


**Figure 3-37. Single Exponential First-Order Curve Fit for Phenyl Azide and Butyric Acid.** The rate constant,  $k1'$ , was determined to be equal to  $4.89 \cdot 10^{-2} \pm 0.30 \cdot 10^{-2} \text{ sec}^{-1}$  with  $R^2$  equal to 0.995 using a single exponential first-order decay curve fit.

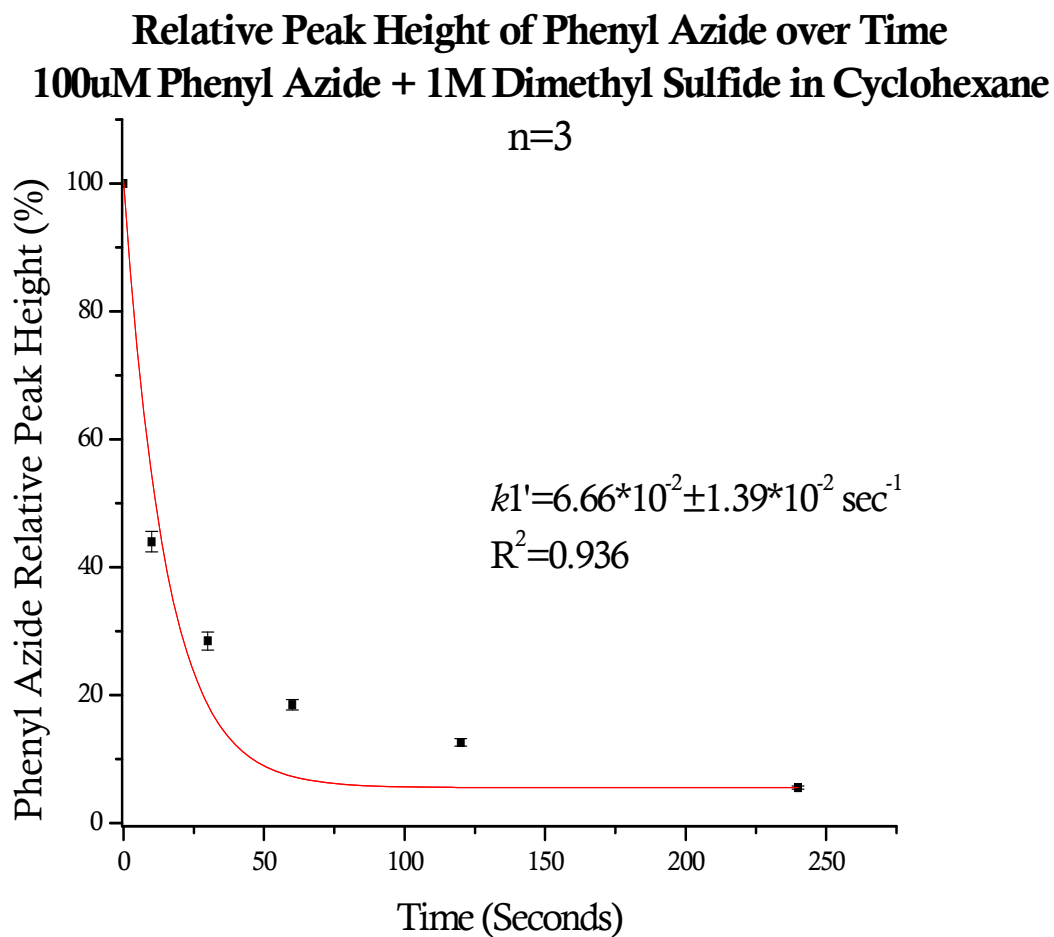


**Figure 3-38. Single Exponential First-Order Curve Fit for Phenyl Azide and Dimethyl Sulfide.** The rate constant,  $k_1'$ , was determined to be equal to  $6.66 \times 10^{-2} \pm 1.39 \times 10^{-2} \text{ sec}^{-1}$  with  $R^2$  equal to 0.936 using a single exponential first-order decay curve fit.

**Single Exponential First-Order Rate Constants  
for the Amino Acid Analogs**

Rank	Native <sup>a</sup>	Model <sup>b</sup>	$k1' \pm SD$ ( $\text{sec}^{-1}$ ) <sup>c</sup>	Fit <sup>d</sup>	Conc. <sup>e</sup> (M)	Solvent <sup>f</sup>
1	PAL	Phenyl Azide	14.8 ± 1.3	1	0	M
2	Met	Dimethyl Sulfide	6.66 ± 1.4	1	1	Cyclohexane
3	Lys	Butylamine	6.17 ± 0.31	1	16	Neat
4	Arg	GAA	5.58 ± 0.74	1	1	M
5	His	Imidazole	5.09 ± 0.59	1	1	M
6	Glu	Butyric Acid	4.89 ± 0.3	1	1	Cyclohexane
7	Lys	Butylamine	4.52 ± 0.2	1	1	Cyclohexane
8	PAL	Phenyl Azide	4.27 ± 0.27	1	0	Cyclohexane
9	BackBone	NEA	2.96 ± 0.4	1	10.6	Neat
10	BackBone	NEA	2.84 ± 0.4	1	1	Cyclohexane
11	Cys	Octanethiol	2.46 ± 0.62	1	1	Cyclohexane
12	Phe	Ethylbenzene	1.81 ± 0.17	1	1	Cyclohexane
13	Cys	Octanethiol	0.33 ± 0.02	1	6	Neat
14	Tyr	Phenol	0.30 ± 0.04	1	1	M

a denotes the abbreviation for the native compound where PAL is DAT photoaffinity ligand, Glu is glutamic acid, Lys is lysine, Met is methionine, BB is peptide backbone, His is histidine, Arg is arginine, Cys is cysteine, Phe is phenylalanine, and Tyr is tyrosine.

b NEA is N-ethylacetamide, GAA is guanidine acetic acid.

c single exponential first order rate constant,  $k1'$ , in  $\text{sec}^{-1}$ . All values  $\times 10^{-2}$ .

d denotes the order of the fit where 1 is 1<sup>st</sup> order. The equation for the kinetic analysis of data was  $y = Ae^{(-k1'*t)/M} + B$ , where A is the amplitude,  $k1'$  is the single exponential first-order rate constant, M is the molar concentration of the amino acid analog, t is the time in seconds, and B is the y offset when the baseline did not go to zero.

e denotes the concentration of the amino acid analog in molarity where 0 concentration of amino acid analog means that there was not an analog present.

f is the solvent used in the reaction where M is 10% methanol (MeOH)/90% phosphate buffered saline (PBS), pH 7.4.

**Table 3-3. Single Exponential First-Order Rate Constants.** When irradiated with itself in an aqueous environment, phenyl azide has the fastest rate constant of all of the models. It is also significantly higher than phenyl azide reacting in a nonpolar environment like cyclohexane.

**Single Exponential First-Order Rate Constants for the  
Amino Acid Analogs Divided by Solvent Conditions**

Rank	Native <sup>a</sup>	Model <sup>b</sup>	$k_1'$ sec <sup>-1</sup> ±SD <sup>c</sup>	Fit <sup>d</sup>	Conc. <sup>e</sup> (M)	Solvent <sup>f</sup>
1	Lys	Butylamine	6.17±0.31	1	16	N
2	BB	NEA	2.96±0.23	1	10.6	N
3	Cys	Octanethiol	0.33±0.02	1	6	N
1	PAL	Phenyl Azide	14.8± 1.3	1	0	M
2	Arg	GAA	5.58±0.74	1	1	M
3	His	Imidazole	5.09±0.59	1	1	M
4	Tyr	Phenol	0.30±0.04	1	1	M
1	Met	Dimethyl Sulfide	6.66±1.4	1	1	C
2	Glu	Butyric Acid	4.89±0.3	1	1	C
3	Lys	Butylamine	4.52±0.2	1	1	C
4	PAL	Phenyl Azide	4.27±0.27	1	0	C
5	BB	NEA	2.84±0.4	1	1	C
6	Cys	Octanethiol	2.46±0.62	1	1	C
7	Phe	Ethylbenzene	1.81±0.17	1	1	C

a denotes the abbreviation for the native compound where PAL is DAT photoaffinity ligand, Glu is glutamic acid, Lys is lysine, Met is methionine, BB is peptide backbone, His is histidine, Arg is arginine, Cys is cysteine, Phe is phenylalanine, and Tyr is tyrosine.

b NEA is N-ethylacetamide, GAA is guanidine acetic acid.

c single exponential first order rate constant,  $k_1'$ , in sec<sup>-1</sup>. All values x 10<sup>-2</sup>.

d denotes the order of the fit where 1 is 1<sup>st</sup> order. The equation for the kinetic analysis of data was  $y=Ae^{((-k_1' * t)/M)} + B$ , where A is the maximum phenyl azide relative peak height (%),  $k_1'$  is the single exponential first-order rate constant, M is the molar concentration of the amino acid analog, t is the time in seconds, and B is the y offset when the baseline did not go to zero.

e denotes the molar concentration of the amino acid analog where 0 concentration of analog means that it was the phenyl azide only and that no analog was present.

f is the solvent used in the reaction where M is 10% MeOH/90% PBS, C is cyclohexane, and N is neat conditions.

**Table 3-4. Single Exponential First-Order Rate Constants Divided by Solvent**

**Conditions.** When ranking the order of the rate constants in different environments, butylamine ranks first in NEAT conditions, the phenyl azide ranks first in an aqueous environment while guanidine acetic acid is second but the first amino acid analog, and dimethyl sulfide ranks first in a nonpolar environment.

## Dimerization of Phenyl Azide

The self reaction of phenyl azide in cyclohexane or in aqueous conditions should be able to be described by the second-order rate equation:  $1/[\text{phenyl azide}] = 1/[\text{phenyl azide}]_0 + k_2t$  (Eq. 3 in the Data Analysis Section of Methods). The inverse of the phenyl azide concentration can be plotted over time to determine the rate constant,  $k_2$ . The dimerization rate,  $r$ , is equal to  $k_2[\text{phenyl azide}][\text{phenyl azide}] = k_2[\text{phenyl azide}]^2$ , where  $[\text{phenyl azide}]$  is the molar concentration of phenyl azide. Upon the determination of  $k_2$ , the rate of dimerization can be calculated. The rate constant,  $k_2$ , for phenyl azide in aqueous conditions was found to be  $1.95 \cdot 10^{-3} \pm 0.36 \cdot 10^{-3} \text{ M}^{-1}\text{sec}^{-1}$  but the fit was inadequate suggesting that something more was happening in the reaction. The rate constant,  $k_2$ , for phenyl azide in cyclohexane was found to be  $2.55 \cdot 10^{-3} \pm 0.49 \cdot 10^{-3} \text{ M}^{-1}\text{sec}^{-1}$  but the fit was inadequate as well.

The total rate of reaction can be described as the combined rate of the phenyl azide dimerization rate and the target reaction rate. The target reaction rate is equal to  $k_1'[\text{phenyl azide}]$ . The dimerization reaction rate is equal to  $k_2[\text{phenyl azide}]^2$ . The total rate is equal to the target reaction rate plus the dimerization reaction rate. For example, the first-order rate constant,  $k_1'$  for phenyl azide reacting with butylamine in cyclohexane was  $4.52 \cdot 10^{-2} \pm 0.2 \cdot 10^{-2} \text{ sec}^{-1}$ . The target reaction rate is  $(4.52 \cdot 10^{-2} \text{ sec}^{-1}) \cdot (1 \cdot 10^{-4} \text{ M}) = 4.52 \cdot 10^{-6} \text{ M/sec}$ . The second-order rate constant,  $k_2$ , for phenyl azide reacting with itself in cyclohexane was  $2.55 \cdot 10^{-3} \pm 0.49 \cdot 10^{-3} \text{ M}^{-1}\text{sec}^{-1}$ . The dimerization reaction rate would then be  $2.6 \cdot 10^{-11} \text{ M/sec}$ . The total rate of reaction for phenyl azide with butylamine =  $4.52 \cdot 10^{-6} \text{ M/sec} + 2.6 \cdot 10^{-11} \text{ M/sec} \approx 4.5 \cdot 10^{-6} \text{ M/sec}$ .

Based on the above, the effect of phenyl azide reacting with itself has minimal effect on the rate of the total reaction. The second-order rate equation for the loss of phenyl azide alone in either aqueous conditions or in nonpolar conditions did not fit the data adequately. Including the rate of phenyl azide dimerization does not change the overall order of reactivity of phenyl azide with the amino acid analogs.

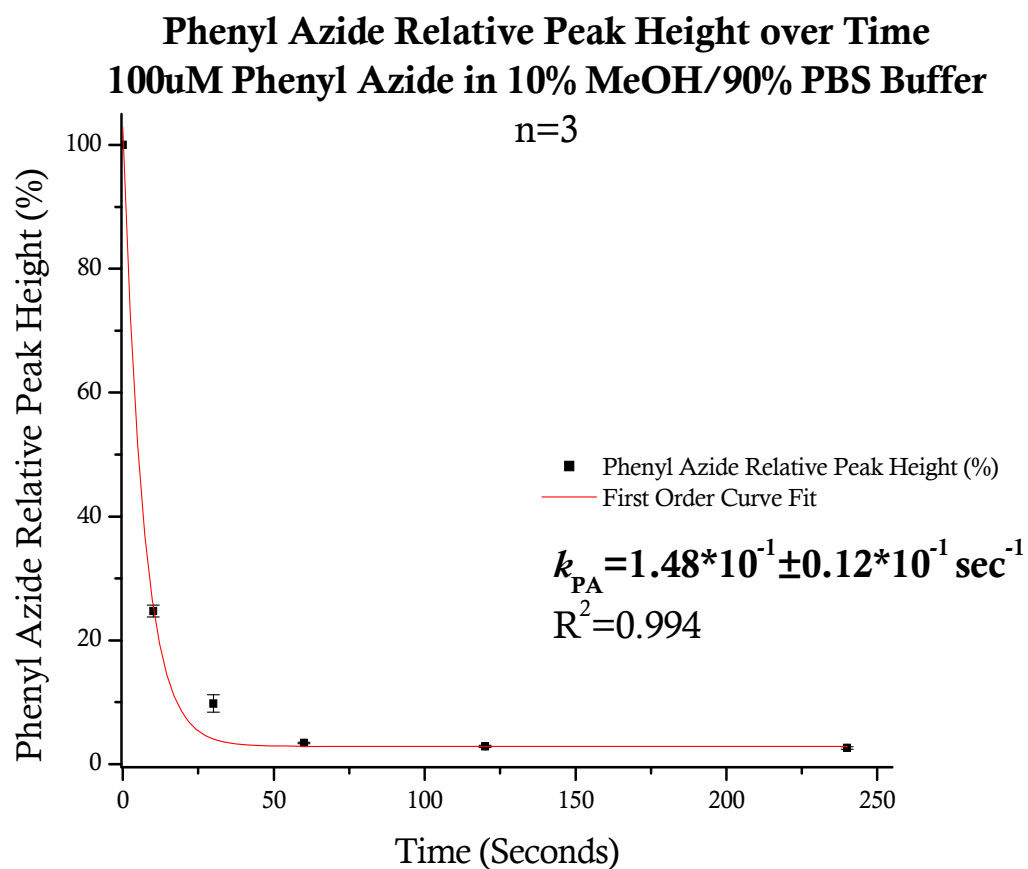


**Figure 3-39. Loss of Phenyl Azide in Aqueous Conditions for 4 Minutes of**

**Irradiation.** The rate constant,  $k_{PA}$ , was determined to be equal to  $1.48 \cdot 10^{-1} \pm 0.12 \cdot 10^{-1} \text{ sec}^{-1}$  with  $R^2$  equal to 0.994 using a single exponential first-order decay curve fit.



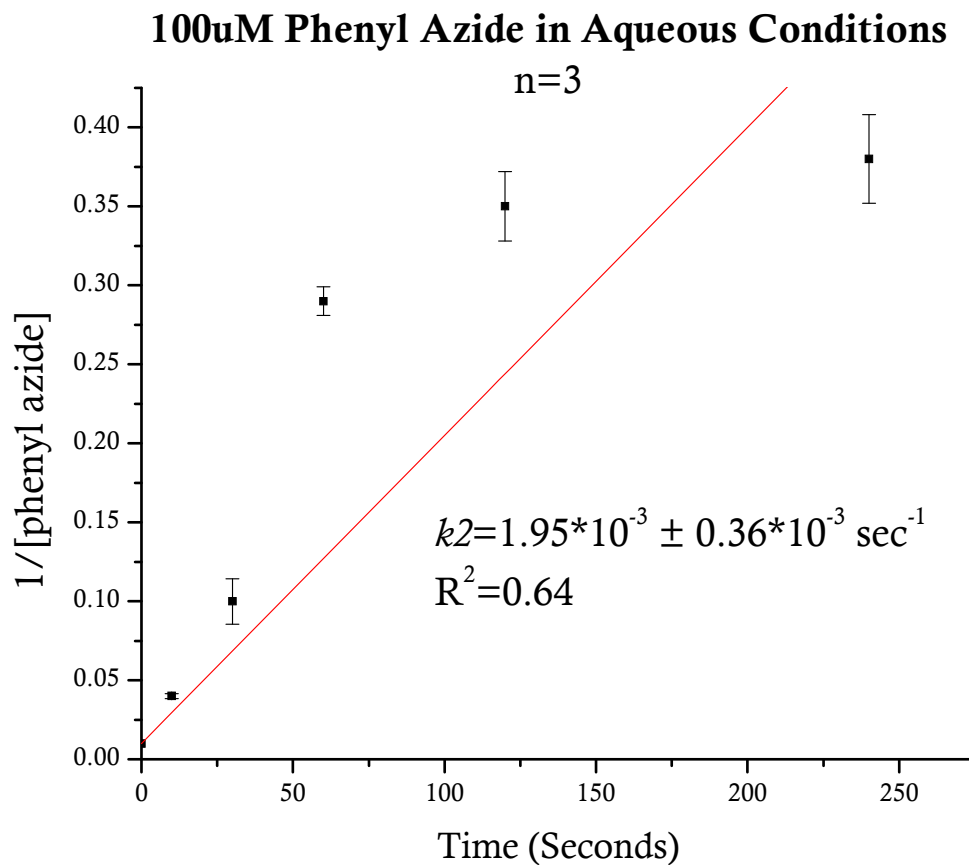


**Figure 3-40. Dimerization of Phenyl Azide in Aqueous Conditions.** The dimerization of phenyl azide can be fit to a second-order rate equation,  $1/[\text{phenyl azide}] = 1/[\text{phenyl azide}]_0 + k_2 t$ , where  $k_2$  is the rate constant in  $\text{M}^{-1}\text{sec}^{-1}$ ,  $[\text{phenyl azide}]_0$  is the initial molar concentration of phenyl azide,  $t$  is time in seconds. The rate constant,  $k_2$ , for phenyl azide reacting with itself in aqueous conditions was  $1.95 \cdot 10^{-3} \pm 0.36 \cdot 10^{-3} \text{ M}^{-1}\text{sec}^{-1}$ .  $N=3$ . The second-order rate equation model did not adequately fit the data.

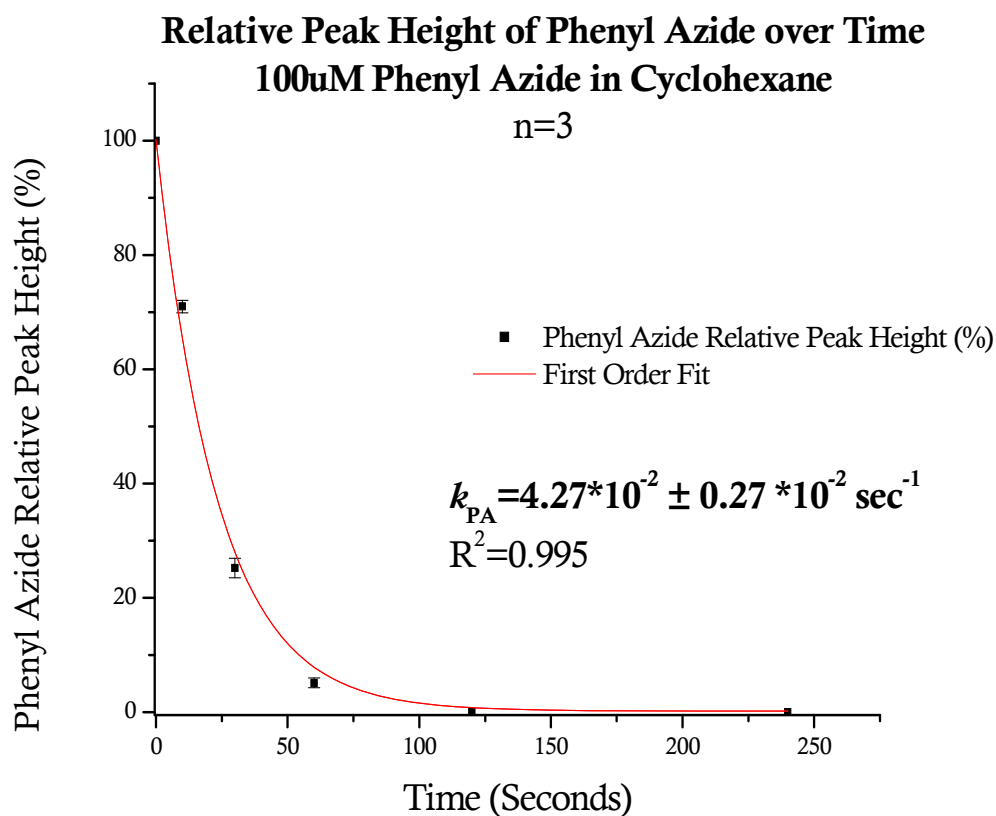


**Figure 3-41. Loss of Phenyl Azide in Cyclohexane for 4 Minutes of Irradiation.** The rate constant,  $k_{PA}$ , was determined to be equal to  $4.27 * 10^{-2} \pm 0.27 * 10^{-2} \text{ sec}^{-1}$  with  $R^2$  equal to 0.995 using a single exponential first-order decay curve fit.

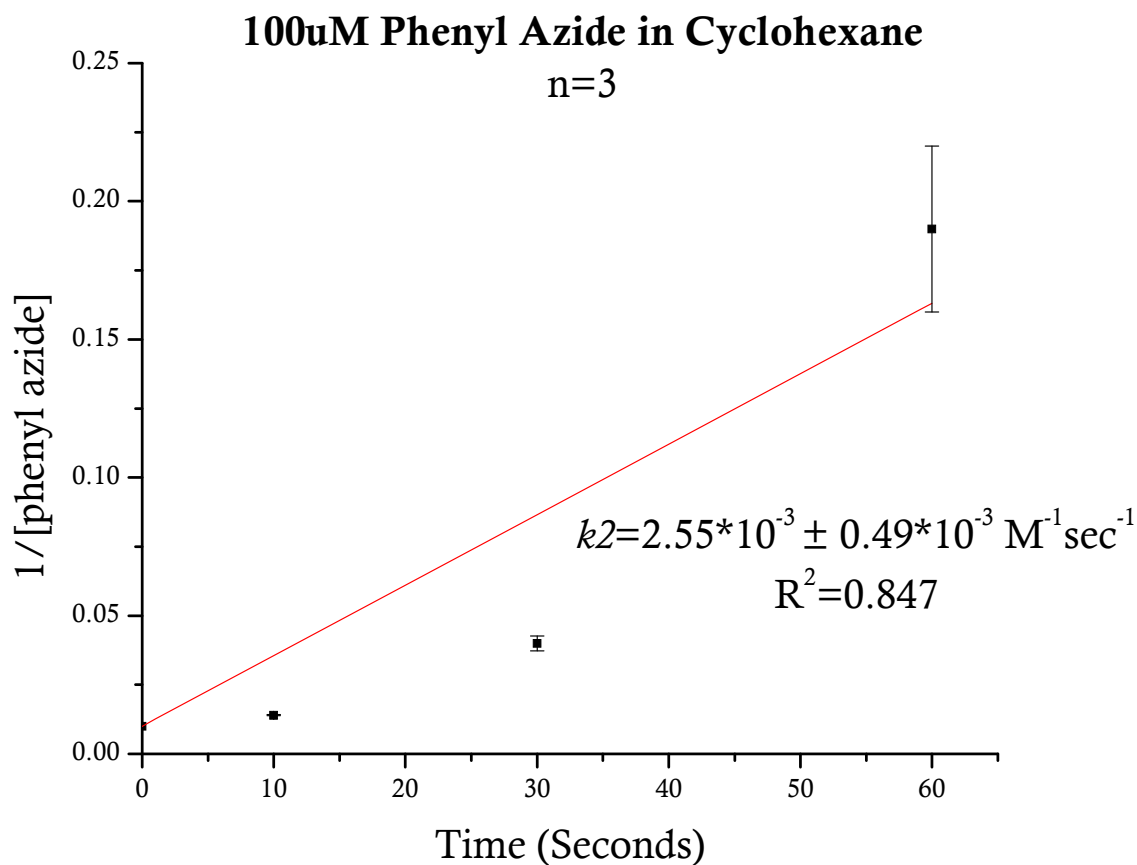


**Figure 3-42. Dimerization of Phenyl Azide in Cyclohexane.** The dimerization of phenyl azide was fit to a second-order rate equation,  $1/[\text{phenyl azide}] = 1/[\text{phenyl azide}]_0 + k_2 t$ , where  $k_2$  is the rate constant in  $\text{M}^{-1} \text{sec}^{-1}$ ,  $[\text{phenyl azide}]_0$  is the initial molar concentration of phenyl azide,  $t$  is time in seconds. The fit using this rate equation was constant,  $k_2$ , for phenyl azide reacting with itself in cyclohexane was  $2.55 \cdot 10^{-3} \pm 0.49 \cdot 10^{-3} \text{ M}^{-1} \text{sec}^{-1}$ .  $N=3$ . The second-order rate equation model did not adequately fit the data.

A.

**Initial Reaction Rates for Phenyl Azide with Amino Acid Analogs  
Irradiated in Cyclohexane**

Amino Acid Analog	Target Reaction Rate= $k_1'$ [PA] (M/sec)
Dimethyl Sulfide	$6.66 \times 10^{-6}$
Butyric Acid	$4.89 \times 10^{-6}$
Butylamine	$4.52 \times 10^{-6}$
<i>N</i> -ethylacetamide	$2.84 \times 10^{-6}$
1-Octanethiol	$2.46 \times 10^{-6}$
Ethylbenzene	$1.81 \times 10^{-6}$

B.

**Initial Reaction Rates for Phenyl Azide with Amino Acid Analogs  
Irradiated in Aqueous Conditions**

Amino Acid Analog	Target Reaction Rate= $k_1'$ [PA] (M/sec)
Guanidine Acetic Acid	$5.58 \times 10^{-6}$
Imidazole	$5.09 \times 10^{-6}$
Phenol	$0.3 \times 10^{-6}$

**Table 3-5. Initial Reaction Rates of Phenyl Azide Reacting with Amino Acid**

**Analogs. A. Initial Reaction Rates of Phenyl Azide with Amino Acid Analogs**

**Irradiated in Cyclohexane.** The initial target reaction rates in cyclohexane were

calculated as  $k_1'$ [PA] =  $k_1'$ [0.0001M] for each amino acid analog. **B. Initial Reaction**

**Rates of Phenyl Azide with Amino Acid Analogs in Aqueous Conditions.** The initial target reaction rates in aqueous conditions were calculated as  $k'1[\text{PA}] = k1'[0.0001\text{M}]$  for each amino acid analog.

### **Double Exponential Rate Constants Applied to the Photoreactions of Phenyl Azide with Amino Acid Analogs**

Two rate constants,  $k_{AA}$  and  $k_{PA}$ , were used to determine the more likely rate constant between phenyl azide and amino acid analogs if the phenyl azide was dimerizing while the azepine product was being formed. For most of the data, a single exponential first-order equation did not fit the data. The double exponential rate equation with two rate constants,  $k_{AA}$  and  $k_{PA}$ , fits the data better, as expected when two constants are used to fit the data. These two processes are the loss of phenyl azide in the presence of amino acid analogs and the loss of phenyl azide in solvent without amino acid analogs.  $k_{PA}$  represents the rate constant of phenyl azide loss when reacting without amino acid analogs in cyclohexane or aqueous conditions while  $k_{AA}$  represents the rate of phenyl azide loss when reacting with the amino acid analogs. The equation used for the exponential decay curve fit was  $A(e^{-k_{AA}t/M} + e^{-k_{PA}t})$ , where A is the maximum phenyl azide relative peak height (%),  $k_{PA}$  is the rate constant for phenyl azide loss when reacting without amino acid analogs, M is the molar concentration of the amino acid analogs,  $k_{AA}$  is the rate constant of the phenyl azide loss when reacting with the amino acid analog, and t is time in seconds. All constants were fixed values, while  $k_{AA}$  varied.

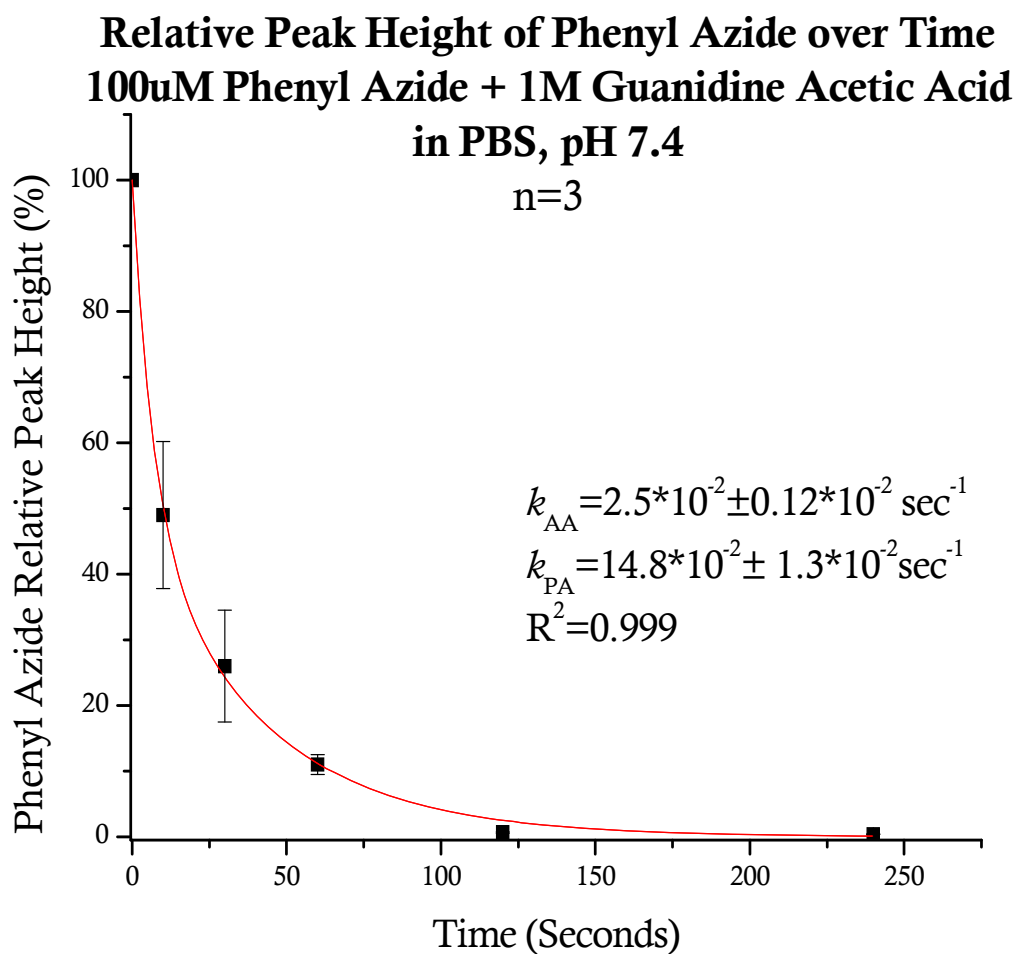


**Figure 3-43. Double Exponential First-Order Curve Fit for Phenyl Azide and Guanidine Acetic Acid.** The rate constant,  $k_{AA}$ , was determined to be equal to  $2.5 \cdot 10^{-2} \pm 0.12 \cdot 10^{-2} \text{ sec}^{-1}$  with  $R^2$  equal to 0.999 using a double exponential first-order decay curve fit.  $k_{PA}$  was fixed at  $14.8 \cdot 10^{-2} \pm 1.3 \cdot 10^{-2} \text{ sec}^{-1}$ .

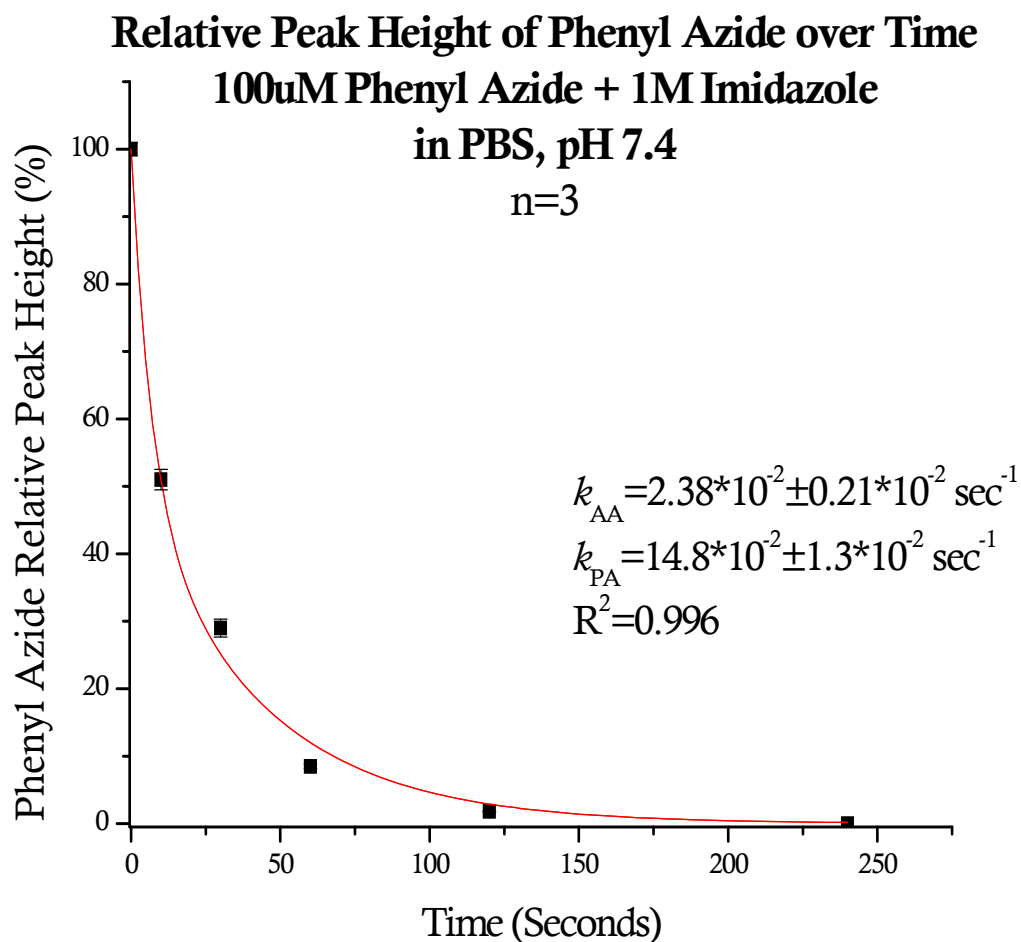


**Figure 3-44. Double Exponential First-Order Curve Fit for Phenyl Azide and Imidazole.** The rate constant,  $k_{AA}$ , was determined to be equal to  $2.38 \cdot 10^{-2} \pm 0.21 \cdot 10^{-2} \text{ sec}^{-1}$  with  $R^2$  equal to 0.996 using a double exponential first-order decay curve fit.  $k_{PA}$  was fixed at  $14.8 \cdot 10^{-2} \pm 1.3 \cdot 10^{-2} \text{ sec}^{-1}$ .



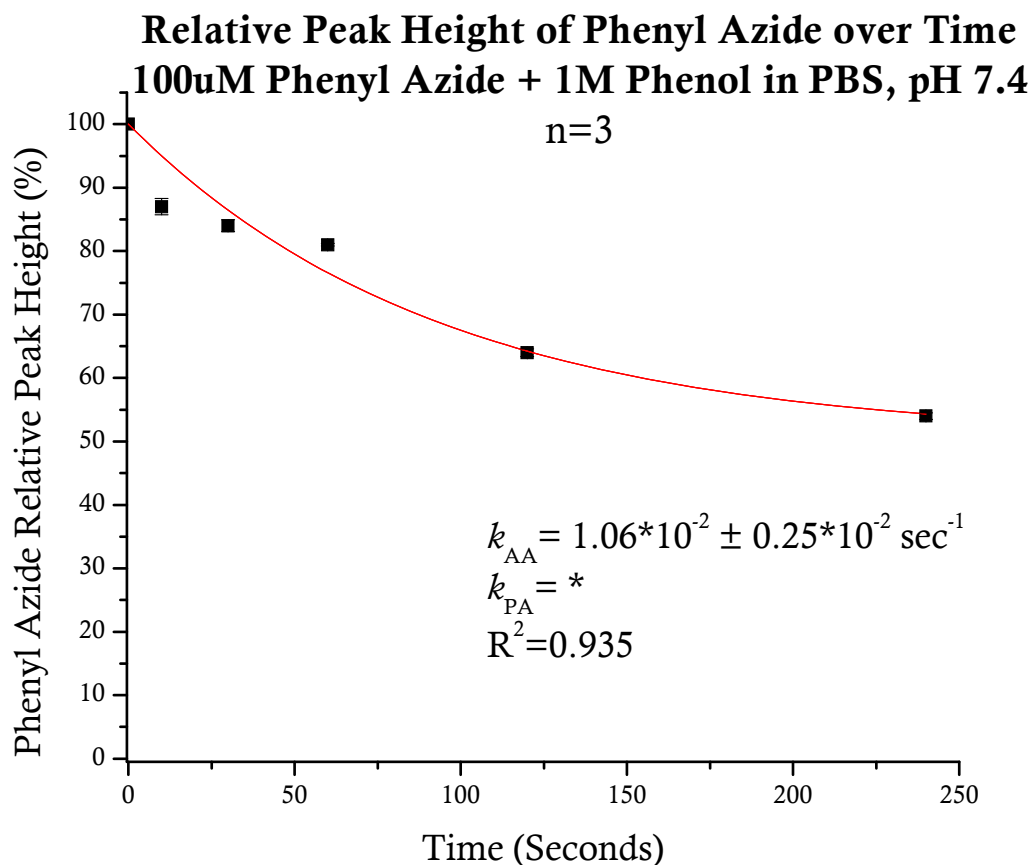


**Figure 3-45. Double Exponential First-Order Curve Fit for Phenyl Azide and Phenol.** The rate constant,  $k_{AA}$ , was determined to be equal to  $1.1 * 10^{-2} \pm 0.003 * 10^{-2} \text{ sec}^{-1}$  with  $R^2$  equal to 0.935 using a double exponential first-order decay curve fit.

\* $k_{AA}$  is not accurate because  $k_{PA}$  was unable to be fixed in the equation and yielded a negative  $k_{PA}$  for this set of data.

**Double Exponential First-Order Rate Constants for  
Phenyl Azide Irradiated with Amino Acid Analogs  
in Aqueous Conditions**

Rank <sup>a</sup>	Native <sup>b</sup>	Model <sup>c</sup>	1 <sup>st</sup> Order Rate Constant for PA <sup>d</sup>	Rate Constant for PA <sup>e</sup>	Rate Constant for A.A. Analogs <sup>f</sup>
			$k_1'$ (sec <sup>-1</sup> ) ±SD	$k_{PA}$ (sec <sup>-1</sup> ) ±SD	$k_{AA}$ (sec <sup>-1</sup> ) ±SD
1	PAL	Phenyl Azide	14.8± 1.3	14.8± 1.3	N/A
2	Arg	GAA	5.58±0.74	14.8± 1.3	2.5±0.12
3	His	Imidazole	5.09±0.59	14.8± 1.3	2.38±0.21
4	Tyr	Phenol	0.30±0.04	*	1.1 ± 0.003

a is the rank order of rate constants based on the single and double exponential first-order fits.

b is the native compound that is being modeled by analogs that are irradiated with phenyl azide, where PAL is the DAT photoaffinity label.

c is the amino acid analog that is irradiated with phenyl azide, where GAA is guanidine acetic acid.

d is the single exponential first-order rate constant,  $k_1'$ , for the data over a 4 minute time course of irradiation. The equation used to fit the data was  $Ae^{-k_1't} + B$ , where A is the maximum phenyl azide relative peak height (%),  $k_1'$  is the rate constant, t is time in seconds, and B is the y offset when the baseline did not go to zero. All constants were fixed values except  $k_1'$ , which varied.

e is the single exponential first-order rate constant,  $k_{PA}$ , for the loss of phenyl azide in aqueous conditions without amino acid analogs, where PA means phenyl azide.

f is the rate constant,  $k_{AA}$ , for the amino acid analog reacting with phenyl azide in aqueous conditions, where AA means amino acid analog. The equation used to fit the data was  $A(e^{-k_{AA}t/M} + e^{-k_{PA}t})$ , where A is the maximum phenyl azide relative peak height (%),  $k_{AA}$  is the rate constant describing the loss of phenyl azide in aqueous conditions with the amino acid analog, M is the molar concentration of the amino acid analog,  $k_{PA}$  is the rate constant describing the loss of phenyl azide reacting in aqueous conditions without amino acid analogs, and t is time in seconds. All constants except  $k_{AA}$  were fixed values.

\*This equation did not fit the data. Repeated manipulations led to a number that was negative for  $k_{PA}$ , when both  $k_{AA}$  and  $k_{PA}$  varied. Thus, the rate constant for a double exponential curve fit with phenol is not reported.

**Table 3-6. Single and Double Exponential First-Order Rate Constants for Amino Acid Analogs in Aqueous Conditions.** The ranking of the double exponential rate constant,  $k_{AA}$ , resulted in the same ranking as the single exponential first-order rate constant,  $k_1'$ , where the arginine model, guanidine acetic acid, was the most reactive.

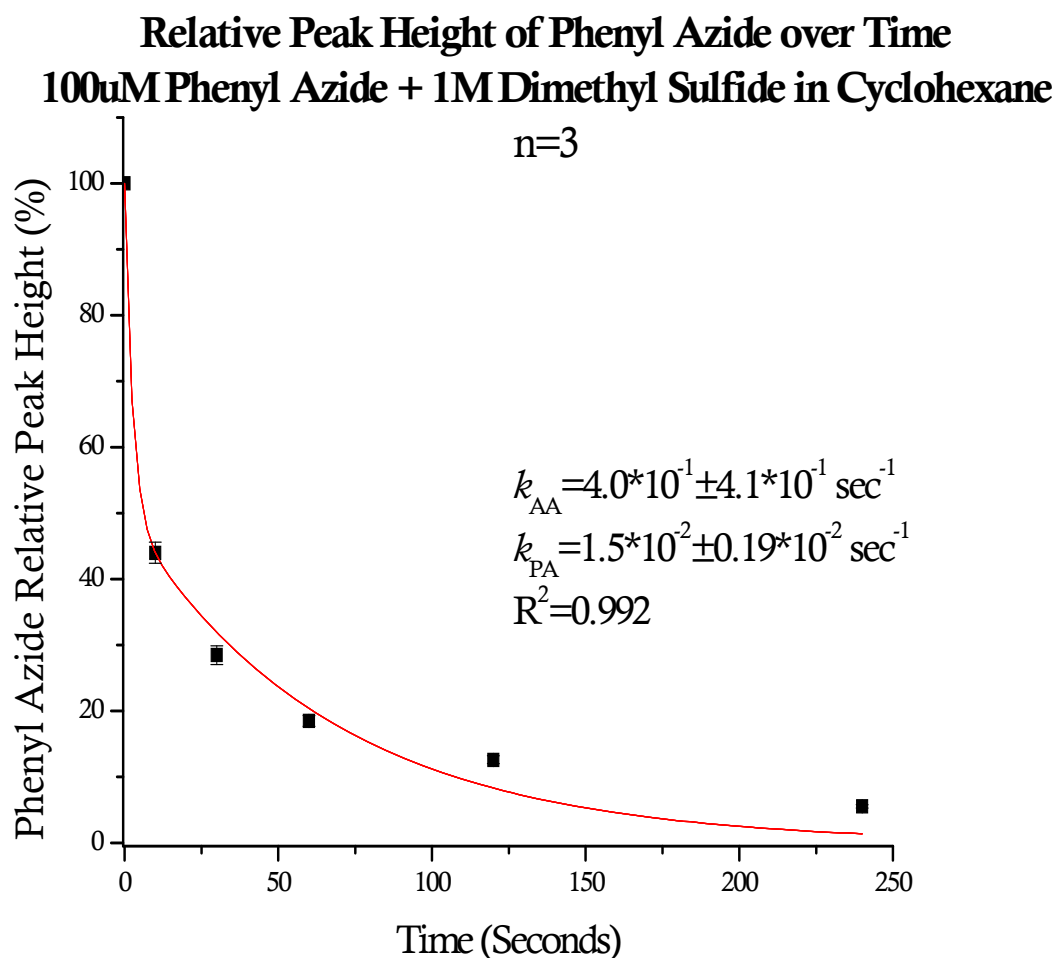


**Figure 3-46. Double Exponential First-Order Curve Fit for Phenyl Azide and Dimethyl Sulfide.** The rate constant,  $k_{AA}$ , was determined to be equal to  $4.0 \cdot 10^{-1} \pm 4.1 \cdot 10^{-1} \text{ sec}^{-1}$  with  $R^2$  equal to 0.992 using a double exponential first-order decay curve fit. This data suggests that one process is occurring because it could not be fit with a fixed  $k_{PA}$  value, accounting for the loss of PA in cyclohexane without analog.  $k_{PA}$  equals  $1.5 \cdot 10^{-2} \pm 0.19 \cdot 10^{-2} \text{ sec}^{-1}$  for this set of data. This is approximately 3 times slower than the fixed value obtained experimentally which is  $4.27 \cdot 10^{-2} \text{ sec}^{-1}$ .  $k_{PA}$  was unable to be fixed at  $4.27 \cdot 10^{-2} \pm 0.27 \cdot 10^{-2} \text{ sec}^{-1}$ .

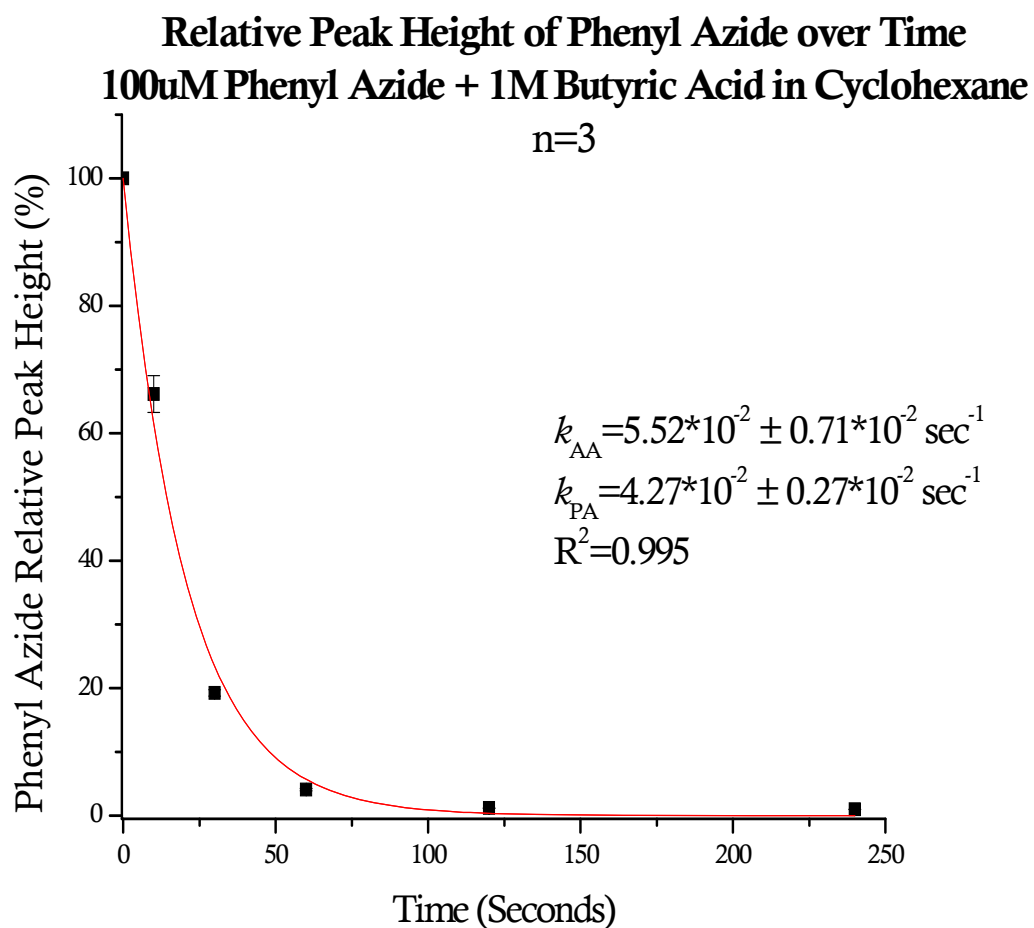


**Figure 3-47. Double Exponential First-Order Curve Fit for Phenyl Azide and Butyric Acid.** The rate constant,  $k_{AA}$ , was determined to be equal to  $5.52 \cdot 10^{-2} \pm 0.71 \cdot 10^{-2} \text{ sec}^{-1}$  with  $R^2$  equal to 0.995 using a double exponential decay curve fit.  $k_{PA}$  was fixed at  $4.27 \cdot 10^{-2} \pm 0.27 \cdot 10^{-2} \text{ sec}^{-1}$ .

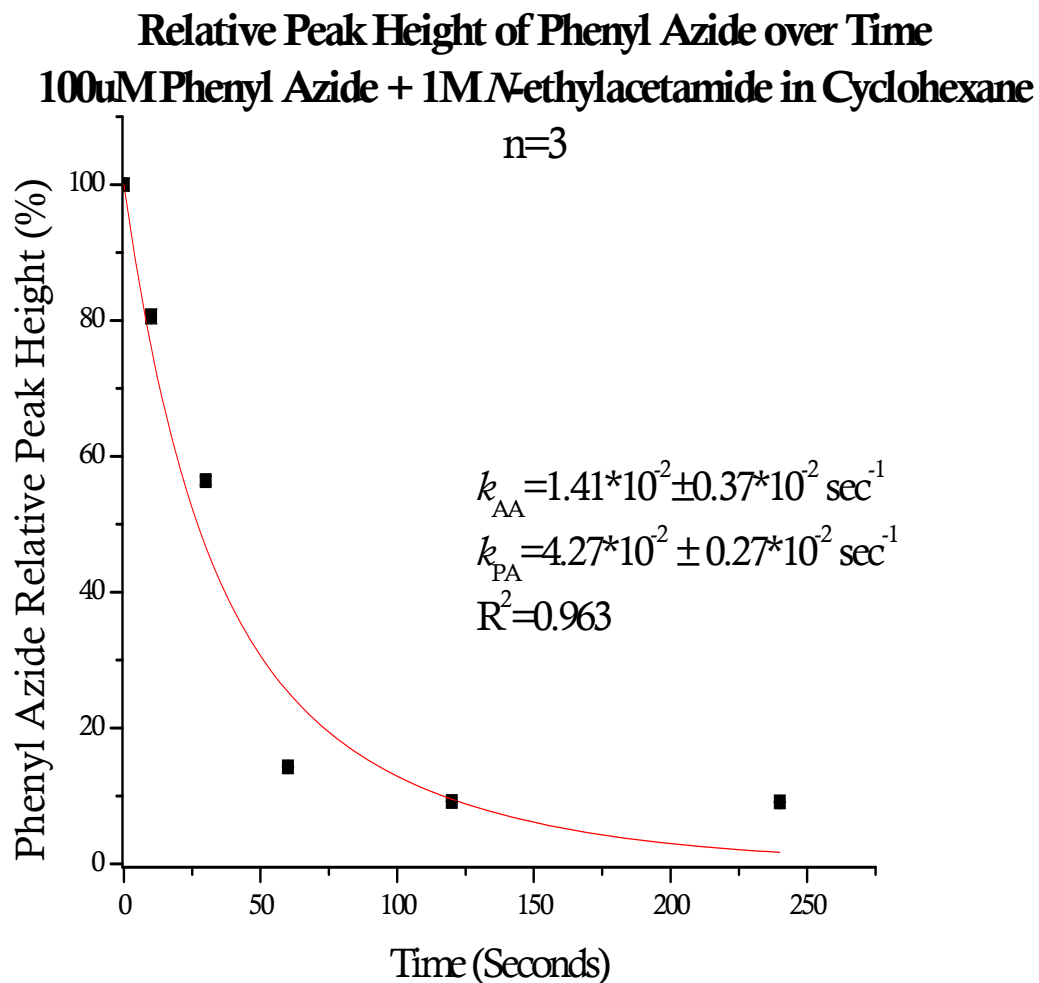


**Figure 3-48. Double Exponential First-Order Curve Fit for Phenyl Azide and N-ethylacetamide.** The rate constant,  $k_{AA}$ , was determined to be equal to  $1.41 \cdot 10^{-2} \pm 0.37 \cdot 10^{-2} \text{ sec}^{-1}$  with  $R^2$  equal to 0.963 using a double exponential decay curve fit.  $k_{PA}$  was fixed at  $4.27 \cdot 10^{-2} \pm 0.27 \cdot 10^{-2} \text{ sec}^{-1}$ .

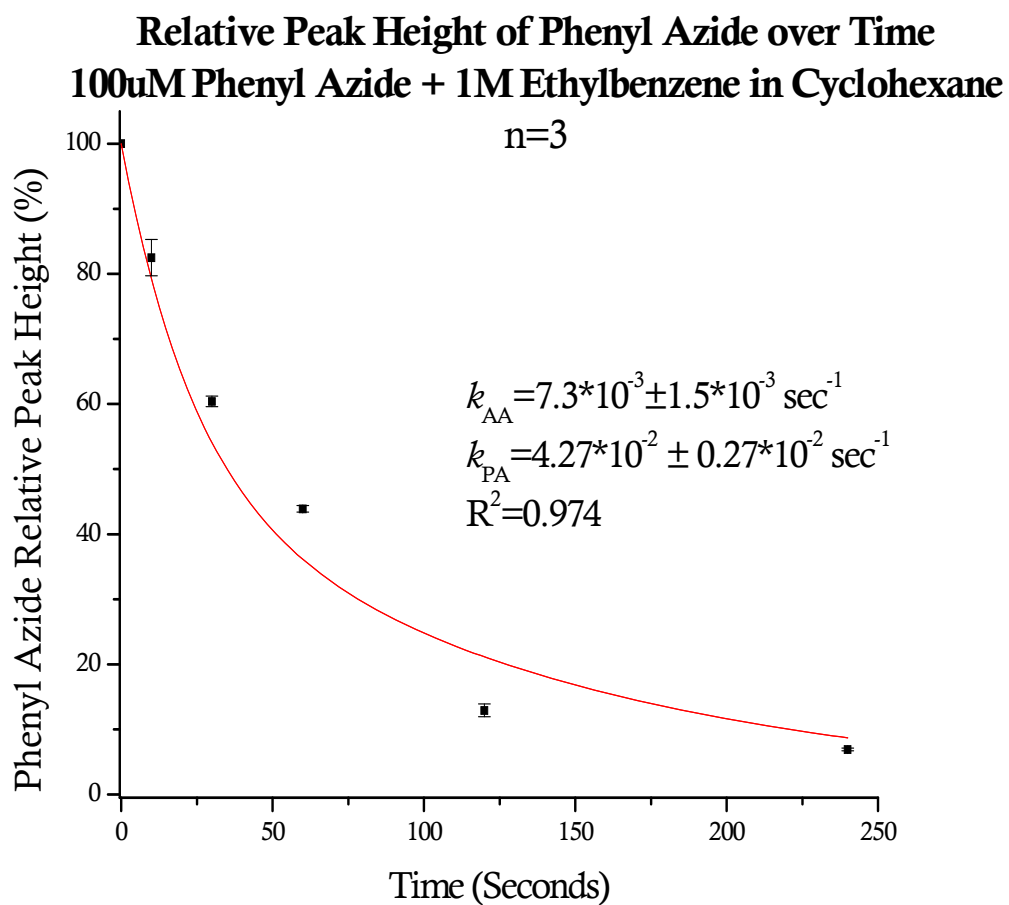


**Figure 3-49. Double Exponential First-Order Curve Fit for Phenyl Azide and Ethylbenzene.** The rate constant,  $k_{AA}$ , was determined to be equal to  $7.3 \cdot 10^{-3} \pm 1.5 \cdot 10^{-3} \text{ sec}^{-1}$  with  $R^2$  equal to 0.974 using a double exponential decay curve fit.  $k_{PA}$  was fixed at  $4.27 \cdot 10^{-2} \pm 0.27 \cdot 10^{-2} \text{ sec}^{-1}$ .

**Rate Constants for Phenyl Azide Irradiated  
with Amino Acid Analogs in Cyclohexane**

Rank <sup>a</sup>	Native <sup>b</sup>	Model <sup>c</sup>	1 <sup>st</sup> Order Rate Constant for PA <sup>d</sup> $k_1' \pm SD$ (sec <sup>-1</sup> )	Rate Constant for PA <sup>e</sup>	Rate Constant for A.A. Analogs <sup>f</sup>
				$k_{PA} \pm SD$ (sec <sup>-1</sup> )	$k_{AA} \pm SD$ (sec <sup>-1</sup> )
1	Met	Dimethyl Sulfide	6.66±1.4	1.5±0.2 <sup>g</sup>	40±41 <sup>g</sup>
2	Glu	Butyric Acid	4.89±0.3	4.27±0.27	5.52±0.71
3	Lys	Butylamine	4.52±0.2	4.27±0.27	4.75±0.43
4	PAL	Phenyl Azide	4.27±0.27	4.27±0.27	N/A
5	BB	NEA	2.84±0.4	4.27±0.27	1.41±0.37
6	Cys	Octanethiol	2.46±0.62	4.27±0.27	0.534±0.12
7	Phe	Ethylbenzene	1.81±0.17	4.27±0.27	0.73±.15

a is the rank order of rate constants based on the single exponential first-order fit.

b is the native compound that is being modeled by analogs that are irradiated with phenyl azide, where PAL is the DAT photoaffinity label and BB is the peptide backbone.

c is the model compound that is irradiated with phenyl azide, where NEA is *N*-ethylacetamide.

d is the single exponential first-order rate constant,  $k_1'$ , for the data over a 4 minute time course of irradiation. The equation used to fit the data was  $Ae^{-k_1't} + B$ , where A is the maximum phenyl azide relative peak height (%),  $k_1'$  is the rate constant, t is time in seconds, and B is the y offset when the baseline did not go to zero. All constants were fixed values except  $k_{AA}$ .

e is the rate constant for phenyl azide reacting with itself in cyclohexane, where PA means phenyl azide.

f is the rate constant for the amino acid analog reacting with phenyl azide in cyclohexane, where AA means amino acid analog. The equation used to fit the data was  $A*(e^{-k_{AA}t} + e^{-k_{PA}t})$ , where A is the maximum phenyl azide relative peak height (%),  $k_{AA}$  is the rate constant describing the loss of phenyl azide in the presence of amino acid analog in cyclohexane, M is the molar concentration of the amino acid analogs,  $k_{PA}$  is the rate constant describing the loss of phenyl azide in cyclohexane without amino acid analogs, and t is time in seconds. All constants were fixed values, while  $k_{AA}$  varied.

g represents the double exponential first-order curve fit of the data. When  $k_{PA}$  was set at a fixed value, the equation would not fit the data. In order for the curve to fit the data, both  $k_{PA}$  and  $k_{AA}$  had to vary. These were the values that were obtained for this fitting.  $k_{AA}$  has an error that is larger than the value itself, which means the approximate value may be a negative number. Therefore, with dimethyl sulfide, the methionine model, there may be one process in which phenyl azide is reacting with the analog only.

**Table 3-7. Single and Double Exponential First-Order Rate Constants for Amino Acid Analogs in Cyclohexane.** The values for the fits using two rate constants allowed for the ranking of the amino acid rate constants with phenyl azide to be nearly the same as the first-order fits.

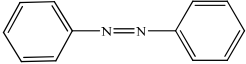
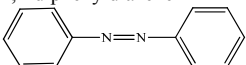
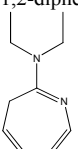
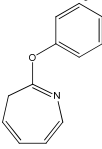
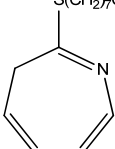
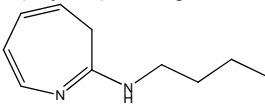
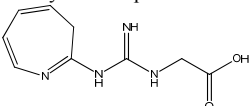
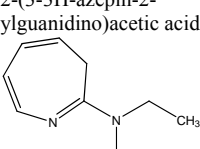
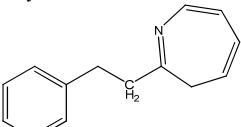
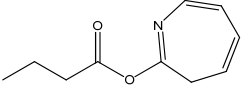
## **Identification of Products by Mass Spectrometry for Aryl Azides Irradiated with Amino Acid Analogs**

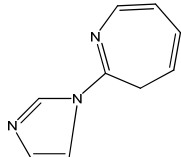
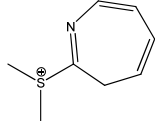
The products that were formed for the irradiation of phenyl azide with amino acid analogs were identified using mass spectrometry. There were such small yields of product during the irradiation that a commercially available aryl azide, *para*-azidoacetophenone (PAAP) was used to produce a larger yield of products to identify by mass spectrometry. The mass spectrometric data for this analysis is also reported in this section. No further analysis was done with the *para*-azidoacetophenone (PAAP).

The expected product for the irradiation of phenyl azide and nucleophiles like diethylamine is *N,N*-diethyl-2*H*-azepin-7-amine (Schrock & Schuster, 1984). This product from the irradiation between phenyl azide and diethylamine was confirmed by mass spectrometry during preliminary investigation of the product formation. The expected product from irradiation of phenyl azide (PA) or *para*-azidoacetylphenone (PAAP) with amino acid analogs was the azepine based on this preliminary information. Therefore, mass spectrometry was used to confirm the products formed from the irradiation of PA or PAAP with amino acid analogs.



### Phenyl Azide (PA) Irradiated with Amino Acid Analogs

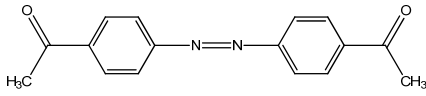
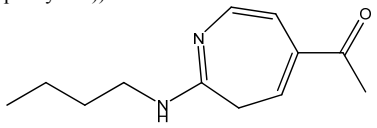
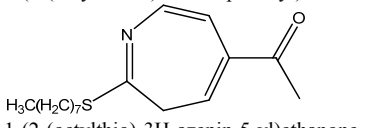
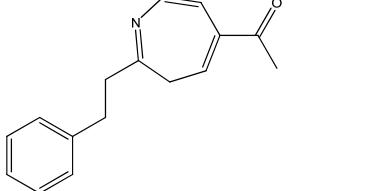
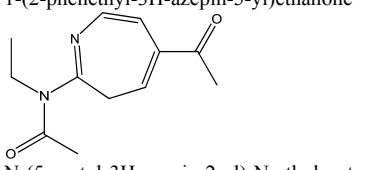
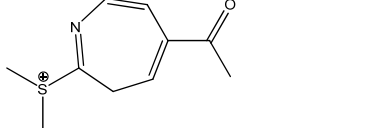
Amino Acid Analog	Monoisotopic Mass	Mass Found $\pm$ Error (ppm)	Product Structure
PA in PBS	182.08439	183.09151 -0.90	 1,2-diphenyldiazene
PA in Cyclohexane	182.08439	183.09159-0.46	 1,2-diphenyldiazene
Diethylamine	164.13134	165.13842 -1.24	 <i>N,N</i> -diethyl-3 <i>H</i> -azepin-2-amine
Phenol	185.08405	186.09129-0.27	 2-phenoxy-3 <i>H</i> -azepine
1-Octanethiol	237.15511	237.15457 -0.98	 2-(octylthio)-3 <i>H</i> -azepine
Butylamine	164.13134	165.13854 -0.52	 <i>N</i> -butyl-3 <i>H</i> -azepin-2-amine
Guanidine Acetic Acid	208.09601	208.09654 +1.06	 2-(3 <i>H</i> -azepin-2-yl)guanidinoacetic acid
<i>N</i> -ethylacetamide	178.11060	179.11784 -0.28	 <i>N</i> -(3 <i>H</i> -azepin-2-yl)- <i>N</i> -ethylacetamide
Ethylbenzene	197.12044	198.12755 - 0.89	 2-phenethyl-3 <i>H</i> -azepine
Butyric Acid	179.09462	180.10172-1.03	 3 <i>H</i> -azepin-2-yl butyrate

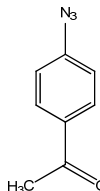
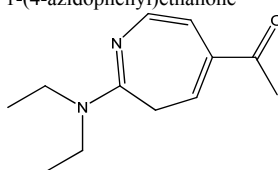
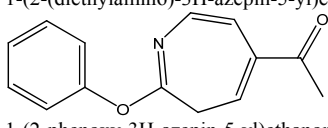
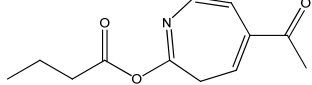
Amino Acid Analog	Monoisotopic Mass	Experimental Mass $\pm$ Error (ppm)	Product Structure
Imidazole	161.09529	160.08685-0.46	 2-(1 <i>H</i> -imidazol-1-yl)-3 <i>H</i> -azepine
Dimethyl Sulfide	154.06904	154.06834-1.02	 (3 <i>H</i> -azepin-2-yl)dimethylsulfonium

**Table 3-8. Mass Spectrometry Analysis of Amino Acid Analogs with Phenyl Azide.**

ESI-MS or APCI-MS was used to determine the products. The confirmed products were within 5 ppm of the theoretical mass to charge values.

***Para*-azidoacetophenone (PAAP) Irradiated with Amino Acid Analogs**

<b>Amino Acid Analog</b>	<b>Theoretical Mass</b>	<b>Experimental Mass ±Error (ppm)</b>	<b>Product Structure</b>
PAAP	266.10552	267.11243-1.40	 <p>1,1'-(4,4'-(diazene-1,2-diyl)bis(4,1-phenylene))diethanone</p>
Butylamine	206.14190	207.14898-1.01	 <p>1-(2-(butylamino)-3H-azepin-5-yl)ethanone</p>
1-Octanethiol	279.16567	280.17241-1.97	 <p>H<sub>3</sub>C(H<sub>2</sub>C)<sub>7</sub>S 1-(2-(octylthio)-3H-azepin-5-yl)ethanone</p>
Ethylbenzene	239.13100	240.13781-2.00	 <p>1-(2-phenethyl-3H-azepin-5-yl)ethanone</p>
<i>N</i> -ethylacetamide	220.12116	221.12807-1.74	 <p>N-(5-acetyl-3H-azepin-2-yl)-N-ethylacetamide</p>
Dimethyl Sulfide	196.07960	196.07883-1.19	 <p>(5-acetyl-3H-azepin-2-yl)dimethylsulfonium</p>

Amino Acid Analog	Theoretical Mass	Experimental Mass	Product Structure
PAAP Control	161.05890	162.06596-1.41	 1-(4-azidophenyl)ethanone
Diethylamine	206.14190	207.14905-0.68	 1-(2-(diethylamino)-3H-azepin-5-yl)ethanone
Phenol	227.09462	228.10174-0.73	 1-(2-phenoxy-3H-azepin-5-yl)ethanone
Butyric Acid	221.10518	Expected product not detected within 5ppm. 221.07586-130.205	 5-acetyl-3H-azepin-2-yl butyrate

**Table 3-9. Mass Spectrometric Analysis of Amino Acid Analogs with *Para*-azidoacetophenone (PAAP).** ESI-MS or APCI-MS were the two methods used to determine the product. A commercially available aryl azide, *para*-azidoacetophenone (PAAP), was irradiated with the model compounds for 4 minutes. The confirmed products were within 5 ppm of the theoretical products.

### **Products from the Irradiation of Phenyl Azide with Amino Acid Analogs**

The irradiated sample of phenyl azide with amino acid analogs was separated by HPLC. The product peak height in mV was recorded for each amino acid analog. In this section, the product peak heights that were detected by the 254 nm wavelength detector on the HPLC will be shown. 1-Octanethiol had the highest absorbance of those analogs irradiated in cyclohexane and in pure analog (NEAT). Guanidine acetic acid had the highest absorbance of the analogs irradiated in aqueous conditions.

**Product Peak Heights for Phenyl Azide Irradiated with Amino Acid Analogs  
in NEAT and Cyclohexane Solvent Conditions**

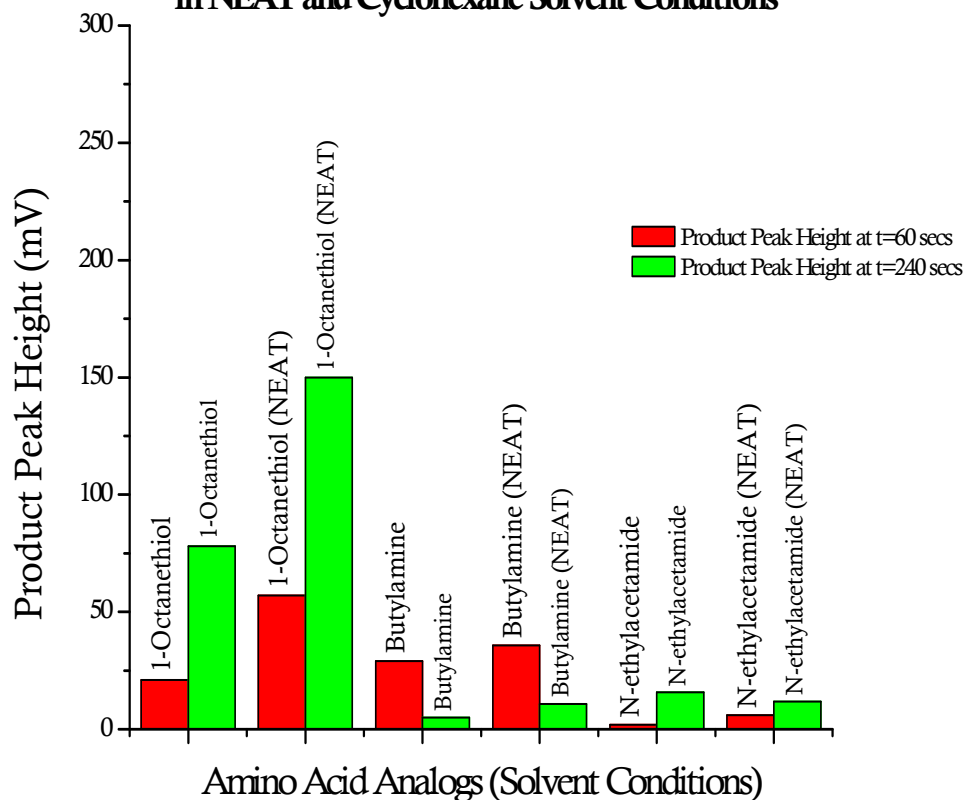


**Figure 3-50. Product Peak Heights for Cysteine, Lysine, and Peptide Backbone**

**Analogs.** Phenyl azide ( $100\mu\text{M}$ ) was irradiated with amino acid analogs for 60 and 240 seconds in cyclohexane and NEAT conditions. 1-Octanethiol had the most product detected under NEAT conditions and in cyclohexane. Butylamine's product formed within 60 seconds and then begins to decompose.

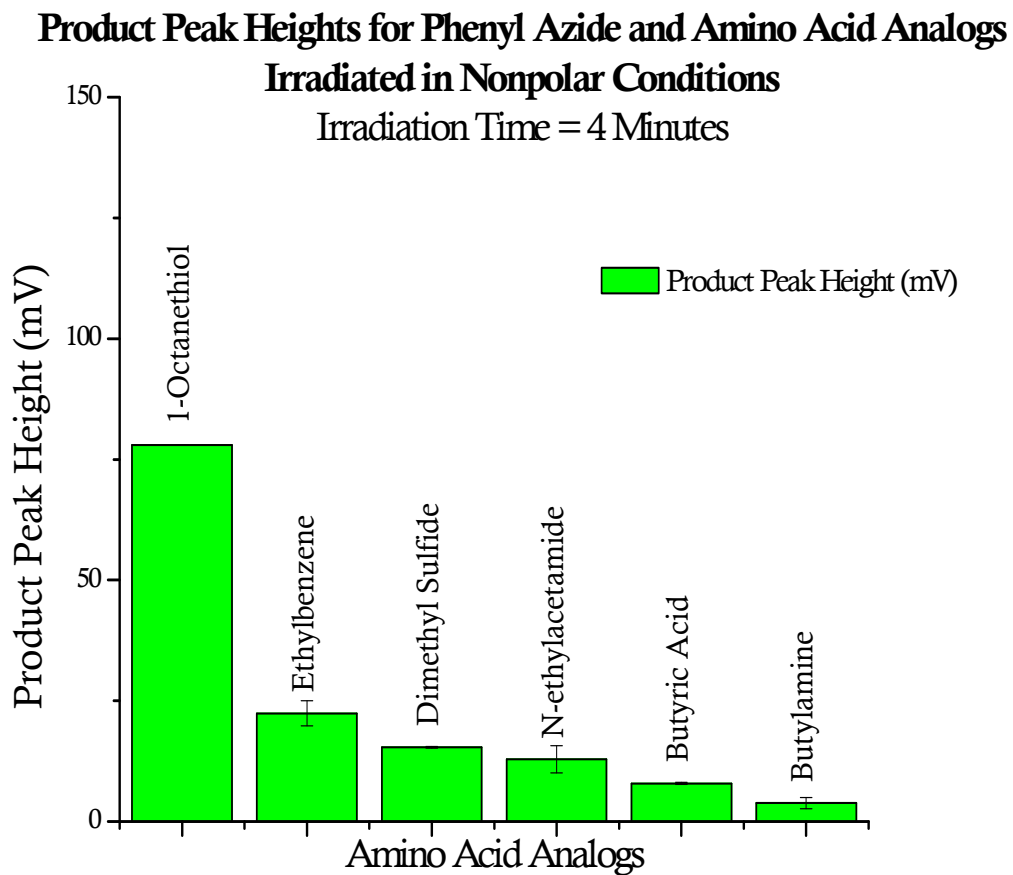


**Figure 3-51. Product Peak Heights in Nonpolar Environment.** 1-Octanethiol is the amino acid analog that forms the most detectable product compared to others in cyclohexane. UV detection is at 254 nm. This figure is not corrected for relative UV response.

**Product Peak Heights for Phenyl Azide and Amino Acid Analogs  
Irradiated in Aqueous Conditions**

Irradiation Time = 4 Minutes

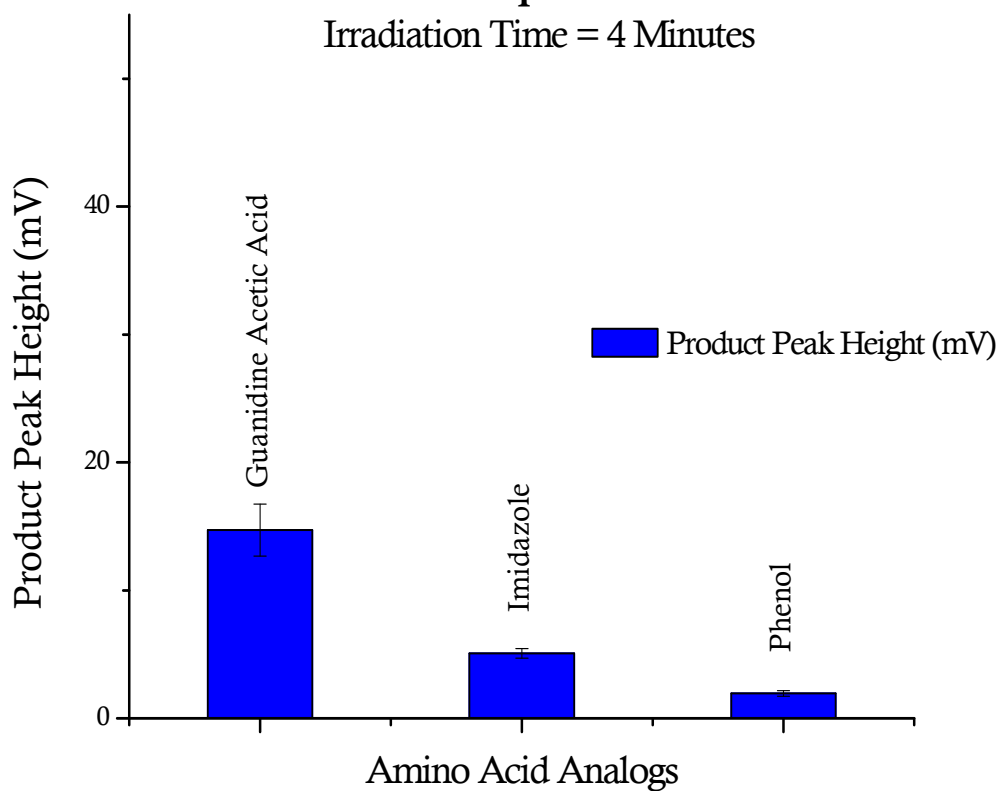


**Figure 3-52. Product Peak Heights in Aqueous Conditions.** In an aqueous environment, phenyl azide irradiated with guanidine acetic acid forms the most detectable product relative to imidazole and phenol.



**Product Peak Heights for Phenyl Azide and Amino Acid Analogs  
Irradiated in NEAT Conditions**

Irradiation Time = 4 Minutes

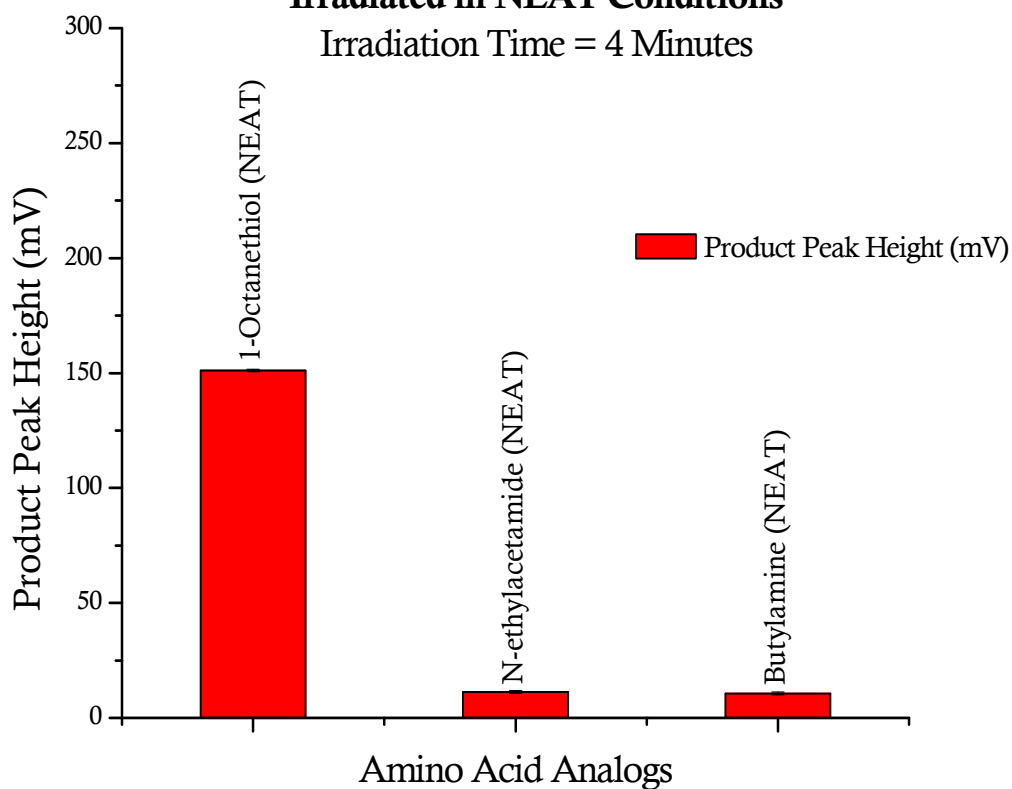


**Figure 3-53. Product Peak Heights in NEAT Conditions.** Under NEAT conditions, phenyl azide was irradiated with 1-octanethiol, which forms the most detectable product relative to *N*-ethylacetamide and butylamine. The UV detection was 254 nm and this figure is not corrected for the UV response.

### Stability of Products in Proteolytic Conditions

The stability of the products formed from irradiation of phenyl azide and the amino acid analogs was tested using basic and acidic proteolytic conditions. Following the photolabeling of hDAT with the photoaffinity ligands, proteolysis was done. After proteolysis, there was little to no sample left to work with. It is possible that the changes in pH during proteolysis may have an effect on the amount of photolabeled hDAT remains. Therefore, the goal of these experiments was to test the stability of basic enzymatic proteolytic conditions and acidic chemical cleavage conditions on the product formed between phenyl azide and the amino acid analogs. The enzymatic proteolysis of hDAT was done with trypsin, thermolysin, or chymotrypsin in a solution of 100mM ammonium bicarbonate (AMBIC), pH 8.9 for 24 hours at 37<sup>0</sup>C in the dark. The chemical cleavage of hDAT was done with 100mM cyanogen bromide (CNBr) in a solution of 70% trifluoroacetic acid (TFA), pH 1 for 24 hours at 25<sup>0</sup>C in the dark.

The products from the irradiation of phenyl azide with amino acid analogs were subjected to 100mM ammonium bicarbonate (AMBIC), pH 8.9 for 4 and 24 hours at 25<sup>0</sup>C. At 4 hours of incubation, the imidazole analog had the most stable product in basic conditions. At 24 hours of incubation, every product formed with the amino acid analogs decomposed. The products were subjected to 70% TFA, pH 1 for 24 hours at 25<sup>0</sup>C. After 24 hours of incubation in acidic conditions, the 1-octanethiol analog formed the most stable product, followed by phenol then imidazole.

### Stability of Products in Basic Conditions

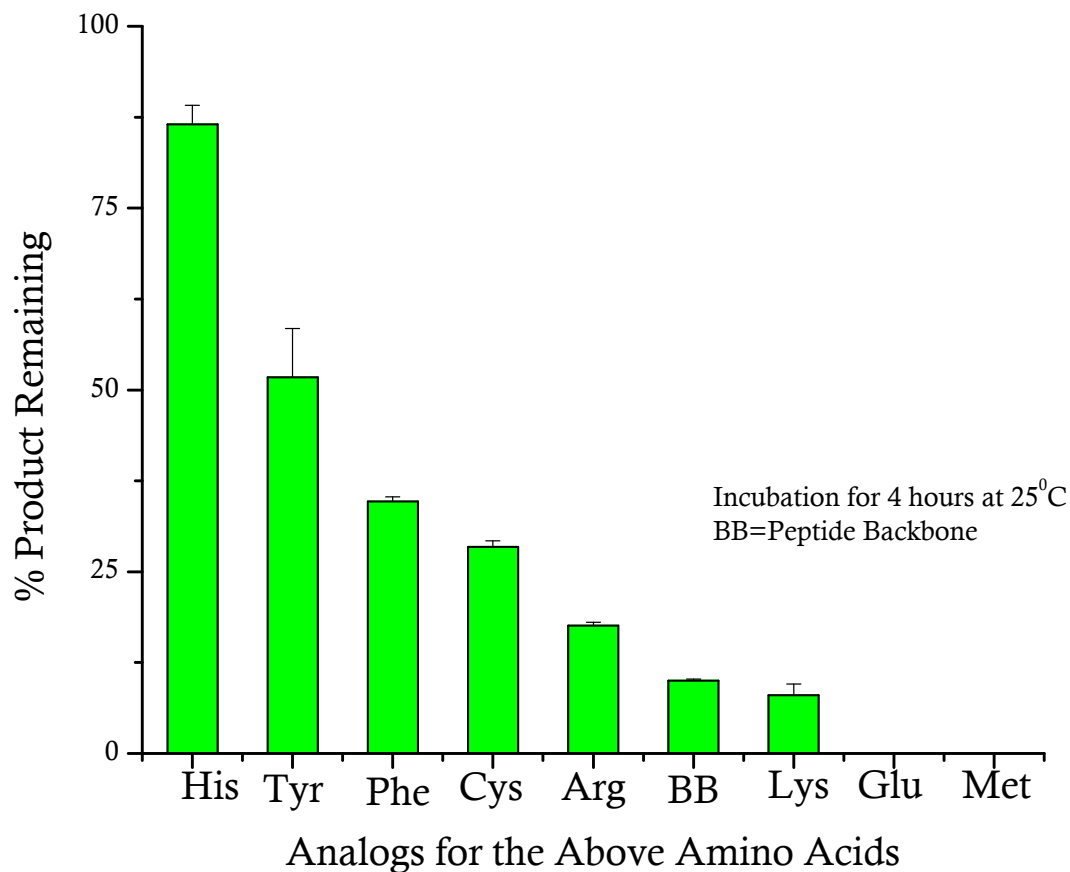


**Figure 3-54. Stability of Products in Basic Proteolytic Conditions.** The analog for histidine (imidazole) has the most stable product in basic conditions. 100mM ammonium bicarbonate, pH 8.9, which is used along with trypsin, chymotrypsin, or thermolysin for enzymatic digestions, was applied to the products from phenyl azide and the amino acid analogs for 4 and 24 hours. The results at 4 hours are shown above. At 24 hours, all products decompose in 100mM AMBIC.

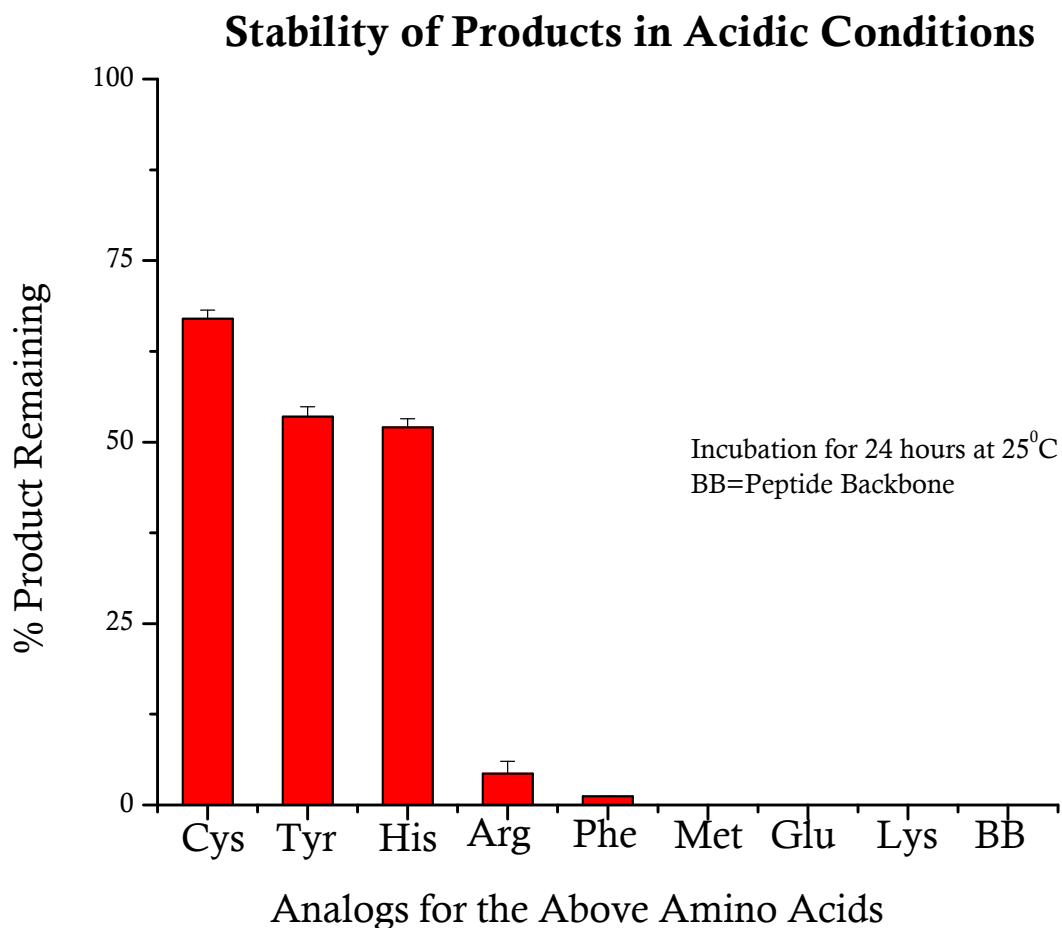


**Figure 3-55. Stability of Products in Acidic Proteolytic Conditions.** The analog for cysteine (1-octanethiol) was the most stable under acidic conditions, relative to the other analogs' products. Tyrosine (phenol) and histidine (imidazole) were also relatively stable in acidic conditions. 70% trifluoroacetic acid, pH 1, which is used along with 100mM cyanogen bromide for chemical cleavages during proteolysis, was applied to the products between phenyl azide and the amino acid analogs for 24 hours at 25<sup>0</sup>C in the dark.

## **Discussion**

## Introduction to the Discussion

Knowledge of the reactivity of aryl azide with amino acid analogs is important because aryl azides are commonly used as photoaffinity labels. Photoaffinity labeling is often used to determine the site of ligand incorporation within a protein. In this dissertation, a small molecule model of the reaction between aryl azido photolabels and amino acids was developed. The rate constant was determined for the reaction of the phenyl azide with analogs of amino acid side chains and the relative rate of reactivity compared. The reactivity of the amino acid analogs are correlated to physical constants such as polarizability, electronegativity, and dielectric constants. The reactivity of aryl nitrenes has been reviewed by Bayley and Staros (1984). The results from this study will be compared to and discussed based on what was previously known about aryl nitrene reactivity.

Photolysis of phenyl azide in the presence of nucleophiles, electrophiles, and acids have been reported to form 3*H*-azepines as the dominant product through the singlet pathway (Rizk *et al.*, 2006; Schrock & Schuster, 1984; Schuster, 1992; Takeuchi, 1981). As a side reaction, small, almost undetectable yields of azobenzene have been reported to occur with phenyl azide in the presence of nucleophiles (Schrock & Schuster, 1984). However, azobenzene is the dominant product formed upon photolysis of phenyl azide alone (Schrock & Schuster, 1984). This dimerization of phenyl azide occurs through the triplet pathway (Budyka *et al.*, 1992; Ong *et al.*, 2003) and occurs in inert solvents (Budyka *et al.*, 1992; Ong *et al.*, 2003) as well as in aqueous conditions (Rizk *et al.*, 2006). In the present study, products formed from the photoreactions of phenyl azide and amino acid analogs were confirmed to be azepines.

Product stability in proteolytic conditions has always been a point of interest for the photolabeling experiments performed with proteins, including hDAT. There was a significant loss of product after proteolysis when hDAT was photolabeled with an aryl azide photolabel like [<sup>125</sup>I]-DEEP. The stability of aryl azide photolabeled products in proteolytic conditions has not been studied before. In this discussion, the possibility of a correlation between the relative reactivity of phenyl azide with the amino acid analogs and the product stabilities in proteolytic conditions is explored.

**Interpretation of Results for Photoreactions of Phenyl Azide  
with the Amino Acid Analogs, Butylamine and 1-Octanethiol**

*Butylamine as a Model for Lysine*

The photoreactions of phenyl azide with butylamine as a model for lysine and with 1-octanethiol as a model for cysteine were highlighted because of their reported reactivities with phenyl nitrenes (Schwartz, 1989). In Schwartz's study, cysteine was the most reactive being greater than  $10^5$  times more reactive with phenyl nitrene than lysine. Lysine was equally as reactive as histidine and greater than 10 times more reactive than that of glycine. Lysine was less reactive than the aromatic amino acids like tyrosine, tryptophan and phenylalanine.

In the present study, butylamine was found to react with phenyl azide with a  $k_1'$  of  $4.52 \cdot 10^{-2} \pm 0.2 \cdot 10^{-2} \text{ sec}^{-1}$ . This rate was one of the fastest compared to the other amino acid analogs. The results of an analysis of variance (ANOVA) showed that dimethyl sulfide ( $k_1' = 6.66 \cdot 10^{-2} \pm 1.4 \cdot 10^{-2} \text{ sec}^{-1}$ ), the analog of methionine was significantly larger than the other analogs ( $p < 0.05$ ), while butyric acid ( $k_1' = 4.89 \cdot 10^{-2} \pm 0.3 \cdot 10^{-2} \text{ sec}^{-1}$ ), the analog for glutamic acid had a larger rate constant but it was not significantly different than butylamine.

A rate constant solely for phenyl azide reacting with the amino acid ( $k_{AA}$ ) was determined to account for the possibility of parallel reactions occurring in the reaction. One rate constant,  $k_{PA}$ , described the loss of phenyl azide in cyclohexane without the amino acid analogs, which was  $4.27 \cdot 10^{-2} \pm 0.27 \cdot 10^{-2} \text{ sec}^{-1}$ . The rate constant of the amino acid analog,  $k_{AA}$ , with phenyl azide was determined to be  $4.75 \cdot 10^{-2} \pm 0.43 \cdot 10^{-2} \text{ sec}^{-1}$  for



butylamine. The rate constant,  $k_{AA}$ , was similar to the first-order rate constant for butylamine ( $4.52 \cdot 10^{-2} \pm 0.2 \cdot 10^{-2} \text{ sec}^{-1}$ ).

The rate constant for phenyl azide and butylamine was also determined in pure target. The rate constant for the photoreaction of phenyl azide and butylamine in neat conditions was  $6.17 \cdot 10^{-2} \pm 0.31 \cdot 10^{-2} \text{ sec}^{-1}$ , which was larger than in cyclohexane. It was also larger than the rate constant for the loss of phenyl azide reacting without amino acid analogs in cyclohexane. This suggests that the formation of phenyl azide into an azepine happens much more rapidly than the dimerization of phenyl azide into azobenzene. The rate of product formation of butylazepine can be measured without having to account for the percentage of azobenzene formation.

Product formation was measured and a rate constant,  $k$  was determined from the irradiation of butylamine and phenyl azide to be  $8.28 \cdot 10^{-2} \pm 0.35 \cdot 10^{-2} \text{ sec}^{-1}$ . The product formed from this reaction was *N*-butyl-3*H*-azepine-2-amine as confirmed by mass spectrometry and proton NMR. The chemical formula of *N*-butyl-3*H*-azepine-2-amine is  $C_{10}H_{16}N_2$ . The theoretical monoisotopic mass is 164.13134. ESI-MS confirmed the product. The experimental chemical formula for  $(M+H)^+$  was  $C_{10}H_{17}N_2$  and the experimental mass was 165.13854, which was within 5 ppm of the theoretical mass.

### ***1-Octanethiol as a Model for Cysteine***

1-Octanethiol was used as a model for cysteine. Cysteines have been reported to be reactive in proteins (Dayon *et al.*, 2006; Javitch, 1998; Javitch *et al.*, 1994; Schwartz, 1989; Stewart *et al.*, 2005) and hence a likely target for the reaction with phenyl azide during photolabeling experiments. Phenyl azide was photoreacted with 1-octanethiol in

cyclohexane over time. Initially, a range of 4 minutes of irradiation was used because it is the time that DAT photolabels are irradiated with the hDAT protein. However, phenyl azide has not been used up within this time frame with 1-octanethiol. Therefore, longer irradiation times were used to get a more accurate rate of reaction for phenyl azide with 1-octanethiol.

The single exponential first-order rate constant with 1-octanethiol was determined at 4 minutes of irradiation to be  $1.97 \times 10^{-2} \pm 0.54 \times 10^{-2} \text{ sec}^{-1}$ . Over twenty minutes of irradiation, the single exponential first-order rate constant was determined to be  $1.49 \times 10^{-2} \pm 0.28 \times 10^{-2} \text{ sec}^{-1}$ . Although longer irradiations gave a somewhat better fit, it was still clear that two processes may be occurring because of the way the data was fit to the single exponential first-order curve and because the rate constant was smaller than that from the loss of phenyl azide alone in cyclohexane ( $4.27 \times 10^{-2} \pm 0.27 \times 10^{-2} \text{ sec}^{-1}$ ). When the data was fit to a curve with a double exponential rate equation that took into account two reactions, most of the points were on the curve unlike the single exponential 1<sup>st</sup> order fit. The  $k_{AA}$  was found to be  $5.34 \times 10^{-3} \pm 1.15 \times 10^{-3} \text{ sec}^{-1}$ . Phenyl azide was also irradiated with pure 1-octanethiol (NEAT). The rate constant from this photoreaction was determined over 4 minutes and then over 60 minutes of time. The rate constant over 4 minutes was  $3.34 \times 10^{-3} \pm 0.16 \times 10^{-3} \text{ sec}^{-1}$  and over 60 minutes it was  $2.98 \times 10^{-3} \pm 0.58 \times 10^{-3} \text{ sec}^{-1}$ . The rate constants were smaller than that of phenyl azide with 1-octanethiol in cyclohexane. This may be due to the absorbance of -SH occurring at 254 nm wavelength (Crews, 1998). It is possible that because it is in excess in cyclohexane and pure during neat conditions that it absorbs the majority of the UV light during the irradiation so that less of the UV radiation is being absorbed by phenyl azide. Since the UV light is

necessary for the formation of the reactive nitrene, if less of the UV is targeting phenyl azide a slower reaction may be occurring.

HPLC analysis showed an increasing absorbance occurring at a retention time of approximately 25 minutes. This fraction was collected and submitted for mass spectrometry analysis. APCI-MS confirmed the azepine product formation. The chemical formula found for the mass spec was  $C_{14}H_{23}NS$  and the experimental mass was 237.15421, which was within 5 ppm of the theoretical mass. The rate constant for the product formation was determined to be  $2.35 \cdot 10^{-3} \pm 0.61 \cdot 10^{-3} \text{ sec}^{-1}$ . The octylthioazepine rate constant for the product formation is much smaller than the rate constant for the butylazepine formation ( $8.28 \cdot 10^{-2} \pm 0.35 \cdot 10^{-2} \text{ sec}^{-1}$ ).

**Interpretation of Results for Photoreactions of Phenyl Azide  
with Amino Acid Analogs in Nonpolar, Aqueous, and NEAT Conditions**

Phenyl azide was irradiated with amino acid analogs over a four-minute time course. This time frame was chosen because the hDAT protein is irradiated with DAT photolabels for four minutes with UV light at 254 nm. The rate constants for each reaction were determined. Lysine, cysteine, phenylalanine, glutamic acid, methionine and peptide backbone analogs were irradiated in a nonpolar environment of cyclohexane. Histidine, arginine, and tyrosine analogs were irradiated in an aqueous environment. Phenyl azide was irradiated alone in both conditions.

***Nonpolar Conditions***

Dimethyl sulfide, a methionine analog, was found to be the most reactive analog in cyclohexane with a rate constant of  $6.66 \times 10^{-2} \pm 1.4 \times 10^{-2} \text{ sec}^{-1}$ . It was larger than phenyl azide dimerization in cyclohexane ( $4.27 \times 10^{-2} \pm 0.27 \times 10^{-2} \text{ sec}^{-1}$ ). Although dimethyl sulfide had the largest rate constant, its rate constant is only 1.5 times larger than the rate constants of butyric acid ( $4.89 \times 10^{-2} \pm 0.3 \times 10^{-3} \text{ sec}^{-1}$ ) and butylamine ( $4.52 \times 10^{-2} \pm 0.2 \times 10^{-2} \text{ sec}^{-1}$ ). 1-Octanethiol and ethylbenzene had the least amount of reactivity with phenyl azide. However, both absorb UV radiation near 254 nm. It is possible that less UV radiation reached the phenyl azide in the presence of the amino acid analogs.

### ***Aqueous Conditions***

In aqueous conditions, the arginine analog resulted in the larger rate constant ( $5.58 \times 10^{-2} \pm 0.74 \times 10^{-2} \text{ sec}^{-1}$ ) compared to the histidine analog ( $5.09 \times 10^{-2} \pm 0.59 \times 10^{-2} \text{ sec}^{-1}$ ). Phenol had the smallest rate constant in aqueous conditions ( $0.30 \times 10^{-2} \pm 0.04 \times 10^{-2} \text{ sec}^{-1}$ ). This may be because the benzene ring of phenol absorbs UV radiation at a wavelength of 254 nm. Because phenol was in a million times excess of phenyl azide, less of the UV radiation was able to reach the phenyl azide. This caused less of the phenyl azide to be activated into the phenyl nitrene which reacts with the hydroxyl group of phenol during the four minute irradiation time period.

### ***NEAT Conditions***

The lysine, cysteine and peptide backbone analogs were irradiated in NEAT conditions. The butylamine (lysine analog) was the most reactive followed by the peptide backbone model and finally the cysteine analog. The cysteine analog was less reactive in this condition than when it was in the cyclohexane. This is not because it is less reactive but moreso because it is in a higher concentration in NEAT conditions. This means that more of the UV radiation was absorbed by the -SH functional group that absorbs near 254 nm. Therefore, it takes longer for the phenyl azide to be activated to form the reactive nitrene to begin the reaction with the -SH group.

### Rate Constants of Amino Acid Analogs in Nonpolar Conditions

Ranking of Rate Constants <sup>a</sup>	Amino Acid Analog <sup>b</sup>	Amino Acid <sup>c</sup>	1 <sup>st</sup> Order Rate Constant, $k_1 \pm \text{SD} \text{ (sec}^{-1}\text{)}^d$	Rate Constant of Amino Acid Analog $k_{AA} \pm \text{SD}$ $\text{(sec}^{-1}\text{)}^e$
1	Dimethyl Sulfide	Methionine	6.66±1.4	40±41 <sup>f</sup>
2	Butyric Acid	Glutamic Acid	4.89±0.3	5.52±0.71
3	Butylamine	Lysine	4.52±0.2	4.75±0.43
4	<i>N</i> -ethylacetamide	Peptide Backbone	2.84±0.4	1.41±0.37
5	1-Octanethiol	Cysteine	2.46±0.62	0.53±0.12
6	Ethylbenzene	Phenylalanine	1.81±0.17	0.73±0.15

a is the rank order of the rate constants based on the single exponential 1<sup>st</sup> order rate constants.

b is the amino acid analog.

c is the amino acid that is being modeled.

d is the 1<sup>st</sup> order rate constant from the single exponential decay equation determined for each amino acid analog irradiated with phenyl azide in cyclohexane.

e is the rate constant of the amino acid analog from the double exponential decay equation, where  $k_{PA}$  was the rate constant for the loss of phenyl azide in cyclohexane is  $4.27 \cdot 10^{-2} \pm 0.27 \cdot 10^{-2} \text{ sec}^{-1}$ .

f represents the fit of the data using the double exponential decay equation. When  $k_{PA}$  was set at a fixed value, the equation would not fit the data. In order for the curve to fit the data, both  $k_{PA}$  and  $k_{AA}$  had to vary. This was the value that was obtained for this fitting.  $k_{AA}$  had an error that was larger than the value itself, which means the value may be a negative number. Therefore, with dimethyl sulfide, the methionine model, there may be one process in which phenyl azide is reacting with the analog only.

**Table 3-10. Rate Constants of Amino Acids in Nonpolar Conditions.** The order of reactivity of phenyl azide with amino acid analogs in cyclohexane remains relatively the

same whether organized by the single exponential first-order rate constants or the rate constant for the amino acid analog,  $k_{AA}$  as determined by the double exponential decay equation.

### Rate Constants of Amino Acid Analogs in Aqueous Conditions

Ranking of Rate Constants <sup>a</sup>	Amino Acid Analog <sup>b</sup>	Amino Acid <sup>c</sup>	1 <sup>st</sup> Order Rate Constant, $k_1' \pm \text{SD} \text{ (sec}^{-1}\text{)}^d$	Rate Constant of the Amino Acid Analog $k_{AA} \pm \text{SD}$ $\text{(sec}^{-1}\text{)}^e$
1	Guanidine Acetic Acid	Arginine	5.58±0.74	2.5±0.12
2	Imidazole	Histidine	5.09±0.59	2.38±0.21
3	Phenol	Tyrosine	0.30±0.04	1.1 ± 0.003

a is the rank order of the rate constants based on the 1<sup>st</sup> order rate constants and the rate constant of the amino acid analog,  $k_{AA}$ .

b is the amino acid analog.

c is the amino acid that is being modeled.

d is the 1<sup>st</sup> order rate constant determined for each amino acid analog irradiated with phenyl azide in aqueous conditions.

e is the rate constant of the amino acid analog with phenyl azide, where  $k_{PA}$  or the rate constant of phenyl azide reacting with itself in aqueous conditions is  $14.8 \times 10^{-2} \pm 1.3 \times 10^{-2} \text{ sec}^{-1}$ .

**Table 3-11. Rate Constants of Amino Acids in Aqueous Conditions.** The order of reactivity for phenyl azide with the amino acid analogs in aqueous conditions is the same whether ranked using the single exponential first-order rate constant,  $k_1'$  or the rate constant,  $k_{AA}$ , from the double exponential rate equation.



### Phenyl Azide Irradiated in Nonpolar and Aqueous Conditions

Phenyl azide was irradiated in the nonpolar environment of cyclohexane and in aqueous conditions. The dimerization of phenyl azide should be described better by a second-order rate constant,  $k_2$ , that takes into account the self-reaction of phenyl azide. However, when fit with the 2<sup>nd</sup> order rate equation, the data did not fit the curve suggesting that there is more going on than previously suspected. The rate constant,  $k_2$ , for the self-reaction of phenyl azide in aqueous conditions was  $1.95 \times 10^{-3} \pm 0.36 \times 10^{-3} \text{ M}^{-1} \text{ sec}^{-1}$ . The second-order rate constant,  $k_2$  for phenyl azide self-reacting in cyclohexane was  $2.55 \times 10^{-3} \pm 0.49 \times 10^{-3} \text{ M}^{-1} \text{ sec}^{-1}$ . The second-order rate constants were calculated but are not accurate enough to draw conclusions upon. There may be other factors beyond the scope of this study causing the data to fit a pseudo first-order rate equation. It was not the intent of this study to understand the dimerization of phenyl azide. While the rate constants are reported, the dimerization of phenyl azide is minimal when there is a large excess of target in the system. Therefore, the effect of the phenyl azide self-reaction was not taken into further account beyond this.

The loss of phenyl azide in cyclohexane resulted in a rate constant,  $k_{PA}$  of  $4.27 \times 10^{-2} \pm 0.27 \times 10^{-2} \text{ sec}^{-1}$ . The loss of phenyl azide in aqueous conditions without amino acid analogs resulted in a single exponential first-order rate constant,  $k_{PA}$  of  $14.8 \times 10^{-2} \pm 1.3 \times 10^{-2} \text{ sec}^{-1}$ . The initial loss of phenyl azide as described by a first-order rate equation happens significantly faster in aqueous conditions than in nonpolar conditions as described by an unpaired t-test where  $p < 0.05$ . Phenyl azide loss in aqueous conditions may be due to the hydrophobic effect, which states that non-polar molecules tend to form intermolecular aggregates in an aqueous medium. If phenyl azide aggregated in the

presence of aqueous conditions, then it also would react with itself more readily.

However, if phenyl azide is more dispersed in cyclohexane then the rate of self-reaction would be limited to how fast the molecules of phenyl azide could get to one another.

The above statements attempt to explain the differences in the two rate constants for phenyl azide loss in aqueous versus nonpolar conditions. Many assumptions can be made regarding this trend but clearer answers cannot be obtained through this study alone. The dimerization of phenyl azide was not the main point of this study and would need to be explored independent of this study in order to fully describe the kinetics of the system.

### **Interpretation of Phenyl Azide Reactivity with Amino Acid Analogs**

The rate constants were correlated to physical properties of functional groups, like polarizability, electronegativity, and dielectric constants (See Appendix). There is little correlation between the rate constants of the amino acid analogs and the dielectric constants of the functional groups. There appears to be little correlation between the polarizability and the rate constants. The electronegativity of the functional groups seems to have the strongest correlation with the rate constants.

Table 3-12 shows a partial list of amino acids that are being labeled by azido photolabels. From this list, one can see that there are a variety of amino acids that can be labeled by azido photolabels. The novelty of using the azido group is that it is not specific and can react with a wide variety of functional groups. Regardless of the amino acids that are in the binding site being explored, these azido photolabels will still form a covalent bond with the protein.

According to table 3-13, there is not a lot of experimental data on the reactivity of aryl nitrenes with amino acid functional groups but the premise is that it can react with many functionalities. The noticeable trend in the table is that while reactivity with different functional groups is high, there is variable stability of the adducts formed.

Few conclusions can be drawn regarding the relative reactivity of phenyl azide with the amino acid analogs. One conclusion is that the reactivity of phenyl azide with the amino acid analogs can be vaguely correlated to the electronegativity of the functional groups. This assumption is limited because knowing the electronegativity does not guarantee that the reactivity of the functional groups will be known. Another conclusion is that the dimethyl sulfide was the most reactive analog compared to the

other analogs irradiated in cyclohexane. Guanidine acetic acid and histidine were the most reactive analogs in aqueous conditions. Butylamine was the most reactive analog in neat conditions. The rate constants of the analogs with phenyl azide were compared using a one-way ANOVA (see Appendix) and those analogs that were significantly different were determined by post-ANOVA multiple comparisons where  $p < 0.05$ .

<b>Aryl azide photolabel</b>	<b>Biological macromolecule</b>	<b>Labeled Amino Acid(s)</b>	<b>Reference</b>
2-azido[alpha-32P]adenosine diphosphate	beta subunit of beef heart mitochondrial F1-ATPase	<b>Leu-342, Ile-344, Tyr-345, and Pro-346</b>	(Garin <i>et al.</i> , 1986)
2',3'-O-(2,4,6-trinitrophenyl)-8-azido-AMP and -ATP	active site of sarcoplasmic reticulum Ca(2+)-ATPase.	<b>Lys-492</b>	(McIntosh <i>et al.</i> , 1992)
azido AG-A (agosterol) 8-azido-ATP	MRP1 beta-subunit of bovine mitochondrial F1-ATPase	<b>Arg -1249 Lys-301, Ile-304, and Tyr-311</b>	(Ren <i>et al.</i> , 2002) (Hollemaans <i>et al.</i> , 1983)
azidophenyl derivative of semotiadil FNAK {(+)-(R)-3,4-dihydro-2-[5-methoxy-2-[3-[N-methyl-N-[2-(3-azidophenoxy)-ethyl]amino]propoxyl]phenyl]-4-methyl-2H-1,4-benzothiazin-3-(4H)-one}	domain III of human serum albumin	<b>Lys-414 Lys-541</b>	(Kawahara <i>et al.</i> , 2002)
N-(4-azido-2-nitrophenyl)-putrescine (ANP) 8-azido-ATP	actin	<b>Cys-374</b>	(Kim <i>et al.</i> , 1998)
aryl azide linked to the phosphate backbone BI-RJ-70, an azido photoaffinity analogue	HisP, a membrane protein of the histidine permease	<b>His-19 and Ser-41</b>	(Mimura <i>et al.</i> , 1990)
	TaqI restriction endonuclease noncatalytic modulatory site, RT1MS on HIV-1 RT	<b>Tyr-161 Tyr-181 and Tyr-188</b>	(Mayer & Barany, 1995) (Cohen <i>et al.</i> , 1991)

**Table 3-12. Partial List of Amino Acids Labeled by Azido Photolabels.** This list

shows that many different classes of amino acids have been identified as being labeled by aryl azides.

### Arylnitrene Reactivity with Amino Acid Functional Groups

Functional Group	Amino acid on which group is found	Comments
C-C	All	Do not react
C=C	None <sup>1</sup>	Electrophilic nitrenes react
C-H	All	Aliphatic CH reacts with strongly electrophilic nitrenes
Aryl	Phe, Tyr, Trp, His	Electrophilic nitrenes insert into aryl CH, by addition followed by rearrangement
N-H	Lys, His, N-terminal	Several possible reaction pathways
Guanidinium	Arg	Probably react, but no experimental data
O-H	Ser, Thr, Tyr	Several possible reaction pathways
S-H	Cys	Several possible reaction pathways
S-S	Cys-Cys	Probably react, but no experimental data; unstable adducts and cleavage of -S <sub>2</sub> -
S-CH <sub>3</sub>	Met	React, but adducts likely to be unstable
COOH	Asp, Glu, C-termini	React, but adducts unstable
CONHR	Asn, Gln, peptide bond	No experimental data; reaction with peptide bond may cause chain cleavage
COOR	Methyl aspartate, methyl glutamate <sup>2</sup>	Probably react, but adducts likely to be unstable
-PO <sub>2</sub> H	Phosphoserine, phosphothreonine, phosphotyrosine <sup>3</sup>	Probably react, but adducts likely to be unstable

<sup>1</sup> Some aromatic residues found in biopolymers have bonds of olefinic character. Many fatty acids found in lipids have double bonds.

<sup>2</sup> Also found in lipids.

<sup>3</sup> Found in greater abundance in lipids and nucleic acids.

(adapted from Bayley and Staros, 1984)

**Table 3-13. Arylnitrene Reactivity with Amino Acid Functional Groups.**

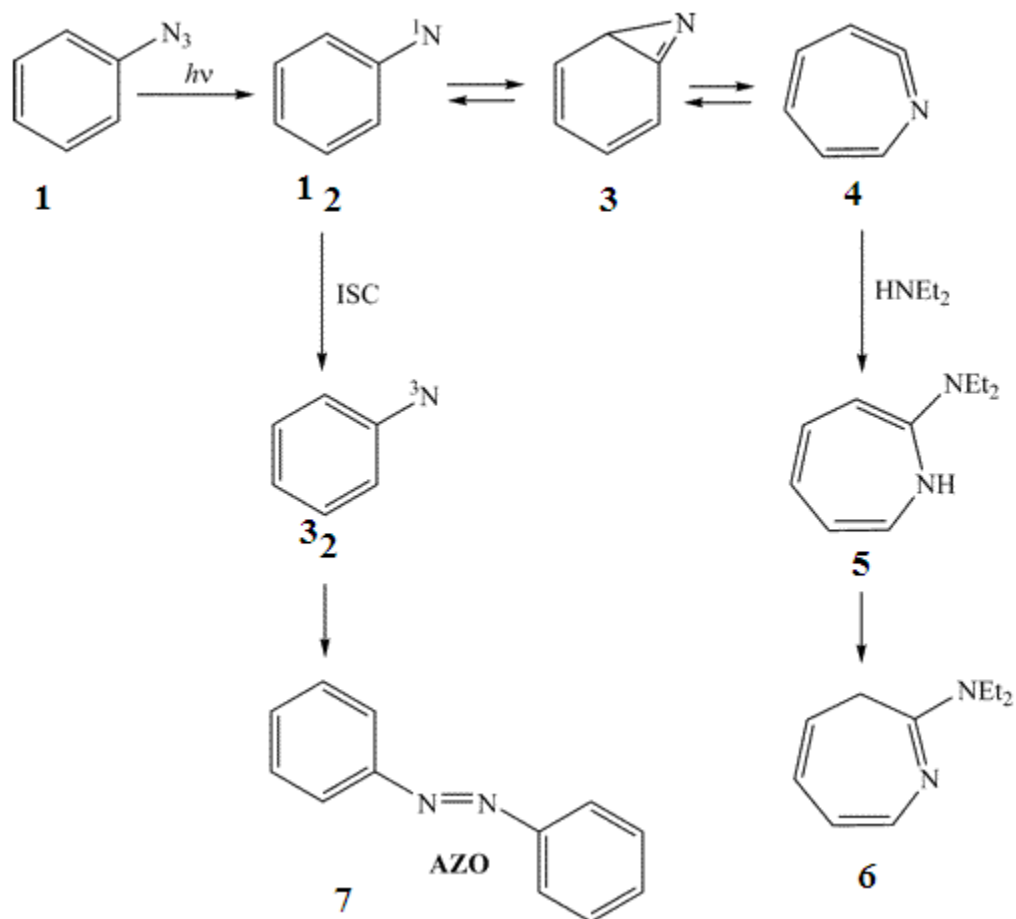
Arylnitrenes are able to react with many different functional groups. This table shows which adducts produced with the aryl nitrenes is proposed to be unstable.

**Discussion of the Product Formation of Azepines  
from the Irradiation of Aryl Azides and Amino Acid Analogs**

Irradiation of phenyl azide in cyclohexane and PBS buffer, pH 7.4 was performed. The formation of azobenzene (**7**) (Scheme 3-4) was confirmed using mass spectrometry in both solvent conditions. Detection of phenyl azide absorbance by HPLC revealed a complete loss of phenyl azide after a 4 minute irradiation time period. Proton NMR as well as mass spectrometry determined that the product could be confirmed as azobenzene. Azobenzene (**7**) is the only product formed from the irradiation of phenyl azide in inert solvents (Schrock & Schuster, 1984) and in aqueous conditions (Rizk *et al.*, 2006). This reaction occurs through the triplet pathway (Scheme 3-4).

Reactions of phenyl azide in the presence of nucleophiles are reported to form azepines through the singlet state pathway (Li *et al.*, 1988a; Rizk *et al.*, 2006; Shields, 1987). In scheme 3-4, phenyl azide (**1**) forms a reactive singlet nitrene (**2**) upon photolysis. In the singlet state, the phenyl nitrene cyclizes rapidly (~1 ns in organic solvents) to form benzazirine (**3**), which immediately opens to form 1, 2, 4,6-azocycloheptatetraene (a 1,2-didehydroazepine or cyclic ketenimine) (Rizk *et al.*, 2006) (**4**, Scheme 3-4). McClelland and co-workers have shown that this photochemistry is also applicable to the photolysis of phenyl azide in aqueous solutions (McClelland *et al.*, 1996).





**Scheme 3-4. Photolysis of Phenyl Azide in Aqueous and Organic Solvents.**

Azobenzene (7) is formed during the photolysis of phenyl azide in aqueous and organic solvents through the triplet pathway. Azepine (6) is the dominate product formed during photolysis of phenyl azide with a nucleophile. This reaction proceeds through the singlet state (adapted from Li *et al.*, 1988b; Rizk *et al.*, 2006; Schrock & Schuster, 1984).

### ***Identification of Butylazepine***

<sup>1</sup>H NMR and ESI-MS was used to confirm the presence of butylazepine from the irradiation of phenyl azide and butylamine but the azepine product has never been isolated for the photoreaction of phenyl azide and butylamine. Azepine has been confirmed and isolated from a reaction of phenyl azide and diethylamine (Li *et al.*, 1988b). The problem with isolating these azepines is that they decompose rapidly under certain conditions, including acidic and basic conditions. Attempts at extracting the product and separating it on a column were unsuccessful. However, the crude mixture contained the butylazepine in very low yields. A proton NMR showed peaks corresponding to the protons of butylazepine in the theoretical NMR generated by ChemDraw. The ESI-MS of the product matched the theoretical mass within 5 ppm. The theoretical monoisotopic mass was 164.13134. The experimental mass (M+H)<sup>+</sup> ± standard deviation (ppm) was 165.13854±0.52 ppm.

### ***Analysis of Azepine Products from Phenyl Azide and Amino Acid Analogs using Mass Spectrometry***

APCI-MS or ESI-MS was used to confirm the formation of azepines in the photolysis of phenyl azide with the amino acid analogs. Table 3-8 in the Results section of Chapter Three shows the mass found for each analog along with its error. All of the errors were within 5 ppm of the theoretical mass.

The azepine product for butyric acid was not confirmed when irradiated with PAAP within 5 ppm in spite of exhaustive methods to obtain the azepine product. The error was 20 ppm, which is higher than the accepted value of 5 ppm. Several factors may

contribute to the lack of confirmation by mass spectrometry. The product may have decomposed rapidly and there was not enough of the product left for the mass spectrometric analysis. The butyric acid is highly acidic and the product could hydrolyze easily because of the excess analog present in the solution. Separation by HPLC, collection of the fraction thought to be the product and analysis of that fraction by mass spectrometry still did not show the azepine. Therefore, azepine formation was not confirmed with PAAP and butyric acid.

### **Absorbance of Products from the Photoreactions of Phenyl Azide and Amino Acid Analogs**

1-Octanethiol had the strongest absorbance of product with phenyl azide versus the other targets in nonpolar conditions. The ethylbenzene product was the second and the dimethyl sulfide was the third. This ranking is not surprising given that  $-SH$  and  $R-S-R$  both absorb near 254 nm (Crews, 1998). The benzene ring of ethylbenzene also absorbs near the 254 nm wavelength set on the HPLC UV detector. Therefore, more product is not necessarily being formed by the 1-octanethiol but more is able to be detected because of the strong absorbance by the  $-SH$  at this wavelength. *N*-ethylacetamide, butyric acid and butylamine do not have functional groups that absorb at this wavelength so the product formed appears to be smaller than that of the other targets when in fact there may be more (Figure 3-56A).

In aqueous conditions, phenol and imidazole had the least absorbance of products formed though they have aromatic rings. Phenol also gave the smallest rate constant. It is possible that when in excess, phenol, which absorbs at 254 nm, absorbs the majority of

the UV radiation. This means that in the presence of phenol, less UV radiation may reach the phenyl azide, resulting in less phenyl nitrene and therefore less product formation. Imidazole, while an aromatic heterocycle, has a maximum UV absorbance at 207 nm which means that less of its product may be detected by the UV wavelength of 254 nm set by the HPLC (Figure 3-56B).

Phenyl azide was irradiated in pure amino acid analog (NEAT). 1-Octanethiol had the most absorbance of product even though it had the smallest rate constant. The reaction did not go to completion until 60 minutes of irradiation time; however, at 4 minutes, it had surpassed butylamine and *N*-ethylacetamide in the detection of product. The smaller rate constant was possibly due to the absorption of UV radiation at 254 nm by 1-octanethiol, therefore, inhibiting the UV absorption by phenyl azide. Once the UV radiation reached phenyl azide to form the reactive nitrene, the reaction time period of 4 minutes was over. Since the 1-octanethiol has the –SH functional group that absorbs near 254 nm, the product had the highest absorbance among the other amino acid analogs (Figure 3-56C).

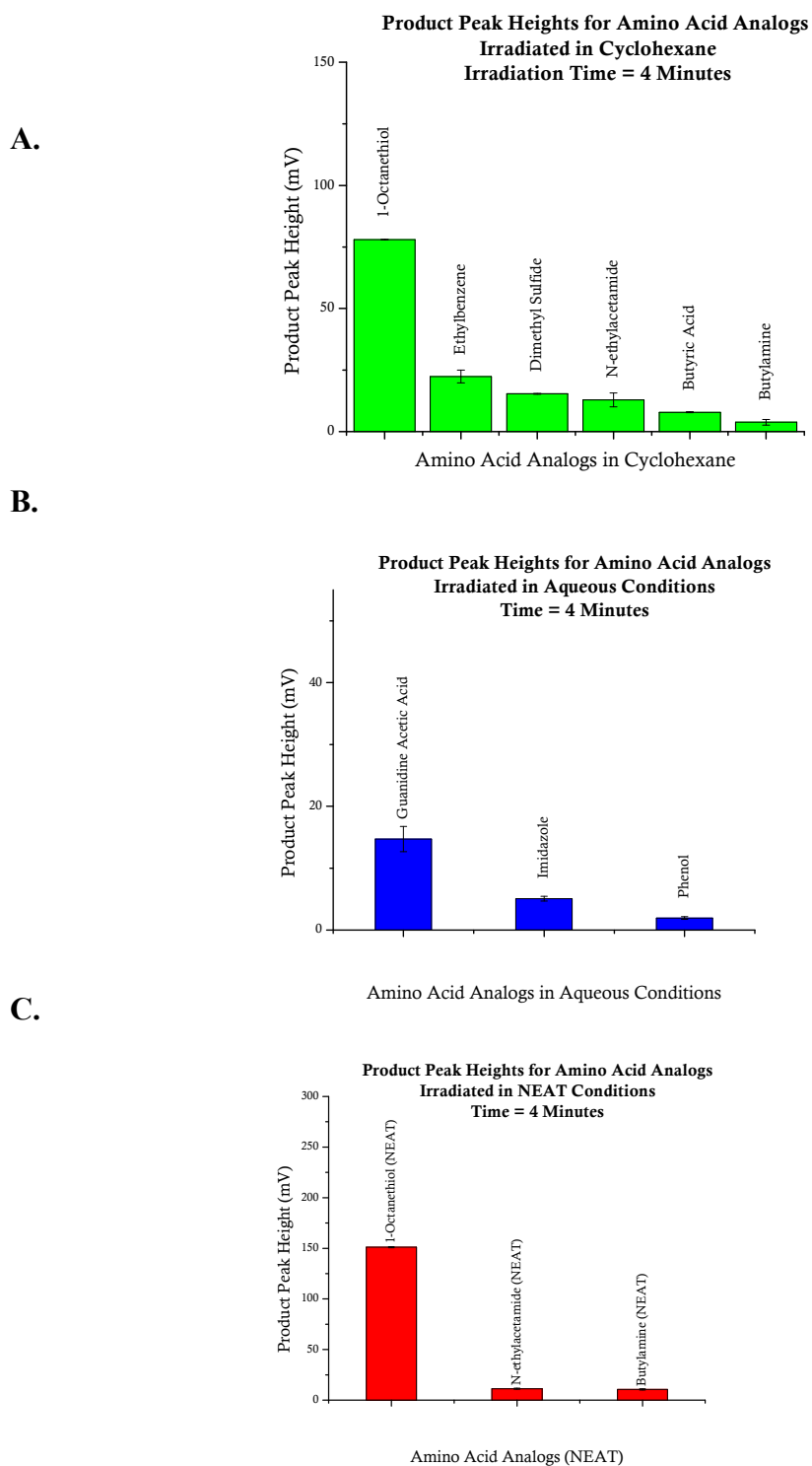


**Figure 3-56. UV Absorbance of Products in Different Solvent Conditions.** A. 1-Octanethiol was the analog with the most UV absorbance of product formed in cyclohexane. B. Guanidine acetic acid was the analog with the most UV absorbance of

product formed in aqueous conditions. C. 1-Octanethiol was the analog with the most absorbance of product formed in NEAT conditions.

## Azepine Product Stability in Proteolytic Conditions

### *Stability of Product in Basic Conditions*

In work to identify the amino acid labeled in hDAT by photoaffinity cocaine analogs, proteolysis of hDAT is done, enzymatically or chemically following the photolabeling and visualization by autoradiography. An in-gel digestion with trypsin in 100 mM ammonium bicarbonate (AMBIC), pH 8.9, was the first digestion performed with [ $^{125}$ I]-DEEP labeled hDAT. The protein was incubated with trypsin in AMBIC for 24 hours at 37 degrees Celsius. A modification of these conditions was used to test the stability of products formed from reaction with phenyl azide and the amino acid analogs. The trypsin was omitted from the tests as well as the temperature. The experiment was limited to exploring pH condition used for tryptic digests, that is, pH 8.9.

Initially, the products were tested at 37<sup>0</sup>C for 24 hours in 100 mM AMBIC, pH 8.9. All products decomposed. Then the experiment was tried at 25<sup>0</sup>C for 24 hours in 100mM AMBIC, pH 8.9 and all of the products decomposed. These results suggested that the elevated temperature did not play a major role in the decomposition of the product. Therefore, the stability of the product was tested at 4 hours at 25<sup>0</sup>C in AMBIC, pH 8.9. All stability tests were done in the absence of light so that any decomposition could not be attributed to light.

Imidazole, a histidine analog, was the most stable compared to the other analogs, retaining 87% of its product. Phenol, the tyrosine analog (52%) and ethylbenzene, the phenylalanine model (35%), were more stable than the other targets under these basic conditions. The least stable products were butyric acid, the glutamate analog and

dimethyl sulfide, the methionine analog. Each of the amino acid analog's product completely decomposed within 4 hours of treatment with AMBIC.

### ***Stability of Product in Acidic Conditions***

Primary and secondary cyanogen bromide cleavages are done to create smaller peptides of labeled hDAT. These CNBr cleavages are performed in a solution of 70% trifluoroacetic acid (TFA). The pH of this solution is 1, a highly acidic solution.

Previously, it had been shown that the TFA in the solution of CNBr causes decomposition of the DAT photolabel, [<sup>125</sup>I]-DEEP (Figure 2-18 and 2-19 in Chapter Two Results Section). The CNBr itself appears to cause no additional decomposition. It has been concluded that the 70% TFA is the major cause of decomposition of the hDAT photolabel, [<sup>125</sup>I]-DEEP. It was therefore tested on the products formed from phenyl azide and the amino acid analogs.

Usually the CNBr cleavages are done over 24 hours at 25<sup>0</sup>C in the dark. Therefore, the products from the irradiation of phenyl azide and amino acid analogs were incubated in the dark for 24 hours with 70% TFA. Decomposition from exposure to the light did not play a role in the decomposition seen with the product. As shown in Table 3-14, the product formed from 1-octanethiol, the cysteine analog, is the most stable in acidic conditions, retaining 67% of its product. The product formed from phenol, the tyrosine analog, is the second most stable in acidic conditions (54%) about the same as the product from imidazole, the histidine analog (52%). Complete decomposition occurred for the products from dimethyl sulfide, the methionine analog, butyric acid, the



glutamate analog, butylamine, the lysine analog, and *N*-ethylacetamide, the peptide backbone analog.

The major product formed from each photoreaction is an azepine. *3H*-azepines are fairly unstable compounds (Odum, 1997). Many factors contribute to the stability of azepines. Temperature, pH, light, and storage conditions can all contribute to the stability of azepines. In this study, pH was used to test the stability because it is the major factor in the digestion of photolabeled hDAT protein. Acidic and basic conditions have different effects on the products formed as can be seen in this study. The most stable products are the histidine analog, imidazole, the tyrosine analog, phenol and the cysteine analog, 1-octanethiol. These compounds maintain at least 50% of their product following the acidic and basic conditions examined.

As stated before, *3H*-azepines are fairly unstable and decompose rapidly. It has been shown that further irradiation of *3H*-azepines lead to the formation of another product that has been characterized by NMR. 2-dimethylamino-*3H*-azepine (**8a**), 2-amino-*3H*-azepine (**8b**) and 2-ethoxy-*3H*-azepine (**8c**) were irradiated directly in pentane. These compounds underwent selective photoelectrocyclization to 3-substituted 2-azabicyclo[3.2.0]hepta-2,6-dienes (**9**) (Scheme 3-5 and 3-6). This knowledge can be applied to the decomposition that is seen when butylamine and phenyl azide are irradiated beyond 60 seconds. Although the azepine has been identified as a product of the photoreactions in this research, decomposition of the azepine is seen in the graph of the product formation over time (Figure 3-7 and 3-11 in the Results Section of Chapter Three). The decomposition could possibly be the cyclization into the bicycloheptadiene shown in Scheme 3-5.

### Product Stability in Proteolytic Conditions

#### A.

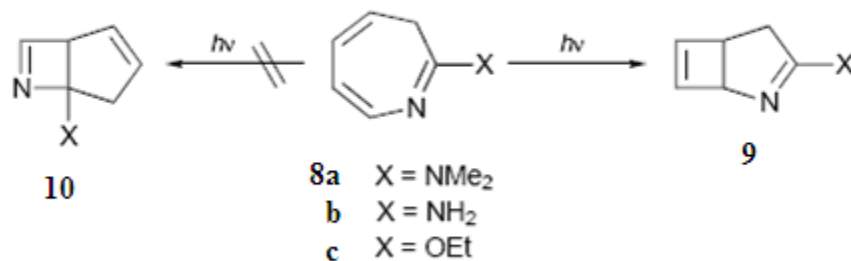
AMBIC Ranking	Amino Acid Analog	% Product Remaining $\pm$ SEM
1	Imidazole	87 $\pm$ 2.7
2	Phenol	52 $\pm$ 6.7
3	Ethylbenzene	35 $\pm$ 0.7
4	1-Octanethiol	28 $\pm$ 0.8
5	Guanidine Acetic Acid	18 $\pm$ 0.5
6	<i>N</i> -ethylacetamide	10 $\pm$ 0.2
7	Butylamine	8 $\pm$ 1.6
8	Butyric Acid	0
8	Dimethyl Sulfide	0

#### B.

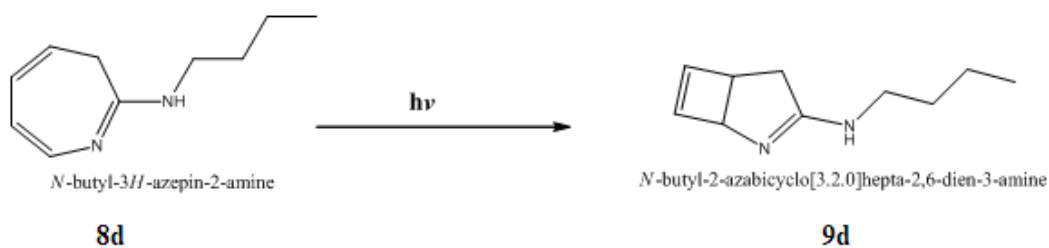
TFA Ranking	Amino Acid Analog	% Product Remaining $\pm$ SEM
1	1-Octanethiol	67 $\pm$ 1.2
2	Phenol	54 $\pm$ 1.4
3	Imidazole	52 $\pm$ 1.2
4	Guanidine Acetic Acid	4 $\pm$ 1.7
5	Ethylbenzene	1 $\pm$ 0.02
6	Dimethyl Sulfide	0
6	Butyric Acid	0
6	Butylamine	0
6	<i>N</i> -ethylacetamide	0

**Table 3-14. Product Stability in Basic and Acidic Conditions.** Imidazole forms the most stable product after application of AMBIC and 1-octanethiol forms the most stable

product in 70% TFA. Butyric acid and dimethyl sulfide forms the least stable products in AMBIC. Ethylbenzene, butyric acid, butylamine and *N*-ethylacetamide forms the least stable products in 70% TFA.



**Scheme 3-5. Photoisomerization of 3H-azepines.** According to Odum and Schmall, 1997, photoelectrocyclization of 3H-azepine substituted in the 2-position with ethoxy, amino and dimethylamino groups yield 3-substituted 2-azabicyclo[3.2.0]hepta-2,6-dienes as the only major volatile product in all cases (Scheme adapted from Odum, 1997).



**Scheme 3-6. Irradiation of *N*-butyl-3H-azepin-2-amine.** Irradiation of butylamine and phenyl azide forms *N*-butyl-3H-azepine-2-amine (**8d**). Further irradiation beyond 60 seconds shows decomposition of the azepine. This decomposition may be due to the formation of *N*-butyl-2-azabicyclo[3.2.0]hepta-2,6-dien-3-amine (**9d**) from further irradiation of *N*-butyl-3H-azepine-2-amine (**8d**). (Scheme adapted from Odum, 1997).

Acidic conditions cause 3*H*-azepine to hydrolyze, breaking the bond between nitrogen and carbon to form an ammonium ion (Figure 3-57) (Noskov *et al.*, 1997). Products of acid hydrolysis of dibenz[b,e]azepines exist only in reaction solutions. Attempts to isolate them (by extraction with solvents from preliminarily neutralized solutions or evaporation) lead to either the initial dibenz[b, e]azepines or their hydrochlorides (Noskov *et al.*, 1997) . An azepinium ion has been observed that is not as stable as a tropylium ion. This ion was seen upon reacting azepines with TiCl<sub>4</sub>, a Lewis acid (Satake *et al.*, 2004). Following irradiation of phenyl azide and amino acid analogs, the products were subjected to 70% TFA, a proteolytic condition of CNBr cleavages.

In this study with butylazepine, decomposition was seen following treatment with acids and bases. These products are caused by the hydrolysis of the azepine into its protonated salt under acidic conditions (Noskov *et al.*, 1998) (Figure 3-58). More than 50% of the products were identified as the protonated salt after 60 minutes of reaction time with acid. An increase of the protonated salt was seen as time reacting with the acid was increased. Therefore, 24 hours of interaction of trifluoroacetic acid (TFA) with the azepine most likely gives the protonated salt seen in Figure 3-58.

### **Correlation of Rate Constants vs. Product Stability in Proteolytic Conditions**

Correlations between phenyl azide reactivity and the product stability in proteolytic conditions were done (see Appendix). Product stability in acidic chemical cleavage conditions does not seem to correlate with the reactivity of phenyl azide with the amino acid analogs as explained by the rate constants. The product stability in basic enzymatic conditions does appear to correlate with the rate constants. This trend suggests

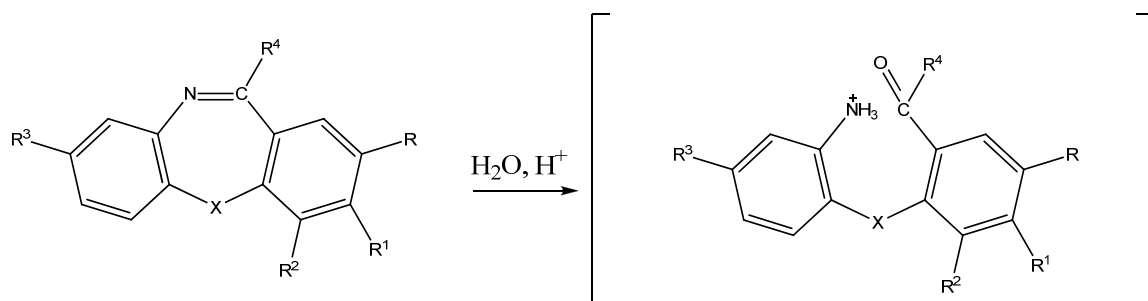


**Figure 3-57. Acid Hydrolysis of Azepine.** Acid hydrolysis of azepine is seen in reaction solutions upon the addition of acid (adapted from Noskov *et al.*, 1997).

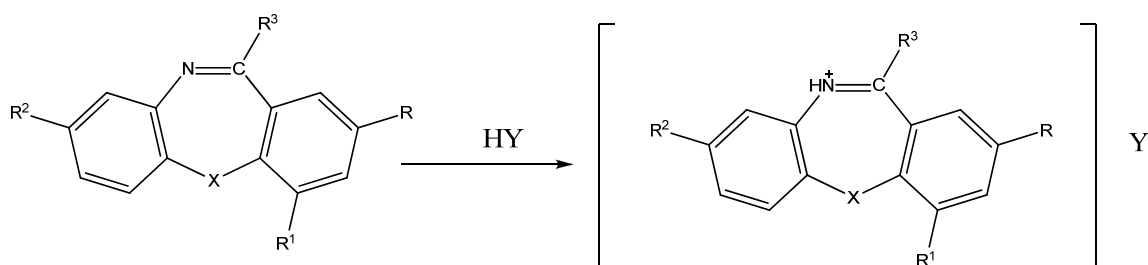


**Figure 3-58. Azepine becomes the Protonated Salt upon Addition of Acid.** The protonated salt is formed from the addition of acid to 3H-azepines (adapted from Noskov *et al.*, 1998). that the most reactive amino acid analog with phenyl azide may not be the most stable product through basic enzymatic conditions.

### **So What Gets Labeled?**

The main purpose of this study of phenyl azide reactivity was to be able to draw some conclusions about what amino acid side chain is the most likely to be labeled by aryl azido photolabels. The argument for using aryl azides as photolabels is well warranted because the azido group reacts with a wide variety of amino acid side chain functional groups. However, aryl azides “rarely give stoichiometric labeling”. In fact, yields of azide photolabeling are generally less than 30% (Fleming, 1995). Another disadvantage is that the adducts formed with the aryl azide may not be stable (Bayley and Staros, 1984) and the bond between the label and the protein could be compromised during post-photolabeling procedures such as proteolysis.

The research done in this study supports the previous assumptions made by others in the field. Phenyl azide did react with each of the amino acid analogs tested. There was less than an order of magnitude of difference in the rate constants obtained for each analog. Reactivity of aryl azides with a particular amino acid residue is limited to the amino acid residues that are in proximity to the azido moiety in the binding site of the protein. The aryl azide may also react with the peptide backbone. This information adds another dimension of understanding to how aryl azides react with amino acid functional groups and the peptide backbone.

A covalent bond may be formed between the aryl azide photolabel and the protein of interest, there may be instability issues surrounding the labeled protein if proteolysis is done in an attempt to map the labeled amino acid. This study sheds new light on how the bond formed from photolabeling with aryl azides may not be stable through the proteolytic digestions that are oftentimes done following the photolabeling. This gives

one a better perspective on the low yields of product left following the work-up of photolabeled proteins, i.e. hDAT, through various procedures.



## References

- Abramson, J., Smirnova, I., Kasho, V., Verner, G., Iwata, S. and Kaback, H. R. (2003)  
The lactose permease of *Escherichia coli*: overall structure, the sugar-binding site  
and the alternating access model for transport. *FEBS Lett*, **555**, 96-101.
- Abramson, J., Smirnova, I., Kasho, V., Verner, G., Kaback, H. R. and Iwata, S. (2003)  
Structure and mechanism of the lactose permease of *Escherichia coli*. *Science*,  
**301**, 610-615.
- Agoston, G. E., Wu, J. H., Izenwasser, S., George, C., Katz, J., Kline, R. H. and  
Newman, A. H. (1997) Novel N-substituted 3 alpha-[bis(4'-  
fluorophenyl)methoxy]tropane analogues: selective ligands for the dopamine  
transporter. *J Med Chem*, **40**, 4329-4339.
- Amara, S. G. and Sonders, M. S. (1998) Neurotransmitter transporters as molecular  
targets for addictive drugs. *Drug Alcohol Depend*, **51**, 87-96.
- Andersen, P. H. (1987) Biochemical and pharmacological characterization of [3H]GBR  
12935 binding in vitro to rat striatal membranes: labeling of the dopamine uptake  
complex. *J Neurochem*, **48**, 1887-1896.
- Andersen, P. H. (1989) The dopamine inhibitor GBR 12909: selectivity and molecular  
mechanism of action. *Eur J Pharmacol*, **166**, 493-504.
- Arnt, J., Christensen, A. V., Hyttel, J., Larsen, J. J. and Svendsen, O. (1982) Effects of  
putative dopamine autoreceptor agonists in pharmacological models related to  
dopaminergic and neuroleptic activity. *Eur J Pharmacol*, **86**, 185-198.

- Autelitano, F., Weill, C., Goeldner, M. and Ilien, B. (1997) Covalent labeling of muscarinic acetylcholine receptors by tritiated aryldiazonium photoprobes. *Biochem Pharmacol*, **53**, 501-510.
- Ball, J. C., Ross, A. (1991) *The effectiveness of Methadone maintenance treatment*. Springer-Verlag, Inc., New York.
- Bartzokis, G., Beckson, M., Newton, T., Mandelkern, M., Mintz, J., Foster, J. A., Ling, W. and Bridge, T. P. (1999) Selegiline effects on cocaine-induced changes in medial temporal lobe metabolism and subjective ratings of euphoria. *Neuropsychopharmacol*, **20**, 582-590.
- Bayley, H. and Knowles, J. R. (1977) Photoaffinity labeling. *Methods Enzymol*, **46**, 69-114.
- Bayley, H. and Knowles, J. R. (1978) Photogenerated Reagents for Membrane Labeling .1. Phenylnitrene Formed within Lipid Bilayer. *Biochem*, **17**, 2414-2419.
- Bayley, H., and J.V. Staros (1984), "Photoaffinity Labeling and Related Techniques", in *Azides and Nitrenes: Reactivity and Utility*, E.F.V. Scriven, Ed., New York: Academic Press, pp. 433-490.
- Bazeas, S. E. (1996) Affinity labels as probes for the study of the nucleotide binding site of enzymes. *Biol. Res.*, **29**, 21-30.
- Berger, P., Janowsky, A., Vocci, F., Skolnick, P., Schweri, M. M. and Paul, S. M. (1985) [3H]GBR-12935: a specific high affinity ligand for labeling the dopamine transport complex. *Eur J Pharmacol*, **107**, 289-290.

- Berger, S. P., Martenson, R. E., Laing, P., Thurkauf, A., Decosta, B., Rice, K. C. and Paul, S. M. (1991) Photoaffinity labeling of the dopamine reuptake carrier protein with 3-azido[3H]GBR-12935. *Mol Pharmacol*, **39**, 429-435.
- Beuming, T., Shi, L., Javitch, J. A. and Weinstein, H. (2006) A comprehensive structure-based alignment of prokaryotic and eukaryotic neurotransmitter/Na<sup>+</sup> symporters (NSS) aids in the use of the LeuT structure to probe NSS structure and function. *Mol Pharmacol*, **70**, 1630-1642.
- Boja, J. W., Patel, A., Carroll, F. I., Rahman, M. A., Philip, A., Lewin, A. H., Kopajtic, T. A. and Kuhar, M. J. (1991) [125I]RTI-55: a potent ligand for dopamine transporters. *Eur J Pharmacol*, **194**, 133-134.
- Boja, J. W., Rahman, M. A., Philip, A., Lewin, A. H., Carroll, F. I. and Kuhar, M. J. (1991) Isothiocyanate derivatives of cocaine: irreversible inhibition of ligand binding at the dopamine transporter. *Mol Pharmacol*, **39**, 339-345.
- Borden, W. T., Gritsan, N. P., Hadad, C. M., Karney, W. L., Kemnitz, C. R. and Platz, M. S. (2000) The interplay of theory and experiment in the study of phenylnitrene. *Acc Chem Res*, **33**, 765-771.
- Bouchet, M. J., Rendon, A., Wermuth, C. G., Goeldner, M. and Hirth, C. (1987) Aryl diazo compounds and diazonium salts as potential irreversible probes of the gamma-aminobutyric acid receptor. *J Med Chem*, **30**, 2222-2227.
- Boyd, N. D., White, C. F., Cerpa, R., Kaiser, E. T. and Leeman, S. E. (1991) Photoaffinity labeling the substance P receptor using a derivative of substance P containing p-benzoylphenylalanine. *Biochem*, **30**, 336-342.

- Brunner, J. (1993) New photolabeling and crosslinking methods. *Annu Rev Biochem*, **62**, 483-514.
- Brunner, J. and Richards, F. M. (1980) Analysis of Membranes Photolabeled with Lipid Analogs - Reaction of Phospholipids Containing a Disulfide Group and a Nitrene or Carbene Precursor with Lipids and with Gramicidin-A. *J Biol Chem*, **255**, 3319-3329.
- Brunner, J., Senn, H. and Richards, F. M. (1980) 3-Trifluoromethyl-3-phenyldiazirine. A new carbene generating group for photolabeling reagents. *J Biol Chem*, **255**, 3313-3318.
- Buck, K. J. and Amara, S. G. (1994) Chimeric dopamine-norepinephrine transporters delineate structural domains influencing selectivity for catecholamines and 1-methyl-4-phenylpyridinium. *Proc Natl Acad Sci U S A*, **91**, 12584-12588.
- Buck, K. J. and Amara, S. G. (1995) Structural domains of catecholamine transporter chimeras involved in selective inhibition by antidepressants and psychomotor stimulants. *Mol Pharmacol*, **48**, 1030-1037.
- Budyka, M. F., Kantor, M. M. and Alifimov, M. V. (1992) Photolysis of Phenyl Azide. *B Russ Acad Sci Ch+*, **41**, 590-591.
- Butzin, C. A., Scarpitti, F. B., Nielsen, A. L., Martin, S. S., Inciardi, J. A. (1999) Measuring the impact of drug treatment: Beyond relapse and recidivism. *Correct Manag Q*, **3**, 1-7.
- Byck, R. (1987) Cocaine Use and Research. In: *Cocaine: Clinical and Biobehavioral Aspects*, (S. Fisher, Raskin, A., and Uhlenhuth, E.H. ed.), pp. 3-20. Oxford University Press, Oxford.

- Cai, S. X., Glenn, D. J. and Keana, J. F. W. (1992) Toward the Development of Radiolabeled Fluorophenyl Azide-Based Photolabeling Reagents - Synthesis and Photolysis of Iodinated 4-Azidoperfluorobenzoates and 4-Azido-3,5,6-Trifluorobenzoates. *J Org Chem*, **57**, 1299-1304.
- Cao, J., Lever, J. R., Kopajtic, T., Katz, J. L., Pham, A. T., Holmes, M. L., Justice, J. B. and Newman, A. H. (2004) Novel azido and isothiocyanato analogues of [3-(4-phenylalkylpiperazin-1-yl)propyl]bis(4-fluorophenyl)amines as potential irreversible ligands for the dopamine transporter. *J Med Chem*, **47**, 6128-6136.
- Carroll, F. I., Howell, L. L. and Kuhar, M. J. (1999) Pharmacotherapies for treatment of cocaine abuse: preclinical aspects. *J Med Chem*, **42**, 2721-2736.
- Carroll, F. I., Lewin, A. H., Abraham, P., Parham, K., Boja, J. W. and Kuhar, M. J. (1991) Synthesis and ligand binding of cocaine isomers at the cocaine receptor. *J Med Chem*, **34**, 883-886.
- Carroll, K. M., Nich, C., Ball, S. A., McCance, E. and Rounsavile, B. J. (1998) Treatment of cocaine and alcohol dependence with psychotherapy and disulfiram. *Addiction*, **93**, 713-727.
- Carroll, S. E. N., B.; Scriven, E. F. V.; Suschitzky, H.; Thomas, D. R. (1977) Decomposition of Aromatic Azides in Ethanethiol. *Tetrahedron Lett*, **36**, 3175-3178.
- Carvelli, L., Moron, J. A., Kahlig, K. M. et al. (2002) PI 3-kinase regulation of dopamine uptake. *J Neurochem*, **81**, 859-869.

- Chait, L. D., Uhlenhuth, E. H. and Johanson, C. E. (1987) Reinforcing and subjective effects of several anorectics in normal human volunteers. *J Pharmacol Exp Ther*, **242**, 777-783.
- Chami, M., Steinfels, E., Orelle, C., Jault, J. M., Di Pietro, A., Rigaud, J. L. and Marco, S. (2002) Three-dimensional structure by cryo-electron microscopy of YvcC, an homodimeric ATP-binding cassette transporter from *Bacillus subtilis*. *J Mol Biol*, **315**, 1075-1085.
- Chan, H. L., Gaffney, P. R., Waterfield, M. D., Anderle, H., Peter Matthiessen, H., Schwarz, H. P., Turecek, P. L. and Timms, J. F. (2006) Proteomic analysis of UVC irradiation-induced damage of plasma proteins: Serum amyloid P component as a major target of photolysis. *FEBS Lett*, **580**, 3229-3236.
- Chang, G. and Roth, C. B. (2001) Structure of MsbA from *E. coli*: a homolog of the multidrug resistance ATP binding cassette (ABC) transporters. *Science*, **293**, 1793-1800.
- Chapman, O. L. L., J. P. (1978) 1-Aza-1,2,4,6-cycloheptatetraene. *J Am Chem Soc*, **100**, 282-285.
- Chen, N. and Reith, M. E. (2008) Substrates dissociate dopamine transporter oligomers. *J Neurochem*, **105**, 910-920.
- Chen, N., Trowbridge, C. G. and Justice, J. B., Jr. (1999) Cationic modulation of human dopamine transporter: dopamine uptake and inhibition of uptake. *J Pharmacol Exp Ther*, **290**, 940-949.

Chen, R., Wei, H., Hill, E. R., Chen, L., Jiang, L., Han, D. D. and Gu, H. H. (2007)

Direct evidence that two cysteines in the dopamine transporter form a disulfide bond. *Mol Cell Biochem*, **298**, 41-48.

Chiapperino, D., Anderson, G. B., Robbins, R. J. and Falvey, D. E. (1996)

Photochemically Generated Arylnitrenium Ions: Laser Flash Photolysis and Product Studies of the Photochemistry of N-tert-Butyl-3-methyl-6-chloroanthranilium Ions. *J Org Chem*, **61**, 3195-3199.

Church, W. H., Justice, J. B., Jr. and Byrd, L. D. (1987) Extracellular dopamine in rat striatum following uptake inhibition by cocaine, nomifensine and benztropine.

*Eur J Pharmacol*, **139**, 345-348.

Ciliax, B. J., Heilman, C., Demchyshyn, L. L., Pristupa, Z. B., Ince, E., Hersch, S. M.,

Niznik, H. B. and Levey, A. I. (1995) The dopamine transporter:

immunochemical characterization and localization in brain. *J Neurosci*, **15**, 1714-1723.

Clarke, R. L., Daum, S. J., Gambino, A. J., Aceto, M. D., Pearl, J., Levitt, M., Cumiskey, W. R. and Bogado, E. F. (1973) Compounds affecting the central nervous system.

4. 3 Beta-phenyltropane-2-carboxylic esters and analogs. *J Med Chem*, **16**, 1260-1267.

Cohen, K. A., Hopkins, J., Ingraham, R. H. et al. (1991) Characterization of the binding

site for nevirapine (BI-RG-587), a nonnucleoside inhibitor of human

immunodeficiency virus type-1 reverse transcriptase. *J Biol Chem*, **266**, 14670-14674.

- Cordonier, C. E., Satake, K., Atarashi, M., Kawamoto, Y., Okamoto, H. and Kimura, M. (2005) Reaction of 2-methoxy-3H-azepine with NBS: efficient synthesis of 2-substituted 2H-azepines. *J Org Chem*, **70**, 3425-3436.
- Coyle, J. T. and Snyder, S. H. (1969) Antiparkinsonian drugs: inhibition of dopamine uptake in the corpus striatum as a possible mechanism of action. *Science*, **166**, 899-901.
- Coyle, J. T. and Snyder, S. H. (1969) Catecholamine uptake by synaptosomes in homogenates of rat brain: stereospecificity in different areas. *J Pharmacol Exp Ther*, **170**, 221-231.
- Crews, P., Rodriguez, J., Jaspars, M. (1998) *Organic Structure Analysis: Topics in Organic Chemistry: A Series of Advanced Textbooks*. Oxford University Press, New York.
- Dahl, S. G., Sylte, I. and Ravna, A. W. (2004) Structures and models of transporter proteins. *J Pharmacol Exp Ther*, **309**, 853-860.
- Damaj, M. I., Slemmer, J. E., Carroll, F. I. and Martin, B. R. (1999) Pharmacological characterization of nicotine's interaction with cocaine and cocaine analogs. *J Pharmacol Exp Ther*, **289**, 1229-1236.
- Dayon, L., Roussel, C. and Girault, H. H. (2006) Probing cysteine reactivity in proteins by mass spectrometric EC-tagging. *J Proteome Res*, **5**, 793-800.
- Degraff, B. A., Gillespie, D. W. and Sundberg, R. J. (1974) Phenyl Nitrene - Flash Photolytic Investigation of Reaction with Secondary-Amines. *J Am Chem Soc*, **96**, 7491-7496.



- Denny, J. B. and Blobel, G. (1984) 125I-labeled crosslinking reagent that is hydrophilic, photoactivatable, and cleavable through an azo linkage. *Proc Natl Acad Sci U S A*, **81**, 5286-5290.
- Desai, R. I., Kopajtic, T. A., Koffarnus, M., Newman, A. H. and Katz, J. L. (2005) Identification of a dopamine transporter ligand that blocks the stimulant effects of cocaine. *J Neurosci*, **25**, 1889-1893.
- Di Chiara, G. and Imperato, A. (1988) Drugs abused by humans preferentially increase synaptic dopamine concentrations in the mesolimbic system of freely moving rats. *Proc Natl Acad Sci U S A*, **85**, 5274-5278.
- Di Simplicio, P., Franconi, F., Frosali, S. and Di Giuseppe, D. (2003) Thiolation and nitrosation of cysteines in biological fluids and cells. *Amino Acids*, **25**, 323-339.
- Doering, W. V. E. and Odum, R. A. (1966) Ring Enlargement in Photolysis of Phenyl Azide. *Tetrahedron*, **22**, 81-93.
- Dole, V. P., Nyswander, M.E. (1983) *The Neurobiology of Opiate Reward Processes*. Elsevier, Amsterdam.
- Dorman, G. and Prestwich, G. D. (1994) Benzophenone photophores in biochemistry. *Biochem*, **33**, 5661-5673.
- Dorman, G. and Prestwich, G. D. (2000) Using photolabile ligands in drug discovery and development. *Trends Biotechnol*, **18**, 64-77.
- Dunkin, I. R., Lynch, M. A., McAlpine, F. and Sweeney, D. (1997) A medium effect in the photolysis of phenyl azide in low-temperature matrices. *J Photoch Photobio A*, **102**, 207-212.

- Dutta, A. K., Fei, X. S., Vaughan, R. A., Gaffaney, J. D., Wang, N., Lever, J. R. and Reith, M. E. (2001) Design, synthesis, and characterization of a novel, 4-[2-(diphenylmethoxy)ethyl]-1-benzyl piperidine-based, dopamine transporter photoaffinity label. *Life Sci*, **68**, 1839-1849.
- Ebadi, M., Sharma, S., Shavali, S. and El Refaey, H. (2002) Neuroprotective actions of selegiline. *J Neurosci Res*, **67**, 285-289.
- Ehret-Sabatier, L., Kieffer, B. (1989). In: *Photochemical Probes in Biochem*, (P. E. Nielsen ed.), pp. 107-122. Kluwer Academic, Boston.
- Esposito, B. P. and Najjar, R. (2002) Interactions of antitumoral platinum-group metallodrugs with albumin. *Coordin Chem Rev*, **232**, 137-149.
- Farrell, M., Ward, J., Mattick, R., Hall, W., Stimson, G. V., des Jarlais, D., Gossop, M. and Strang, J. (1994) Methadone maintenance treatment in opiate dependence: a review. *BMJ*, **309**, 997-1001.
- Feldman, R. S., Quenzer, L. F. (1984) *Fundamentals of Neuropsychopharmacology*. Sinauer and Associates, Inc., Sunderland.
- Ferrer, J. V. and Javitch, J. A. (1998) Cocaine alters the accessibility of endogenous cysteines in putative extracellular and intracellular loops of the human dopamine transporter. *Proc Natl Acad Sci U S A*, **95**, 9238-9243.
- Fischer, F. and Poetsch, A. (2006) Protein cleavage strategies for an improved analysis of the membrane proteome. *Proteome Sci*, **4**, 2.
- Fisher, S., Raskin, A., and Uhlenhuth, E.H. (1987) Cocaine: Clinical and Biobehavioral Aspects. Oxford University Press, Oxford.

- Fleming, S. A. (1995) Chemical Reagents in Photoaffinity Labeling. *Tetrahedron*, **51**, 12479-12520.
- Garin, J., Boulay, F., Issartel, J. P., Lunardi, J. and Vignais, P. V. (1986) Identification of amino acid residues photolabeled with 2-azido[ $\alpha$ -<sup>32</sup>P]adenosine diphosphate in the beta subunit of beef heart mitochondrial F1-ATPase. *Biochem*, **25**, 4431-4437.
- Garner-O'Neale, L.D., Bonamy, A.F., Meek, T. L., and Patrick, B.G. (2003) Calculating group electronegativities using the revised Lewis-Langmuir equation. *Journal of Molecular Structure (Theochem)* **639**:151-156.
- Garrido, M. J. and Troconiz, I. F. (1999) Methadone: a review of its pharmacokinetic/pharmacodynamic properties. *J Pharmacol Toxicol Methods*, **42**, 61-66.
- Giros, B. and Caron, M. G. (1993) Molecular Characterization of the Dopamine Transporter. *Trends Pharmacol Sci*, **14**, 43-49.
- Giros, B., Jaber, M., Jones, S. R., Wightman, R. M. and Caron, M. G. (1996) Hyperlocomotion and indifference to cocaine and amphetamine in mice lacking the dopamine transporter. *Nature*, **379**, 606-612.
- Goeldner, M. P. and Hirth, C. G. (1980) Specific Photoaffinity-Labeling Induced by Energy-Transfer - Application to Irreversible Inhibition of Acetylcholinesterase. *P Natl Acad Sci-Biol*, **77**, 6439-6442.
- Goeldner, M. P., Hirth, C. G., Kieffer, B. and Ourisson, G. (1982) Photosuicide Inhibition - a Step Towards Specific Photoaffinity-Labeling. *Trends Biochem Sci*, **7**, 310-312.

- Goeldner, M. P., Hirth, C. G., Rossi, B., Ponzio, G. and Lazdunski, M. (1983) Specific Photoaffinity-Labeling of the Digitalis Binding-Site of the Sodium and Potassium-Ion Activated Adenosine-Triphosphatase Induced by Energy-Transfer. *Biochem*, **22**, 4685-4690.
- Gold, M. S. (1997) Cocaine (and Crack): Clinical Aspects (181-198). In: *Substance Abuse: A Comprehensive Textbook*, (Lowinson ed.), pp. 181-198. Williams & Wilkins, Baltimore.
- Goldman, D. W., Pober, J. S., White, J. and Bayley, H. (1979) Selective Labeling of the Hydrophobic Segments of Intrinsic Membrane-Proteins with a Lipophilic Photogenerated Carbene. *Nature*, **280**, 841-843.
- Gorelick, D. A., Gardner, E. L. and Zheng-Xiong, X. (2004) Agents in Development for the Management of Cocaine Abuse. *Drugs*, **64**, 1547-1573.
- Griffiths, R. R., Bigelow, G.E., Henningfield, J.E. (1980) Similarities in Animal and Human Drug-taking Behavior. In: *Advances in Substances Abuse*, (N. K. Mello ed.), Vol. 1, pp. 1-90. JAI Press, Inc., Greenwich.
- Grigoriadis, D. E., Wilson, A. A., Lew, R., Sharkey, J. S. and Kuhar, M. J. (1989) Dopamine transport sites selectively labeled by a novel photoaffinity probe: 125I-DEEP. *J Neurosci*, **9**, 2664-2670.
- Gritsan, N. P. and Platz, M. S. (2006) Kinetics, spectroscopy, and computational chemistry of arylnitrenes. *Chem Rev*, **106**, 3844-3867.
- Gritsan, N. P. and Pritchina, E. A. (1992) The Mechanism of Photolysis of Aromatic Azides. *Usp Khim*, **61**, 910-939.

- Gritsan, N. P. and Pritchina, E. S. (1989) Mechanism of Photochemical-Transformations of Aromatic Azides. *J Inform Rec Mater*, **17**, 391-404.
- Haberny, K. A., Walsh, S. L., Ginn, D. H., Wilkins, J. N., Garner, J. E., Setoda, D. and Bigelow, G. E. (1995) Absence of acute cocaine interactions with the MAO-B inhibitor selegiline. *Drug Alcohol Depend*, **39**, 55-62.
- Handlon, A. L. and Oppenheimer, N. J. (1988) Thiol reduction of 3'-azidothymidine to 3'-aminothymidine: kinetics and biomedical implications. *Pharm Res*, **5**, 297-299.
- Hanstein, W. G., Hatefi, Y. and Kiefer, H. (1979) Radiochemical synthesis and photochemical properties of the uncoupler 2-azido-4-nitrophenol, a versatile photoaffinity labeling reagent. *Biochem*, **18**, 1019-1025.
- Harvey, J. A., Kosofsky, B. (1998) Cocaine: Effects on the Developing Brain. Vol. 846. Annals of the New York Academy of Sciences.
- Hastrup, H., Karlin, A. and Javitch, J. A. (2001) Symmetrical dimer of the human dopamine transporter revealed by cross-linking Cys-306 at the extracellular end of the sixth transmembrane segment. *Proc Natl Acad Sci U S A*, **98**, 10055-10060.
- Herman, B. H., Elkashef, A., and Vocci, F. (2005) Agents in the development for the management of cocaine abuse. *Drugs*, **64**, 1547-1573.
- Hersch, S. M., Yi, H., Heilman, C. J., Edwards, R. H. and Levey, A. I. (1997) Subcellular localization and molecular topology of the dopamine transporter in the striatum and substantia nigra. *J Comp Neurol*, **388**, 211-227.
- Hollemans, M., Runswick, M. J., Fearnley, I. M. and Walker, J. E. (1983) The sites of labeling of the beta-subunit of bovine mitochondrial F1-ATPase with 8-azido-ATP. *J Biol Chem*, **258**, 9307-9313.

- Hubbard, J. W., Srinivas, N. R., Quinn, D. and Midha, K. K. (1989) Enantioselective aspects of the disposition of dl-threo-methylphenidate after the administration of a sustained-release formulation to children with attention deficit-hyperactivity disorder. *J Pharm Sci*, **78**, 944-947.
- Huff, R. A., Vaughan, R. A., Kuhar, M. J. and Uhl, G. R. (1997) Phorbol esters increase dopamine transporter phosphorylation and decrease transport Vmax. *J Neurochem*, **68**, 225-232.
- Hughes, J. C. and Cook, C. C. (1997) The efficacy of disulfiram: a review of outcome studies. *Addiction*, **92**, 381-395.
- Hurd, Y. L. and Ungerstedt, U. (1989) Cocaine: an in vivo microdialysis evaluation of its acute action on dopamine transmission in rat striatum. *Synapse*, **3**, 48-54.
- Hyttel, J. (1982) Citalopram--pharmacological profile of a specific serotonin uptake inhibitor with antidepressant activity. *Prog Neuropsychopharmacol Biol Psychiatry*, **6**, 277-295.
- Indarte, M., Madura, J. D. and Surratt, C. K. (2008) Dopamine transporter comparative molecular modeling and binding site prediction using the LeuT(Aa) leucine transporter as a template. *Proteins*, **70**, 1033-1046.
- Janowsky, A., Schveri, M. M., Berger, P., Long, R., Skolnick, P. and Paul, S. M. (1985) The effects of surgical and chemical lesions on striatal [3H]threo-(+/-)-methylphenidate binding: correlation with [3H]dopamine uptake. *Eur J Pharmacol*, **108**, 187-191.
- Janowsky, A., Vocci, F., Berger, P., Angel, I., Zelnik, N., Kleinman, J. E., Skolnick, P. and Paul, S. M. (1987) [3H]GBR-12935 binding to the dopamine transporter is

- decreased in the caudate nucleus in Parkinson's disease. *J Neurochem*, **49**, 617-621.
- Javitch, J. A. (1998) Probing structure of neurotransmitter transporters by substituted-cysteine accessibility method. *Methods Enzymol*, **296**, 331-346.
- Javitch, J. A., Li, X., Kaback, J. and Karlin, A. (1994) A cysteine residue in the third membrane-spanning segment of the human D2 dopamine receptor is exposed in the binding-site crevice. *Proc Natl Acad Sci U S A*, **91**, 10355-10359.
- Ji, T. H. (1979) The application of chemical crosslinking for studies on cell membranes and the identification of surface reporters. *Biochim Biophys Acta*, **559**, 39-69.
- Jin, C., Navarro, H. A., Page, K. and Carroll, F. I. (2008) Synthesis and monoamine transporter binding properties of 2beta-[3'-(substituted benzyl)isoxazol-5-yl]- and 2beta-[3'-methyl-4'-(substituted phenyl)isoxazol-5-yl]-3beta-(substituted phenyl)tropanes. *Bioorg Med Chem*.
- Johanson, C. E., Fischman, M.W. (1989) The Pharmacology of Cocaine Related to Its Abuse. *Pharmacol Rev*, **41**, 3-52.
- Kaback, H. R., Dunten, R., Frillingos, S., Venkatesan, P., Kwaw, I., Zhang, W. and Ermolova, N. (2007) Site-directed alkylation and the alternating access model for LacY. *Proc Natl Acad Sci U S A*, **104**, 491-494.
- Kalivas, P. W. a. V., N.D. (2007) The Neural Basis of Addiction: A Pathology of Motivation and Choice. *Focus*, **5**, 208-219.
- Katz, J. L., Kopajtic, T. A., Agoston, G. E. and Newman, A. H. (2004) Effects of N-substituted analogs of benztropine: diminished cocaine-like effects in dopamine transporter ligands. *J Pharmacol Exp Ther*, **309**, 650-660.

- Katz, J. L., Libby, T. A., Kopajtic, T., Husbands, S. M. and Newman, A. H. (2003) Behavioral effects of rimcazole analogues alone and in combination with cocaine. *Eur J Pharmacol*, **468**, 109-119.
- Kawahara, K., Kuniyasu, A., Masuda, K., Ishiguro, M. and Nakayama, H. (2002) Efficient identification of photolabelled amino acid residues by combining immunoaffinity purification with MS: revealing the semotiadil-binding site and its relevance to binding sites for myristates in domain III of human serum albumin. *Biochem J*, **363**, 223-232.
- Kauer, J. C., Ericksonviitanen, S., Wolfe, H. R. and Degrado, W. F. (1986) Para-Benzoyl-L-Phenylalanine, a New Photoreactive Amino-Acid - Photolabeling of Calmodulin with a Synthetic Calmodulin-Binding Peptide. *J Biol Chem*, **261**, 695-700.
- Keana, J. F. W. and Cai, S. X. (1989) Functionalized Perfluorophenyl Azides - New Reagents for Photoaffinity-Labeling. *J Fluorine Chem*, **43**, 151-154.
- Keil, B. (1992) *Specificity of Proteolysis*. Springer-Verlag, New York.
- Kiefer, H., Lindstrom, J., Lennox, E. S. and Singer, S. J. (1970) Photo-affinity labeling of specific acetylcholine-binding sites on membranes. *Proc Natl Acad Sci U S A*, **67**, 1688-1694.
- Kieffer, B. L., Goeldner, M. P. and Hirth, C. G. (1981) Aryldiazonium Salts as Photo-Affinity Labeling Reagents for Proteins. *J Chem Soc Chem Commun*, 398-399.
- Kilty, J. E., Lorang, D. and Amara, S. G. (1991) Cloning and expression of a cocaine-sensitive rat dopamine transporter. *Science*, **254**, 578-579.



- Kim, E., Phillips, M., Hegyi, G., Muhlrads, A. and Reisler, E. (1998) Intrastrand cross-linked actin between Gln-41 and Cys-374. II. Properties of cross-linked oligomers. *Biochem*, **37**, 17793-17800.
- Kitayama, S., Dohi, T. and Uhl, G. R. (1994) Phorbol esters alter functions of the expressed dopamine transporter. *Eur J Pharmacol*, **268**, 115-119.
- Kitayama, S., Shimada, S., Xu, H., Markham, L., Donovan, D. M. and Uhl, G. R. (1992) Dopamine transporter site-directed mutations differentially alter substrate transport and cocaine binding. *Proc Natl Acad Sci U S A*, **89**, 7782-7785.
- Kline, R. H., Izenwasser, S., Katz, J. L., Joseph, D. B., Bowen, W. D. and Newman, A. H. (1997) 3'-Chloro-3 alpha-(diphenylmethoxy)tropane but not 4'-chloro-3 alpha-(diphenylmethoxy)tropane produces a cocaine-like behavioral profile. *J Med Chem*, **40**, 851-857.
- Koller-Becker, H. (1962) Carl Koller and cocaine. *Psychoanal. Q.*, **32**, 309-373.
- Kolpashchikov, D. M. (2003) Superselective labelling of proteins: Approaches and techniques. *J Biomol Struct Dyn*, **21**, 55-64.
- Koob, G. F. (2000) Neurobiology of addiction - Toward the development of new therapies. *Ann Ny Acad Sci*, **909**, 170-185.
- Koob, G. F. and Bloom, F. E. (1988) Cellular and Molecular Mechanisms of Drug-Dependence. *Science*, **242**, 715-723.
- Kotzyba-Hibert, F., Kapfir, I., and Goeldnek, M. (1995) Recent Trends in Photoaffinity Labeling. *Angew Chem Int Ed Eng*, **34**, 1296-1312.

- Kotzyba-Hibert, F., Lagenbuch-Cachat, J., Jaganathen, J., Goeldner, M. and Hirth, C. (1985) Aryldiazonium salts as photoaffinity labels of the nicotinic acetylcholine receptor PCP binding site. *FEBS Lett*, **182**, 297-301.
- Kreek, M. J., Bart, G., Lilly, C., Laforge, K. S. and Nielsen, D. A. (2005) Pharmacogenetics and human molecular genetics of opiate and cocaine addictions and their treatments. *Pharmacol Rev*, **57**, 1-26.
- Kubota, Y., Satake, K., Ikui, R., Okamoto, H., Kimura, M. (2003) Nucleophilic Reactions of 5-*tert*-Butyl-2-methoxy-3*H*-azepine with Alkoxides and Alkylolithium Reagents. *Bull Chem Soc Jpn*, **76**, 805-811.
- Kulkarni, S. S., Newman, A. H. and Houlihan, W. J. (2002) Three-dimensional quantitative structure-activity relationships of mazindol analogues at the dopamine transporter. *J Med Chem*, **45**, 4119-4127.
- Laemmli, U. K. (1970) Cleavage of structural proteins during the assembly of the head of bacteriophage T4. *Nature*, **227**, 680-685.
- Langenbuchcachat, J., Bon, C., Mulle, C., Goeldner, M., Hirth, C. and Changeux, J. P. (1988) Photoaffinity-Labeling of the Acetylcholine Binding-Sites on the Nicotinic Receptor by an Aryldiazonium Derivative. *Biochem*, **27**, 2337-2345.
- Lever, J. R., Zou, M. F., Parnas, M. L., Duval, R. A., Wirtz, S. E., Justice, J. B., Vaughan, R. A. and Newman, A. H. (2005) Radioiodinated azide and isothiocyanate derivatives of cocaine for irreversible labeling of dopamine transporters: synthesis and covalent binding studies. *Bioconjug Chem*, **16**, 644-649.

- Lew, R., Grigoriadis, D., Wilson, A., Boja, J. W., Simantov, R. and Kuhar, M. J. (1991) Dopamine transporter: deglycosylation with exo- and endoglycosidases. *Brain Res*, **539**, 239-246.
- Lew, R., Vaughan, R., Simantov, R., Wilson, A. and Kuhar, M. J. (1991) Dopamine transporters in the nucleus accumbens and the striatum have different apparent molecular weights. *Synapse*, **8**, 152-153.
- Leyva, E., Platz, M.S., Persy, G, Wirz, J. (1986) Photochemistry of Phenyl Azide: The Role of Singlet and Triplet Phenylnitrene as Transient Intermediates. *J Am Chem Soc*, **108**, 3783-3790.
- Leyva, E., Chang, D. H. S., Platz, M. S., Watt, D. S., Crocker, P. J. and Kawada, K. (1991) The Photochemistry of Iodo, Methyl and Thiomethyl Substituted Aryl Azides in Toluene Solution and Frozen Polycrystals. *Photochem Photobiol*, **54**, 329-333.
- Leyva, E., Munoz, D. and Platz, M. S. (1989) Photochemistry of Fluorinated Aryl Azides in Toluene Solution and in Frozen Polycrystals. *J Org Chem*, **54**, 5938-5945.
- Li, Y. Z., Kirby, J., George, M., Poliakoff, M. and Schuster, G. B. (1988) Photochemistry of Aryl Azides - Formation and Reactivity of Dehydroazepines. *Abstr Pap Am Chem S*, **196**, 322-ORGN.
- Li, Y. Z., Kirby, J. P., George, M. W., Poliakoff, M. and Schuster, G. B. (1988) 1,2-Didehydroazepines from the Photolysis of Substituted Aryl Azides - Analysis of Their Chemical and Physical-Properties by Time-Resolved Spectroscopic Methods. *J Am Chem Soc*, **110**, 8092-8098.

- Liapakis, G., Simpson, M. M. and Javitch, J. A. (2001) The substituted-cysteine accessibility method (SCAM) to elucidate membrane protein structure. *Curr Protoc Neurosci*, **Chapter 4**, Unit 4 15.
- Lide, D.R. Ed., CRC Handbook of Chemistry and Physics; CRC Press, Inc., Boca Raton, FL, 1995.
- Loland, C. J., Norgaard-Nielsen, K. and Gether, U. (2003) Probing dopamine transporter structure and function by Zn<sup>2+</sup>-site engineering. *Eur J Pharmacol*, **479**, 187-197.
- Long, S. B., Campbell, E. B. and Mackinnon, R. (2005) Voltage sensor of Kv1.2: structural basis of electromechanical coupling. *Science*, **309**, 903-908.
- Lowinson, J. H., Ruiz, P. and Millman, R. B. (1992) *Substance abuse: a comprehensive textbook*. Williams & Wilkins, Baltimore.
- Lutolf, M. P., Tirelli, N., Cerritelli, S., Cavalli, L. and Hubbell, J. A. (2001) Systematic modulation of Michael-type reactivity of thiols through the use of charged amino acids. *Bioconjugate Chem*, **12**, 1051-1056.
- Lwowski, W. (1970) *Nitrenes: Reactive intermediates in organic chemistry*. Interscience Publishers, New York.
- Madras, B. K., Spealman, R. D., Fahey, M. A., Neumeyer, J. L., Saha, J. K. and Milius, R. A. (1989) Cocaine receptors labeled by [3H]2 beta-carbomethoxy-3 beta-(4-fluorophenyl)tropane. *Mol Pharmacol*, **36**, 518-524.
- Maisonneuve, I. M., Keller, R. W. and Glick, S. D. (1990) Similar effects of D-amphetamine and cocaine on extracellular dopamine levels in medial prefrontal cortex of rats. *Brain Res*, **535**, 221-226.

- Maloteaux, J. M., Vanisberg, M. A., Laterre, C., Javoy-Agid, F., Agid, Y. and Laduron, P. M. (1988) [3H]GBR 12935 binding to dopamine uptake sites: subcellular localization and reduction in Parkinson's disease and progressive supranuclear palsy. *Eur J Pharmacol*, **156**, 331-340.
- Marcinek, A., Leyva, E., Whitt, D. and Platz, M. S. (1993) Evidence for Stepwise Nitrogen Extrusion and Ring Expansion Upon Photolysis of Phenyl Azide. *J Am Chem Soc*, **115**, 8609-8612.
- Marcusson, J. and Eriksson, K. (1988) [3H]GBR-12935 binding to dopamine uptake sites in the human brain. *Brain Res*, **457**, 122-129.
- Matsumoto, R. R., Hewett, K. L., Pouw, B., Bowen, W. D., Husbands, S. M., Cao, J. J. and Hauck Newman, A. (2001) Rimcazole analogs attenuate the convulsive effects of cocaine: correlation with binding to sigma receptors rather than dopamine transporters. *Neuropharmacol*, **41**, 878-886.
- Mayer, A. N. and Barany, F. (1995) Photoaffinity cross-linking of TaqI restriction endonuclease using an aryl azide linked to the phosphate backbone. *Gene*, **153**, 1-8.
- McCance-Katz, E. F., Kosten, T. R. and Jatlow, P. (1998) Disulfiram effects on acute cocaine administration. *Drug Alcohol Depend*, **52**, 27-39.
- McClelland, R. A., Kahley, M.J., Davidse, P.A., and Hadzialic, G. (1996) Acid-Base Properties of Arylnitrenium Ions. *J Am Chem Soc*, **118**, 4794-4803.
- McClelland, R. A. and Postigo, A. (2006) Solvent effects on the reactivity of fluorenyl nitrenium ion with DNA-like probes. *Biophys Chem*, **119**, 213-218.

- McIntosh, D. B., Woolley, D. G. and Berman, M. C. (1992) 2',3'-O-(2,4,6-trinitrophenyl)-8-azido-AMP and -ATP photolabel Lys-492 at the active site of sarcoplasmic reticulum Ca(2+)-ATPase. *J Biol Chem*, **267**, 5301-5309.
- McNicoll, N., Escher, E., Wilkes, B. C., Schiller, P. W., Ong, H. and De Lean, A. (1992) Highly efficient photoaffinity labeling of the hormone binding domain of atrial natriuretic factor receptor. *Biochem*, **31**, 4487-4493.
- Mcnicoll, N., Escher, E., Wilkes, B. C., Schiller, P. W., Ong, H. and Delean, A. (1992) Highly Efficient Photoaffinity-Labeling of the Hormone Binding Domain of Atrial-Natriuretic-Factor Receptor. *Biochem*, **31**, 4487-4493.
- Meijer, E. W., Nijhuis, S. and Vanvroomhoven, F. C. B. M. (1988) Poly-1,2-Azepines by the Photopolymerization of Phenyl Azides - Precursors for Conducting Polymer-Films. *J Am Chem Soc*, **110**, 7209-7210.
- Miller, G. M., Yatin, S. M., De La Garza, R., 2nd, Goulet, M. and Madras, B. K. (2001) Cloning of dopamine, norepinephrine and serotonin transporters from monkey brain: relevance to cocaine sensitivity. *Brain Res Mol Brain Res*, **87**, 124-143.
- Miller, W. T. and Kaiser, E. T. (1988) Probing the Peptide Binding-Site of the Camp-Dependent Protein-Kinase by Using a Peptide-Based Photoaffinity Label. *Proc Natl Acad Sci USA*, **85**, 5429-5433.
- Mimura, C. S., Admon, A., Hurt, K. A. and Ames, G. F. (1990) The nucleotide-binding site of HisP, a membrane protein of the histidine permease. Identification of amino acid residues photoaffinity labeled by 8-azido-ATP. *J Biol Chem*, **265**, 19535-19542.

- Mindell, J. A., Maduke, M., Miller, C. and Grigorieff, N. (2001) Projection structure of a Cl<sup>-</sup>-type chloride channel at 6.5 Å resolution. *Nature*, **409**, 219-223.
- Morawietz, J. and Sander, W. (1996) Photochemistry of Fluorinated Phenyl Nitrenes: Matrix Isolation of Fluorinated Azirines. *J Org Chem*, **61**, 4351-4354.
- Moron, J. A., Zakharova, I., Ferrer, J. V. et al. (2003) Mitogen-activated protein kinase regulates dopamine transporter surface expression and dopamine transport capacity. *J Neurosci*, **23**, 8480-8488.
- Nagendra, S. N., Faiman, M. D., Davis, K., Wu, J. Y., Newby, X. and Schloss, J. V. (1997) Carbamoylation of brain glutamate receptors by a disulfiram metabolite. *J Biol Chem*, **272**, 24247-24251.
- Nestler, E. J. (2005) Is there a common molecular pathway for addiction? *Nat Neurosci*, **8**, 1445-1449.
- Newman, A. H., Allen, A. C., Izenwasser, S. and Katz, J. L. (1994) Novel 3 alpha-(diphenylmethoxy)tropane analogs: potent dopamine uptake inhibitors without cocaine-like behavioral profiles. *J Med Chem*, **37**, 2258-2261.
- Newman, A. H. and Kulkarni, S. (2002) Probes for the dopamine transporter: new leads toward a cocaine-abuse therapeutic--A focus on analogues of benztropine and rimcazole. *Med Res Rev*, **22**, 429-464.
- NIDA (1997) Epidemiologic Trends in Drug Abuse. In: *Highlights and Executive Summary of the Community Epidemiology Work Group*, Vol. 1 Pub. No. 98-4207. Supt. of Docs., Washington, D.C.
- NIDA (1998) Crack and Cocaine. In: *NIDA InfoFacts*.

- NIDA (2003) National Institute on Drug Abuse. Epidemiologic Trends. In: *Drug Abuse: Advance Report*. Community Epidemiology Work Group, NIH Pub No: 03-5363A, Washington, D.C.
- NIDA (2003) National Survey Results on Drug Use From the Monitoring the Future Survey.
- NIDA (2004) Cocaine Abuse and Addiction. In: *NIDA Research Report*. NIH, Bethesda.
- Nielsen, J. A., Chapin, D. S. and Moore, K. E. (1983) Differential effects of d-amphetamine, beta-phenylethylamine, cocaine and methylphenidate on the rate of dopamine synthesis in terminals of nigrostriatal and mesolimbic neurons and on the efflux of dopamine metabolites into cerebroventricular perfusates of rats. *Life Sci*, **33**, 1899-1907.
- Nirenberg, M. J., Chan, J., Liu, Y., Edwards, R. H. and Pickel, V. M. (1997) Vesicular monoamine transporter-2: immunogold localization in striatal axons and terminals. *Synapse*, **26**, 194-198.
- Nirenberg, M. J., Chan, J., Pohorille, A., Vaughan, R. A., Uhl, G. R., Kuhar, M. J. and Pickel, V. M. (1997) The dopamine transporter: comparative ultrastructure of dopaminergic axons in limbic and motor compartments of the nucleus accumbens. *J Neurosci*, **17**, 6899-6907.
- Nirenberg, M. J., Vaughan, R. A., Uhl, G. R., Kuhar, M. J. and Pickel, V. M. (1996) The dopamine transporter is localized to dendritic and axonal plasma membranes of nigrostriatal dopaminergic neurons. *J Neurosci*, **16**, 436-447.



- Norregaard, L., Frederiksen, D., Nielsen, E. O. and Gether, U. (1998) Delineation of an endogenous zinc-binding site in the human dopamine transporter. *EMBO J*, **17**, 4266-4273.
- Noskov, V. G., Kalinina, I.L.N., Noskova, M. N., Kruglyak, Y. L., Bezrukov, A.P., Strukov, I.O.G., Kurochkin, V.K. (1997) Dibenz [b,e] azepines. Part 3. Acid hydrolysis. . *Pharmaceutical Research*, **31**, 619-620.
- Noskov, V. G., Kalinina, L.N., Noskova, M.N.,Kruglyak, Y.L., Strukov, O.G., and Kurochkin, V.K. (1998) 11H-Dibenz[b,e]azepines. Part 4. Protonated and N-alkylated compounds of Dibenz[b,f]-1,4-ox(this)azepine. *Pharmaceutical Chemistry Journal*, **32**, 38-40.
- Odum, R., Schmall, B. (1997) Photoisomerization of 3H-Azepines. *Journal of Chemical Research*, **S**, 276-277.
- Olsen, J. V., Ong, S. E. and Mann, M. (2004) Trypsin cleaves exclusively C-terminal to arginine and lysine residues. *Mol Cell Proteomics*, **3**, 608-614.
- ONDCP (1998) *The National Drug Control Strategy: A Ten Year Plan*.
- ONDCP (2003) Office of National Drug Control Policy Cocaine Fact Sheet.
- O'Neil, K. T., Erickson-Viitanen, S. and DeGrado, W. F. (1989) Photolabeling of calmodulin with basic, amphiphilic alpha-helical peptides containing p-benzoylphenylalanine. *J Biol Chem*, **264**, 14571-14578.
- Ong, S. Y., Chan, P. Y., Zhu, P. Z., Leung, K. H. and Phillips, D. L. (2003) Time-resolved resonance Raman study of triplet aryl nitrenes and their dimerization reaction. *J Phys Chem A*, **107**, 3858-3865.

- Pan, D., Gatley, S. J., Dewey, S. L., Chen, R., Alexoff, D. A., Ding, Y. S. and Fowler, J. S. (1994) Binding of bromine-substituted analogs of methylphenidate to monoamine transporters. *Eur J Pharmacol*, **264**, 177-182.
- Pandurangi, R. S., Katti, K. V., Barnes, C. L., Volkert, W. A. and Kuntz, R. R. (1994) High Yields of Nitrene Insertion into Unactivated C-H Bonds - First-Example of X-Ray Crystallographic and F-19 Nmr Analysis of the Photochemically Produced C-H Inserted Adduct. *J Chem Soc Chem Commun*, 1841-1842.
- Pani, L., Kuzmin, A., Diana, M., De Montis, G., Gessa, G. L. and Rossetti, Z. L. (1990) Calcium receptor antagonists modify cocaine effects in the central nervous system differently. *Eur J Pharmacol*, **190**, 217-221.
- Parnas, M. L., Gaffaney, J. D., Zou, M. F., Lever, J. R., Newman, A. H. and Vaughan, R. A. (2008) Labeling of dopamine transporter transmembrane domain 1 with the tropane ligand N-[4-(4-azido-3-[125I]iodophenyl)butyl]-2beta-carbomethoxy-3beta-(4-chloro phenyl)tropane implicates proximity of cocaine and substrate active sites. *Mol Pharmacol*, **73**, 1141-1150.
- Patai, S. (1971) *The chemistry of the azido group*. Interscience Publishers, London, New York.
- Pathak, M. M., Yarov-Yarovoy, V., Agarwal, G., Roux, B., Barth, P., Kohout, S., Tombola, F. and Isacoff, E. Y. (2007) Closing in on the resting state of the Shaker K(+) channel. *Neuron*, **56**, 124-140.
- Platz, M. S. (1995) Comparison of phenylcarbene and phenylnitrene. *Accounts Chem Res*, **28**, 487-492.

- Poe, R., Schnapp, K., Young, M. J. T., Grayzar, J. and Platz, M. S. (1992) Chemistry and Kinetics of Singlet (Pentafluorophenyl)Nitrene. *J Am Chem Soc*, **114**, 5054-5067.
- Prestwich, G. D., Dorman, G., Elliott, J. T., Marecak, D. M. and Chaudhary, A. (1997) Benzophenone photoprobes for phosphoinositides, peptides and drugs. *Photochem Photobiol*, **65**, 222-234.
- Qian, Y., Melikian, H. E., Rye, D. B., Levey, A. I. and Blakely, R. D. (1995) Identification and characterization of antidepressant-sensitive serotonin transporter proteins using site-specific antibodies. *J Neurosci*, **15**, 1261-1274.
- Ravna, A. W., Sylte, I. and Dahl, S. G. (2003) Molecular model of the neural dopamine transporter. *J Comput Aided Mol Des*, **17**, 367-382.
- Reed, B. (2001) Photoaffinity Labeling and Peptide Mapping of the Human Dopamine Transporter (Doctoral dissertation, Emory University, 2001). *Dissertation Abstracts International*, **62**(11), 5103.
- Reid, A. A., Monn, J. A., Jacobson, A. E., Rice, K. C. and Rothman, R. B. (1989) Characterization of NMDA-coupled and dopamine reuptake carrier coupled [3H]-TCP binding sites in guinea pig brain. *NIDA Res Monogr*, **95**, 530-531.
- Reith, M. E., Zimanyi, I. and O'Reilly, C. A. (1989) Role of ions and membrane potential in uptake of serotonin into plasma membrane vesicles from mouse brain. *Biochem Pharmacol*, **38**, 2091-2097.
- Ren, X. Q., Furukawa, T., Aoki, S., Sumizawa, T., Haraguchi, M., Nakajima, Y., Ikeda, R., Kobayashi, M. and Akiyama, S. (2002) A positively charged amino acid proximal to the C-terminus of TM17 of MRP1 is indispensable for GSH-

- dependent binding of substrates and for transport of LTC<sub>4</sub>. *Biochem*, **41**, 14132-14140.
- Riordan, H. J., Flashman, L. A., Saykin, A. J., Frutiger, S. A., Carroll, K. E. and Huey, L. (1999) Neuropsychological correlates of methylphenidate treatment in adult ADHD with and without depression. *Arch Clin Neuropsychol*, **14**, 217-233.
- Ritz, M. C., Lamb, R. J., Goldberg, S. R. and Kuhar, M. J. (1987) Cocaine receptors on dopamine transporters are related to self-administration of cocaine. *Science*, **237**, 1219-1223.
- Rizk, M. S., Shi, X. and Platz, M. S. (2006) Lifetimes and reactivities of some 1,2-didehydroazepines commonly used in photoaffinity labeling experiments in aqueous solutions. *Biochem*, **45**, 543-551.
- Sallee, F. R., Fogel, E. L., Schwartz, E., Choi, S. M., Curran, D. P. and Niznik, H. B. (1989) Photoaffinity labeling of the mammalian dopamine transporter. *FEBS Lett*, **256**, 219-224.
- SAMHSA (2002) Substance Abuse and Mental Health Services Administration. National Survey on Drug Use and Health.
- Satake, K., Saitoh, H., Kimura, M., and Morosawa, S. (1988) An Alternative Synthetic Route to 3H-Azepines: Thermal Isomerization of 2, 4- and 3,5-Di-t-butyl-3a,5a-dihydro-3H-cyclobuta[b]pyrroles. *J Chem Soc Chem Commun*, 1121-1123.
- Satake, K., Okuda, R., Hashimoto, M., Fujiwara, Y., Watadani, I., Okamoto, H., Kimura, M., and Morosawa, S. (1991) Synthesis and Characterization of 2H-, 3H- and 4H-Azepine: The First Observation of the Thermal Distribution Equilibrium of Azepines. *J Chem Soc Chem Commun*, 1154-1156.

- Satake, K., Kubota, Y., Cordonier, C., Okamoto, H., and Kimura, M. (2004) Synthesis of a Delocalized Azepinium Ion and Investigation of Its Electrophilic Character. *Angew Chem*, **116**, 754-756.
- Sawaki, Y., Kshikawa, S., Iwamura, H. (1987) Reactivity of Nitroso Oxides. Oxygen Transfer as an Electrophilic Peroxy Radical. *J Am Chem Soc*, **109**, 584.
- Schaich, K. M. (1980) Free radical initiation in proteins and amino acids by ionizing and ultraviolet radiations and lipid oxidation--Part 22: ultraviolet radiation and photolysis. *Crit Rev Food Sci Nutr*, **13**, 131-159.
- Schnapp, K. A. and Platz, M. S. (1993) A laser flash photolysis study of di-, tri- and tetrafluorinated phenylnitrenes; implications for photoaffinity labeling. *Bioconjug Chem*, **4**, 178-183.
- Schnapp, K. A., Poe, R., Leyva, E., Soundararajan, N. and Platz, M. S. (1993) Exploratory photochemistry of fluorinated aryl azides. Implications for the design of photoaffinity labeling reagents. *Bioconjug Chem*, **4**, 172-177.
- Scholze, P., Norregaard, L., Singer, E. A., Freissmuth, M., Gether, U. and Sitte, H. H. (2002) The role of zinc ions in reverse transport mediated by monoamine transporters. *J Biol Chem*, **277**, 21505-21513.
- Schrock, A. K. and Schuster, G. B. (1984) Photochemistry of Phenyl Azide - Chemical-Properties of the Transient Intermediates. *J Am Chem Soc*, **106**, 5228-5234.
- Schultes, R. E. (1987) Coca and Other Psychoactive Plants: Magico-Religious Roles in Primitive Societies of the New World In: *Cocaine: Clinical and Biobehavioral Aspects*, (S. Fisher, Raskin, A., and Uhlenhuth, E.H. ed.), pp. 212-249. Oxford University Press, Oxford.

- Schuster, G. B., Platz, M.S. (1992) Photochemistry of Phenyl Azide. In: *Advances in Photochemistry*, (D. Volman, Hammond, G., Neckers, D. ed.), Vol. 17, pp. 69-143. John Wiley and Sons, New York.
- Schwartz, M. A. (1989) Studying the Cytoskeleton by Label Transfer Crosslinking: Uses and Limitations. In: *Photochemical Probes in Biochem*, (P. E. Nielsen ed.), pp. 157-168. Kluwer Academic Publishers.
- Seigneuret, M. and Garnier-Suillerot, A. (2003) A structural model for the open conformation of the mdr1 P-glycoprotein based on the MsbA crystal structure. *J Biol Chem*, **278**, 30115-30124.
- Sen, N., Shi, L., Beuming, T., Weinstein, H. and Javitch, J. A. (2005) A pincer-like configuration of TM2 in the human dopamine transporter is responsible for indirect effects on cocaine binding. *Neuropharmacol*, **49**, 780-790.
- Shaked, Z., Szajewski, R. P. and Whitesides, G. M. (1980) Rates of Thiol-Disulfide Interchange Reactions Involving Proteins and Kinetic Measurements of Thiol Pka Values. *Biochem*, **19**, 4156-4166.
- Shi, L. and Javitch, J. A. (2002) The binding site of aminergic G protein-coupled receptors: the transmembrane segments and second extracellular loop. *Annu Rev Pharmacol Toxicol*, **42**, 437-467.
- Shields, C. J., Chrisope, D.R., Schuster, G.B., Dixon, A.J., Poliakoff, M., and Turner, J.J. (1987) Photochemistry of Aryl Azides: Detection and Characterization of a Dehydroazepine by Time-Resolved Infrared Spectroscopy and Flash Photolysis at Room Temperature. *J Am Chem Soc*, **109**, 4723-4726.

- Shields, C. J., Falvey, D. E., Schuster, G. B., Buchardt, O. and Nielsen, P. E. (1988) Competitive Singlet Singlet Energy-Transfer and Electron-Transfer Activation of Aryl Azides - Application to Photo-Cross-Linking Experiments. *J Org Chem*, **53**, 3501-3507.
- Shimada, S., Kitayama, S., Lin, C. L., Patel, A., Nanthakumar, E., Gregor, P., Kuhar, M. and Uhl, G. (1991) Cloning and expression of a cocaine-sensitive dopamine transporter complementary DNA. *Science*, **254**, 576-578.
- Shoptaw, S., Yang, X., Rotheram-Fuller, E. J., Hsieh, Y. C., Kintaudi, P. C., Charuvastra, V. C. and Ling, W. (2003) Randomized placebo-controlled trial of baclofen for cocaine dependence: preliminary effects for individuals with chronic patterns of cocaine use. *J Clin Psychiatry*, **64**, 1440-1448.
- Shrivastava, I. H. and Bahar, I. (2006) Common mechanism of pore opening shared by five different potassium channels. *Biophys J*, **90**, 3929-3940.
- Siepen, J. A., Keevil, E. J., Knight, D. and Hubbard, S. J. (2007) Prediction of missed cleavage sites in tryptic peptides aids protein identification in proteomics. *J Proteome Res*, **6**, 399-408.
- Singh, A., Thornton, E. R. and Westheimer, F. H. (1962) The photolysis of diazoacetylchymotrypsin. *J Biol Chem*, **237**, 3006-3008.
- Smith, R. A. G. and Knowles, J. R. (1973) Aryldiazirines - Potential Reagents for Photolabeling of Biological Receptor Sites. *J Am Chem Soc*, **95**, 5072-5073.
- Smith, R. A. G. and Knowles, J. R. (1975) Preparation and Photolysis of 3-Aryl-3h-Diazirines. *J Chem Soc Perk T 2*, 686-694.
- Snyder, S. H. (1996) *Drugs and the Brain*. Scientific American Library, New York.

- Snyder, S. H. and Coyle, J. T. (1969) Regional differences in H<sup>3</sup>-norepinephrine and H<sup>3</sup>-dopamine uptake into rat brain homogenates. *J Pharmacol Exp Ther*, **165**, 78-86.
- Sofuoglu, M. and Kosten, T. R. (2005) Novel approaches to the treatment of cocaine addiction. *CNS Drugs*, **19**, 13-25.
- Soundararajan, N. and Platz, M. S. (1990) Descriptive Photochemistry of Polyfluorinated Azide Derivatives of Methyl Benzoate. *J Org Chem*, **55**, 2034-2044.
- Spanagel, R. and Weiss, F. (1999) The dopamine hypothesis of reward: past and current status. *Trends Neurosci*, **22**, 521-527.
- Staros, J. V., Bayley, H., Standring, D. N. and Knowles, J. R. (1978) Reduction of aryl azides by thiols: implications for the use of photoaffinity reagents. *Biochem Biophys Res Commun*, **80**, 568-572.
- Stead, L. F., Perera, R., Bullen, C., Mant, D. and Lancaster, T. (2008) Nicotine replacement therapy for smoking cessation. *Cochrane Database Syst Rev*, CD000146.
- Stewart, A. J., Blindauer, C. A., Berezenko, S., Sleep, D., Tooth, D. and Sadler, P. J. (2005) Role of Tyr84 in controlling the reactivity of Cys34 of human albumin. *FEBS J*, **272**, 353-362.
- Takeuchi, H., Koyama, K. (1981) Photolysis and Thermolysis of Phenyl Azide in Acetic Acid. *Chem Commun*, 202-204.
- Tomizawa, M., Maltby, D., Medzihradzsky, K. F. et al. (2007) Defining nicotinic agonist binding surfaces through photoaffinity labeling. *Biochem*, **46**, 8798-8806.



- Torres, G. E., Carneiro, A., Seamans, K., Fiorentini, C., Sweeney, A., Yao, W.D., and Caron, M.G. (2003) Oligomerization and Trafficking of the Human Dopamine Transporter. *J Biol Chem*, **278**, 2731-2739.
- Torres, G. E., Gainetdinov, R.R., and Caron, M.G. (2003) Plasma Membrane Monoamine Transporters: Structure, Regulation and Function. *Nat Rev Neurosci*, **4**, 13-25.
- Torres, G. E. (2006) The dopamine transporter proteome. *J Neurochem*, **97 Suppl 1**, 3-10.
- Torres, J., Stevens, T.j., and Samso, M. (2003) Membrane Proteins: the 'Wild West' of Structural Biology. *Trends Biochem Sci*, **28**, 137-144.
- Treptow, W., Maigret, B., Chipot, C. and Tarek, M. (2004) Coupled motions between pore and voltage-sensor domains: a model for Shaker B, a voltage-gated potassium channel. *Biophys J*, **87**, 2365-2379.
- Tsao, M. L. and Platz, M. S. (2003) Photochemistry of ortho, ortho' dialkyl phenyl azides. *J Am Chem Soc*, **125**, 12014-12025.
- Turro, N. (1978) *Modern Molecular Photochemistry*. Benjamin/Cummings, Menlo Park.
- Uchimura, N. and North, R. A. (1990) Actions of cocaine on rat nucleus accumbens neurones in vitro. *Br J Pharmacol*, **99**, 736-740.
- Uhl, G. R., Hall, F. S. and Sora, I. (2002) Cocaine, reward, movement and monoamine transporters. *Mol Psychiatry*, **7**, 21-26.
- Uhl, G. R. and Lin, Z. (2003) The top 20 dopamine transporter mutants: structure-function relationships and cocaine actions. *Eur J Pharmacol*, **479**, 71-82.

- Uhl, G. R., O'Hara, B., Shimada, S., Zaczek, R., DiGiorgianni, J. and Nishimori, T. (1991) Dopamine transporter: expression in *Xenopus* oocytes. *Brain Res Mol Brain Res*, **9**, 23-29.
- Ukairo, O. T., Bondi, C. D., Newman, A. H., Kulkarni, S. S., Kozikowski, A. P., Pan, S. and Surratt, C. K. (2005) Recognition of benztropine by the dopamine transporter (DAT) differs from that of the classical dopamine uptake inhibitors cocaine, methylphenidate, and mazindol as a function of a DAT transmembrane 1 aspartic acid residue. *J Pharmacol Exp Ther*, **314**, 575-583.
- Vaughan, R. A. (1995) Photoaffinity-labeled ligand binding domains on dopamine transporters identified by peptide mapping. *Mol Pharmacol*, **47**, 956-964.
- Vaughan, R. A. (1998) Cocaine and GBR photoaffinity labels as probes of dopamine transporter structure. *Methods Enzymol*, **296**, 219-230.
- Vaughan, R. A., Agoston, G. E., Lever, J. R. and Newman, A. H. (1999) Differential binding of tropane-based photoaffinity ligands on the dopamine transporter. *J Neurosci*, **19**, 630-636.
- Vaughan, R. A., Gaffaney, J. D., Lever, J. R., Reith, M. E. and Dutta, A. K. (2001) Dual incorporation of photoaffinity ligands on dopamine transporters implicates proximity of labeled domains. *Mol Pharmacol*, **59**, 1157-1164.
- Vaughan, R. A., Huff, R. A., Uhl, G. R. and Kuhar, M. J. (1997) Protein kinase C-mediated phosphorylation and functional regulation of dopamine transporters in striatal synaptosomes. *J Biol Chem*, **272**, 15541-15546.

- Vaughan, R. A. and Kuhar, M. J. (1996) Dopamine transporter ligand binding domains. Structural and functional properties revealed by limited proteolysis. *J Biol Chem*, **271**, 21672-21680.
- Vaughan, R. A., Parnas, M. L., Gaffaney, J. D. et al. (2005) Affinity labeling the dopamine transporter ligand binding site. *J Neurosci Methods*, **143**, 33-40.
- Vaughan, R. A., Sakrikar, D. S., Parnas, M. L., Adkins, S., Foster, J. D., Duval, R. A., Lever, J. R., Kulkarni, S. S. and Hauck-Newman, A. (2007) Localization of cocaine analog [125I]RTI 82 irreversible binding to transmembrane domain 6 of the dopamine transporter. *J Biol Chem*, **282**, 8915-8925.
- Vaughan, R. A., Simantov, R., Lew, R. and Kuhar, M. J. (1991) A rapid binding assay for solubilized dopamine transporters using [3H]WIN 35,428. *J Neurosci Methods*, **40**, 9-16.
- Vodovozova, E. L. (2007) Photoaffinity labeling and its application in structural biology. *Biochem (Mosc)*, **72**, 1-20.
- Vogel, E., Altenbach, H., Drossard, J., Schmickler, H., Stegelmeier, H. (1980) 1H-Azepine: NMR Spectroscopic and Chemical Characterization. *Angew Chem Int Ed Engl*, **19**.
- Volkow, N. D., Wang, G. J., Fowler, J. S. et al. (1999) Methylphenidate and cocaine have a similar in vivo potency to block dopamine transporters in the human brain. *Life Sci*, **65**, PL7-12.
- Wang, J., Kubicki, J. and Platz, M. S. (2007) An ultrafast study of phenyl azide: the direct observation of phenylnitrenium ion. *Org Lett*, **9**, 3973-3976.

- Watt, D. S., Kawada, K., Leyva, E. and Platz, M. S. (1989) Exploratory Photochemistry of Iodinated Aromatic Azides. *Tetrahedron Lett*, **30**, 899-902.
- White, E. H., Perks, H. M. and Roswell, D. F. (1978) Labeling of Amide Linkages in Active-Site Mapping - Carbonium-Ion and Extended Photoaffinity Labeling Approaches. *J Am Chem Soc*, **100**, 7421-7423.
- Woolverton, W. L. and Johnson, K. M. (1992) Neurobiology of Cocaine Abuse. *Trends Pharmacol Sci*, **13**, 193-200.
- Xu, L., Kelkar, S. V., Lomenzo, S. A., Izenwasser, S., Katz, J. L., Kline, R. H. and Trudell, M. L. (1997) Synthesis, dopamine transporter affinity, dopamine uptake inhibition, and locomotor stimulant activity of 2-substituted 3 beta-phenyltropane derivatives. *J Med Chem*, **40**, 858-863.
- Yamashita, A., Singh, S. K., Kawate, T., Jin, Y. and Gouaux, E. (2005) Crystal structure of a bacterial homologue of Na<sup>+</sup>/Cl<sup>-</sup>-dependent neurotransmitter transporters. *Nature*, **437**, 215-223.
- Yernool, D., Boudker, O., Jin, Y. and Gouaux, E. (2004) Structure of a glutamate transporter homologue from *Pyrococcus horikoshii*. *Nature*, **431**, 811-818.
- Young, M. J. T. and Platz, M. S. (1989) Polyfluorinated Aryl Azides as Photoaffinity-Labeling Reagents - the Room-Temperature Ch Insertion Reactions of Singlet Pentafluorophenyl Nitrene with Alkanes. *Tetrahedron Lett*, **30**, 2199-2202.
- Younger, C. G. and Bell, R. A. (1992) Photolysis of 3,4-Diamidophenyl Azides - Evidence for Azirine Intermediates. *J Chem Soc Chem Commun*, 1359-1361.

- Zhou, Z., Zhen, J., Karpowich, N. K., Goetz, R. M., Law, C. J., Reith, M. E. and Wang, D. N. (2007) LeuT-desipramine structure reveals how antidepressants block neurotransmitter reuptake. *Science*, **317**, 1390-1393.
- Zimanyi, I., Jacobson, A. E., Rice, K. C., Lajtha, A. and Reith, M. E. (1989) Long-term blockade of the dopamine uptake complex by metaphit, an isothiocyanate derivative of phencyclidine. *Synapse*, **3**, 239-245.
- Zimanyi, I., Lajtha, A. and Reith, M. E. (1989) Comparison of characteristics of dopamine uptake and mazindol binding in mouse striatum. *Naunyn Schmiedebergs Arch Pharmacol*, **340**, 626-632.
- Zomot, E., Bendahan, A., Quick, M., Zhao, Y., Javitch, J. A. and Kanner, B. I. (2007) Mechanism of chloride interaction with neurotransmitter: sodium symporters. *Nature*, **449**, 726-730.

## Appendix

### A. The Amino Acid Sequence of the Flag 6XHis Tagged

#### Human Dopamine Transporter

##### FLAG 6XHIS HDAT SEQUENCE

**M<sub>1</sub>DYKDHDGDYKDHDIDYKDDDDKLTMGGSHHHHHHGMASMTGGQQMG  
RDLYDDDDKVPKDPVWWSSTPSVPM**SKSKCSVGLMSSVVAPAKEPNAVGPKEVELILVKEQNGVQLTSSTLTNPRQSPVEAQDRETWGGKIDFLLSVIGFAVDLANVWRFPYLCYKNGGGAFLVPYLLFMVIAGMPLFYMELALGQFNREGAAGVWKICPILKGVGFTVILISLYVGFFYNVIIAWALHYLFSSFTTELPWIHCNNSWNSPNCSDAHPGDSSGDSSGLNDTFGTPAAEYFERGVLHLHQSHGIDDLGPPRWQLTACLVLVIVLLYFSLWKGVKTSKGKVVWITATMPYVVL TALLRGVTLPGAIDGIRAYLSVDFYRLCEASVWIDAATQVCFSLGVGFGVLIASFSSYNKFTNNCYRDAIVTTSINSLTSFSSGFVVFSLGYMAQKHSVPIGDVAKDGPGLIFIYPEAIAATLPLSSAWAVVFFIMLLTLGIDSAMGGMESVITGLIDEFQLLHRHRELFTLFIVLATFLLSLFCVTNGGIYVFTLLDHFAAGTSILFGVLEAIGVAWFYGVGQFSDDIQQMTGQRPSLYWRLCWKLVSFCFLLFVVVVSIVTFRPPHYGAYIFPDWANALGWVIATSSMAMVPIYAA YKFCSLPGSFREKLAYAIAPEKDRELVDRGEVRQFTLRHWLKV<sub>692</sub>

##### M1...P72 FLAG HIS TAG

M<sub>1</sub>DYKDHDGDYKDHDIDYKDDDDKLTMGGSHHHHHHGMASMTGGQQMGRDLYDDDDKVPKDPVWWSSTPSV<sub>72</sub>

##### BEGINS THE DOPAMINE TRANSPORTER-NTERMINAL END

M<sub>1(73)</sub>SKSKCSVGLMSSVVAPAKEPNAVGPKEVELILVKEQNGVQLTSSTLTNPRQSPVEAQDRETWG

##### TMD1

K<sub>65(137)</sub>KIDFLLSVIGFAVDLANVWRFPYL<sub>89(161)</sub>

##### EXTRACELLULAR LOOP 1

C<sub>90(162)</sub>YKNGG<sub>95(167)</sub>

##### TMD2

G<sub>96(168)</sub>AFLVPYLLFMVIAGMPLFYMELA<sub>119(191)</sub>

##### INTRACELLULAR LOOP 1

L<sub>120(192)</sub>GQFNREGAAGVWKICPILKGVG<sub>142(214)</sub>

##### TMD3

F<sub>143(215)</sub>TVILISLYVGFFYNVIIAWALHY<sub>166(238)</sub>

**EXTRACELLULAR LOOP 2 (GLYCOSYLATION ON N & DISULFIDE BRIDGE CYS)**

L<sub>167(239)</sub>FSSFTTELPWIHCNNSWNSPNCSDAHPGDSSGDSSGLNDTFGTTPAAEYFE  
RGVLHLHQSHGIDD<sub>232(304)</sub>

**TMD4**

L<sub>233(305)</sub>GPPRWQLTACLVLVIVLLYFSLW<sub>256(328)</sub>

**INTRACELLULAR LOOP 2**

K<sub>257(329)</sub>GVKTSGK<sub>264(336)</sub>

**TMD5**

V<sub>265(337)</sub>VWITATMPYVVL TALLLRGVTL P<sub>288(360)</sub>

**EXTRACELLULAR LOOP 3**

G<sub>289(361)</sub>AIDGIRAYLSVDFYRLCEAS<sub>310(382)</sub>

**TMD6**

V<sub>311(383)</sub>WIDAATQVCFSLGVGFGVLI AFS<sub>333(405)</sub>

**INTRACELLULAR LOOP 3**

S<sub>334(406)</sub>YNKFTNNCYRDAI<sub>347(419)</sub>

**TMD 7**

V<sub>348(420)</sub>TTSINSLTSFSSGFVVFSFLGYM<sub>372(444)</sub>

**EXTRACELLULAR LOOP 4**

A<sub>373(445)</sub>QKHSVPIGDVAKDGPGLIFIIYPE<sub>396(468)</sub>

**TMD 8**

A<sub>397(469)</sub>IATLPLSSAWAVVFFIMLLTLGI<sub>420(492)</sub>

**INTRACELLULAR LOOP 4**

D<sub>421(493)</sub>SAMGGMESVITGLIDEFQLLHRH<sub>444(516)</sub>

**TMD9**

R<sub>445(517)</sub>ELFTLFIVLATFLLSLFCVT<sub>465(537)</sub>

**EXTRACELLULAR LOOP 5**

N<sub>466(538)</sub>GGIYVFTLLD<sub>476(548)</sub>

**TMD 10**H<sub>477(549)</sub>FAAGTSILFGVLI EAIGVAWFY G<sub>500(572)</sub>**INTRACELLULAR LOOP 5**V<sub>501(573)</sub>GQFSDDIQMTGQRPSLYW<sub>520(592)</sub>**TMD 11**R<sub>521(593)</sub>LCWKL VSPCFLLFVVVVSIVTFR<sub>544(616)</sub>**EXTRACELLULAR LOOP 6**P<sub>545(617)</sub>PHYGAY<sub>552(624)</sub>**TMD 12**I<sub>553(625)</sub>FPDWANALGWVIATSSMAMVPIY<sub>575(647)</sub>**C-TERMINAL END (INTRACELLULAR)**A<sub>576(648)</sub>AYKFCSLPGSFREKLAYAIAPEKDREL VDRGEVRQFTLRHWLKV<sub>620(692)</sub>



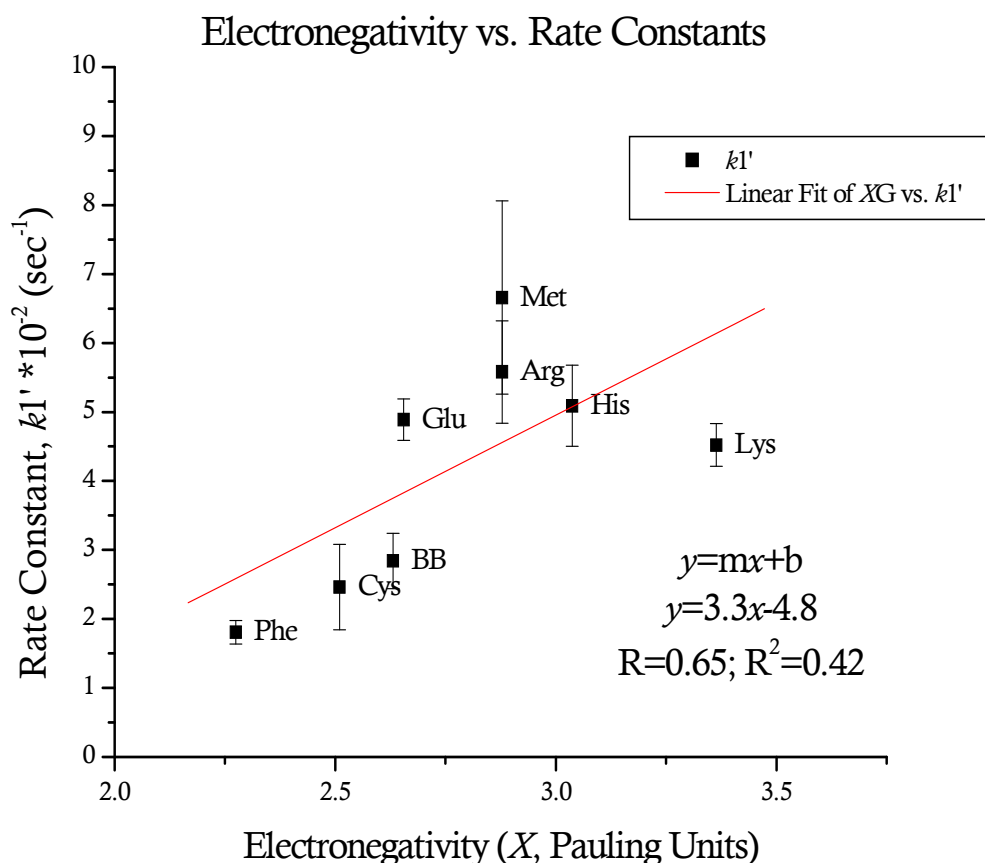
### B. Correlations of Physical Properties vs. Rate Constants

POLARIZABILITY ( $10^{-24}\text{cm}^3$ )	ELECTONEGATIVITY ( $\chi$ ) PAULING UNITS	DIELECTRIC CONSTANT, $\epsilon$	AMINO ACID
*	I=2.958, P=2.878, S=3.037	6.20	ARG
5.67 (ACETAMIDE)	2.631	ACETIC ACID 135.0	PEPTIDE BACKBONE
8.38	2.655		GLU
7.41 (ETHANETHIOL)	2.510	6.667 ETHANETHIOL	CYS
10.8 (ETHYL SULFIDE)		6.70	MET
13.5	2.878	4.71	LYS
11.1	3.364	12.4	TYR
15.04		2.446	PHE
7.5	S=3.037, I=2.958		HIS

\* Refers to values that were unable to be found or have not yet been reported in the literature. For electronegativity values, I means imine group, P means primary amine, and S means secondary amine. Relative peak height is measured in percent as the remaining amount of phenyl azide following 4 minutes of irradiation. Guanidine acetic acid, imidazole, and phenol were irradiated in 10% MeOH/90% PBS buffer, pH7.4. All others were irradiated in cyclohexane.

(values for physical constants obtained from Lide, 1995; Garner-O'Neale *et al.*, 2003)

#### Table of Physical Constants for the Amino Acid Analog Functional Groups.



### Correlation Between Phenyl Azide Reactivity and Electronegativity.

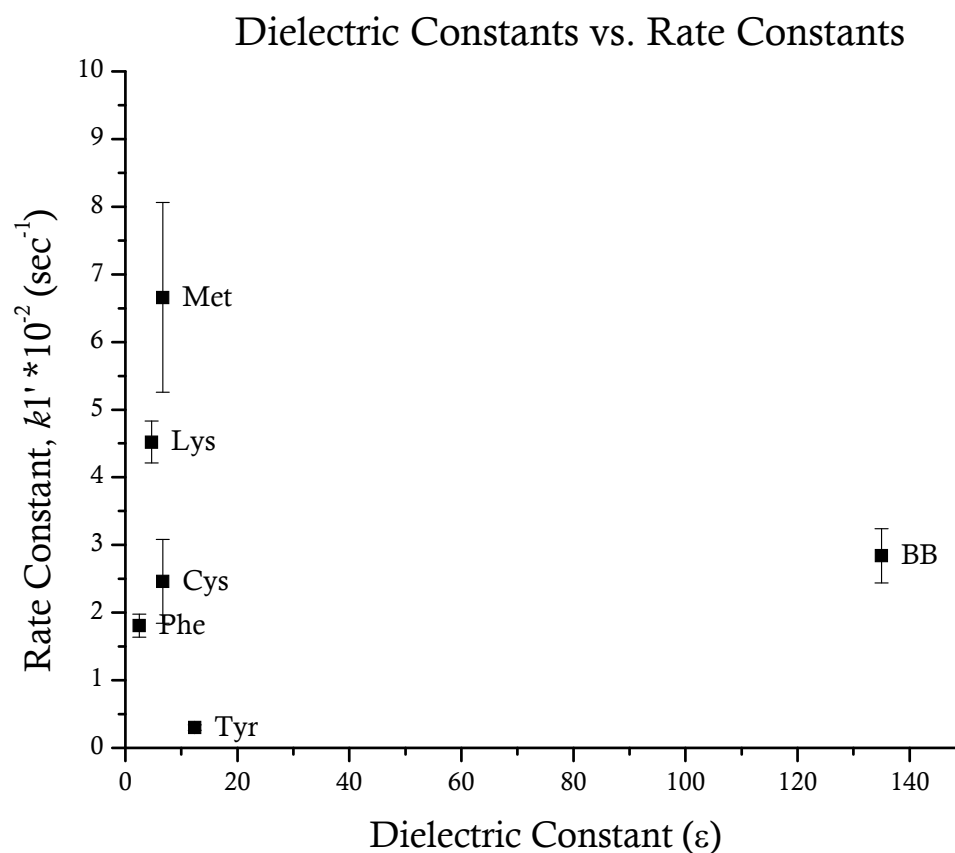
Electronegativity ( $\chi$ ) is a chemical property that describes the ability of a functional group to attract electrons or electron density towards itself in a covalent bond.

The most commonly used method of calculation is that originally proposed by Pauling.

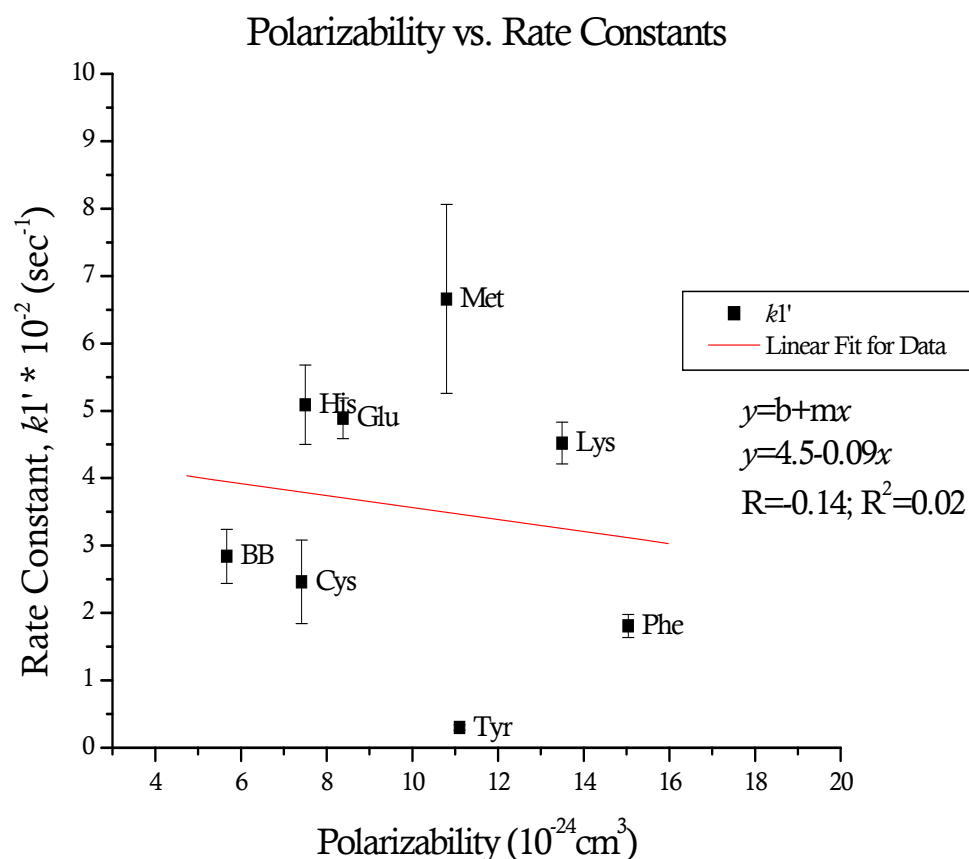
This gives a dimensionless quantity, commonly referred to as the Pauling scale, on a relative scale running from 0.7 to 4.0 (i.e. hydrogen = 2.2). There does seem to be a

correlation between phenyl azide reactivity and electronegativity of the functional

groups. The more electronegative the functional group is, the larger the rate constant is.



**Correlation Between the Phenyl Azide Reactivity and Dielectric Constant.** The dielectric constant is the ratio of the permittivity of a substance to the permittivity of free space. It is an expression of the extent to which a material concentrates electric flux, and is the electrical equivalent of relative magnetic permeability. As the dielectric constant increases, the electric flux density increases. The dielectric constant is described as epsilon ( $\epsilon$ ). There does not seem to be a correlation between the phenyl azide reactivity and the dielectric constants of the amino acid functional groups.



**Correlation Between the Phenyl Azide Reactivity and Polarizability.** Polarizability is the measure of how the electron cloud around an atom responds to changes in its electronic environment. Van der Waals forces (London forces) are also affected by polarizability. The larger atoms (large van der Waals/London forces) are more polarizable than the smaller atoms. Polarizability has the SI units of  $\text{C} \cdot \text{m}^2 \cdot \text{V}^{-1} = \text{A}^2 \cdot \text{s}^4 \cdot \text{kg}^{-1}$  but is more often expressed as polarizability volume with units of  $\text{cm}^3$  or in  $\text{\AA}^3 = 10^{-24} \text{ cm}^3$ . There is not much of a correlation between the reactivity of phenyl azide with amino acid analogs and the polarizability of the functional groups.

## C. ANOVA Data Tables for the Rate Constants

## ANOVA (Nonpolar Conditions)

	Sum of Squares	df	Mean Square	F	Significance
<b>Between Groups</b>	49.618	5	9.924	22.356	<0.001
<b>Within Groups</b>	5.327	12	0.444		
<b>Total</b>	54.945	17			

## Multiple Comparisons of Rate Constants in Nonpolar Conditions

Analogues in Cyclohexane		P<0.05	t
A.A.1	A.A. 2		
Dimethyl Sulfide	Butyric Acid	Yes	3.253
	Butylamine	Yes	3.933
	N-ethylacetamide	Yes	7.021
	1-Octanethiol	Yes	7.720
	Ethylbenzene	Yes	8.914
Butyric Acid	Dimethyl Sulfide	Yes	3.253
	Butylamine	No	0.680
	N-ethylacetamide	Yes	3.768
	1-Octanethiol	Yes	4.466
	Ethylbenzene	Yes	5.661
Butylamine	Dimethyl Sulfide	Yes	3.933
	Butyric Acid	No	0.680
	N-ethylacetamide	No	3.088
	1-Octanethiol	Yes	3.786
	Ethylbenzene	Yes	4.981
N-ethylacetamide	Dimethyl Sulfide	Yes	7.021
	Butyric Acid	Yes	3.768
	Butylamine	No	3.088
	1-Octanethiol	No	0.698
	Ethylbenzene	No	1.893
1-Octanethiol	Dimethyl Sulfide	Yes	7.720
	Butyric Acid	Yes	4.466
	Butylamine	Yes	3.786
	N-ethylacetamide	No	0.698
	Ethylbenzene	No	1.195
Ethylbenzene	Dimethyl Sulfide	Yes	8.914
	Butyric Acid	Yes	5.661
	Butylamine	Yes	4.981
	N-ethylacetamide	No	1.893
	1-Octanethiol	No	1.195

**One-Way ANOVA of Rate Constants in Cyclohexane.** A one-way ANOVA was used to test for differences in the rate constants among 6 amino acid analogs irradiated in cyclohexane. There was a significant difference across the six rate constants,  $F(5,12)=22.356, p<0.001$ . The post-ANOVA comparisons of the six amino acid analogs indicate that the dimethyl sulfide (methionine analog) ( $k_1'=6.66$ ) gave a significantly larger rate constant than any other amino acid analog ( $p<0.05$ ).

## ANOVA (Aqueous Conditions)

	Sum of Squares	df	Mean Square	F	Significance
<b>Between Groups</b>	51.063	2	25.531	85.360	<0.001
<b>Within Groups</b>	1.795	6	0.299		
<b>Total</b>	52.857	8			

## Multiple Comparisons of Rate Constants in Aqueous Conditions

Analog in Aqueous Conditions		P<0.05	t
A.A.1	A.A. 2		
Guanidine Acetic Acid	Imidazole	No	1.098
	Phenol	Yes	11.826
Imidazole	Guanidine Acetic Acid	No	1.098
	Phenol	Yes	10.729
Phenol	Guanidine Acetic Acid	Yes	11.826
	Imidazole	Yes	10.729

**One-Way ANOVA of Rate Constants in Aqueous Conditions.** A one-way ANOVA was used to test for differences in the rate constants among 3 amino acid analogs irradiated in aqueous conditions. There was a significant difference across the three rate constants,  $F(2,6)=25.663$ ,  $p<0.001$ . The post-ANOVA comparisons of the three amino acid analogs indicate that the guanidine acetic acid (arginine analog) ( $kI'=5.58$ ) gave a significantly larger rate constant than phenol ( $kI'=0.3$ ) ( $p<0.05$ ). The imidazole (histidine analog) ( $kI'=5.09$ ) gave a significantly larger rate constant than phenol ( $kI'=0.3$ ) ( $p<0.05$ ). Comparisons between the rate constants of the guanidine acetic acid (arginine) and imidazole (histidine) were no significantly different at  $p<0.05$ .

**ANOVA (NEAT Conditions)**

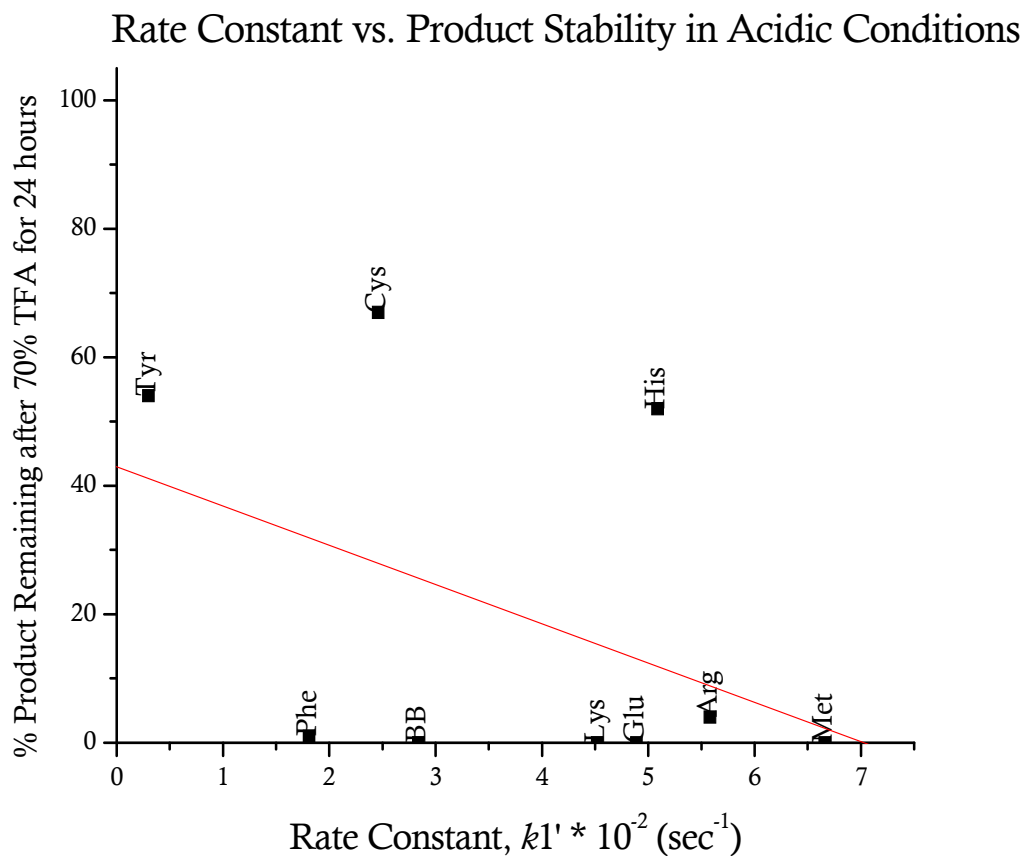
	<b>Sum of Squares</b>	<b>df</b>	<b>Mean Square</b>	<b>F</b>	<b>Significance</b>
<b>Between Groups</b>	51.327	2	25.663	515.327	<0.001
<b>Within Groups</b>	0.299	6	0.050		
<b>Total</b>	51.625	8			

**Multiple Comparisons of Rate Constants in NEAT Conditions**

<b>Analogs in NEAT Conditions</b>		<b>P&lt;0.05</b>	<b>t</b>
<b>A.A.1</b>	<b>A.A. 2</b>		
Butylamine	1-Octanethiol	Yes	31.987
	N-ethylacetamide	Yes	17.582
1-Octanethiol	Butylamine	Yes	31.987
	N-ethylacetamide	Yes	14.405
N-ethylacetamide	Butylamine	Yes	17.582
	1-Octanethiol	Yes	14.405

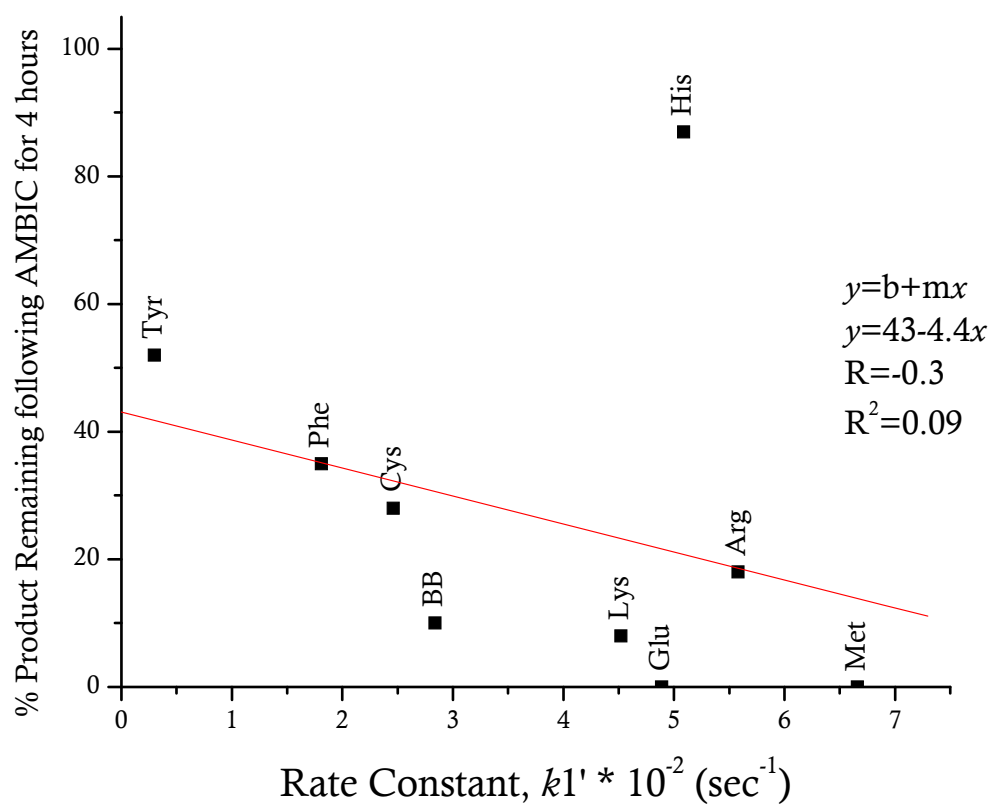
**One-Way ANOVA of Rate Constants in NEAT Conditions.** A one-way ANOVA was used to test for differences in the rate constants among 3 amino acid analogs irradiated in NEAT conditions. There was a significant difference across the three rate constants,  $F(2,6)=85.360$ ,  $p<0.001$ . The post-ANOVA comparisons of the three amino acid analogs indicate that the rate constant for the butylamine (lysine) ( $kI'=6.17$ ) was significantly larger than N-ethylacetamide (peptide backbone) ( $kI'=2.96$ ) and 1-octanethiol (cysteine) ( $kI'=0.33$ ). Comparisons between the rate constants of N-ethylacetamide (peptide backbone) ( $kI'=2.96$ ) and 1-octanethiol ( $kI'=0.33$ ) show that there was a significant difference at  $p<0.05$ .



**D. Correlations of Rate Constants vs. Product Stability in Proteolytic Conditions**

**Correlation Between the Phenyl Azide Reactivity and Product Stability in Acidic Conditions.** There does not seem to be a trend between reactivity of phenyl azide and product stability in acidic conditions. It seems to be random.

### Rate Constant vs. Product Stability in Basic Conditions



#### Correlation Between the Phenyl Azide Reactivity and Product Stability in Basic

**Conditions.** There appears to be a trend between reactivity and product stability in basic conditions. The correlation suggests that the level of reactivity of the analog with phenyl azide does not mean that the product formed will be the most stable in basic enzymatic digestion conditions.